Yearbook

2018

Institute of Technical Physics and Materials Science

http://www.mfa.kfki.hu/

Hungarian Academy of Sciences
Centre for Energy Research

Institute of Technical Physics and Materials Science

MTA EK MFA Yearbook 2018

Director: Prof. Béla Pécz

Address: Konkoly-Thege Miklós út 29-33,
H-1121 Budapest, Hungary
Postal: P.O.Box 49, H-1525 Budapest, Hungary
Phone: +36-1-392 2225
Fax: +36-1-392 2226
E-mail: info@mfa.kfki.hu
URL: http://www.mfa.kfki.hu/

Editors: Krisztina Szakolczai, Zsolt Zolnai
Published by: EK MFA, Budapest, Hungary, 2019

CONTENT

Director's foreword

As the director of MFA, it is my pleasure to welcome the reader. I recommend browsing the present yearbook which continues the series of the former ones and contains results achieved in 2018.

2018 started as an extremely successful year for MFA from the point of projects gained and infrastructure renewed. Also the results of our colleagues were appreciated by different authorities and prize committees. However, we faced a strong 'brain drain' by the industry. Parallel to this, a tough debate started between our government and the Hungarian Academy of Sciences (MTA) on the re-structuring of the academic research network. The public debate, which exposed the possibilities to move some institutions to universities and/or forming a new research network outside the MTA supervision did not make easier our situation. While the salaries remained low, this kind of near future transition did not bring new young people into our staff.
From the point of view of infrastructure, we could open with a ceremony our new aberration corrected microscope laboratory. After a long time of application submission, getting the fund, testing and tendering a new FEI THEMIS 200 TEM/STEM microscope was installed and the staff started to use that in June of 2018. Thanks to the image corrector the new microscope demonstrated the resolution of 89 pm resolving the so called diamond dumbbells. According to our original application we consider this microscope (the first aberration corrected one in the country) as an open laboratory for the Hungarian Materials Science. Therefore, I expect many requests from our universities institutions and also from industrial partners. The work in that field is also supported by a new dual beam microscope (FEI SCIOS2), what was also installed in 2018.

It was my pleasure to greet Joseph Gyulai, our former director on the occasion of his 85th birthday. A scientific workshop was organised on which several speakers from Hungary and also from Germany gave talks on common scientific results, progress in research fields which were generated by Professor Gyulai and of course many of the speakers recalled some events from their memories on the common work with Joseph Gyulai.

In the last quarter of the year the MEMS Laboratory started a split operation as Microsystems (led by Péter Fürjes) and Nanosensors (led by János Volk). The two young leaders will focus more on their selected research fields and run together the clean room facilities.

I congratulate to my colleagues: Péter László Biró gained the highest scientific award of the country, i.e. the Széchenyi Prize, Ferenc Vonderviszt was awarded by the Knight's Cross of Order of Merit of Hungary. György Molnár defended his Thesis for the Doctor of Academy (D.Sc.) title. We are also proud of those three PhD students (Gábor Piszter, Boglárka Kovács and Ferenc Bíró), who were supervised by colleagues at MFA and defended their thesis successfully in 2018 and got the PhD degree from different universities. Péter Vancsó was awarded the Junior Prima prize for his excellent results achieved in the simulation of 2D materials. Levente Tapasztó received the ELFT (Roland Eötvös Physical Society) prize of Zoltán Gyulai for his outstanding results in solid state physics.

I hope that the Readers of this yearbook will find further interesting scientific details on the following pages. Here I note that the former MFA Yearbooks are available electronically at http://www.mfa.kfki.hu/hu/yearbook.

Béla Pécz, D.Sc., Director

Organizational structure

Director	**Béla PÉCZ**

Scientific Departments	
Thin Film Physics Department	Katalin BALÁZSI
Complex Systems Department	György SZABÓ
Photonics Department	Péter PETRIK
Nanosensorics Laboratory	János VOLK
Microsystems Department	Péter FÜRJES
Nanostructures Department	Levente TAPASZTÓ
"Lendület" group - 2D Materials	Levente TAPASZTÓ
"Lendület" group - Topological Nanostructures	Péter NEMES-INCZE
"Lendület" group - NanoBioSensorics	Róbert HORVÁTH

Directly supervised functions	
Head of Scientific Advisory Council	János LÁBÁR
Scientific secretary, projects and PR	Krisztina SZAKOLCZAI
Quality control, MTMT, REAL admin	Andrea BOLGÁR
Technical support	Károly BODNÁR
Financial administration	Zsuzsanna KELEMEN
Informatics	Gergely TAMÁS
Technology transfer (IPR)	Antal GASPARICS

Key Financial Figures of MFA

The turnover realised by the institute always reflect the national and international political and financial system and also the efforts of the institute. The domestic subsidies did not change in the last few years; however the overhead and the salaries increased. The periodicity of the Hungarian grants resulted in decreasing income from domestic projects. Despite the efforts of the colleagues only a few H2020 proposals are above the line. Since 2015 MFA is part of the Centre of Energy Research. The financial operation is only partly transparent, our financial status completely not plannable, totally unpredictable by our own grant administration group. The data shown here for 2015-2018 are based upon our own database and estimates.

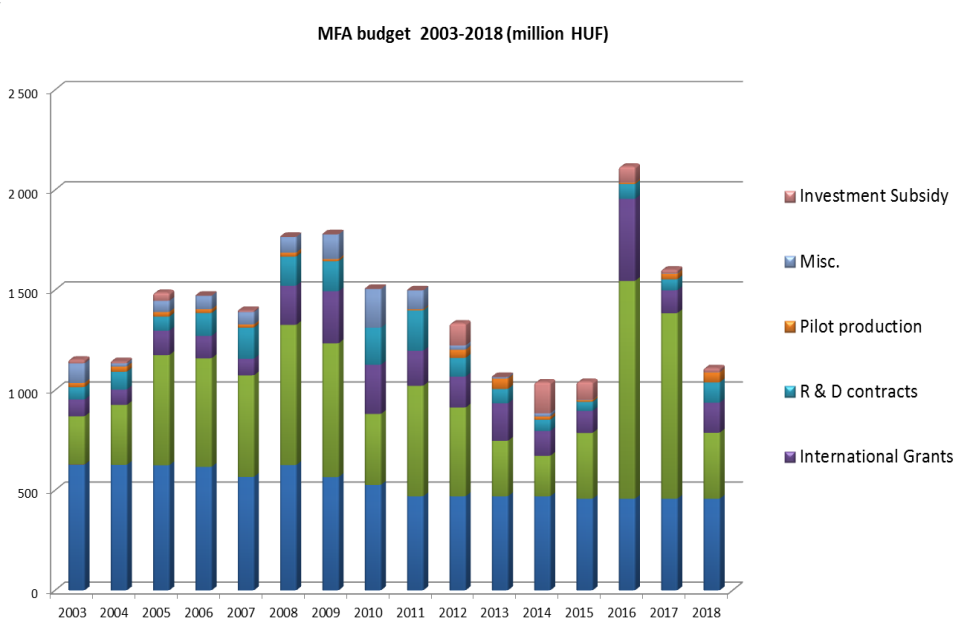

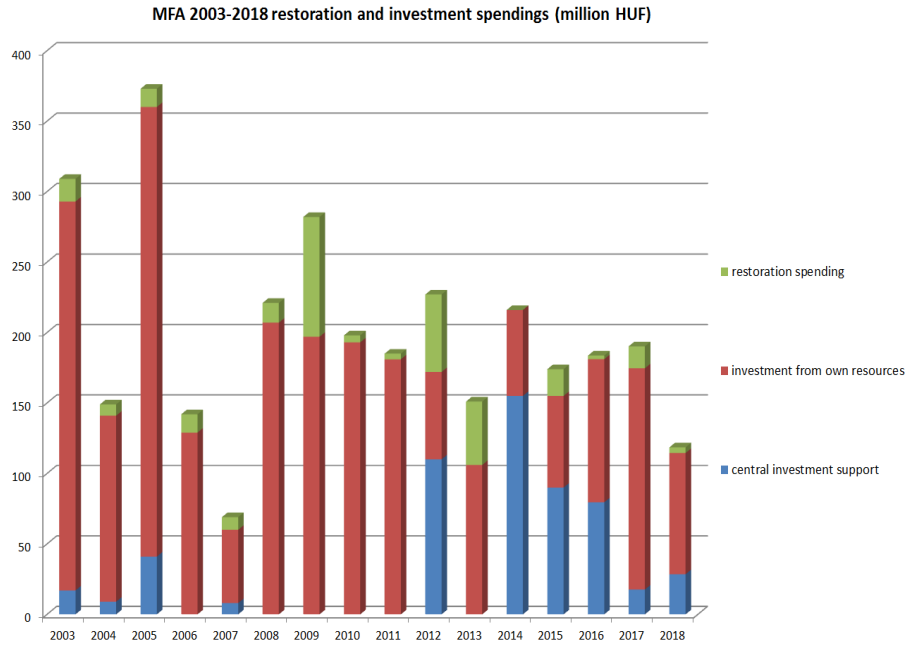

Publications and Citations of MFA

According to the Thomson-Reuters ISI "Web of Knowledge", and MTMT databases, the Institute has an average publication activity of ca. 100 scientific papers in IF journals a year. The number decreased a bit in the last years, but recently MFA researchers publich in journals with higher impact factor.

MFA and its predecessor's publications

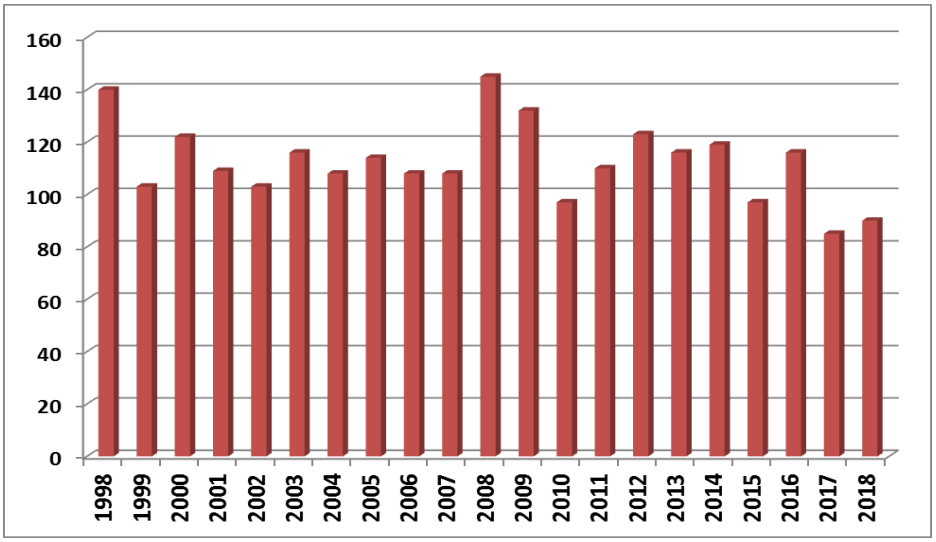

MFA and its predecessor's citations

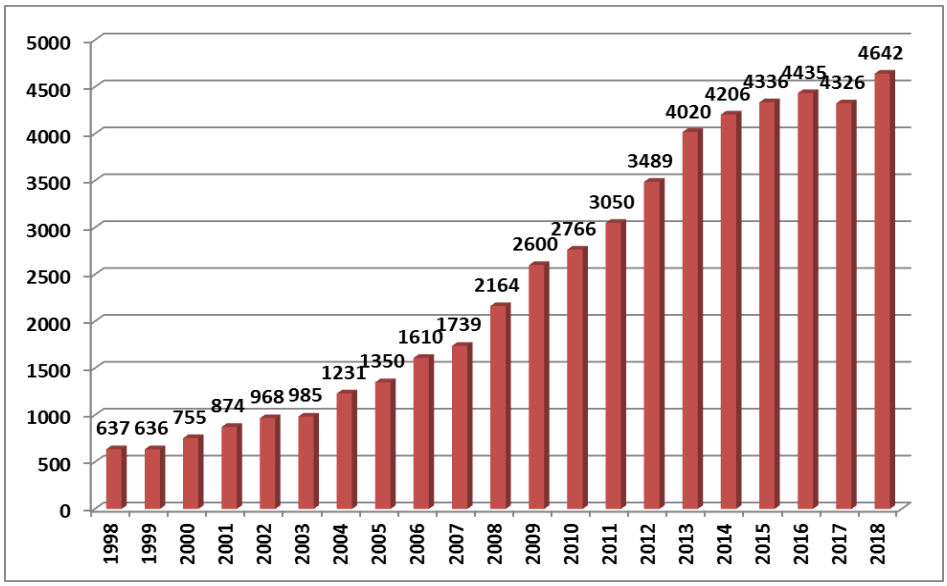

Prizes and Distinctions

	**BIRÓ, László Péter**	Széchenyi Prize
	**VONDERVISZT, Ferenc**	Order of Merit of the Republic of Hungary Knight's Cross
	**BIRÓ, László Péter**	Scientific Prize of Érd City
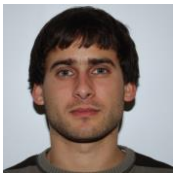	**VANCSÓ, Péter**	Junior Prima Award
	**PÁLINKÁS, András**	New National Excellence Fellowship
	**BÁRSONY, István**	Professor Emeritus of the Hungarian Academy of Sciences
	**SERÉNYI, Miklós**	Professor Emeritus of the Hungarian Academy of Sciences
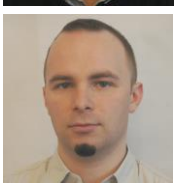	**Tapasztó, Levente**	ELFT Zoltán Gyulai Prize

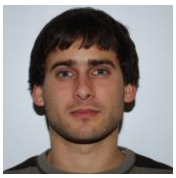

VANCSÓ, Péter

Academia Europaea Burgen Scholar Excellence Award

PETRIK, Péter

MFA Prize (Institute)

NEMES-INCZE, Péter

MFA Prize (Postdoctoral)

PETŐ, János

MFA Prize (Ph.D. student)

RADÓ, János

MFA Prize (Ph.D. student)

CORA, Ildikó

Ferenczi György Memorial Prize

Dr. László Péter Biró a physicist was awarded the Érd Science Prize. The award can be given to those who have excelled in one of the disciplines and thus contributed to the reputation of the City of Érd. (source: erdmost.hu)

Dr. Levente Tapasztó was awarded the ELFT Zoltán Gyulai Prize.

SCIENTIFIC REPORTS

A new generation electron microscope for the open laboratory of the Hungarian materials science

VEKOP-2.3.3-15-2016-00002

Béla Pécz, János Lábár

A new laboratory with the first spherical aberration corrected TEM/STEM in Hungary was opened on 11th of June 2018 in our Institute. The work started years earlier, when members of the Thin Film Physics Department took study trips to different laboratories in order to learn the technique. The first proposal was submitted to NKFIH in 2016, then with their specific support a second step proposal to our Ministry of Economy. It was a continuous work for two years to get the support, select the appropriate model and carry out a very rigid public procurement procedure. Finally, a Thermo Fisher Scientific FEI THEMS 200 model was selected with an image corrector. The preparation of the appropriate room started with moving an old microscope to another room, as the group wanted to keep and run the existing 200 kV analytical and the 300 kV high resolution (equipped with an EELS) microscopes beside the new one. A far more sophisticated installation environment with a very stable, precise temperature controlled air condition and stray magnetic field cancel system was constructed.

Figure 1*. The new microscope in the laboratory.*

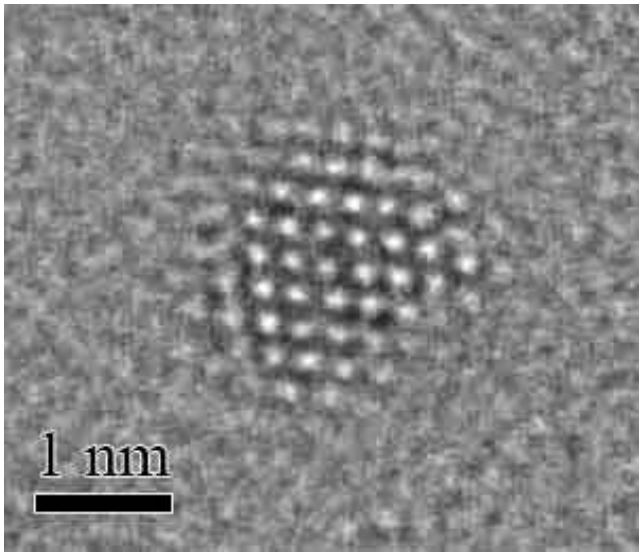

The onsite tests after installation exceeded our expectations and the factory guaranteed parameters. Factory stated TEM resolution at 200 kV is 0.09 nm, i.e. 90 pm. The tests show that a resolution of 70 pm is attainable.

Figure 2*. The image to the left shows a small gold particle at atomic resolution. As the spherical aberration (C_s) is intentionally set to a very small negative value, the atoms appear with bright contrast on the image.*

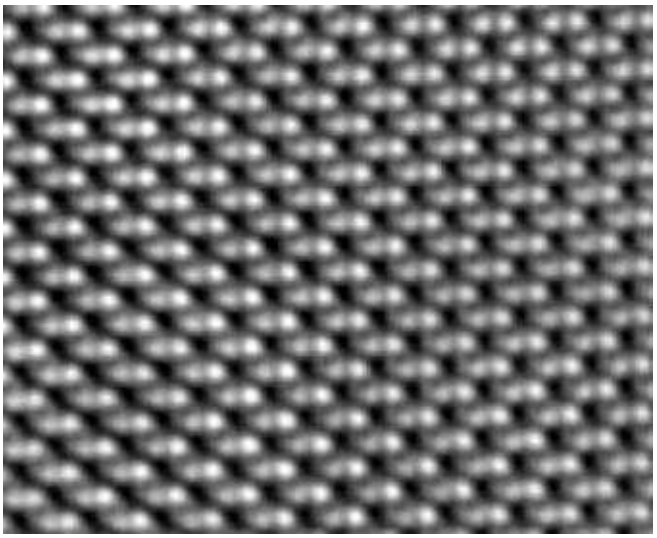

In the following we will show some examples proving the superior capability of the microscope

Figure 3*. Diamond lattice imaged in TEM mode revealing the diamond dumbbells with the distance of 89 pm, (400) lattice spacing in diamond. This is a very important demonstration of the resolution power. In the case we do not have the resolution below 90 pm these two close dots (i.e. two rows of carbon atoms) are imaged as one intensity spot in the high resolution image.*

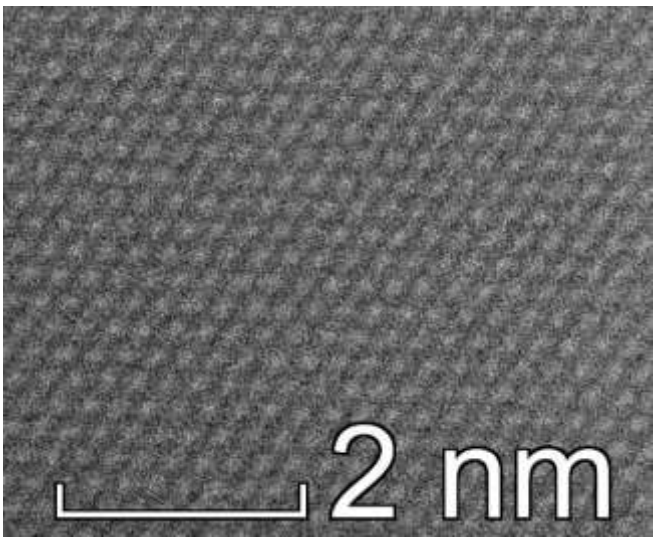

The microscope can be operated at 80 kV still having a very good resolution thanks to the spherical aberration corrector. Sensitive materials including 2D layers can be investigated at that low voltage operation.

Figure 4. *Graphene foil in high resolution imaged at 80 kV.*

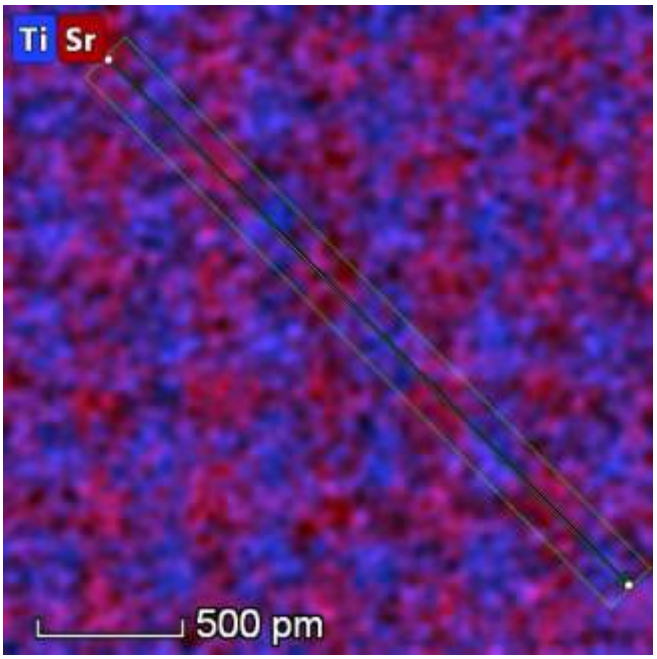

The analytical measurements in the new microscope are provided by the SuperX system comprised of 4 EDS detectors built into the column. There is no need to tilt the sample in order to get a good signal to noise ratio.

Figure 5. *Although this is not a probe corrected microscope the power of the EDS mapping can be demonstrated on a $SrTiO_3$ thin specimen in which the Ti and Sr atoms can be distinguished, see the image left.*

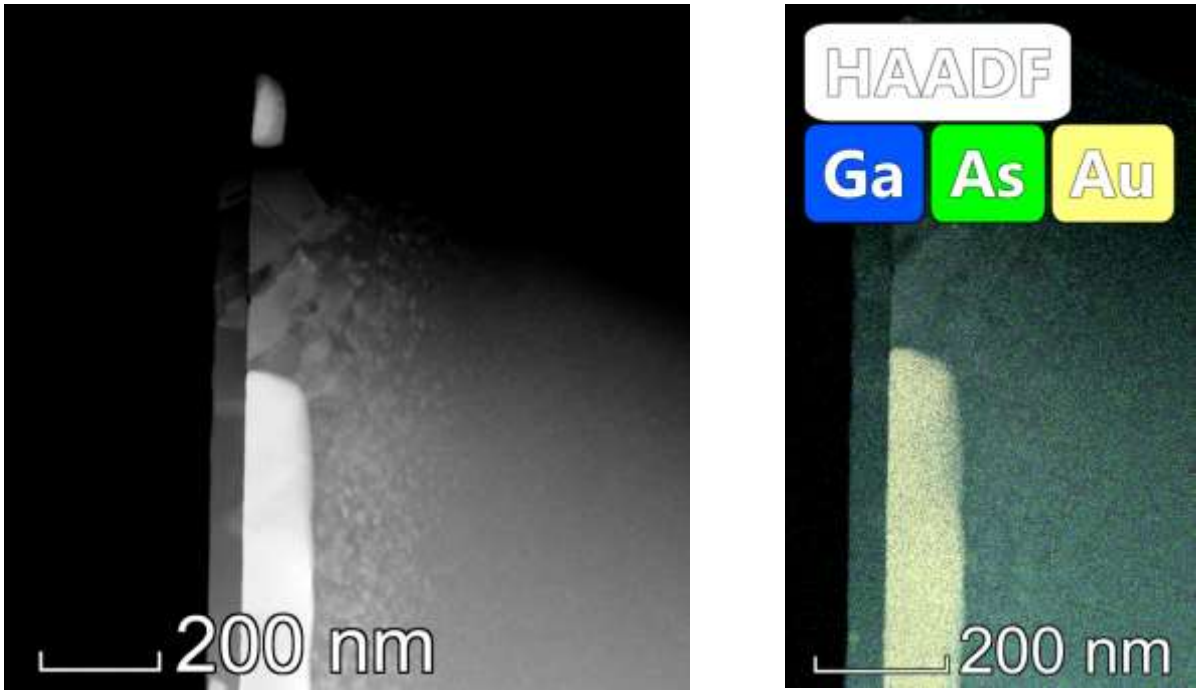

***Figure 6**. The above images are taken in STEM mode. The left one is an HAADF (High-angle annular dark-field) image showing gold grains with high intensity, as the brightness is monotonically increasing with the atomic number (Z^2). This itself makes possible to map the details of any specimen in which we can observe variations of Z. However, the right side image is a spectrum image taken on the same area of the sample (Au/GaAs sample ion beam mixed and annealed) We can observe not only gold crystallites (in the reality they contain already some gallium therefore the colour in the EDS map is darker than the yellow colour of gold) is embedded into GaAs, but a thin GaAs on the top of the sample as well. The results were presented at the Workshop dedicated to the 85th birthday of Prof. J. Gyulai.*

The new contrast mechanism of the corrected TEM, namely imaging with negative C_s, facilitated the identification of the crystallographic phase of a precipitate by comparing the experimental image to the simulated images of the possible phases. An Al-alloy with low (0.14wt%) Zr-content contained spherical precipitates embedded in the Al-matrix. EDS analysis showed that the precipitate contains Zr and Al, but the elemental ratio could not be determined due to the undefined contribution of the surrounding, encapsulating Al-matrix. Two phases appeared in the literature to describe such spherical Al-Zr precipitates, both with identical cubic crystal structure. The difference between the two is that in the first, Al atoms sit at the corners of the cube and Zr atoms at the centres of all faces and in the second their positions (and so the proportion of the elements) are reversed. We recorded an experimental image with negative C_s from a region that contained such a precipitate of 12 nm diameter, together with the surrounding matrix. Simulated images were also calculated for both phases and for the Al-matrix.

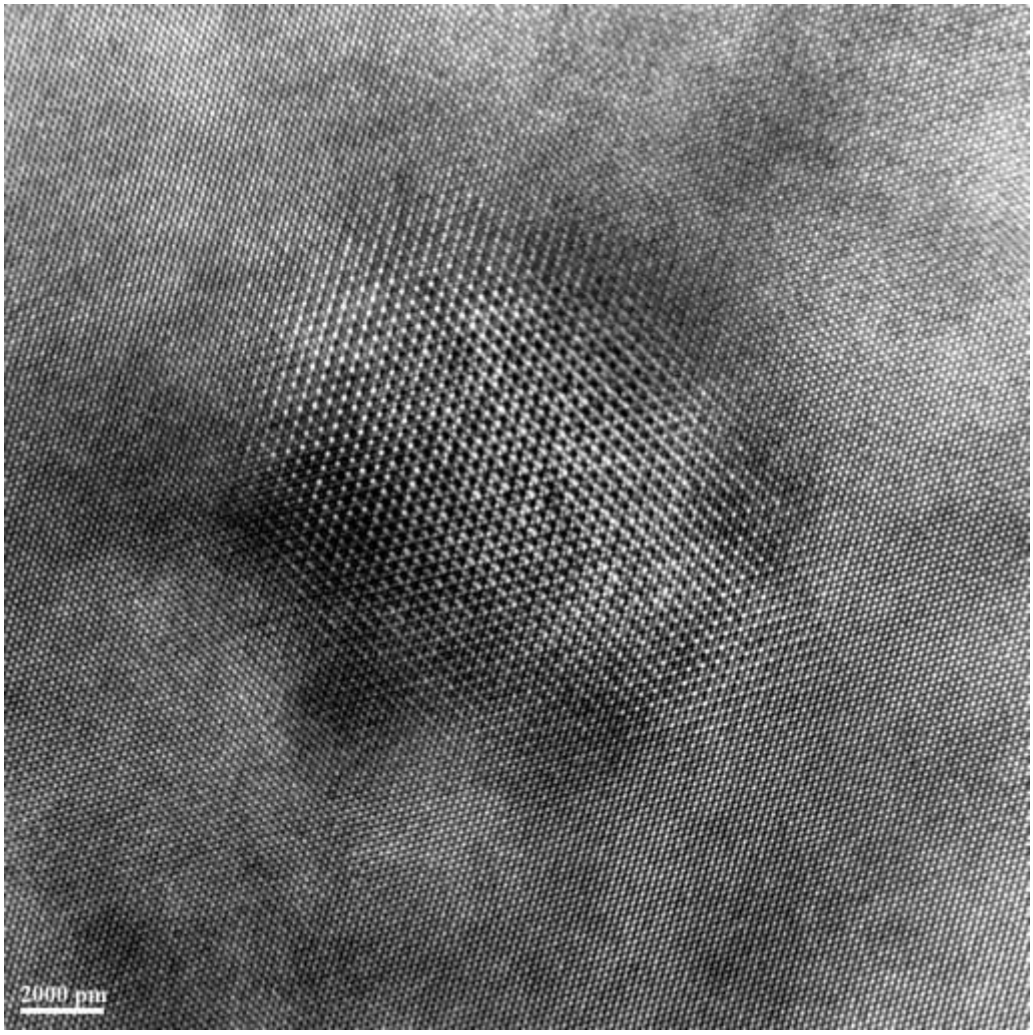

Figure 7. *A magnified, selected region of the above image shows (below) the transition from the Al-matrix to the precipitate. There is serious overlap between the matrix and the precipitate in the transitional region. Atomic columns are bright with negative C_s. Structural features with the same size are marked with blue in the matrix, in the transitional region and in the precipitate.*

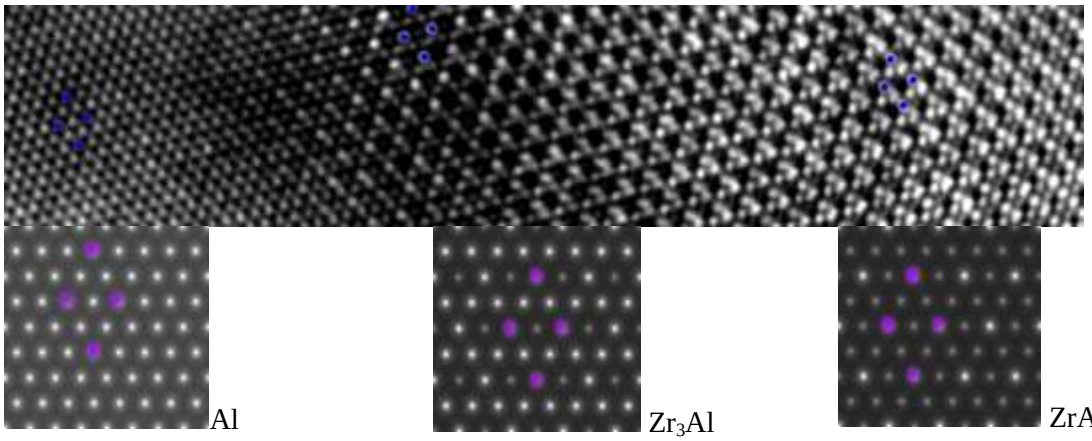

Figure 8. *The projected potentials were calculated with the JEMS program for the [111] direction of all three structures. The same tructural features are also marked in the simulated images.*
It can be seen that on the one hand there is perfect match between measured and simulated images for the matrix. On the other hand, simulated image for phase Zr_3Al perfectly matches the measured (four times bright triangles with a darker spot in the middle), while the simulated image of the other phase is completely different, making phase identification unambiguous. The precipitate is cubic Zr_3Al.

Single-atom catalysts based on doped MoS_2 single layers for efficient hydrogen evolution

ERC StG, Lendület,* Korea-Hungary Joint Laboratory, *Graphene Flagship

J. Pető, P. Vancsó, G. Dobrik, T. Ollár (EK-FKL), Z. Popov (MISis-Moscow), C. Hwang (KRISS-Korea), P.B. Sorokin (MISis-Moscow) and L. Tapasztó

Single atom catalysts have recently shifted into the spotlight of heterogeneous catalysis research. Among their major appeals are the ultimate efficiency of material utilization and the simple and well-defined nature of the active centers, holding the promise of rational catalyst design. The major challenges are the preparation of a high density of firmly bound individual single-atomic centers, as well as establishing reliable structure-activity relationships. Both platinum group and transition metal atoms were found to be catalytically active in single-atomic form. Embedded in the proper matrix, also non-metal atoms can become catalytically active centers. We demonstrate that 2D crystals can provide an efficient template for realizing single-hetero-atom catalysts with a high density of non-metal single-atomic active sites. Such single-atom catalysts obtained through substitutional doping of 2D MoS_2 crystals with oxygen can provide the advantages of an easy and versatile synthesis, a supreme site density, and a well-controlled and characterized active site structure.

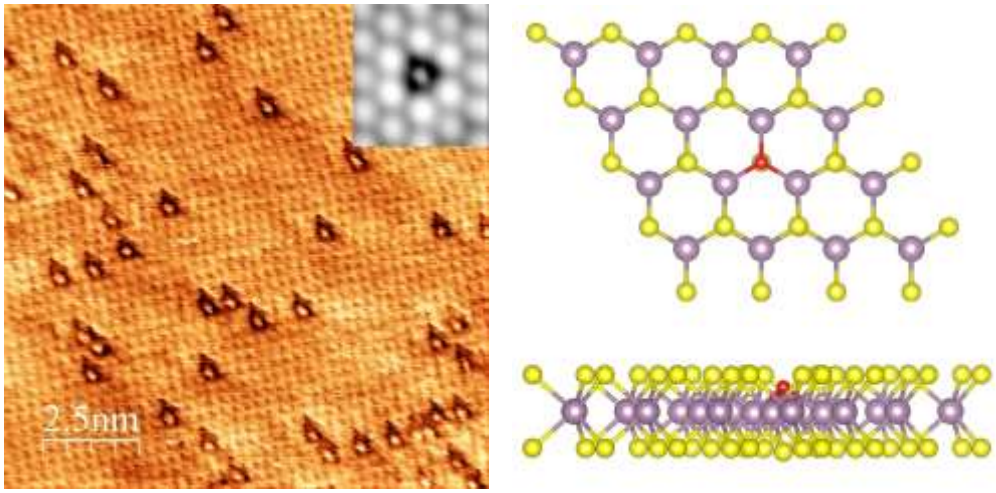

***Figure 1**. Atomic resolution STM image of MoS_2 monolayers showing single oxygen atoms replacing individual S atoms in the crystal lattice. Calculated atomic structure of the oxygen substitution sites (red) in 2D MoS_2 host crystals (Mo-grey, S- yellow).*

By means of atomic resolution STM investigations we were able to image a novel oxidation reaction of the MoS_2 single-layers at single-atom level, providing unexpected insights. In contrast to the generally accepted view, our results clearly evidence that the basal plane of 2D MoS_2 crystals spontaneously oxidized upon long-term ambient exposure. Instead of O chemisorption or full conversion to MoO_3, a novel oxygen substitution mechanism has been revealed, where individual S atoms of the basal plane are one by one replaced by oxygen atoms giving rise to a new 2D $MoS_{2-x}O_x$ solid solution crystal. As MoS_2 single layers are the most widely investigated 2D materials besides graphene, the ability to chemically modify their single atomic sites provides a novel strategy for highly efficient defect engineering as well as synthesizing novel 2D crystals with tunable chemical compositions.

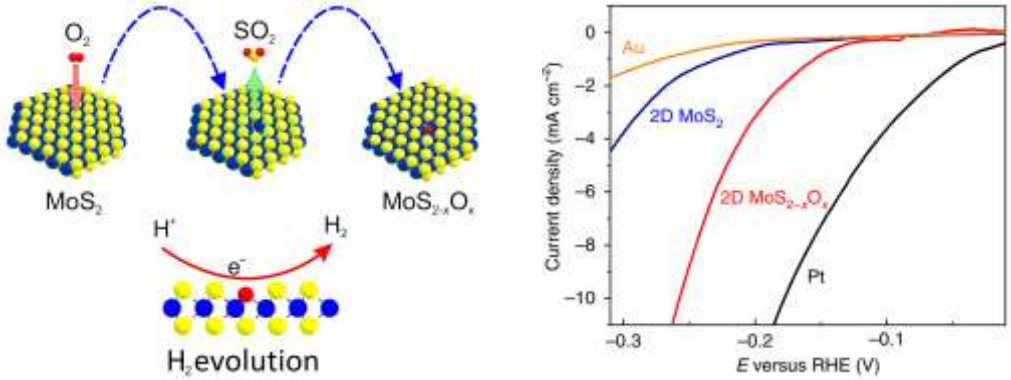

Figure 2: *Oxygen atoms spontaneously incorporate into the structure of MoS_2 single layers under ambient conditions giving rise to solid solution type 2D molybdenum oxy-sulfide crystals. The single atomic oxygen substitution sites catalytically activate the basal plane of MoS_2 for hydrogen evolution as evidenced by the voltammogram curves*.

Most importantly, we have observed a significantly enhanced catalytic activity for hydrogen evolution of 2D $MoS_{2-x}O_x$ as compared to its pure 2D MoS_2 form. We have shown that the individual O atom dopants are responsible for significantly increasing the catalytic activity. The Tafel slope for $MoS_{2-x}O_x$ crystals was decreased to 67 mV dec^{-1} as compared to pristine MoS_2 (98 mV dec^{-1}) and approached that of the Pt (54 mV dec^{-1}). Introducing the electronegative O atoms generates sites with higher electron affinity (−0.88 e^-), which gives rise to localized negative charges attracting H^+ to participate in reductive coupling to form H_2. Consequently, 2D $MoS_{2-x}O_x$ crystals emerge as highly efficient, non-precious, earth-abundant catalysts for H_2 evolution with a high density of single-atomic active sites on their basal plane. Upon optimization, such catalysts hold the potential to closely approach the catalytic activity of platinum at much lower costs.

Synthesizing single atom catalysts with well dispersed identical active centers is highly challenging. Even today, the relatively low site density is a major limiting factor for the activity of single atom catalysts, as the stable anchoring (strong bonding) of individual heteroatoms to substrates is required for preventing their aggregation. Our results evidence that 2D transition metal chalcogenides can provide ideal substrates for the stable anchoring of various heteroatoms, through substituting single atoms from the host crystal lattice with various heteroatoms. These findings open the way towards developing non-metal single atom catalysts by using transition metal chalcogenide single-layers as an active substrate, opening new perspectives in single atom catalysis.

Nanostructures Laboratory & 2D 'Lendület' Research Group

Head: Dr. Levente Tapasztó, Ph.D., senior research fellow

Research Staff

- Zsolt Endre HORVÁTH, D.Sc., Deputy Head of Laboratory
- Prof. László Péter BIRÓ, Corr. Member of the HAS
- Gergely DOBRIK, Ph.D.
- Krisztián KERTÉSZ, Ph.D.
- Antal Adolf KOÓS, Ph.D.
- Géza István MÁRK, Ph.D.
- Péter NEMES-INCZE, Ph.D.
- Zoltán OSVÁTH, Ph.D.
- Gábor PISZTER, Ph.D.
- Péter SÜLE, Ph.D.
- Péter VANCSÓ, Ph.D.

Ph.D. students / Diploma workers

- Péter KUN, Ph.D. student
- András PÁLINKÁS, Ph.D. student
- János PETŐ, Ph.D. student
- Márton SZENDRŐ, Ph.D. student

Main expertise of the Nanostructures Laboratory lies in synthesis and atomic scale characterization of various nanostructures. In recent years, research efforts were focused on two-dimensional (2D) materials. Research areas cover synthesis of various 2D crystals, their characterization with atomic resolution, and nanoengineering. Furthermore, studying electronic properties thereof, and fabrication of proof of concept electronic devices based on 2D materials and their nanostructures. Most intensively investigated materials are: graphene, dichaclogenide single layers of various transition metals, layered topological insulator crystals, as well as photonic nanoarchitectures of biological origin.

The major achievements of the Nanostructures Laboratory during 2018 were the following:

- In the framework of the ERC Starting Grant project they showed that the substitution of sulfur atoms with oxygen atoms in monolayer MoS_2 creates catalytically active single-atomic sites, which are capable of enhancing the hydrogen evolution reaction. The $MoS_{2-x}O_x$ crystals can be a cheaper alternative to platinum catalysts. Their results were published in Nature Chemistry and numerous academic (Nature Review Chemistry, phys.org, Nanowerk) and general media (PR Newswire, Fox14, index.hu) picked up on these accomplishments.
- In the framework of the „Lendület" project they were able to show that the naturally occurring Pt_2HgSe_3 crystal has a 110 meV wide topological band gap and identified the corresponding edge states. This is the first experimental evidence for the topological insulator nature of the Pt_2HgSe_3 crystal, a layered 2D material which can be used under ambient conditions.
- In the framework of the Korea-Hungary Joint Laboratory for Nanosciences they showed that mechanical deformation causes a direct to indirect band gap transition and a semiconductor to metal transition in monolayer MoS_2 at relatively low (~2%) elastic deformations. These results open up new and efficient possibilities for bandgap engineering of 2D MoS_2 crystals.
- In the framework of the Graphene Flagship project using atomic resolution scanning tunneling microscopy they identified in $MoSe_2$ monolayers grown by Chemical Vapor Deposition (CVD) a special type of grain boundary running along the zig-zag lattice direction that does not perturb significantly the electronic structure. This makes possible the growth of macroscopic 2D $MoSe_2$ crystals with high electronic quality using the CVD technique.

- In the framework of an NKFIH OTKA project they used Raman spectroscopy measurements to show that in the graphene/gold nanoparticle hybrid systems a fully reversible mechanical strain can be induced by a focused laser beam. The method can be used for the dynamic control of mechanical deformation in graphene.
- In the framework of an NKFIH OTKA project they showed that the nanostructures at the origin of the green and blue coloration of the wings of Albulina metallica butterflies can be used for selective chemical vapor sensing. They showed that the sensing efficiency and selectivity can be significantly improved if the scales containing different nanoarchitectures are integrated into sensor arrays.

Direct-indirect bandgap and semiconductor-metal transitions in MoS_2 single-layers at moderate strain

ERC StG, Korea-Hungary Joint Laboratory, Lendület

J. Pető, P. Vancsó, G. Dobrik, P. Nemes-Incze, G. Kukucska (ELTE), J. Koltai (ELTE), L. Tapasztó

Strain-engineering the properties of 2D MoS_2 crystals have been intensely investigated for the last couple of years. Tuning the band structure by applying mechanical strain can provide an efficient way to fit the properties of the material to the specific requirements of various electronic and opto-electronic applications. Theoretical studies predict a steady decrease of the bandgap upon increasing of uni- and biaxial strain. Furthermore, it is expected that increasing the strain leads to a direct-indirect bandgap transition that was predicted to occur between 0,47 – 2,7 % strain depending on the theoretical model, while increasing the strain up to about 10% is predicted to give rise to a semiconductor-metal transition. Photoluminescence (PL) measurements confirmed that tensile strain can reduce the optical bandgap of 2D MoS_2 crystals. However, the experimental demonstration of the direct-indirect gap and semiconductor-metal transitions remained challenging.
Here we study MoS_2 nanobubbles emerging at the interface of MoS_2 single layers with Au(111) substrate. Such bubbles are shown to induce a few percent of biaxial tensile strain in the MoS_2 lattice. We employed Raman spectroscopy to determine the amount of strain in MoS_2 nanobubbles, and scanning tunneling microscopy (STM) and spectroscopy investigations to directly measure the fundamental bandgap of the strained MoS_2 monolayers.

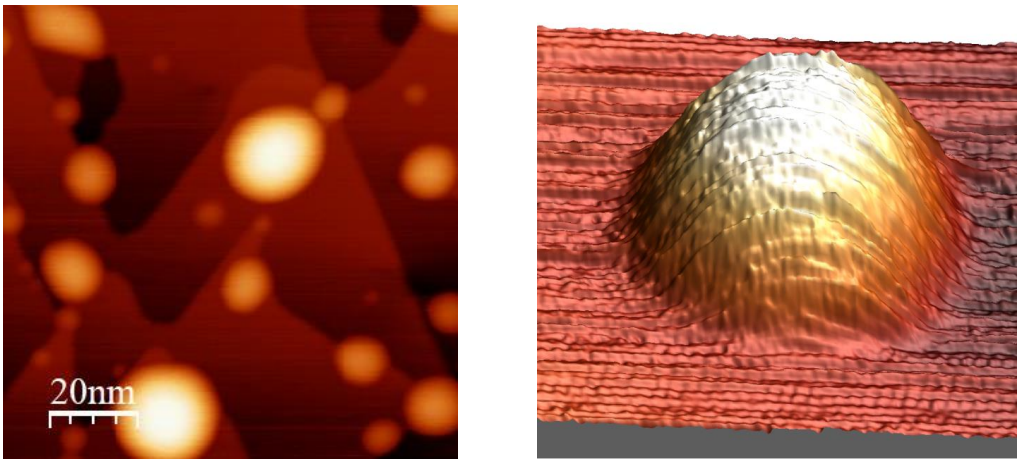

Figure 1. *Nanobubble formation at the MoS_2/Au(111) interface. a) STM image revealing the presence of several nanoscale MoS_2 bubbles. b) 3D STM image of an individual MoS_2 nanobubble.*

In order to experimentally determine the amount of mechanical strain induced in the MoS_2 lattice in the bubble areas, we performed confocal Raman spectroscopy measurements and calculations. The best agreement was found when considering 2% of bi-axial tensile strain.
By tunneling spectroscopy on MoS_2 nanobubbles, we were able to measure the fundamental bandgap of MoS_2 single layers subjected to 2% of biaxial tensile strain. We found that this strain decreases the bandgap of 1.4 ± 0.15 eV below the 1.7 eV optical gap, evidencing that the direct to indirect bandgap transition has already occurred at 2% tensile strain, in good agreement with DFT calculations. Furthermore, the combination of a few percent of tensile strain with the intrinsic *n* doping of the MoS_2 layers can provide a metallic character to MoS_2 single-layers already starting from modest strain values (2-3%).

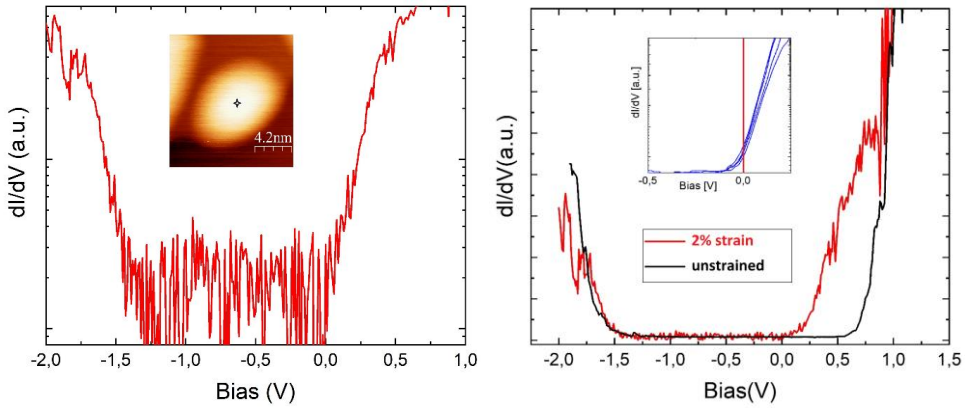

Figure 2: *a) Tunneling spectrum on a MoS_2 nanobubble revealing a bandgap of about 1.4 eV. b) Comparison of the tunneling spectra of strained and unstrained MoS_2 monolayer. The inset shows that the Fermi level of strained bubbles can shift inside the conduction band, conferring a metallic character to the strained MoS_2 crystal.*

To understand the mechanism of the strain-induced changes in the band structure, we have performed DFT calculations. These calculations show that at 2% of tensile strain the bandgap is reduced by about 0.46 eV, and becomes an indirect gap between the K and Γ points of the Brillouin-zone, in good agreement with our experiments. Furthermore, the calculations evidence that the bandgap reduction is almost entirely due to the downshift of the conduction band, again in excellent agreement with our experimental observation (Fig 2b).

These findings experimentally demonstrate a particularly efficient strain-engineering of the fundamental gap, which can be exploited in electronic applications, for example, by strain patterning type I heterojunctions. Furthermore, our results also clearly reveal the limitations of the strain-engineering approach. The direct-indirect transition restricts the opto-electronic applications, while the semiconductor-metal transition puts a strong limit on electronic applications above 2% of strain, where the 2D MoS_2 crystals acquire a metallic character.

Measuring the edge states of Pt_2HgSe_3, a room temperature two-dimensional topological insulator candidate

Lendület LP2017-9, ERC StG NanoFab2D, H2020 Graphene Flagship

K. Kandrai, P. Vancsó, G. Kukucska (ELTE), J. Koltai (ELTE), Á. Hoffmann, A. Vymazalová (Czech Geological Survey), L. Tapasztó, P. Nemes-Incze

The realization that the geometrical concept of topology has a profound influence on the band structure of solids is no doubt one of most surprising and wide-reaching discoveries in the last decades of condensed matter research. Materials that are characterized by the $\mathbb{Z}_2$ topological invariant are insulating in the bulk and have conductive edge channels on their surfaces or edges. These edge states carry dissipationless current and could be a platform to realize topological quantum computation. A prototype of this is actually graphene, but the fact that the material is a topological insulator remains a theoretical curiosity, due to the negligible spin orbit coupling (SOC) strength of carbon. Therefore, the hunt is on for materials that have a large topologically non-trivial band gap, preferably in the room temperature regime (>77 meV).

Jacutingaite (Pt_2HgSe_3), a naturally occurring layered mineral has been recently predicted to be a topological insulator, with a band gap above room temperature. One can consider it a "heavy metal" version of graphene, with large SOC. By performing scanning tunneling microscopy (STM) measurements on the material, we reveal the honeycomb-like configuration of the basal plane states (see Fig 1a, b). Our density functional theory (DFT) calculations predict a topologically non-trivial gap of 110 meV. This value is reproduced by tunneling conductance measurements on the bulk basal plane. Its topological character is confirmed by calculating the $\mathbb{Z}_2$ invariant. In Fig. 1e we can observe how the density of states within the gap increases, if we move the tip of the STM closer to a monolayer step edge on the surface. This observation is expected if the topological edge state resides within the band gap. By mapping the tunneling conductance within the gap, as a function of position, it becomes clear that the increased density of states follows the step edge, with a decay of ~5 Å into the bulk, as expected from DFT calculations (see Fig. 2).

The identification of the topological edge states makes Pt_2HgSe_3, a prime candidate for applications of 2D topological insulators, with the promise of achieving room temperature dissipationless transport, or the realization of a topological superconductor.

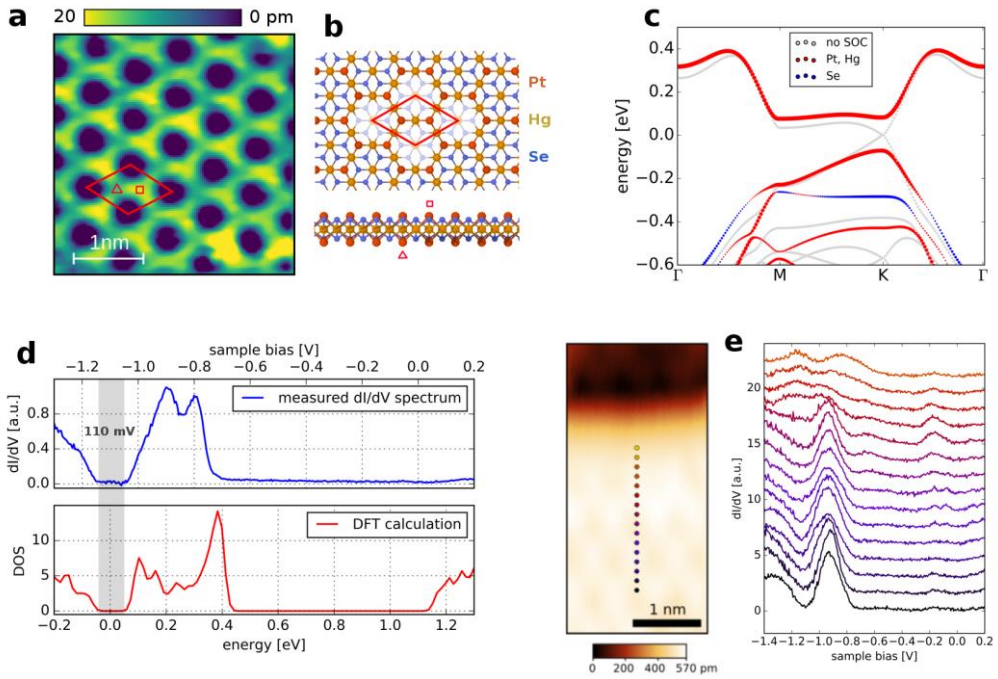

Figure 1. *STM measurements on Pt_2HgSe_3. (a) Atomic resolution STM image of the basal plane, showing the honeycomb structure of Pt_2HgSe_3. (b) Atomic lattice of a single layer of Pt_2HgSe_3. (c) DFT calculation of its bands. Grey plot shows the bands of a single layer without spin orbit coupling. Red and blue bands are calculated with spin orbit coupling taken into account. The color represents the contribution of Pt and Hg atoms. (d) Density of states measured on the basal plane (blue) and calculated via DFT (red). (e) Tunneling conductance measurements nearing a monolayer edge, showing the appearance of states inside the predicted topological band gap.*

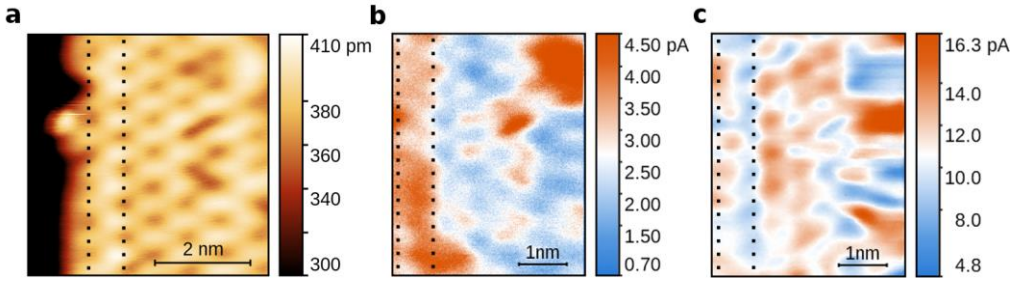

Figure 2. *Images of the topological edge state. (a) STM topographic image of a monolayer step edge. Tunneling conductance images measured at the edge, at a sample voltage inside the band gap: (b) and out of the band gap in the conduction band: (c).*

Highly ordered grain boundaries in CVD $MoSe_2$ single layers.

ERC StG NanoFab2D, Graphene Flagship

A. A. Koós, P. Vancsó, G. Dobrik, L. P. Biró and L. Tapasztó

The chemical vapour deposition (CVD) growth method is one of the most widely investigated techniques to achieve a scalable growth of macroscopic area 2D crystals. However, CVD grown layers also suffer from a few drawbacks as compared to high quality, but microscopic exfoliated 2D transition metal dichalcogenide (TMDC) flakes. In general, CVD grown layers are expected to contain a much higher concentration of grain boundaries that are known to substantially affect their electronic and optical properties. Grain boundaries in TMDC materials are often characterized by structural disorder and a substantial local modification of the band gap that both act as source of charge carrier scattering, degrading the electronic quality of CVD grown sheets. Nevertheless, growing large area single crystalline domains is highly challenging. Even if one can drastically reduce the nucleation site density, it requires an extremely slow growth process. Consequently, growing macroscopic areas of TMDC single layers of high structural and electronic quality is a particularly important, yet unsolved challenge.

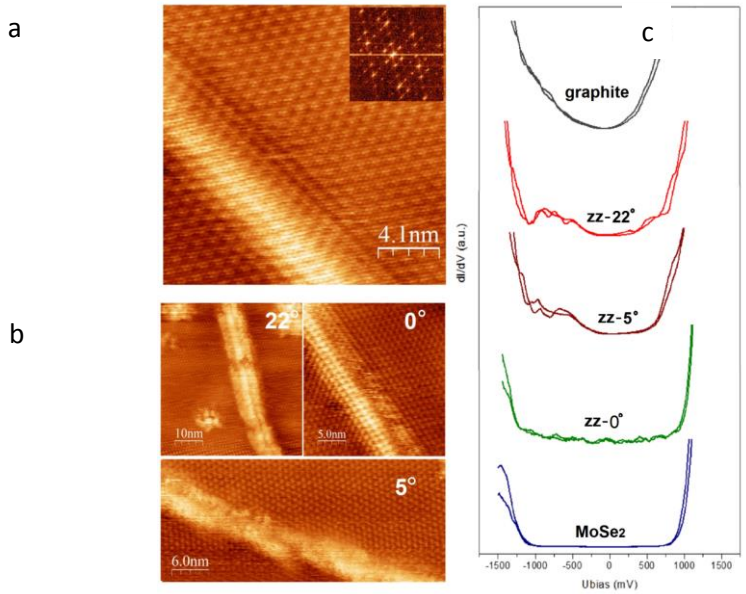

Figure 1. *a,b) Atomic resolution STM images of mirror twin grain boundaries in CVD $MoSe_2$ running along various crystallographic orientations measured relative to the zigzag direction. c) Representative tunneling spectra of various grain boundaries.*

In general, grain boundaries provide a strong intrinsic limitation to the structural and electronic quality of the CVD grown single layers. Consequently, revealing their atomic and electronic structure is of particular importance. We were able to achieve atomic resolution STM images on or around several $MoSe_2$ grain boundaries, as shown in Fig 1. All atomic resolution STM images evidence that the atomic lattices on the two sides of a $MoSe_2$ grain boundary have closely matching orientations. The prevalence of this special class of grain boundaries is due to the rotationally aligned CVD growth of $MoSe_2$ on graphite. We found that the most often observed mirror twin boundaries (MTBs) running along the zigzag directions are highly ordered, while those enclosing an angle with the zigzag direction (but still preserving the rotational alignment of the two sides) are characterized by a more disordered atomic structure. To get insight into the electronic structure of the $MoSe_2$ grain boundaries, we have also performed tunnelling spectroscopy measurements on various GBs (Fig. 1c). Tunneling spectra on disordered MTBs enclosing a nonzero angle with the zigzag crystallographic direction display a substantially reduced band gap due to emerging midgap electronic defect states. By contrast, tunnelling

spectra of zigzag grain boundaries are very similar to those recorded on the defect free $MoSe_2$ regions, evidencing that zzMTBs do not perturb strongly the electronic properties of the crystal. To understand the electronic properties of the experimentally observed zzMTBs in more details, we have performed DFT calculations on several possible zzMTB geometries.

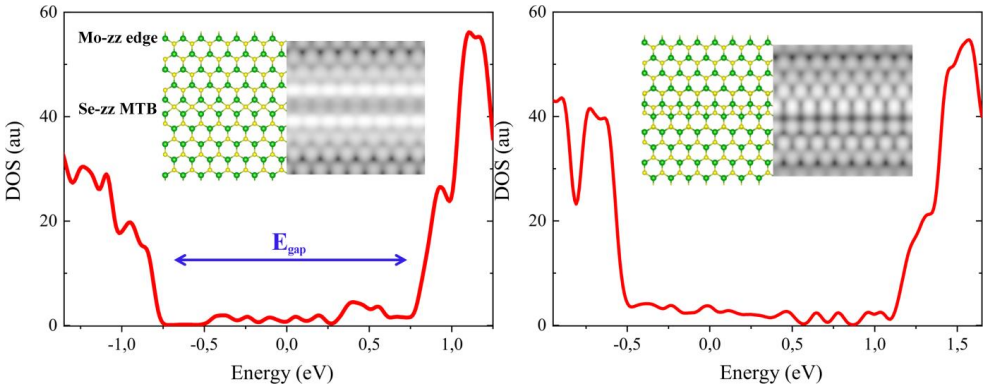

Figure 2. *Calculated atomic and electronic structure of various $MoSe_2$ MTBs with (Se) zigzag orientation. The inset shows the simulated STM images of the corresponding atomic structures.*

We have shown that in contrast to other types of grain boundaries, mirror twin boundaries running parallel to the zigzag crystallographic direction of the $MoSe_2$ lattice are characterized by a highly ordered atomic structure and leave the electronic structure almost unaffected; while grain boundaries with other orientations display a more disordered structure and substantially modify the band gap locally. Zigzag mirror twin boundaries do not degrade the electronic quality of CVD grown $MoSe_2$ single layers.

Mechanical strain puts a twist on Dirac fermions in graphene

Lendület LP2017-9, ERC StG NanoFab2D, H2020 Graphene Flagship

P. Kun, G. Kukucska (ELTE), G. Dobrik, J. Koltai, J. Kürti (ELTE), L. P. Biró, L. Tapasztó, P. Nemes-Incze

One of the hallmark properties of graphene is that backscattering of charge carriers is prohibited for smooth potentials. This is a major characteristic of the massless Dirac quasiparticles in graphene and was recognized early on, in the very first charge transport measurements of single graphite layers. Forbidden backscattering in perfect graphene is intimately linked to the pseudospin property of Dirac fermions and lies at the heart of the exceptional electrical properties of graphene.

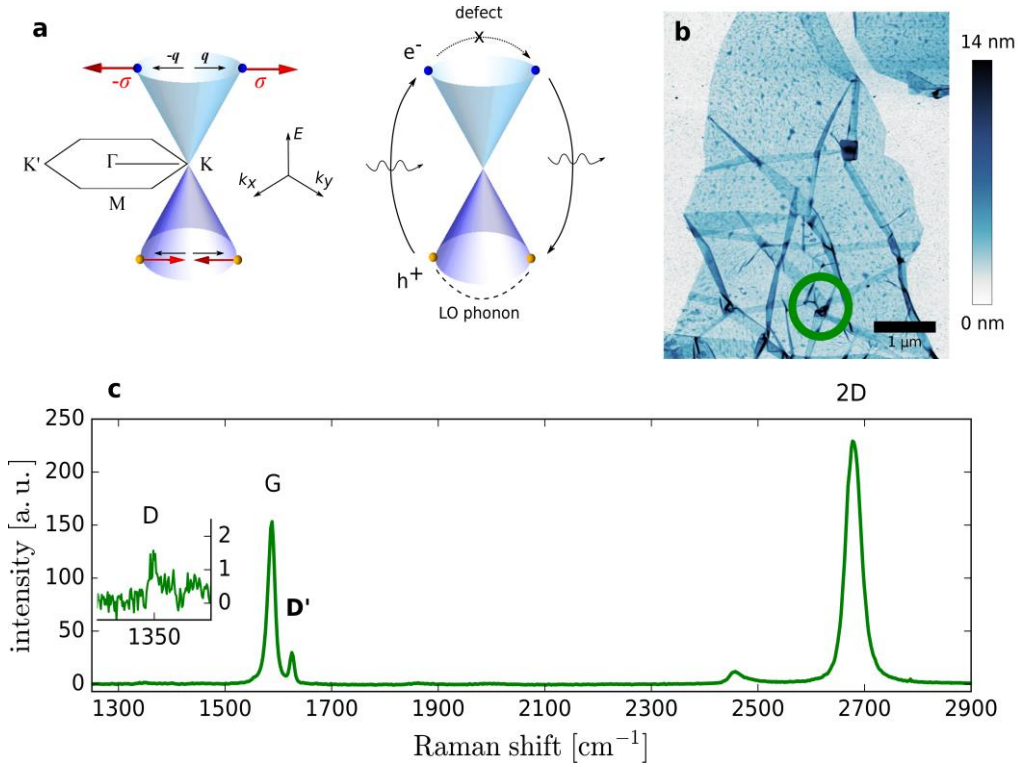

Figure 1. *Anomalous D' peak intensity in Raman spectroscopy measurements on crumpled graphene. (a) Pseudospin conservation and intra-valley scattering in graphene, emphasizing the process leading to the D' peak. (b) AFM image of a crumpled graphene sample, with the Raman measurement position shown by green circle. (c) Raman spectrum measured on the crumpled graphene, showing a D' peak with an intensity 300 times the D peak intensity.*

The "spin-like" property is a result of the crystal symmetry of graphene and determines the phase that the Dirac wave function acquires while scattering. In non-perfect graphene, if mechanical strain is present, the resulting deformation of the crystal lattice can be described as a pseudo-magnetic field. Charge carriers propagating in such strained areas acquire an additional phase, similarly to the Aharonov–Bohm effect. The "twist" in the wavefunction due to this extra phase can lift the ban on complete backscattering, as we show in an optical experiment.

For the first time, we have presented experimental evidence that pseudospin effects have a dramatic influence on the double resonant Raman spectra, more precisely on the intensity of the D' peak (see Fig. 1). Until now, this defect induced peak has only been observed for lattice defects (vacancy, grain boundary, etc.) and not for smooth potentials (pseudomagnetic field patterns). Each type of defect has a specific D' peak to D peak intensity ratio, characteristic of the defect in question. We measure this

fingerprint on crumpled single layer graphene and find an anomalously high D' peak intensity. Since the D' peak involves complete backscattering (see Fig. 1a), increased intensity is a hallmark of increased backscattering due to the pseudo-magnetic field. Numerical calculations reproduce the measured "Raman fingerprint", taking into account the pseudo-magnetic field pattern produced by the crumpling (see Fig. 2).

Our results lead to a better understanding of charge carrier scattering in strained graphene. This is especially important, since strain fluctuations are thought to be the bottleneck limiting the mobility of high-quality graphene devices.

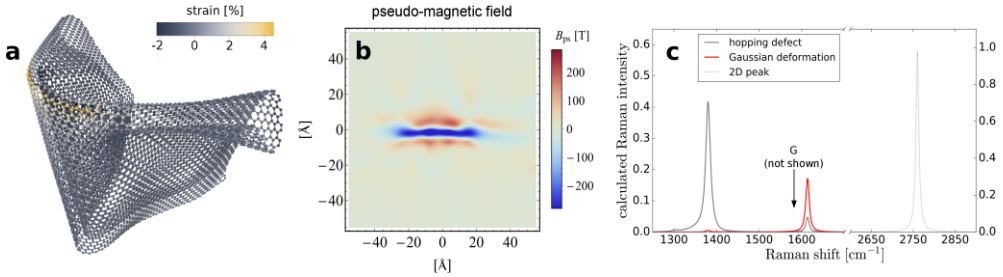

Figure 2. *Calculated Raman spectra on crumpled graphene. (a) Molecular dynamics simulation of a twice folded rectangular graphene layer. (b) Calculated pseudo-magnetic field (B_{ps}) within the rectangular graphene layer. (c) Calculated peak intensities of the doubly resonant processes (D, D', 2D). For scattering on strain patterns (red peak), the calculation reproduces the measured D' and D peak intensities.*

Kun, P., Kukucska, G., Koltai, J., Kürti, J., Biró, L. P., Tapasztó, L. & Nemes-Incze, P. Strong intravalley scattering on graphene corrugations revealed by Raman spectroscopy. *arXiv* (2018). at http://arxiv.org/abs/1801.08861

Dynamic strain in gold nanoparticle supported graphene induced by focused laser irradiation

OTKA K 119532

A. Pálinkás, P. Kun, A. A. Koós, and Z. Osváth

Graphene on noble-metal nanostructures constitutes an attractive nanocomposite with possible applications in sensors or energy conversion. In this work we study the properties of hybrid graphene/gold nanoparticle structures by Raman spectroscopy and Scanning Probe Methods. While we found that successive high intensity laser irradiation increased gradually the doping and the defect concentration in SiO_2 supported graphene, the same irradiation procedure did not induce such irreversible effects in the graphene supported by gold nanoparticles (NPs). Moreover, the laser irradiation induced dynamic hydrostatic strain in the graphene on Au NPs, which turned out to be completely reversible. A thin gold film of 5 nm was deposited onto a SiO_2(285 nm)/Si substrate by an electron-beam evaporation system (AJA). Gold nanoparticles were formed on areas of 5×5 μm^2 by local laser heating of the gold layer using a confocal Raman microscope (WITec) and a focused, 6 mW laser-power @633 nm. CVD graphene was transferred onto the substrate (gold layer and gold NPs) using thermal release tape (TRT) method. Multiple Raman-spectroscopy measurements were performed on each selected region with low (0.6 mW) and high (6 mW) laser power. The samples' morphology was investigated by Atomic Force Microscopy both before and after the laser annealing.

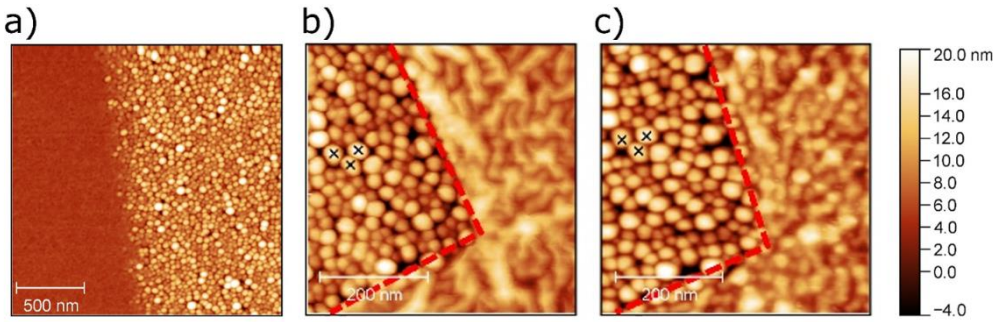

Figure 1. (a) *AFM image showing the border of as-evaporated (left) and annealed (right) gold region.* ***(b-c)*** *AFM images showing both graphene covered and bare gold NPs, b) before, and c) after subsequent laser annealing. The corner-like graphene edge is marked with red dashed line, while three individual bare gold NPs are marked with black symbols.*

The AFM image in Fig. 1a shows both the as-evaporated gold layer (left side) and an irradiated part (right side) with the borderline in the middle. Dome-like gold NPs formed on the irradiated part with diameter of 32 nm and height of 11 nm in average. Fig. 1b and 1c show AFM images of the same corner-like graphene edge, right after the transfer process and after multiple high power laser annealing, respectively. The initially formed nanoparticles remained unchanged after subsequent laser annealing (see for example the NPs marked with black crosses in Fig. 1. b-c, and the configuration of the NPs surrounding them). We can observe in Fig. 1b that the covering graphene is rippled in various longish shapes. In turn, in Fig. 1c the individual NPs are well outlined beneath the graphene, meaning that graphene follows better the shape of NPs after laser annealing. We performed successive Raman maps with 488 nm and 633 nm laser excitation on graphene/Au NPs in a 5×5 μm^2 area with 20×20 pixels. Low (0.6 mW) and high (6 mW) power measurements were performed alternately. The higher laser power was used explicitly to anneal locally the samples, while with low powers we characterized the effect of the applied heating.

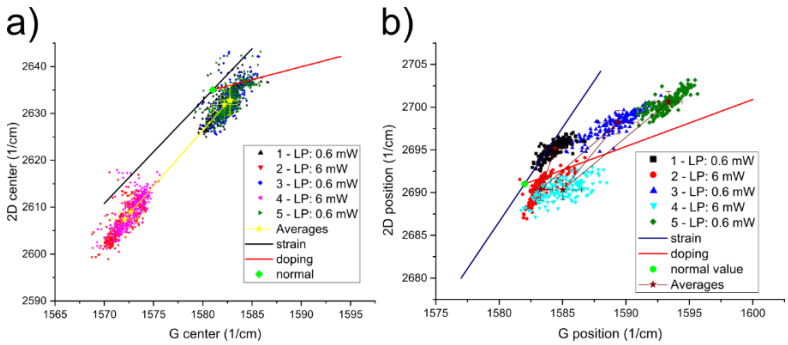

Figure 2. *Correlation plot of the 2D-G Raman peak positions of (a) Au NPs supported and (b) Si/SiO_2 supported graphene. Subsequent Raman data measured with laser power of 0.6 mW (1, 3, 5) and 6 mW (2, 4).*

In Fig. 2 we plotted the correlation plots of the 2D-G Raman peak positions of graphene. The average of the first low power measurement was at (ω_G; ω_{2D})=(1582.2; 2631.9 cm^{-1}), which corresponds to a small tensile strain ε_{hidr1} = 0.08% and p-doping of E_F = -89 meV. The following high power measurements (data sets no. 2 and 4) show a significant shift of both G and 2D peaks, which is nearly parallel with respect to the pure hydrostatic strain slope. We fitted the average values and found a slope of 2.37±0.02, which is close to 2.2 (the "strain" slope). Note that the effect is reproducible, the peak shifts are very similar in the two cases. The induced dynamic hydrostatic strain is ε_{hidr2} = 0.48%. Furthermore, the low power measurements are also very reproducible, the data sets no. 3 and 5 have averages close to the first one. On average, neither the strain nor the doping was changed significantly, as shown in Fig. 2a. For comparison, we prepared a sample where graphene was transferred directly to a standard, SiO_2(285 nm)/Si substrate. In Fig. 2b we plotted the corresponding 2D-G peak positions. After high intensity laser irradiation, significant increase in the p-type doping occurred, as is clearly seen from subsequent low intensity correlation plot data (sets no. 3 and 5, respectively). The shift of the averages follows the pure p-doping slope of 0.55 very well.

These results point out the role of the substrate in the laser irradiation induced effects on graphene, and can have implications in the development of graphene/plasmonic nanoparticle based high temperature sensors. The paper was published in NANOSCALE 10, 13417 (2018).

Optical vapor sensing on single wing scales and on whole wings of the Albulina metallica butterfly

OTKA K 111741, OTKA K 115724

K. Kertész, G. Piszter, Zs. Bálint, and L. P. Biró

Nowadays, monitoring the air quality of homes, work places, and industrial facilities is becoming more and more important. For the efficient characterization of the ambient atmosphere, gas and vapor sensors are required which combine high sensitivity and chemically selective detection of volatile organic compounds with low power consumption and fast response time and operate in ambient air. Sensors based on photonic-crystal–type nanoarchitectures may offer an optimal solution to this problem due to the fast development of the response signal (color change) and relatively easy optical readout combined with small size.

The *Albulina metallica* butterfly species is specific in that males have structural colors on both of their wing surfaces (Fig. 1). In our earlier work, we showed that the vivid wing colorations are generated by quasi-ordered, "pepper-pot"–type photonic nanoarchitectures. We showed, that despite the almost-identical scanning electron microscope images of the photonic nanoarchitectures (Fig. 1), there are minor but characteristic differences between the two sides in respect to the size and distribution of the air holes filling the chitin matrix. Direct space analysis of the electron microscope images showed that the typical first-neighbor distance of the embedded air holes is characteristically different for the blue and gold-green wing scales causing the different structural colors.

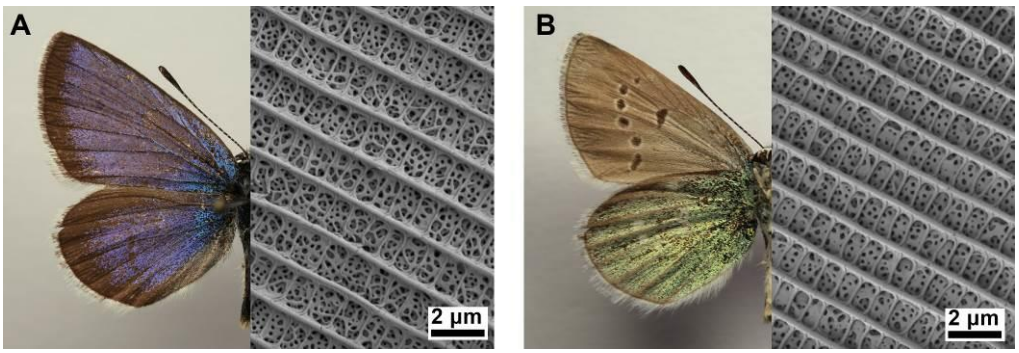

Figure 1*. Photos of an imagine and scanning electron micrographs of wing scales of Albulina metallica male specimen. The (**A**) blue and (**B**) gold-green wing surfaces are shown.*

Selective chemical sensing of two qualitatively similar, but quantitatively different, "pepper-pot"–type photonic nanoarchitectures, which occur in the dorsal (blue) and ventral (gold-green) cover scales in the wings of the male *Albulina metallica* butterflies, were investigated using ten different vapors. The capillary condensation of vapors yielded characteristic response curves in relative reflectance both for the chemical substances and for the two different structures in the concentration range of 5% to 50% vapor in artificial air. This shows that, by combining different nanoarchitectures in an array of sensors, selectivity can be enhanced by using the "fingerprinting" of various vapors and storing the characteristic responses on the different elements of the array.

As the complete wings are optically complex objects, we also investigated the behavior of single scales, both by using a microscope and collecting the signals not from the entire wing, but from one single scale only, and by removing single scales from the wing and placing them on microscope slides for individual characterization. Complete immersion of separated single scales in ethanol showed significant changes from blue to green, and from gold-green to red (Fig. 2A). We also performed vapor sensing measurements on ten blue and ten gold-green single wing scales while applying a 50% concentration of chloroform and water vapors. The average of the ten measurements on each side and for each vapor is

plotted in Fig. 2B. It was shown, that single scales exhibit similar, chemically selective sensing both in reflected light and transmitted light as was found on the whole wings.
The effect of stacked wing scales on the vapor-sensing properties was also investigated. We measured transmittance of light across one, two, and three stacked scales during 50% ethanol vapor exposition. It was found that the optical response increases with the number of stacked scales showing that by increasing the volume of interaction between the vapors and the nanoarchitectures the sensitivity can be significantly enhanced.

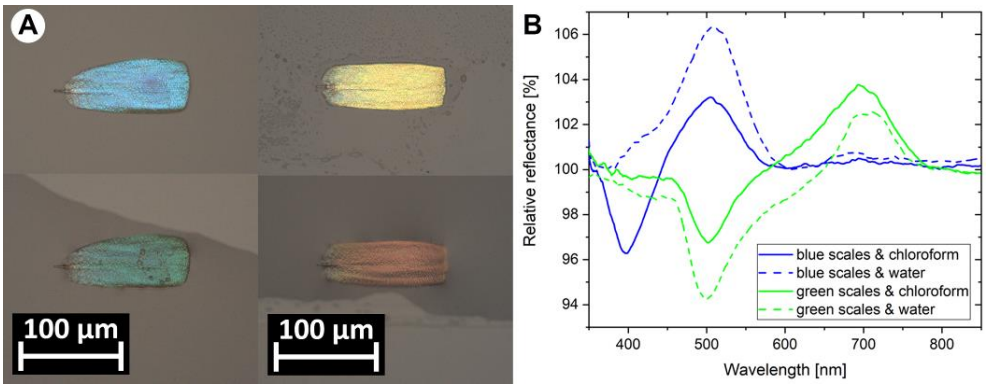

***Figure 2**. (**A**) Reflected light optical micrographs of Albulina metallica single scales in air (upper) and submerged in ethanol (lower): the color changes from blue to green and from gold-green to red, respectively. (**B**) Average of vapor sensing signals (in reflected light) on single blue and gold-green Albulina metallica wing scales using 50% chloroform and water vapors, as noted. Measurements were performed on single scales still attached to the wing membrane.*

These findings show that naturally tuned photonic nanoarchitectures can be used to construct miniature sensor arrays consisting of one or a few scale stacks with different chemical selectivity, enabling the production of small (approximately 100 µm size) and material specific vapor sensors with optical readout.

Photonics Department

Head: Dr. Peter PETRIK, D.Sc., scientific advisor

Research Staff

- Emil AGÓCS, Ph.D., on leave
- Csaba S. DARÓCZI, dr. univ.
- András DEÁK, Ph.D., Head of Chemical Nanostructures Laboratory
- Miklós FRIED, D.Sc., Head of Ellipsometry Laboratory
- Antal GASPARICS, Ph.D.
- András HÁMORI, dr. univ., retired
- Norbert NAGY, Ph.D.
- György JUHÁSZ, dr. univ., retired
- György KÁDÁR, D.Sc., Prof. emeritus
- Tivadar LOHNER, D.Sc., Prof. emeritus
- János MAKAI, C.Sc., retired
- Judit NÁDOR, Ph.D.
- Ferenc RIESZ, C.Sc.
- Miklós SERÉNYI, D.Sc.
- Gábor VÉRTESY, D.Sc.
- Dániel ZÁMBÓ, Ph.D.

Students

- Bálint FODOR, Ph.D.
- Benjamin KALAS, Ph.D.
- Szilárd POTHORSZKY, Ph.D.
- Alekszej ROMANENKO, M.Sc., PhD
- Dániel SZEKRÉNYES, Ph.D.
- Alex SZENDREI, B.Sc.

Technical Staff

- Tímea CSÁNYI

The Photonics Department develops unique methods and tools (e.g. spectroscopy, magnetic testing, biosensors, flatness, cleanliness of surfaces, contamination of water) for the **non-destructive optical and magnetic characterization** of surface nanostructures and materials. One of the most important tasks of the Department is patenting and application of the methods in international projects with partners representing the industry and the high technology.

Major result of the Photonics Department in the year of 2018:

The increased Raman scattering emerging form **plasmonic nanovoids** has been quantified by using reporter nanoparticles (gold nanoparticles loaded with a known number of Raman reporter molecule). Inhomogeneous distribution of capping molecules over the surface of a patchy gold nanorod has been created and the structure of the molecular patch directly investigated by single-particle AFM and scattering microspectroscopy techniques as well. It has been shown that for gold nanorods that experience a strong and abrupt change of the environment along their surface (e.g. well-defined nanoscale substrate inhomogeneity), the classical damped harmonic oscillator generally applied for the description of the single-particle scattering spectra of plasmonic nanoparticle, does not hold.
The applicability of the nondestructive method „**Magnetic adaptive testing**" has been studied and the following results have been achieved: 1) Magnetic parameters (among others) in general also depend on the size of the samples to be measured, and results of measurements, performed on different size samples cannot be compared with each other. It has been shown, that by proper choice of the size of magnetizing yoke, the degradation of the material can be correctly determined even in that case if different sizes of samples are measured. 2) Detectability of an artificial slot (local material thinning) has been investigated by this method, when a nonmagnetic spacer (air gap) was placed

between sample and magnetized yoke. It has been found that if the thickness of this spacer was not larger than 0.15 mm, it had no influence on the detectability of the slot. 3) A new measuring probe has been designed and built for studying the influence of neutron irradiation on nuclear reactor pressure vessel steel, and this probe was successfully tested on irradiated samples. These results show the excellent applicability of this method for inspection of material degradation and they are encouraging for possible future practical applications.

- The evaluation protocol and validation of **capillary bridge surface investigations** have been improved for the testing of surface cleanliness and chemical properties.
- A **cyclic voltammetry sensor** has been created for the measurement of As and Ni using immobilization of flagellar filaments. It has been shown that using this method, concentrations corresponding to the toxicity threshold can be detected.
- An *in situ* optical method has been developed for the characterization of surface **oxidation of Zr tubes used for fuel cladding in nuclear power plants**. The method can be used for the monitoring of surface layers during annealing.
- Flow cells utilizing surface-enhanced measurements by multi-layers or plasmon enhancement have been developed for the high-sensitivity **optical investigation of solid-liquid interfaces**.
- A model has been developed for the temperature dependence of bubble formation in **hydrogenated a-$Si_xGe_{(1-x)}$ layers**. The model makes it possible to determine a critical temperature for the degradation, which has a significant practical importance in the semiconductor and photovoltaic device technology.
- Optimal grid positions have been determined for **quantitative Makyoh-topography**. The effects of deviations from the optimal positions have been analyzed and proven experimentally.
- a-$Si_xGe_{(1-x)}$ layers with linearly changing composition over a lateral distance of 20 mm have been prepared using **combinatorial deposition and characterized using focused mapping ellipsometry**. It has been shown that besides the composition also the optical properties are changing linearly with the lateral position.

Optical Spectroscopy of Individual Nanoscale Objects

OTKA FK 128327, OTKA KH 129578, OTKA K 112114 , OTKA K 119532

D.P. Szekrényes S. Pothorszky, D. Zámbó, N. Nagy, Z. Osváth, Z. Zolnai and A. Deák

The preparation and investigation of well-defined nanostructured materials contributes to a better understanding of their structure-property relationship. This is an essential background for the development of advanced functional systems in the field of photonics and optoelectronics.

In our research, we use a broad range of experimental approaches and techniques to prepare well-defined nanostructured materials and to study their interaction with light. In the highlighted projects we employ noble metal derived nanostructures, which show a very intense absorption and scattering due to the appearance of localized surface plasmon resonances. By combining optical microscopy, imaging spectroscopy and high sensitivity detection, we are able to carry out absorption or scattering measurements even down to the single nanoparticle level. This in turn allows access to a more rigorous interpretation of the relationship between the optical properties and the structure or surface properties of the investigated nanostructures.

One possible method for the preparation of nanostructured plasmonic surfaces is nanosphere templating of thermoplastic polymer layers. The gold-coated polymer replica of a Langmuir-Blodgett film consisting of sub-micron silica spheres can be used to create localized and propagating surface plasmons at the nanostructured substrate. This structure was used to investigate the signal enhancement related to indentations in the gold surface layer during micro-Raman scattering experiments.[1] The indentations were prepared based on the above mentioned colloidal templating and the voids filled with 4-mercaptobenzoic acid (MBA) loaded gold nanospheres. The periodic void structure has been designed to allow selective excitation of a single void in a way that at the laser wavelength of the micro-Raman setup, the cavity-type plasmon modes localized at the metallic void interface can be effectively excited. The surface modification of the gold particles by MBA was studied in detail and the number of MBA molecules present on a single gold nanoparticle inferred from optical and electrophoretic-mobility measurements to be ca. 210. Correlative scanning electron microscopy and micro-Raman measurements allowed the investigations at the single void level. Raman signal from a single MBA loaded gold nanoparticle in the cavity was already detectable. The number of particles present at a single void-site provided a straightforward way to control the number of molecules excited during the experiments. By measuring the signal strength as a function of particle number, trapped inside a single nanovoid and comparing it with a reference sample (clusters of given number of particles on a flat gold surface), a 25-fold experimental signal enhancement attributed to the nanostructured nature of the interface could be inferred.

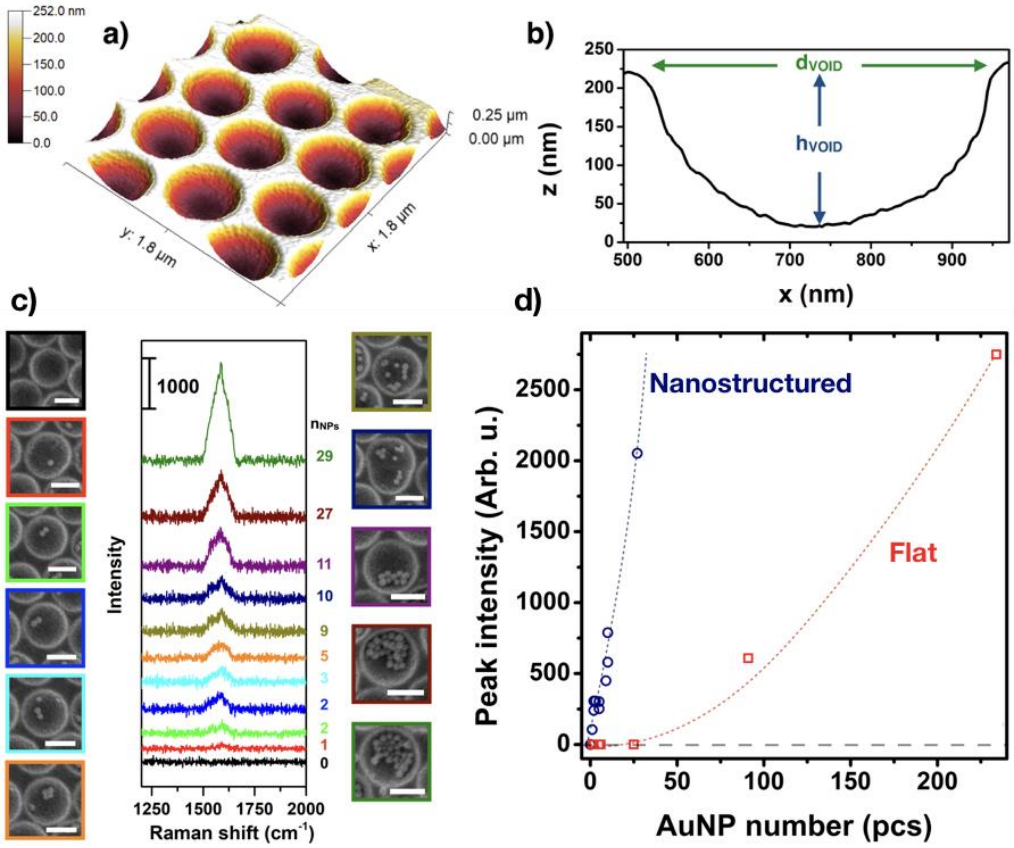

Figure 1. *AFM image of the metallic void array (a) and a typical height profile across an individual void (b). Raman spectra obtained from exciting individual voids containing different number of MBA coated gold nanoparticles (c). Intensity of the 1578 cm^{-1} peak of MBA as a function of excited particle number measured on the nanostructured and the reference flat gold surface (d).*

We are investigating the surface-chemical patch formation on individual gold nanorods.[2] When thiol-group containing molecules are added to the sol of gold nanorods, they will bind irreversibly to the particle surface and replace any physically bound stabilizing ligands (cetyltrimethylammonium ammonium bromide in the present case). It is known from the literature that at sufficiently low concentration levels, these thiol-group containing molecules preferentially bind at the tip of the nanorods. In a recent study we have shown that correlative (measuring the very same objects) scanning-probe and optical micro-spectroscopic measurements performed on individual gold particles provide direct experimental evidence on the inhomogeneous ligand distribution of tip-selectively cysteamine-modified gold nanorods. At higher (10^{-2} mM) cysteamine concentration, a well-defined patch is formed at the tips of the gold nanorods. At lower cysteamine concentration binding of the cysteamine still takes place at the rod tips, but it only provides a partial coverage, allowing other thiol molecules to bind at the rod tip. The findings allow for a more rational design of functional patchiness at the nanoparticle level.

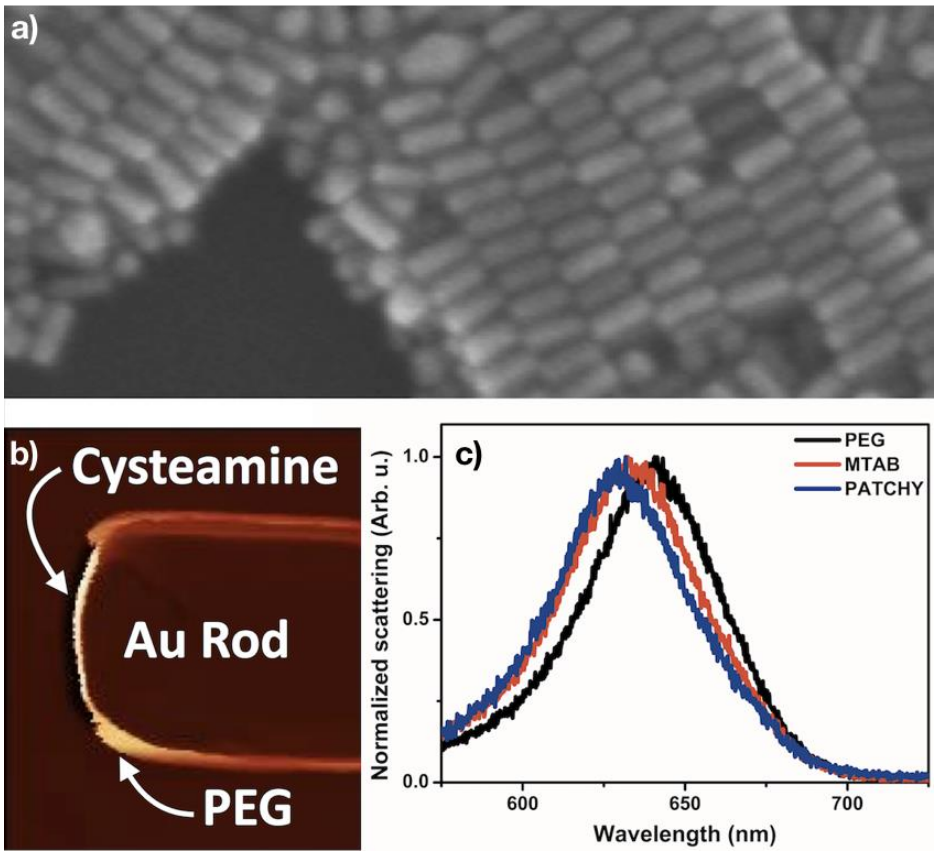

Figure 2. *SEM image of the as synthesized 115×55 nm gold nanorods (a). Single particle AFM image showing the well-defined surface chemical patch developed at the tip of the nanorod (b). Scattering spectra of individual nanorods having different surface coatings (c).*

Not only the spatially different molecular coating at the nanoparticle surface, but also local, nanometric substrate inhomogeneities might significantly influence the scattering spectra of supported plasmonic nanoparticles by means different plasmon resonance damping mechanisms.[3] To study this in detail, ITO substrates were modified by the combination of nanosphere lithography and ion-bombardment to create a nanopattern with sharp boundaries between the irradiated and masked regions. Then, single particle scattering spectra of gold nanorods distributed over the nanopattern are investigated in detail. For nanorods located purely on either the masked or implanted areas, the spectra can be adequately interpreted in terms of a classical damped harmonic oscillator model, taking the chemical interface damping into account. When the particles overlap the masked and irradiated areas, however, markedly different behavior is found depending on the actual arrangement. For the rods experiencing a symmetric inhomogeneity (that is by bridging between two masked regions), damping varies smoothly with the extent of substrate inhomogeneity. For the asymmetric case (rods overlapping the boundary between the implanted and masked zones) a sudden increase of the damping is found, which is rather independent on the specific extent of substrate inhomogeneity. Comparing the damping variations with the related intensity changes indicates that substrate inhomogeneity at such length scales results in a different behavior than predicted by the classical damped harmonic oscillator model applied for nanoparticles encapsulated or homogeneously surrounded by molecular coatings.

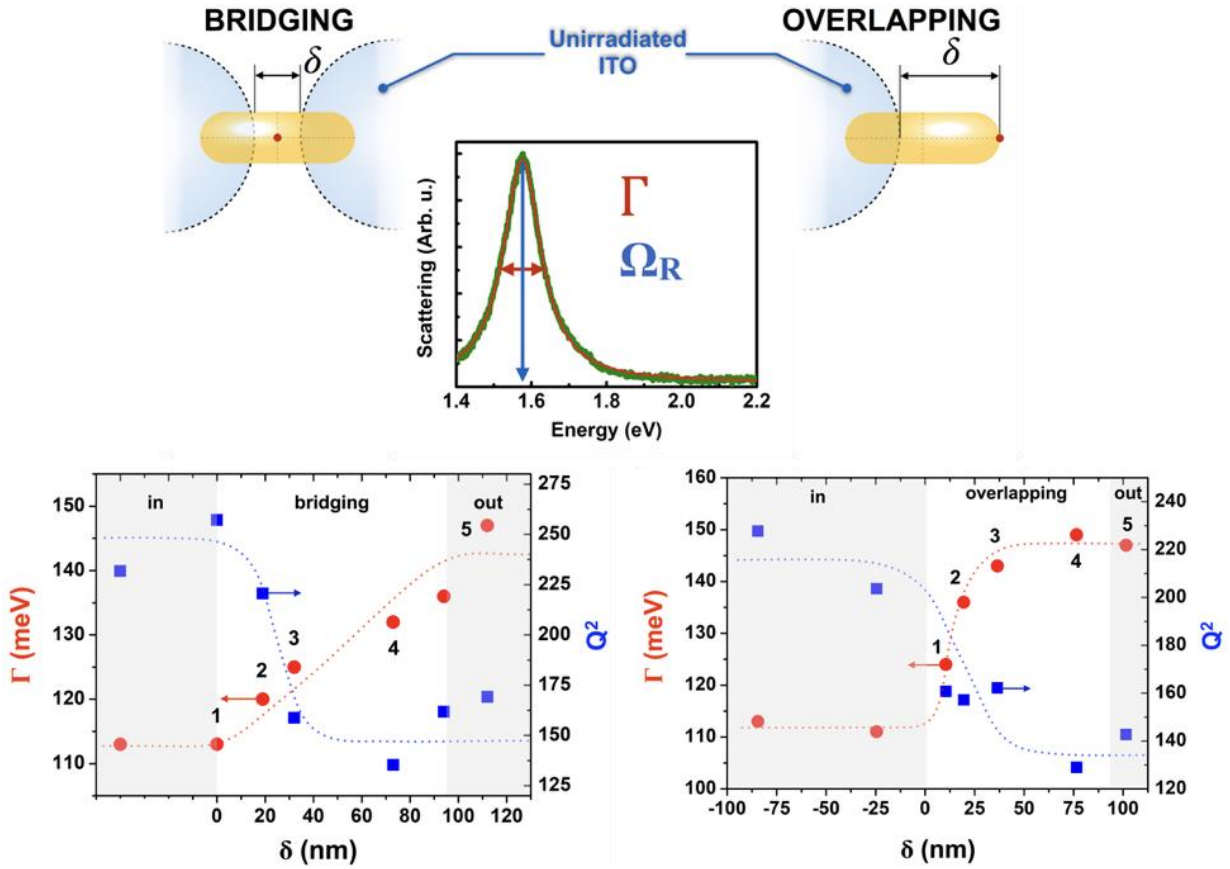

Figure 3. *Schematics depicting the two main spatial arrangements of a nanorod over a Xe^+ irradiated nanopattern derived using a nanosphere monolayer mask (top). The width of the resonance (**Γ**) and the corresponding quality factor (Q^2) plotted as a function of the relative position of the rod over the nanopattern (bottom).*

References

(1) Zámbó, D.; Szekrényes, D. P.; Pothorszky, S.; Nagy, N.; Deák, A. SERS Activity of Reporter-Particle-Loaded Single Plasmonic Nanovoids. *J. Phys. Chem. C* **2018**, *122* (41), 23683–23690. https://doi.org/10.1021/acs.jpcc.8b06716.

(2) Szekrenyes, D. P.; Pothorszky, S.; Zambo, D.; Osváth, Z.; Deák, A. Investigation of Patchiness on Tip-Selectively Surface Modified Gold Nanorods. *J. Phys. Chem. C* **2018**, *122* (3), 1706–1710. https://doi.org/10.1021/acs.jpcc.7b11211.

(3) Zolnai, Z.; Zámbó, D.; Osváth, Z.; Nagy, N.; Fried, M.; Németh, A.; Pothorszky, S.; Szekrényes, D. P.; Deák, A. Gold Nanorod Plasmon Resonance Damping Effects on a Nanopatterned Substrate. *J. Phys. Chem. C* **2018**, *122* (43), 24941–24948. https://doi.org/10.1021/acs.jpcc.8b07521.

Non-destructive Evaluation (NDE) System for the Inspection of Operation-Induced Material Degradation in Nuclear Power Plants

EU H2020 755330 - NOMAD

A. Gasparics and G. Vértesy

The long-term operation (LTO) of existing nuclear power plants (NPPs) has already been accepted in many countries as a strategic objective to ensure adequate supply of electricity over the coming decades. In order to estimate the remaining useful lifetime of NPP components, LTO requires reliable tools. The objective of EU H2020 project: "Nondestructive Evaluation System for the Inspection of Operation-Induced Material Degradation in Nuclear Power Plants" (NOMAD – https://nomad-horizon2020.eu/) is the development, demonstration and validation of a non-destructive evaluation tool for the local and volumetric characterization of the embrittlement in operational reactor pressure vessels (RPVs). In order to address these objectives, the following steps will be taken:

- Development and demonstration of an NDE tool for the characterization of RPV embrittlement, especially accounting for material heterogeneities and exceeding the existing information from surveillance programs.
- Extension of the existing database of RPV material degradation by adding correlations of mechanical, microstructural and NDE parameters as well as including quantification of reliability and uncertainty.
- Application of the developed tool to cladded material resembling the actual RPV inspection scenario.

NOMAD takes into account the priorities of reactor operation, responding to stringent safety requirements from regulators, and seeks to foster convergence of nuclear safety approaches. The approach to be developed within NOMAD will deliver information complementary to and exceeding the information obtained by destructive tests of surveillance samples, which are currently assumed to represent the whole component and do not take into account possible local material variations. NOMAD aims to fulfil requirements for nuclear safety in the framework of assessment of lifetime operation. Thereby, it covers the specific challenge and scope of the call: Continually improving safety and reliability of Generation II and III reactors.

The NOMAD consortium gathers nine important institutions in the field of European nuclear energy and development of the non-destructive techniques, all stakeholders in the assessment of the lifetime operation of NPPs. The consortium has been formed by Fraunhofer Institute for Nondestructive Testing IZFP (Germany, coordinator), SCK•CEN Belgian Nuclear Research Centre (Belgium), VTT Technical Research Centre of Finland Ltd. (Finland), SVTI Swiss Association for Technical Inspections (Switzerland), Coventry University (Great Britain), Hungarian Academy of Science - Centre for Energy Research (Hungary), Paul Scherrer Institut (Switzerland), Tecnatom S.A. (Spain), HEPENIX Technical Service Ltd. (Hungary).

Our Institute contributes to the NOMAD project with own micromagnetic testing method: so called Magnetic Adaptive Testing (MAT). MAT is a recently developed method for nondestructive characterization of ferromagnetic materials which is based on systematic measurement and evaluation of minor magnetic hysteresis loops. This method will be tested and evaluated regarding its applicability for the determination of the material changes and the variation of the material properties during exposure to neutron irradiation.

As shown in our several previous research activities, MAT provides more sensitivity for material degradation than the major hysteresis loop and has an improved feature of measurement error suppression. An additional significant advantage of this method is that there is no need for magnetic saturation of the measured samples, which eases the practical application.

A specially designed Permeameter with a magnetizing/sensing yoke is applied for measurement of families of minor loops of the magnetic circuit differential permeability. The magnetizing coil is fed with

a triangular waveform current with step-wise increasing amplitudes and with a fixed slope magnitude in all the triangles. The voltage signal in the pick-up coil is proportional to the differential permeability of the magnetic circuit. The MAT evaluation delivers large set of so-called magnetic descriptors from the measured data. The optimal descriptor as an output is selected by carful correlation analysis.
Even in the early phase of the project realization, we could obtain promising experimental results on Charpy and on block type specimens that were aged by thermal treatments or neutron irradiations. An example obtained on Charpy specimens are made of 22NiMoCr37 material can be seen below; where the optimally selected MAT descriptor is seen as the function of the neutron fluence. Here we got monotonous correlation with the degree of irradiation, the scattering was ~5%, while the difference between samples irradiated by 5.1 x 10^{19} n/cm^{2}and 1 x 10^{20} n/cm^2 achieved the 13% and 30%, respectively.

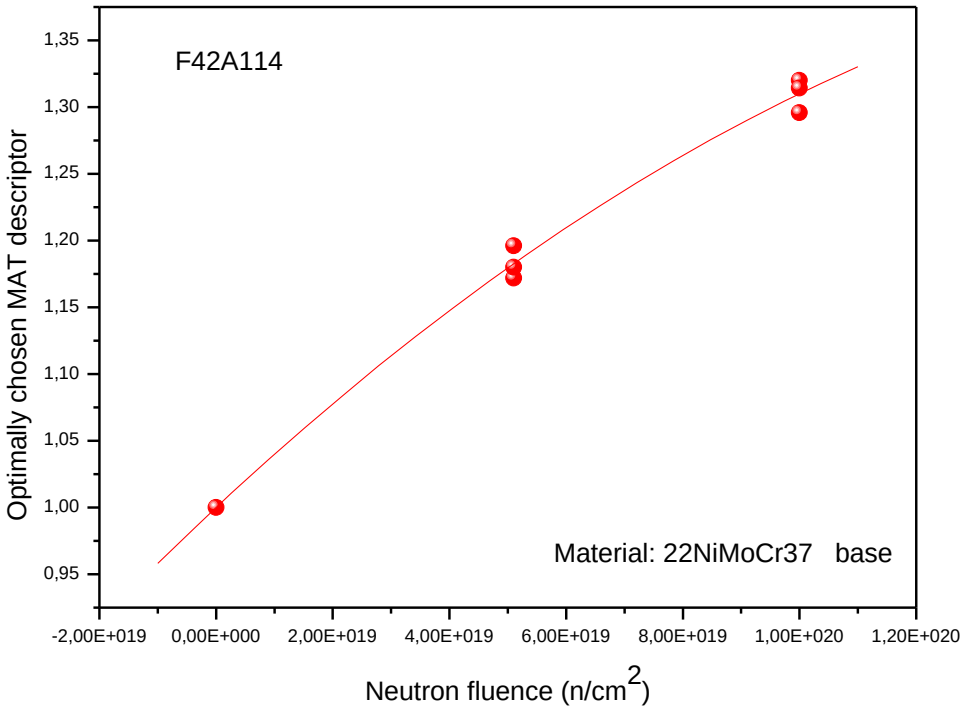

Figure 1. *Charpy specimens are made of 22NiMoCr37 material*

References:
G. Vértesy, A. Gasparics, I. Szenthe, F. Gillemot, I. Uytdenhouwen: ”Inspection of reactor steel degradation by magnetic adaptive testing” in Special Issue "Non-destructive Inspection" of Materials — Open Access Journal (https://www.mdpi.com/journal/materials/special_issues/NDI_18) 2019.
G. Vértesy, A. Gasparics, I. Szenthe, F. Gillemot: ” Magnetic nondestructive inspection of reactor steel cladded blocks” in Global Journal of Advanced Engineering Technologies and Sciences (GJAETS - https://www.gjaets.com) 2019.

Investigation of the role of a nonmagnetic spacer in local wall thinning measurement

OTKA K 111662

G. Vértesy, A. Gasparics

Local wall thinning is a very serious and frequent defect type in pipes used in industry. To avoid severe accidents, inspection of the thickness reduction of pipes is a very important task. In most cases the wall thinning inspection should be done from the *outer* side of the pipe, because - even though this phenomenon frequently occurs *inside* the tube due to the stream of coolant flowing inside the pipe - long length of the pipe usually prevents any testing from inside. A more difficult problem is to detect the local wall thinning at locations under an enforcement shield that covers the pipe outside where a branch pipe is connected to the main one. If pipes are made of ferromagnetic materials (e.g. steel), magnetic methods are suitable as nondestructive testing methods for the inspection of local wall thinning even at locations under enforcement shields. A recently developed nondestructive method, called Magnetic adaptive testing (MAT), which is based on systematic measurement of minor magnetic hysteresis loops, was successfully applied for the detection of local wall thinning in ferromagnetic plates. It was shown that even a relatively small, local modification of the sample thickness could be detected with adequate signal/noise ratio from the other side of the specimen. The measurements gave good results also, if the investigated plate was covered by other plate(s).

In spite of a great number of publications in this area, the influence of an air gap/nonmagnetic spacer between the magnetizing yoke and the sample surface is discussed in a very limited way. In practical cases some air gaps always necessarily exist, even between polished surfaces, the question is only the thickness of the air gap. The surfaces of tubes, and other objects to be inspected are frequently painted, which by itself produces a nonmagnetic spacer, not to speak about the frequent case, where the surfaces are rough, dirty or corroded. The problem becomes even more pronounced if the wall thinning to be detected is under an enforcement shield, because in this case also some air gap – due to the surface roughness of the plates – always exist between the two ferromagnetic plates.
The purpose of the present work is to investigate the influence of the air gap(s) – which is nothing else but a nonmagnetic spacer between the plate surfaces – in local wall thinning experiments performed by MAT. We investigated how the artificially applied nonmagnetic spacer between a magnetizing yoke and a sample surface, and also between the two plates, influences the measured signal, and the detectability of the artificially made slot in the bottom plate. We studied what was the thickest nonmagnetic spacer, which still made possible (in the case of the given configuration) the detection of local wall thinning.
Detectability of a 10 mm wide and 3 mm deep artificial slot, placed at the bottom of a 6 mm thick steel plate was investigated by Magnetic adaptive testing when the measurement was performed through another 6 mm thick steel plate. The result of measurement is given in Fig. x for that case where the artificial slot is detected through another steel plate, and a nonmagnetic spacer is placed between the magnetizing yoke and surface of the upper plate. MAT degradation functions are normalized by the degradation function measured far from the slot. Similar results were obtained if the spacer was placed between the two steel plates, and also if spacers were placed both between upper surface and magnetizing yoke and between the two plates. The sum of air gap thicknesses is important.

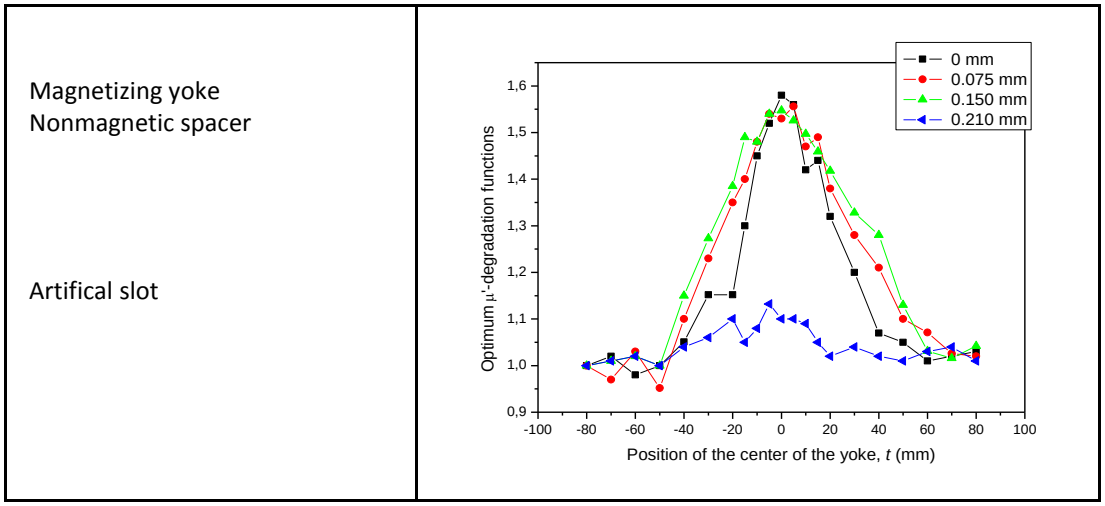

Figure 1. *Left: Sketch of the measurement. The double arrow indicates the direction of the movement of the magnetizing yoke. Right: Optimally chosen MAT-degradation functions vs. the position of the centre of the magnetizing yoke for three non-magnetic spacers with different thicknesses (0.075, 0.150 and 0.210 mm) placed between the yoke and the plate surface, and for the reference case (without spacer).*

It is evident from the measurements that the slot was clearly detectable in the given arrangements, in accordance with our previous experience. Existence of the 10 mm wide and 3 mm deep slot generated more than 50% change in the optimally chosen MAT μ'-degradation functions. It was found that if the thickness of the air gap (or sum of the thicknesses of air gaps) was not larger than 0.15 mm, it had no influence on detectability of the slot. This result shows the excellent applicability of MAT in this case, and it is encouraging for possible future practical applications.

The empirical results were modelled by electromagnetic simulation and it was shown that air gap caused a dramatic decrease of the relative change of the magnetic flux, when the presence of a bottom slot was detected. The magnetic flux change due to the presence of a slot is less than 1 percent if a 0.10 mm wide air gap is considered in the given geometry. However, in spite of this very limited change, detection of the slot is possible with a good signal/noise ratio.

The possible explanation of this unexpectedly good sensitivity is that during the MAT evaluation the *derivative of permeability* is used. Due to any air gap, the flux density in the open magnetic circuit decreases dramatically – as proved by the simulation – but the primarily measured signal is proportional to the differential permeability, μ, of the circuit. This differentiation improves the signal to noise ratio significantly.

Next factor, which supports the good results is, that the degradation functions are always normalized by a reference value. It means that even a small difference becomes large by this normalization.

Contact angle measurements with *r-ϑ* type capillary bridges

OTKA FK 128901

N. Nagy

Measurement of low contact angles is challenging. The investigated surface is immersed in the test liquid in case of the captive bubble method, therefore the characterization of swelling or porous layers is problematic. In case of the Wilhelmy balance method, the samples must have regular geometry and identical surfaces along the contact line, therefore coatings and thin films cannot be characterized. The developed indirect method combines the accuracy of the Wilhelmy method and the general usability of the sessile drop method.

The method is based on the use of a liquid bridge as a probe: the capillary bridge of the test liquid is stretched between the rim of the base of a cylinder and the investigated surface under equilibrium conditions. The advancing contact angle on the sample can be measured during the stepwise decrease of the bridge length. The receding contact angle is determined during the retraction of the cylinder. The contact angle is calculated from Delaunay's analytical solution, while the necessary parameters are determined from the measured capillary force and from the automated analysis of the captured image of the liquid bridge. The contact angle on the cylinder's rim changes continuously during the decrease and increase of the bridge length. The bridge is formed from a pendant drop. This unique feature ensures that the advancing contact line finds dry (not prewetted) surface.

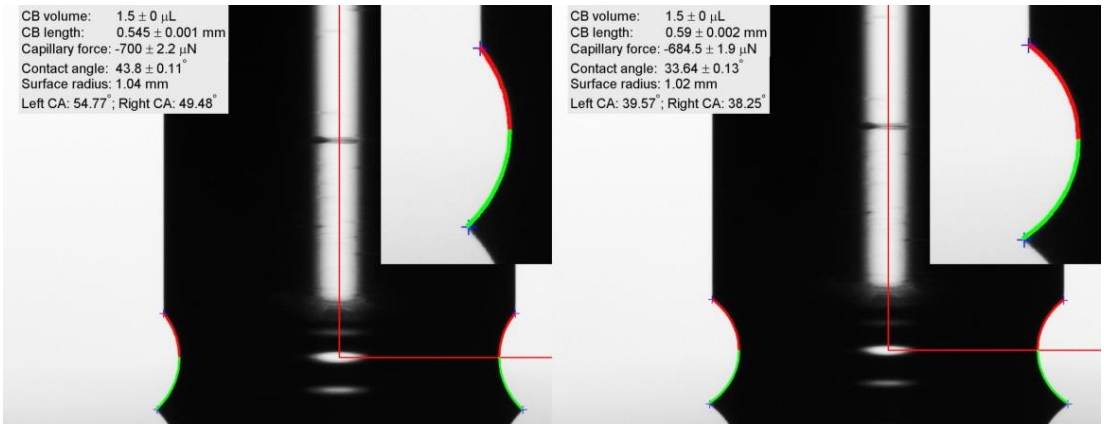

Figure 1. *Typical results of the evaluation (left: approaching, right: reversal phase). The measurement was carried out on a thermal SiO_2 surface. The insets show the left magnified contours. Blue crosses: margins of the liquid bridge identified by the program; red lines: coordinate system; red and green curves: analytical solution for the top and bottom half of the capillary bridge, respectively. The main determined parameters are listed in the upper left corner.*

Precalculated look-up tables were built up for *nodoid* type axisymmetric liquid bridges in the relevant parameter space. Parameter sensitivity investigations can be carried out based on these tables avoiding the difficulty of solution of the inverse problems. Another advantage of these tables can be found during the evaluation: the significant difference between measured and precalculated values indicates that the bridge is not axisymmetric or it is not in equilibrium. This verification ensures that the determined contact angle is reliable without the use of a second camera.

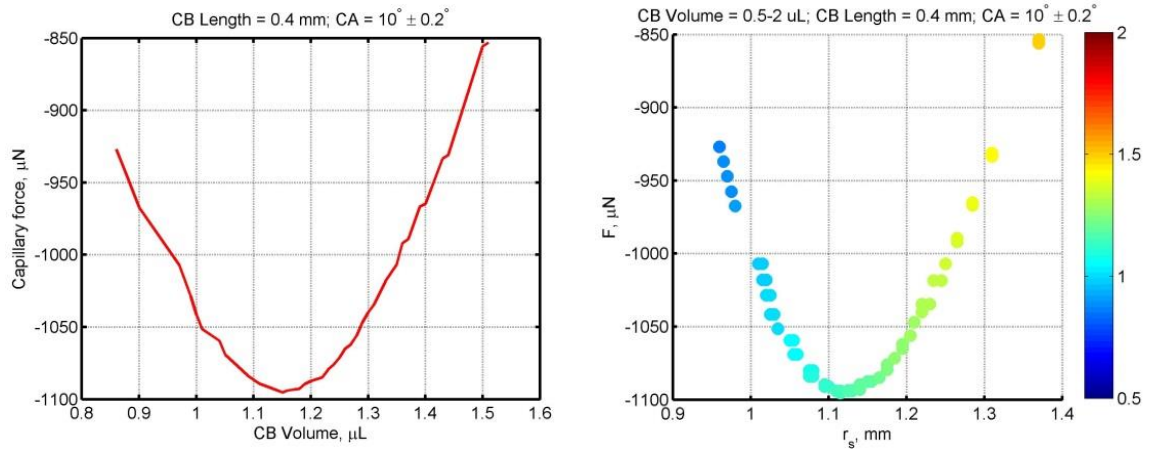

Figure 2. *Sensitivity of the capillary force (F) and the contact radius (r_s) on the volume change of the capillary bridge. The color bar shows the bridge volume. The capillary force of an evaporating liquid bridge can increase or decrease depending on the actual bridge geometry. The direction of change is determined by the change of the curvature of the nodoid surface.*

The method was proved to be valid and highly sensitive, while its repeatability is so good as the repeatability of the sessile drop method with two times longer contact lines. The capability of the measurement of ultra-low contact angles was demonstrated on acid-treated superhydrophilic glass surfaces. The capillary force, as well as, the contact angle does not exhibit hysteresis on these surfaces. For more details, please refer:

N. Nagy: Contact angle determination on hydrophilic and superhydrophilic surfaces by using *r-ϑ* type capillary bridges, *Langmuir*, under review.

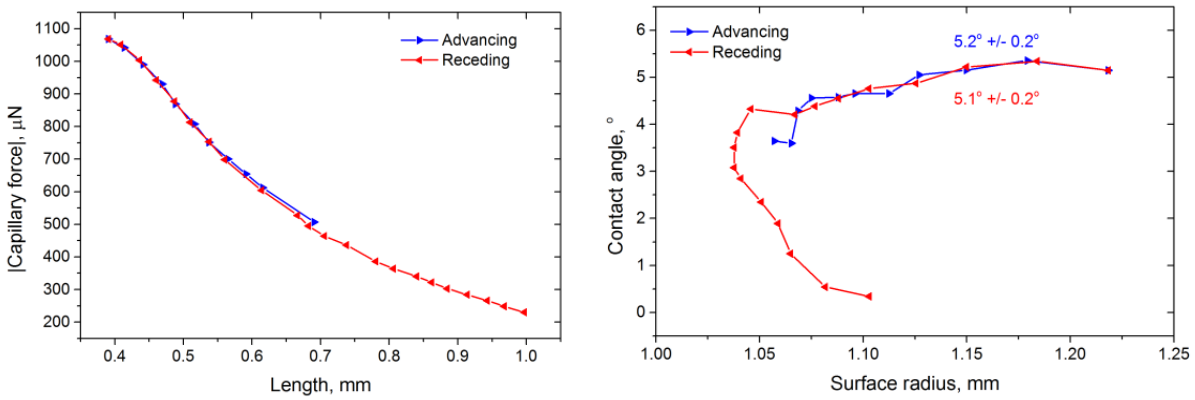

Figure 3. *Capillary force and contact angle measured on an acid-treated glass slide. The capillary force does not exhibit hysteresis. The advancing and receding contact angles are equal wihtin their standard deviation.*

In situ monitoring of ZrO_2 surfaces during oxidation

NVKP_16-1-2016-0014, OTKA K 115852

P. Petrik, A. Romanenko, B. Kalas, L. Peter, T. Novotny, E. Perez-Fero, E. Agocs, T. Lohner, Z. Hozer

One of the major applications of Zr is its use as cladding tubes in nuclear power plants. The corrosion and oxidation of different Zr alloys is an intensively investigated major safety issue. We used ellipsometry to characterize surfaces of zirconium tubes and plates for nuclear applications. We have shown earlier that ellipsometry can be used even on the surface of tubes with a diameter of 9.1 mm, when applying proper focusing. We also determined reference refractive indices for both zirconium and zirconium oxide, and demonstrated the capability of ellipsometry for the determination of the thickness and refractive index of the surface oxide applying different oxidation parameters. In this study, we characterized processed zirconium surfaces using the technique developed in our previous work. We used both ultra violet-visible-near infrared and mid-infrared ellipsometry to study the thicknesses of the surface layers as well as the dielectric functions of both the layers and the substrate. We also developed a heat cell that allows multiple angle of incidence ellipsometry measurement at elevated temperatures. We used this setup to monitor the temporal behavior of hydrogenated and oxidized zirconium surfaces. (P. Petrik, A. Romanenko, B. Kalas, L. Péter, T. Novotny, E. Perez-Feró, B. Fodor, E. Agocs, T. Lohner, S. Kurunczi, M. Stoica, M. Gartner, Z. Hózer, "Optical Properties of Oxidized, Hydrogenated, and Native Zirconium Surfaces for Wavelengths from 0.3 to 25 μm - A Study by Ex Situ and In Situ Spectroscopic Ellipsometry, Phys. Status Solidi. (2019) 1800676. doi:10.1002/pssa.201800676).

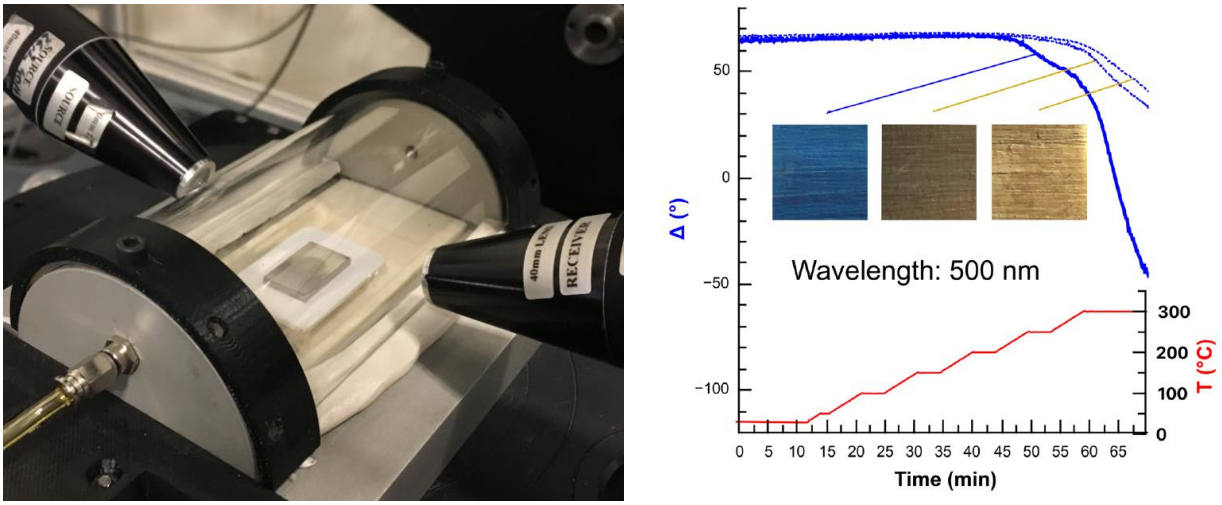

Figure 1. *Left-hand side: Hydrogen-filled E125 zirconium wafer mounted on the heating stage in the cell for environmental ellipsometry. The ring-shaped spot in the middle of the wafer is the part that has been processed using electrochemical hydrogenation. Right-hand side: In situ ellipsometry measurements on three identical zirconium substrates of an E125 alloy processed under different conditions. The red curve shows the temperature profile. Blue curves are the* Δ *(phase shift – the ellipsometric angle that is more sensitive to the change of thickness of the surface layer) values measured by ellipsometry at the wavelength of 500 nm (dotted lines show measurement under Ar flow). The solid line is a measurement in air at a temperature of 28 ◦C and humidity of 41%. In the inset, showing the samples after the heat treatment, the different colors reveal different thicknesses of surface layers caused by oxidation.*

Multilayers for tunable resonance in ellipsometric biosensors

OTKA K 115852 and M-ERA.NET WaterSafe

B. Kalas, A. Romanenko, K. Ferencz, P. Petrik

For biosensing applications Bloch surface waves (BSW) can be utilized that are excited at the surface of one-dimensional photonic crystals (1DPC). In the ultraviolet (UV) wavelength range numerous proteins have characteristic absorption peak so measuring in this range selective measurements can be carried out. The main advantage of BSW-based sensors compared to the structures used in surface plasmon resonance (SPR) is the tunability of the resonance wavelength at which the biosensor operates. The resonance wavelength can be easily tailored by changing the layer thicknesses or by modulating the optical properties of the applied materials. Other advantage of BSW is that by using 1DPC structures narrower dip and bigger propagation length (and thus enhanced biosensor performance) can be achieved in the wavelength spectra due to the small absorption (no metal layers are applied in the structures).
In this work we realised a structure by alternating SiO_2 and ZrO_2 nanolayers and thus we constructed a 1DPC suitable for biosensing application in the UV range. The optical measurements were carried out in a self-made Kretschmann-Raether flow cell combined with a spectroscopic ellipsometer (Woollam M-2000DI).

B. Kalas, E. Agocs, A. Romanenko, P. Petrik, In Situ Characterization of Biomaterials at Solid-Liquid Interfaces Using Ellipsometry in the UV-Visible-NIR Wavelength Range, Phys. Status Solidi. (2019) 1800762. doi:10.1002/pssa.201800762.

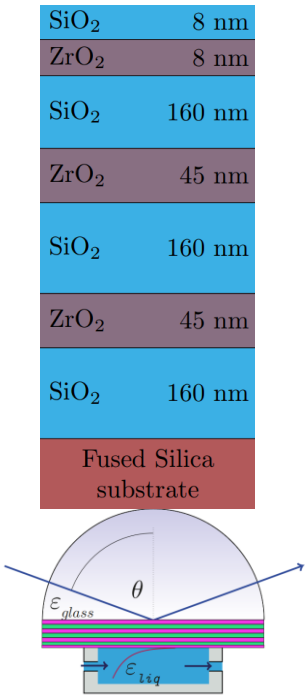

Figure 1. *The schematic figures of the 1DPC structures and the used flow cell.*

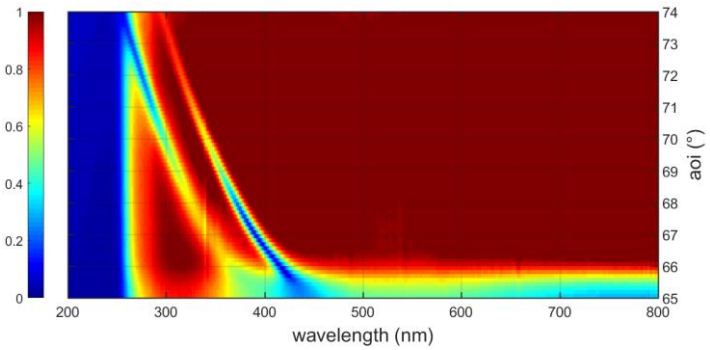

Figure 2. *The measured reflection map (normalized intensity of p-polarized reflection) of the 1DPC structure in the flow cell. The vertical axis shows the angle of incidence in degrees.*

Sustainable autonomous system for nitrites/nitrates and heavy metals monitoring of natural water sources

M-ERA.NET-2014 „WaterSafe", OTKA NN 117847

M. Fried A. Saftics, S. Kurunczi, P. Petrik, Z. Labadi

The international (with Romanian and University of Pannonia partners) project („WaterSafe") aimed to develop a new autonomous system based on micro electrochemical sensors and ultra-thin solar cells for concentration measurement of different ionic species in natural water sources.
It focused on three directions: 1) new materials with high efficiency in solar energy harvesting and fabrication of small ultra-thin solar cells together with the power stabilizing device, able to supply the needed voltage to the sensors and electronics module; 2) new microsensors and materials for detection of nitrites/ nitrates and heavy metals in water; 3) low cost autonomous energy system integration and fabrication.

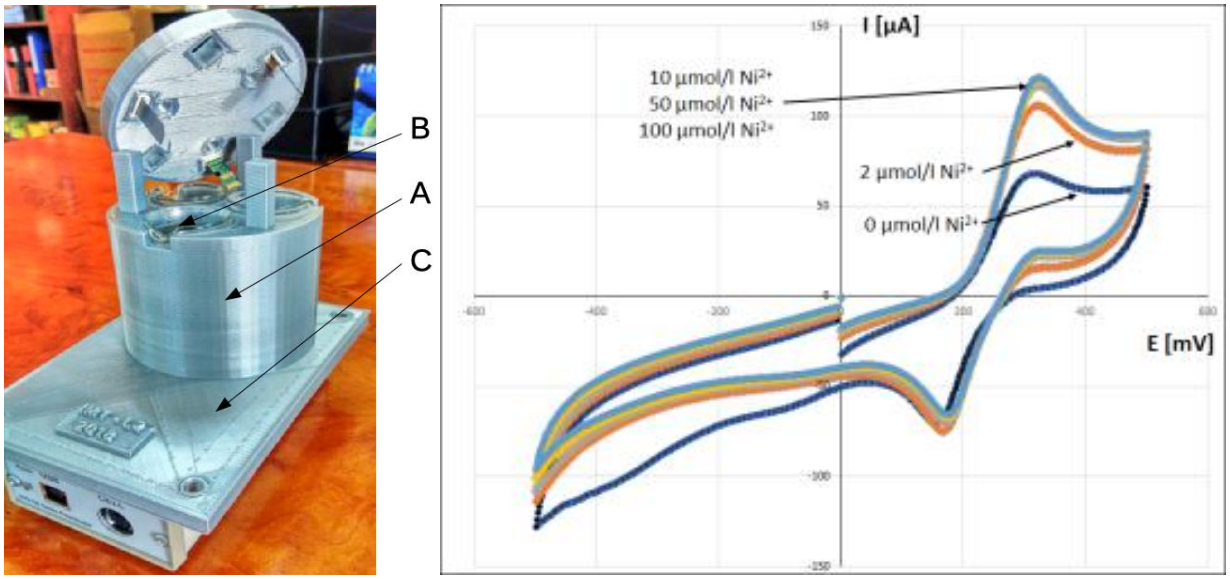

Figure 1. *(Left-hand side) Measurement set-up: A -cylindrical camera B - 3 electrochemical cells C - data acquisition and display. (Right-hand side) CV curves of Ni sensing filament layers with different Ni concentrations.*

We (MFA) investigated the developed (by University of Pannonia) metal-ion-bonding (Ni, As) special proteins (flagellar filaments) by optical (Spectroscopic Ellipsometry) and electrochemical (Cyclic Voltametry) methods. We performed promising electrochemical measurements with these new types of sensor-chips. The latest results were checked by comparative control measurements performed by partners from NANOM (Brasov, Romania), proving that the sensor-chip (protein) stability is good enough and even the sensor chips can be re-used after 1 month and chemical cleaning. This later investigation series prove that the prepared chips can be used after several months and more than once.
More information about the results of the project can be read on the webpage of the project: **http://www.icf.ro/pr_2016/WaterSafe/Obtained_results.html**

Diffusion and reaction kinetics governing surface blistering in RF sputtered a-Si_xGe_{1-x}:H thin films

M. Serényi, A. Hámori and B. Kalas

The structural and surface quality of the material is one of the most critical issues regarding of their large scale application in electronic devices based on hydrogenated amorphous silicon (a-Si:H) [1], germanium (a-Ge:H) [2] and a-SiGe:H. Atomic hydrogen migration occurs in the amorphous network. The high temperatures applied during growth of those materials, e. g. during chemical vapor deposition, or device operations enhance the diffusion of H atoms, in particular of those liberated from their bonds to the host atoms. Such enhanced diffusion favors the migration of H atoms towards nanovoids where they very likely form molecular H_2 since the reaction $2MeH \rightarrow H_2 + Me\text{-}Me$ is an exothermic one (Me indicates the host atom: Si or Ge). The accumulation on the wall of voids causes the evolution of hydrogen bubbles and then the formation of blisters. Some efforts have been made to understand the microscopic mechanisms determining the rupture of the MeH bonds and formation of H_2 rich voids at the origin of the blisters in order to prevent them. The objective of this work was to find a way to determine the threshold temperature below which surface blistering does not occur in hydrogenated a-Si_xGe_{1-x}, $0 \leq x \leq 1$. This is achieved by a theoretical model that takes into account both the kinetics of the rupture of the MeH bonds and, in particular, the diffusion of the atomic H. The experimental results suggesting our theoretical approach have been obtained by Secondary Neutral Mass Spectrometry and by surface light reflectivity measurements, as regards of the time of the onset of blistering and its activation energy by Arrhenius plots. The data supplied by the latter plots allow the validation of the theoretical model. The calculated critical temperature for blistering is of the same order of magnitude as the experimentally observed one. The experimentally determined Vegard's law-like dependence of the blistering activation energy [3,4] on the Si concentration in the a-Si_xGe_{1-x} alloys is interpreted by a simple formula and related 3D-like diagram.

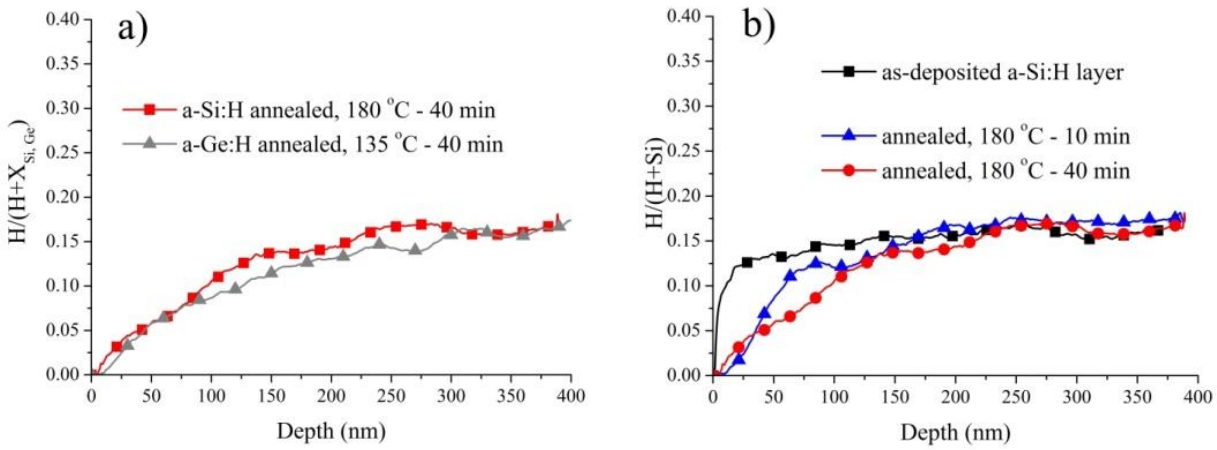

Figure 1. *SNMS depth profile of hydrogen in annealed a-Si and a-Ge layer after 40 minutes of annealing (a), and after 10 and 40 minutes in a-Si layer (b)*

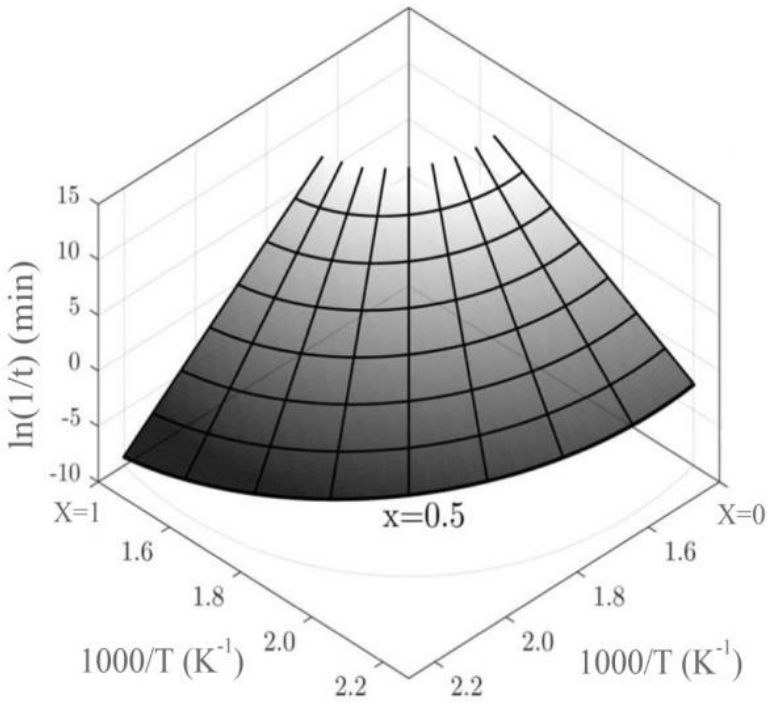

Figure 2. *Graphical representation of blistering onset vs. temperature in a polar coordinate system. The left-hand vertical plane belongs to the Si and the right one to the Ge Arrhenius plot.*

References:

[1] C. Frigeri, M. Serényi, Zs. Szekrényes, K. Kamarás, A. Csik, N. Q. Khánh, Effect of heat treatments on the properties of hydrogenated amorphous silicon for PV and PVT applications, Sol. Energy 119 (2015) 225-232. https://doi.org/10.1016/j.solener.2015.07.004

[2] M. Serényi, C. Frigeri, A. Csik, N. Q. Khánh, A. Németh, Z. Zolnai, On the mechanisms of hydrogen induced blistering in RF sputtered amorphous Ge, CrystEngComm 19 (2017) 1486-1494. https://doi.org/10.1039/C7CE00076F

[3] M. Serényi, C. Frigeri, R. Schiller, Vegard's-law-like dependence of the activation energy of blistering on the x composition in hydrogenated a-Si_xGe_{1-x} , J. Alloys Compd. 763 (2018) 471-477. https://doi.org/10.1016/j.jallcom.2018.05.269

[4] M. Serényi, A. Csík, A. Hámori, B. Kalas, I. Lukács, Zs. Zolnai and C. Frigeri, Diffusion and reaction kinetics governing surface blistering in radio frequency sputtered hydrogenated a-Si_xGe_{1-x} ($0 \leq x \leq 1$) thin films, Thin Solid Films in press.

Makyoh topography

Ferenc Riesz

Makyoh topography is an optical tool for the qualitative flatness testing of specular surfaces, based on the defocused detection of a collimated light beam reflected from the tested surface. By inserting a square grid into the path of the illuminating beam, the height map can be calculated by integrating the gradients obtained from the distortion of the grid's reflected image (quantitative extension).
In the past year, activities were concentrated both on methodology and applications.
Applying the grid creates not only the structured illumination necessary to calculate the large-scale surface shape, but aids in qualitative visual evaluation as well. If the grid's image is sharp, the simultaneous qualitative observation of the sample morphology in high resolution is possible within the same image, in addition to the low-resolution height map. We have studied the conditions for this sharpness [rie18]. A sharpness criterion was given based on a wave optics model, while the necessary instrumental settings were calculated using geometrical optics. In addition, it was shown that only lens-based set-ups allow positioning of the grid to be sharp on the Makyoh image; for mirror-based set-ups this is not possible because of geometrical instrumental constraints (Fig. 1).

[rie18] F. Riesz, Structured-illumination Makyoh-topography: optimum grid position and its constraints, Surf. Topogr. Metrol. Prop. 6 (2018) 45009. doi:10.1088/2051-672x/aaeb86 .

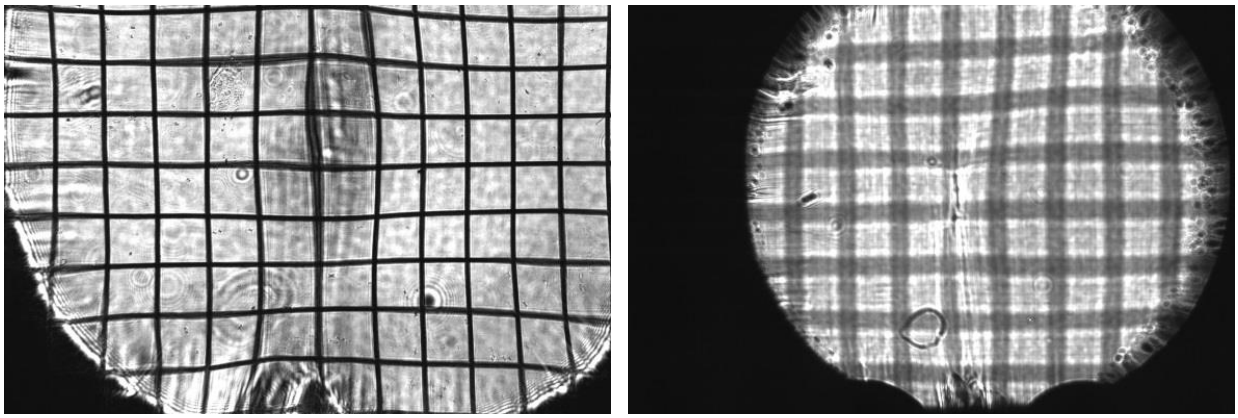

Figure 1. *Makyoh-topography image of a silicon wafer using structured illumination. Left panel: lens-based set-up, showing a sharp grid image; right panel: mirror-based set-up, showing diffraction effects masking the Makyoh image.*

For in-house research, deformation measurements of Si-based thin-film (SiO_x, SiN_x) structures were performed for stress evaluation.

Refractive Index Variation of Magnetron-Sputtered a-$Si_{1-x}Ge_x$ by "One-Sample Concept" Combinatory

OTKA K 115852 and M-ERA.NET WaterSafe

T. Lohner, B. Kalas, P. Petrik, Z. Zolnai, M. Serényi and G. Sáfrán

Gradient a-$Si_{1-x}Ge_x$ layers have been deposited by "one-sample concept" combinatorial DC magnetron sputtering onto one-inch-long silicon slabs (Fig. 1.). Characterizations by electron microscopy, ion beam analysis and ellipsometry show that the layers are amorphous with a uniform thickness, small roughness and compositions from x = 0 to x = 1 changing linearly with the lateral position.
By focused-beam mapping ellipsometry we show that the optical constants also vary linearly with the lateral position, implying that the optical constants are linear functions of the composition (Fig. 2.). Both the refractive index and the extinction coefficient can be varied in a broad range for a large spectral region. The precise control and the knowledge of layer properties as a function of composition is of primary importance in many applications from solar cells to sensors.

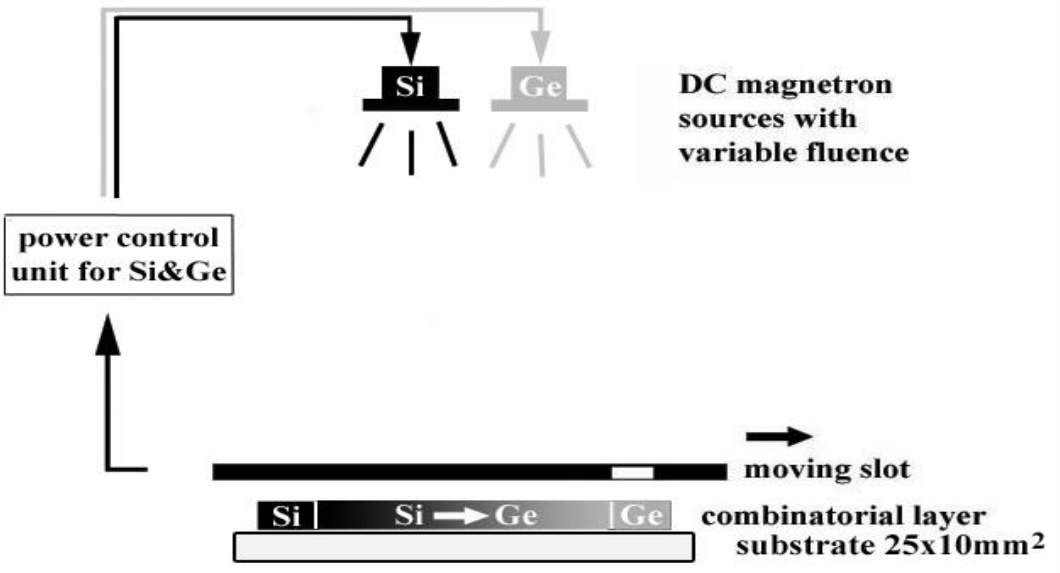

Figure 1. *Set-up used for the combinatorial deposition of the a-$Si_{1-x}Ge_x$ layer.*

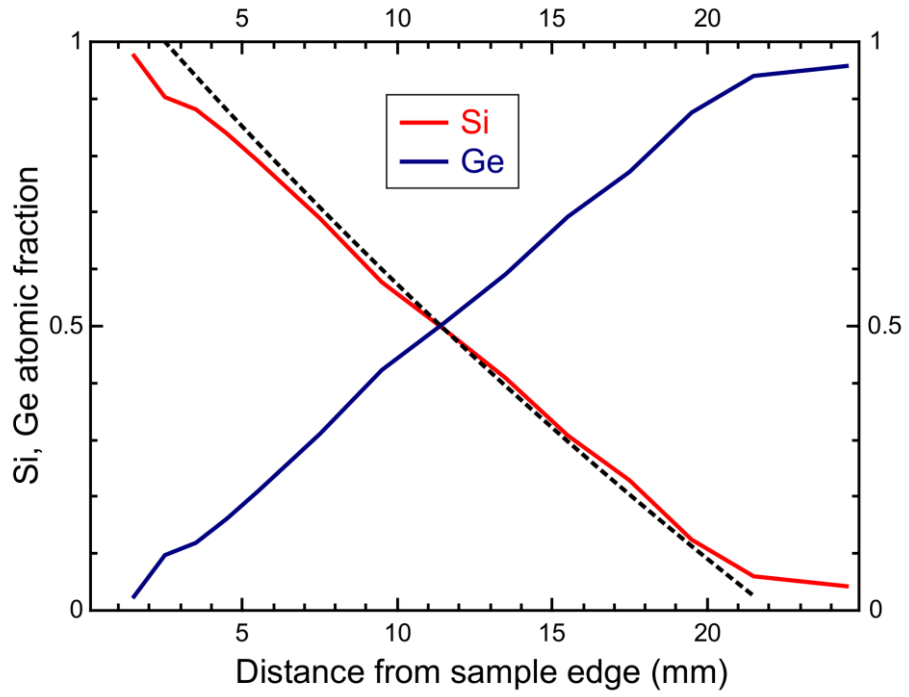

Figure 2. *Atomic fraction as a function of position along the center line of the combinatorial sample measured by Rutherford backscattering spectrometry. The black dotted line shows the distribution of the atomic fractions of Si and Ge based on the calibration using energy dispersive spectrometry (EDS) in a scanning electron microscopy.*

Microtechnology Department

Head: Dr. Gábor BATTISTIG, DSc., senior research fellow

Research Staff

- Zsófia BAJI Ph.D. (on maternity leave)
- István BÁRSONY, Member of HAS
- Gábor BATTISTIG DSc.
- Orsolya BÁLINT-HAKKEL Ph.D.
- Ferenc BÍRÓ, Ph.D.
- Csaba DÜCSŐ Ph.D.
- Péter FÖLDESY Ph.D.
- Péter FÜRJES Ph.D.
- Zoltán HAJNAL Ph.D.
- Nguyen Quoc KHÁNH, Ph.D.
- István LUKÁCS Ph.D.
- György MOLNÁR DSc.
- Andrea Edit PAP Ph.D. (part time)
- Vilmos RAKOVICS Ph.D.
- István RÉTI Ph.D.
- Zoltán Szabó PhD.
- János VOLK Ph.D.
- Zsolt ZOLNAI Ph.D.

Technical Staff

- János FERENCZ (engineer)
- Levente ILLÉS (engineer)
- Csaba LÁZÁR (engineer)
- Petra HERMANN (engineer)
- Róbert HODOVÁN (engineer)
- Erika TUNYOGI (engineer)
- György ALTMANN (technician)
- Gabriella BÍRÓ (technician)
- Tibor CSARNAI (technician)
- Magda ERŐS (retired, part time)
- Attila NAGY (technician)
- Károlyné PAJER (technician)
- Csilla ARIAS-SOTONÉ FARAGÓ (technician)
- Attila NAGY (technician)
- Magda VARGA (technician)
- Zsuzsanna Brigitta SIK (technician)

Postgraduate students

- Anita BÁNYAI
- Eszter HOLCZER
- Eszter TÓTH
- János RADÓ
- László PÓSA
- Saeedeh SOLEIMANI

The tasks of the Microtechnology Department are

***Fundamental research on*:**

- novel sensing principles;
- novel functional materials and nanostructures;
- novel 3D micromachining techniques.

Research and development of physical, chemical/biochemical sensors, and integrated micro- and nanosystems:

- **MEMS** – R&D on gas sensors, vectorial force and other mechanical sensors, thermal sensors, infrared LED devices, CMOS compatible and related micromachining techniques.
- **BioMEMS** – Development and integration of specific microfluidic, nanofluidic, bio-electrode systems, their application in biochemistry, physiology and medical diagnostics.
- **NEMS** – Synthesis and characterization of quasi-one-dimensional semiconducting nanostructures, semiconductor nanodevices, as well as their integration in functional sensors, optoelectronic and photovoltaic devices.

Modelling, structural and device characterization methods (available as support for research partners as well):

- Electrical characterization;
- Thermo-mechanical characterization;
- Optical characterisation;
- Scanning Microprobes;
- SEM, TEM, EDX;
- Ion beam analysis methods;
- Spectroscopic Ellipsometry;
- Fourier-Transform Infrared Spectroscopy.

The Department runs a unique semiconductor manufacturing facility in Hungary comprising two clean labs (300 m^2 + 160 m^2 - Class 100-10000) *a complete Si-CMOS processing line and a mask shop*. The technology allows to manufacture layers, patterned structures and devices on 3" and 4" Si and glass wafers with line resolution of 1 μm and down to ≈10 nm by optical and by e-beam lithography, respectively.

Competences (available as service for academic, industrial partners and customers):

- High temperature annealing, diffusion and oxidation; Rapid Thermal Treatment;
- Low Pressure Chemical Vapour Deposition of poly-Si, SiO_2 and Si_3N_4 layers;
- Low Temperature Chemical Vapour Deposition;
- Plasma Enhanced Atomic Layer Deposition;
- Physical Thin Film Depositions – Electron beam evaporation, DC and RF Sputtering;
- Ion implantation;
- Reactive Ion Etching, Deep Reactive Ion Etching;
- Photolithography with back-side alignment and Nanoimprinting;
- E-beam lithography;
- Nanopatterning, deposition and etching by Focused Ion-Beam;
- Wafer-bonding;
- Wet chemical treatments;
- Electro-chemical porous Si formation;
- Liquid Phase Epitaxy of III-V compound semiconductors;
- Mask design, laser pattern generator;

- Polymer (PDMS, SU8, Polyimide) structuring by photolithography & micro-molding techniques;
- Chip dicing, packaging especially for sensor applications;
- Materials and structural analysis & characterization: SEM, FIB, EDX, FTIR, Atomic Force Microscopy, Electrochemical Impedance Spectroscopy, Stylus Profiler;
- Electrical and functional modelling and characterization;
- Multi-domain Finite Element Modelling of physical processes.

For detailed information please visit our web-sites:
www.mems.hu, www.biomems.hu, www.nems.hu
or contact us by e-mail: **dragon@mfa.kfki.hu**

Nanosensorics Research Group

Group leader: János Volk
Group members: G. Battistig, Zs. Baji, I.E. Lukács, Gy. Molnár, N.Q. Khánh, A.E. Papp, L. Pósa, J. Radó, S. Soleimani, M. Szappanos, E. Tunyogi, Zs. Zolnai

Ongoing projects:

- Kombinált mikro-nanotechnológiai eljárások és ellenőrzésük lokális analitikai technikákkal: a mintázatképzéstől az alkalmazások felé OTKA K112114
- ZnO és Ga2O3 nanostruktúrák készítése atomi réteglevalasztással OTKA 116579
- Korszerű funkcionális anyagok hálózatba szervezhető autonóm érzékelőkhöz (KoFaH) NVKP_16-1-2016-0018
- Mikrotechnológiai infrastruktúra korszerűsítése az európai kompatibilitás eléréséhez VEKOP-2.3.3-15-2016-00010
- Ultrarövid fény- és elektronimpulzusokkal indukált atomi és molekuláris folyamatok vizsgálata az ELI-ALPS-nál, módszer- és eszközfejlesztés 2018-1.2.1-NKP-2018-00010
- Nemzeti Kvantumtechnológiai Program - HUNQTECH Kvantumbitek előállítása, megosztása és kvantuminformációs hálózatok fejlesztése / Creating, and sharing quantumbits and developing quantum information networks 2017-1.2.1-NKP-2017-00001

KoFAH - Advanced Functional Materials for Autonomous Sensor Networks (www.kofah.hu)[1]

In 2018, we continued the work on i) piezoelectric thin films, ii) piezo-MEMS sensors and vibrational energy harvesters as well as on iii) the integration of sensor node demonstrators, such as vibration analyser, tyre sensor, and intelligent bondage.
The project parallelly comprises all three levels: material (i), device (ii) and system (iii).

Material: piezoelectric thin films

In order to conduct research on advanced CMOS compatible piezoelectric thin films a new sputtering system was purchased and installed. Apart from general use of the tool the project-specific goal is to deposit piezoelectric AlN, and alloyed XAlN (X=Sc, Cr, etc.) layers. High quality piezoelectric layers are essential components of the micro-vibration energy harvesters and actuators targeted by the project.
The setup containing three-magnetrons with the appropriate SW enable both automatic and manual operation. Two of the magnetrons can be operated in DC or pulse DC mode, whereas the third one is working in RF mode. The system can handle various size substrates ranging from small pieces up to 6” wafers. The ultimate vacuum of the load-lock equipped deposition chamber is $< 1x10^{-7}$mbar. Deposition or reactive deposition of single layers and multilayer structures as well as co-deposition is also possible.

[1] Korszerű funkcionális anyagok hálózatba szervezhető autonóm érzékelőkhöz (KoFaH) NVKP_16-1-2016-0018

Figure 1 *The VAKSIS sputtering system in operation in the clean-room of the Lab (building 29.b)*

The related tender was successfully completed in 2017 and the contract with VAKSIS Co, Turkey signed in September 2017. In order to provide the required footprint and services our staff removed an outdated system and reorganized the lab. The company delivered and installed the system in due time (May 2018), so the introduced technology became an organic part of the processing line (Fig. 1.). Though special emphasis was put on the formation of piezoelectric layers, other projects will also benefit from the facility.

The optimization of AlN deposition conditions through more than 50 tests led to a reasonable trade-off between deposition rate (400-500 nm/h) and thickness uniformity (±2-3%), whereas the optimum sample temperature was found to be around 300 °C. According to cross-sectional SEM analysis and X-ray diffraction the optimized AlN layers show columnar crystal structure with high degree of c-axis orientation. The obtained longitudinal piezoelectric charge constant was around 3 pC/N for 0.7-1.4 um thick AlN , which agrees well with literature data. These preliminary tests provide a solid starting point for the upcoming research on high-piezoelectric-constant XAlN alloys.

Device:

a) Piezo-MEMS sensors

In 2018 we continued the work on spiral shaped piezo-MEMS accelerometers and started research also on metal substrate based vibrational energy harvesters. In the former part we demonstrated a low-volume, stress-free, piezoelectric micro-electromechanical system (MEMS) cantilever array for fully implantable hearing aids [1]. The 9-element spiral-matrix is sensitive to middle part of audible frequency range (1200-2300Hz) through the proper resonant frequency of the individual spirals tuned by dimensions of the cantilevers based on the results of Comsol simulations.

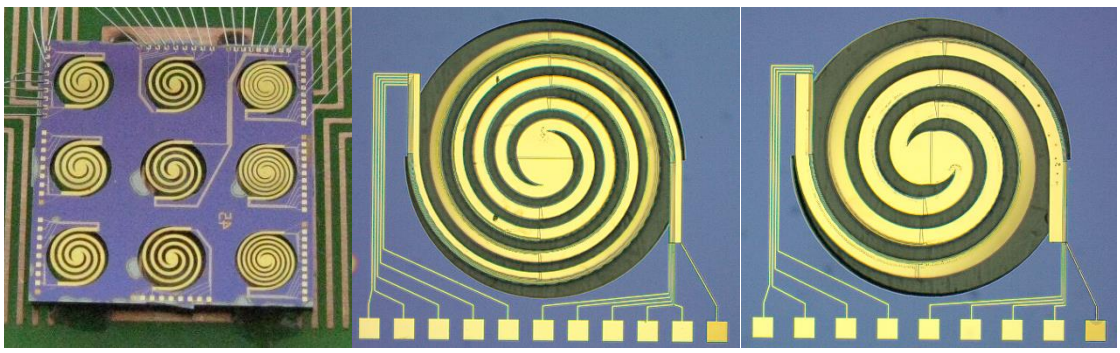

(a) (b) (c)

Figure 2 *9-element wire bonded Fermat-spiral array (a) and two typical cantilevers (four- and three-turn types, b and c, respectively).*

Moreover, each spiral was designed with a multielectrode structure fitted to various mode shapes (Fig 3) to collect more than one ambient frequencies with a single cantilever.

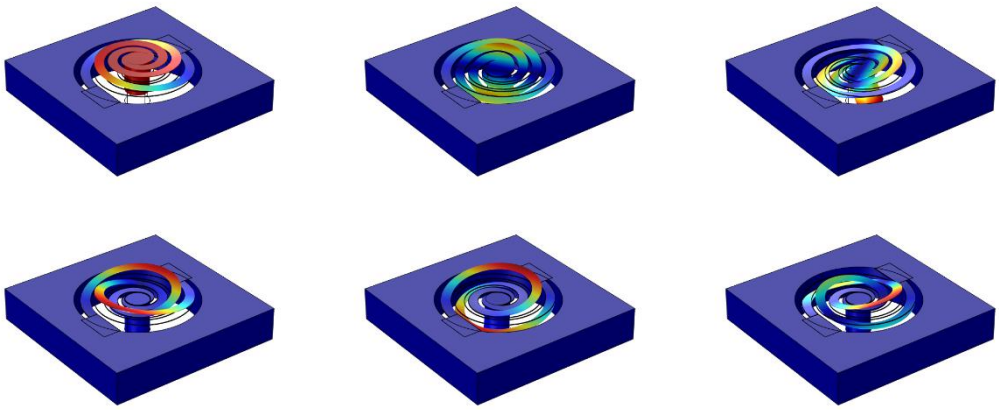

Figure 3 *Simulation of various mode designs for multi-frequency accelerometers to optimize the electrode positions.*

The test device was fabricated by a 30-step micromachining process. Fermat spiral geometry ensures the reduced device footprint, which was formed by deep-reactive ion etching (DRIE). The uniformity of cantilever thickness is controlled by the Si-on-Insulator (SOI) wafer. The biocompatible piezoelectric material aluminum nitride (AlN) was deposited by reactive radio frequency (RF) sputtering from an AlN target.
The fundamental resonances and upper harmonics were collected for each cantilever by the laser Doppler vibrometer at the Technical University of Vienna. During the measurement the cantilevers were mounted on a minishaker which was excited by white-noise signal. The results show a good agreement between the theoretical and measured frequencies. In 2019, we will measure the generated electrical signal vs. the excitation frequency and acceleration, and test the mode selectivity of the optimized electrodes.

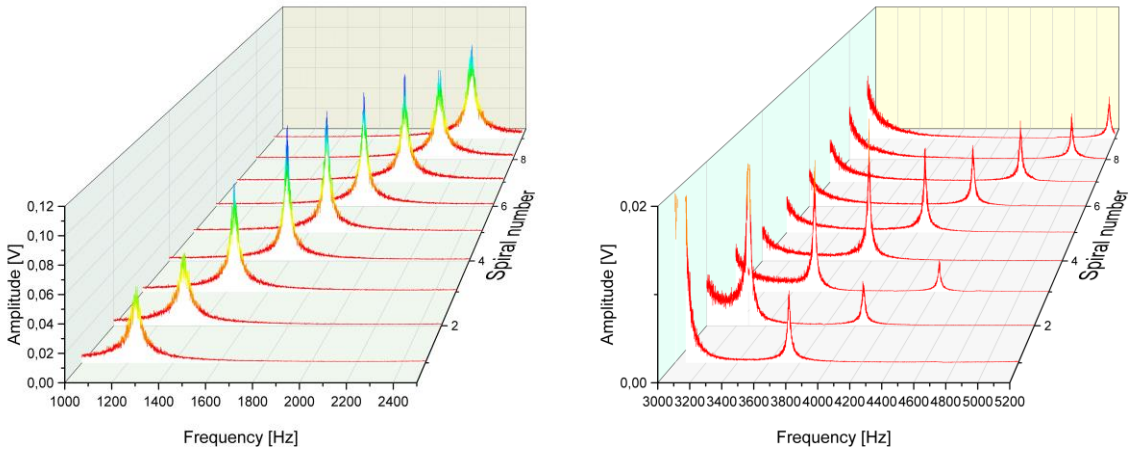

(a) *(b)*

Figure 4 *Laser Doppler vibrometer input voltage during white-noise excitation.*
The resonant frequencies fall in the range of 1200-2300 Hz (a) and harmonics in 3000-5200 Hz (b) depending on the geometry.

b) Piezo-on-metal harvester

As a second objective of the Device work-package, we started to optimize piezo-cantilevers for energy harvesting as well. In order to supply sufficient electrical power for autonomous sensor nodes using RF communication we need energy harvesters larger than the standard MEMS structures. For the 1-10

cm^2 area-range standard Si based technology is often found to be too expensive. Moreover, in harsh vibrational environment and for demanding applications, such as medical implants, the mechanical robustness of single crystalline Si is insufficient.

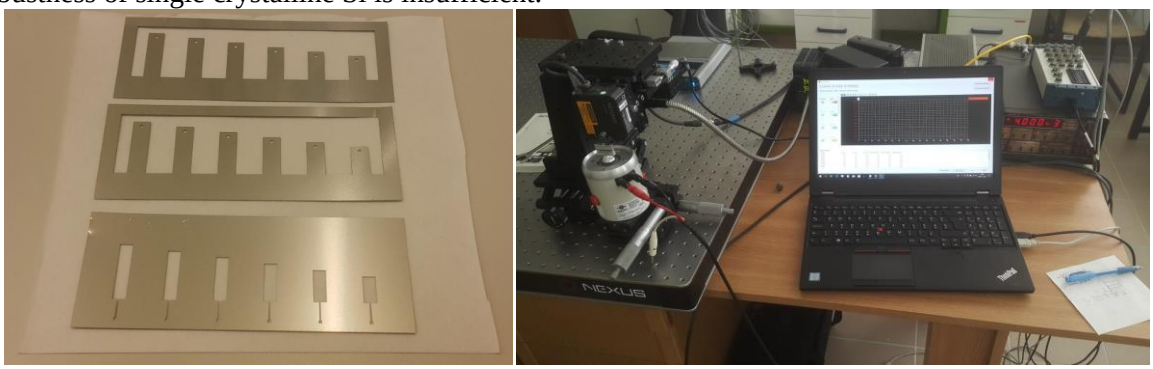

(a) *(b)*

Figure 5 *Ni and stainless-steel cantilever arrays after laser cutting (left upper and center image) and the geometrically fitting stencil mask for top contact deposition (bottom left image) (a). Measurement setup for testing the output voltage and power of the piezo/metal harvester at controlled frequency and acceleration (b).*

Hence, our aim was to combine MEMS technology with metal substrates. Stainless steel has a 50 times higher fracture toughness than single crystal Si. Moreover, the cantilever geometry was shaped at room temperature by high precision stencil laser cutting tool by our industrial partner (Alpha Assemby), which provides an economic technology compared to Si 3D micromachining. As harvester substrates we compared Ni (100 um) and stainless-steel (SUS 304, 80 and 120 um) sheets. Figure 5a shows the Ni and stainless-steel cantilever arrays. The length of the cantilevers was varied between 12-22 mm, expecting resonance frequencies in the 150-650 Hz range.
The simplified fabrication technology was implemented in the cleanroom. Pulsed DC sputtered AlN piezo layer of 1.2 um was deposited first in our new vacuum system (Vaksis) followed by the electron beam deposition of the top electrode through a stencil mask (Fig. 5a). Individual cantilever beams were simply cut by scissors and wire bonded before mounting them on the shaker based measurement setup (Fig. 5b). The obtained open circuit voltage was 430 mV at an acceleration of 9.81 m/s^2 (1G) for the 18 mm cantilever at resonance (201 Hz). At an optimal load resistance of 220 kΩ and output power of 540 μW was obtained [2], whichrequires significant improvement in 2019. Nevertheless, we could demonstrate a simple, room temperature hybrid fabrication process for metal-MEMS harvesters.

System:

a) Tyre deformation monitor

3D MEMS force sensors mounted at the internal sidewalls of vehicle tyres continuously provide information about the actual mechanical deformation of the tyre in operation (Fig. 6). The monitoring of the elastic deformation and its sudden changes offers feedback about the load and friction via characterizing the shape of the tyre sidewalls.

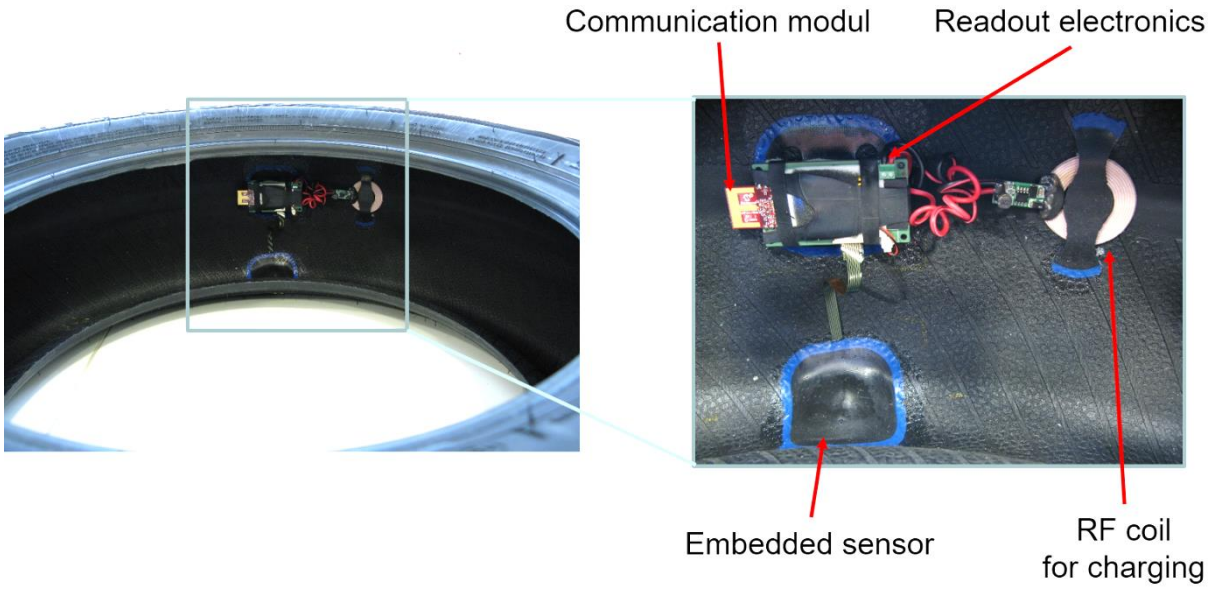

Figure 6 *The integrated tyre monitoring test tool*

The tyre deformation on a vehicle is proportional to the acting forces on the wheel – longitudinal, lateral, and vertical - carrying information on the contact between the tyre and road surface (figure 7). The accomplished application uses RF communication between the rotating wheels and vehicle control. The signal per rotation depends on the number of sensors mounted in the wheel. The sampling frequency of 100 Hz fits well with the sampling frequency of the CAN bus communication of a car. We also integrated an RF coil for external charging of the battery of the readout electronics.

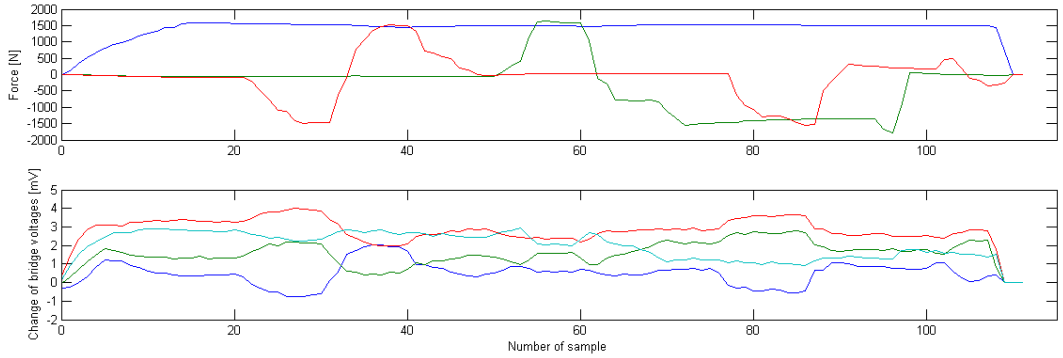

F_x F_y F_z

Figure 7 *The correlation between the out-of-balance voltages of the 3D force sensor and the acting forces on the tyre.*

A tyre equipped with an integrated sensor is being used on an autonomous Nissan Leaf for the preliminary test in co-operation with MTA SZTAKI (Fig. 8). Among the other positive results, we demonstrated the long operating lifetime of the system by operating the sensor for >100 km running mileage.

(a) *(b)*

Figure 8 *The test tyre mounted on the Nissan Leaf with the readout electronics placed in the trunk during the charging process.*

b) Vibration analyser

Our vibration analyser – or VibrAn for short – is a complex, wireless, ambient energy powered and easy-to-use solution for vibration analysis. It was designed to incorporate the latest commercial technologies and achievements in the field of energy harvesting and wireless sensor networks with an emphasis on energy efficient spectrum estimation algorithms for embedded systems. This solution is implemented on a small printed circuit board and contains all the necessary commercial circuit components for hybrid energy harvesting; acceleration sensing; data acquisition, data storage and analysis; as well as wireless communication (Fig. 9) [3].

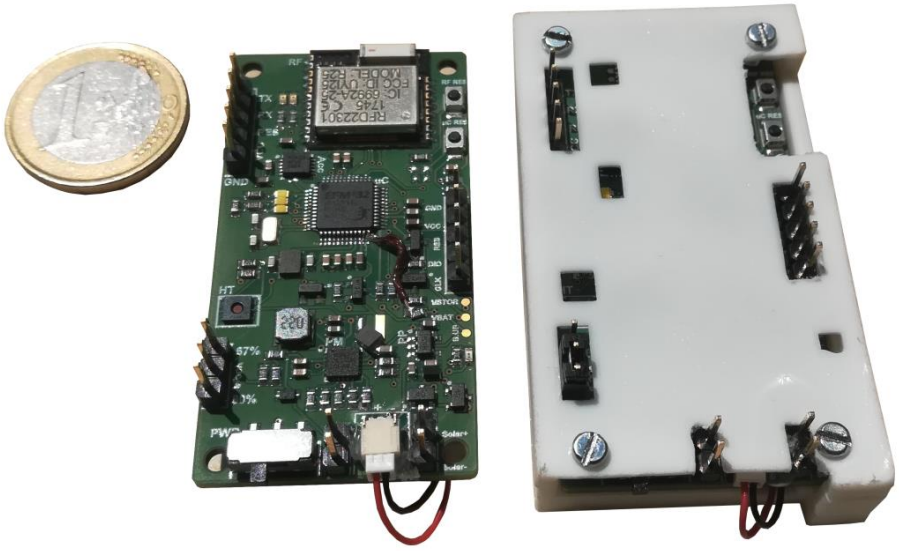

Figure 9 *The second version of VibrAn with and without case (Euro for scale)*

The on-board microcontroller was programmed to select the most energy-efficient data handling algorithm (direct transfer or embedded analysis) based on the weighed combination of user settings and ambient energy (Fig. 10). We tested and calibrated the system in laboratory environment with reference sensors, as well as on a vibrating duct in order to simulate real life applications.

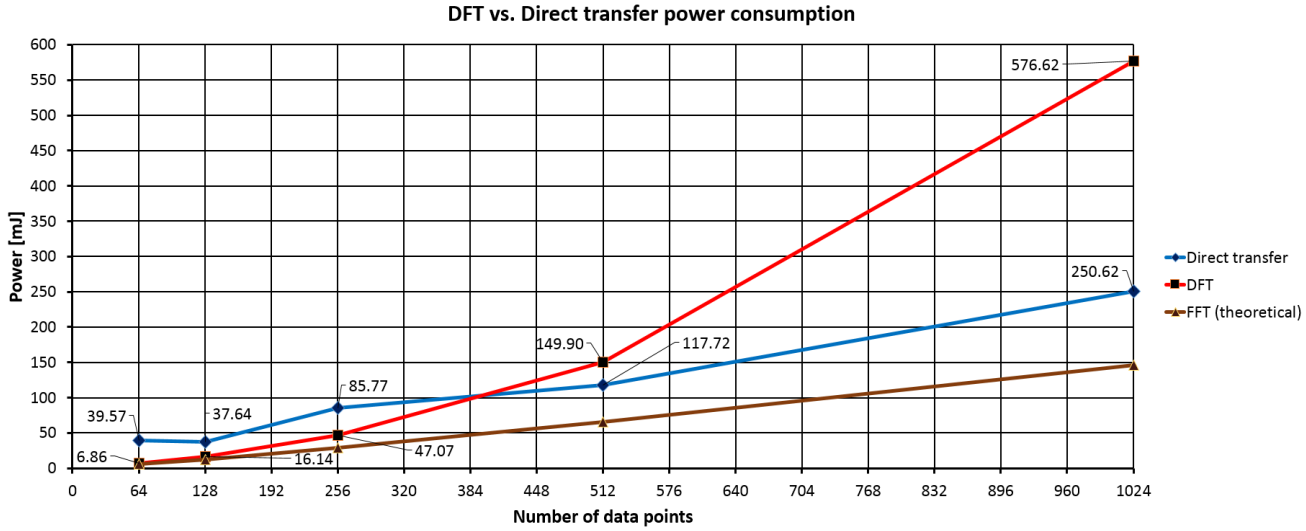

Figure 10 *Power consumption comparison of three different data handling methods*

The accelerometer is able to measure vibrations up to 100 Hz without aliasing, however, around 200 Hz it is guaranteed to appear. The maximum extracted power from the piezoelectric beam was 781 µW with resistive load, and 244 µW with complex load (energy management IC). The highest measured efficiency of the energy management chip (BQ25570) was 81%. In order to perform a 2000 data acceleration measurement (with RF data transmission) with the system 30 mW average power was needed. If this measurement was to be solely powered by energy harvesting, it around 2-3 hours would be required to harvest the necessary amount of energy. In the real life application (Fig. 11) we managed to harvest a total of 2.25 mJ energy in 4 hours and 20 minutes.

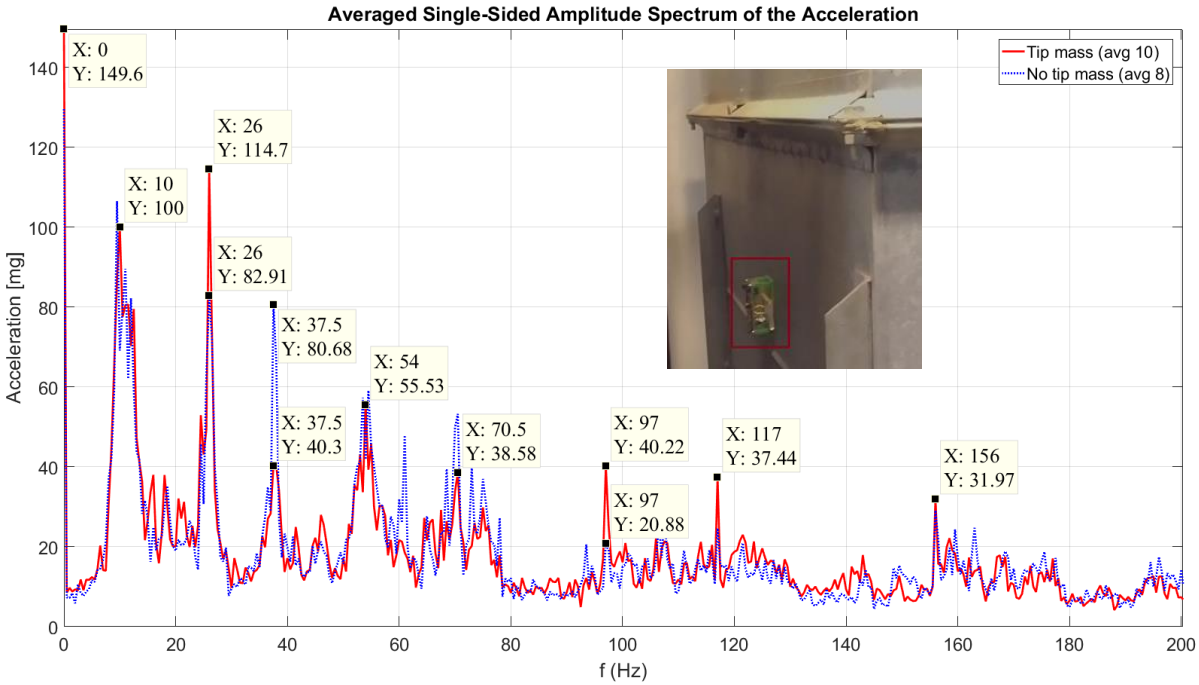

Figure 11 *The vibration spectrum recorded by the sensor on the side-wall of the an air-duct in the engine room for air-conditioning of the clean room facility. The sensor offers early failure detection of air conditioner's fan.*

The presented small device consists of commercially available components, provides an interface to study and test vibrational energy harvesters. In order to maximize the harvested energy, the main

vibrational frequency of the piezoelectric cantilever can be tuned by a moving mass. The proposed system can support the R&D on energy harvesters by providing an interface to test new designs. Future work will focus on improving energy harvesting by incorporating our own energy harvester and decreasing RF communication power consumption by designing our own low power RF protocol. The final target is to achieve an autonomous system transforming the ambient energy into electrical energy.

References

[1] János, Radó; Péter, Udvardi; Saeedeh, Soleimani; Lucky, Kenda Peter; István, Bársony; Péter, Révész; János, Volk: Low-Frequency Piezoelectric Accelerometer Array for Fully Implantable Cochlear Implants PROCEEDINGS 2 : 13 Paper: 1059 (2018).
[2] Tóth Máté Károly: Vibrációs energiahasznosító eszközök készítése és minősítése, BSc szakdolgozat, BM-VIKE, supervisor: J. Volk
[3] Szappanos, Miklós; Radó, János; Battistig, Gábor; Földesy, Péter; Volk, János Energy

Investigation of memristive structures[2]

Resistive switches or memristors are two terminal passive electric components, whose resistance can be reversible varied between two or several states by the voltage is applied. They are built as a capacitor like metal-insulator-metal structure, in which the two electrodes are connected by a conductive filament of nanometer dimension. Despite their simple structure they show complex operation, which offers many promising applications. Using them as simple memory cell (RRAM) is close to commercialization. Memristors have approached or even exceeded the specifications of contemporary flash memories . However, their more promising complex applications, such as their integration as memory and processing unit in neuromorphic computing are still subjects of intensive research..

The NEMS group joined the cooperation with the group of András Halbritter at the Department of Physics of BME in studying resistive switches in 2017 . That group has large experience in charactzerisation of memristive systems (Ag_2S, AgI, SiO_x or Nb_2O_5) using an STM arrangement. Relying on our nanofabrication expertise and facilities, the target of this collaboration is the development, characterization and optimization of on-chip resistive switches. The deviceswere initially fabricated by electron beam lithography, thanfurther scaled down to <10 nm by controlled electrical breakdown process. Recently nanofabricated Ag_2S and SiO_x resistive switches were successfully prepared and this research was continued in in 2018. The devices are fabricated at MFA while the electrical characterizations are performed at BME. In 2018 OTKA grant (K 128534) was obtained for the collaborative research on nanometer scale resistive switching memory devices lead by András Halbritter.

In case of Ag based resistive switching devices the 1/f type noise was studied at BME using the STM setup vs. the surrounding solid electrolyte (Ag_2S, AgI). As control experiments noise measurements were performed on pure Ag nanowires lacking any resistive switching media (see Figure 1, black dots). These Ag nanobridges were lithographically designed at MFA and thinned by feedback-controlled electromigration technique (see insets of Figure 1). The measurements revealed that the magnitude of the noise not, only the total resistance does depend on the surrounding material. This result implies that the noise arises from the internal fluctuation of the Ag nanowire rather than from

[2] In cooperation with Budapest University of Technology and Economics, Faculty Of Natural Sciences, Institute Of Physics

environmental effects. The resistance dependence of the noise is quantitatively captured by a theoretical model (fitted lines in Figure 1). The article is under review at Nanoscale.

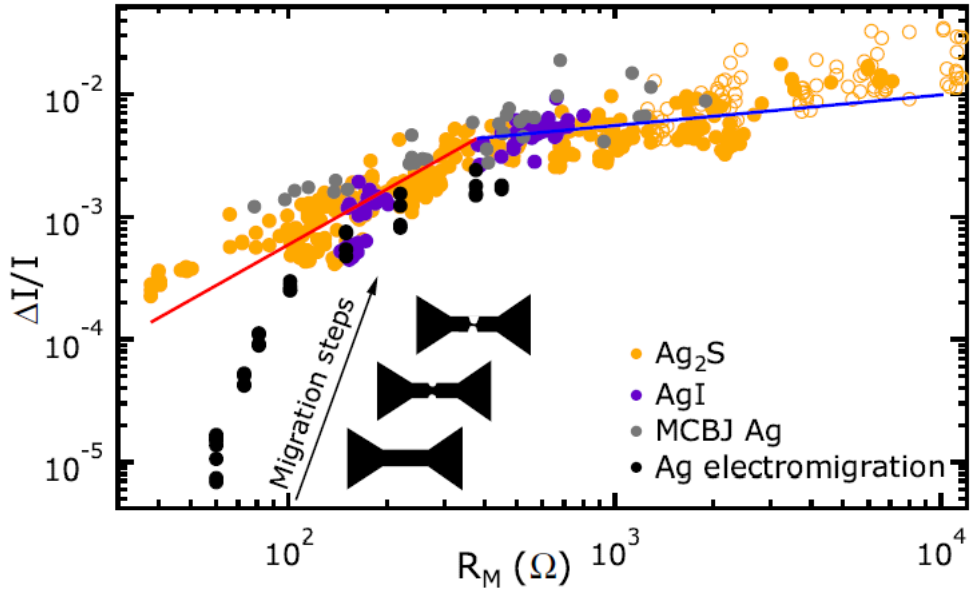

Figure 1. *The current noise ratio values as a function of the mean resistance. Ag nano filaments were formed in STM based Ag_2S (yellow) and AgI (purple) memristive nanojunctions, as well as in pure Ag MCBJs (grey) and electromigrated Ag nanobridges (black). The blue and red lines represent the best fit to the Ag_2S data.*

In SiO_x memristors the switching is based on the amorphization and crystallization of a Si rich region. In this memristive system a dead time effect can be observed: once the device is switched OFF, it is blocked in the OFF state for the period of the dead time. Tuning its length would have essential role in the application of SiO_2 RRAM. Based on our paper, published in 2017, we further investigated the nature of the dead time. The measurements revealed that the dead time shows clear dependence on the pressure, but the Ar plasma treatment of the SiO_2 surface has no effect, whatsoever. Furthermore, an aging effect was observed, as we "wrote and erased the device" several times, the length of the dead time increased.

Similar to the Ag based memristors, noise measurements were performed on graphene-SiO_x resistive switching devices. The active region of the SiO_x switch is formed between graphene electrodes in a gap of few nm (see red region in Figure 2.c). This nanogap is created by electrical breakdown of ian nitially contiguous graphene nanostripe, cut by electron-beam lithography (Figure 2.a). By optimizing the geometry of the patterned graphene and the electrical breakdown protocol, we could breake the graphene constrictions in a controlled way. The constrictions could be narrowed step by step and finally few nm (<5 nm) dimension gaps were generated. The low-frequency 1/f type noise was measured at several stages of the breakdown process and finally obtained in the tunneling regime. Afterwards, the SiO_x switching site was formed in the nanogap, and the noise was measured at the different memristor states. This systematic measurement allows the separation of the noise by the graphene electrodes from the noise of the resistive switch. In the near future noise measurement during the dead time is planned.

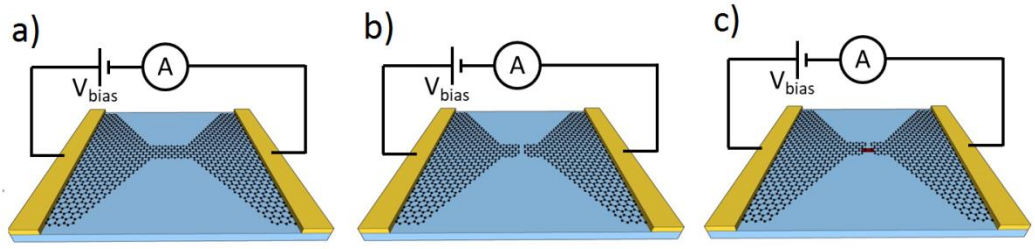

Figure 2. Illustration of the processing steps for forming of a nanometer-dimension SiO_x switch.

Beside both memristive systems above, transition metal-oxides such as niobium oxide, tantalum oxide, vanadium oxide are also well-established resistive switching compounds. We plan to study those memristive systems at ultrasmall dimensions. The size limitsfor well controlled RRAM operation have to be established. Since BME had a significant experience in Nb_2O_5 layer contacted in STM arrangement, it was the first material, which was realized in on-chip implementation. In the Nanotechnology laboratoryseveral devices were fabricated to study the effects of the structure (vertical or lateral arrangement) and electrode materials (graphene, gold, niobium). The structures were patterned by electron beam lithography, while the niobium oxide was deposited by reactive sputtering. The test measurements showed promising results, we could reproduce the same switching effects as observed in the STM arrangement. In the near future further optimizations are needed to result in more stable devices. Fabrication and process optimisation of VO_2 based samples is also in progress.

Large-angle dual scattering contribution in the MEIS spectra of thin gold layers and gold nanoparticles[3]

In this work we show the role of large-angle dual scattering (DS) events appearing as a wide background in the medium energy ion scattering (MEIS) spectra of gold nanostructures. The facility at the International Institute of Accelerator Applications at Huddersfield, UK, has been used for the analysis of thin Au layers deposited on glass substrate and plasmonic Au-silica core-shell nanoparticles (NPs) deposited on Si substrate. The typical Au layer thickness was 10-20 nm and the core/shell nanoparticle size was 25/40 nm. MEIS analysis has been performed with 100 keV He^+ ions for scattering angles of 90° and 125°. Note, these conditions are standard in MEIS experiments. In the size range of 10-100 nm, both for thin layers and spherical particles, besides small-angle multiple scattering, large-angle dual (and plural) scattering also gives strongly increasing contribution to the single scattering (SS) spectra of gold. The estimation of the DS yield is essential for quantitative spectrum evaluation and preliminary optimization of the measurement conditions.

The single scattering MEIS spectra of planar Au layers and spherical Au nanoparticles were simulated with the RBS-MAST [1] and SIMNRA [2] codes, considering the detailed 3D sample geometry. The surface roughness of the Au layers and the spherical shape and first neighbour configuration of the nanoparticles was considered. Atomic force microscopy (AFM) and field emission scanning electron microscopy (FESEM) have been applied as complementary characterization methods.
In our case dual scattering offers significant yield in a wide energy range, which consists of (i) an additional peak overlapping the single scattering spectra of gold and (ii) a smooth low energy background overlapping the glass or Si substrate signal. For 90º and 125º scattering angles the DS peak to SS peak ratios in the (i) energy range seem to be quite similar. The low energy (ii) DS yields, however, strongly differ resulting in 10-15%, and only 2-3% signal levels compared to the corresponding SS peak heights for the two different scattering angles.
We estimate the DS yield contribution in two different manners: with individual particle trajectory simulations provided by the SIMNRA code [2], and with calculations based on a simplified geometrical model for DS events using parametrized functions for He^+ stopping, cross-sections, and charge neutralization processes [3]. For planar Au layers SIMNRA simulations and the results of the simplified geometrical model show good agreement for the dual scattering yields. Similar DS yield calculations had been performed for thin ZnO and Cu_2O layers [4]. The results show that the procedure can be applied for a wide range of different materials in the calculation of MEIS spectra.

[3] Kombinált mikro-nanotechnológiai eljárások és ellenőrzésük lokális analitikai technikákkal: a mintázatképzéstől az alkalmazások felé - OTKA K112114

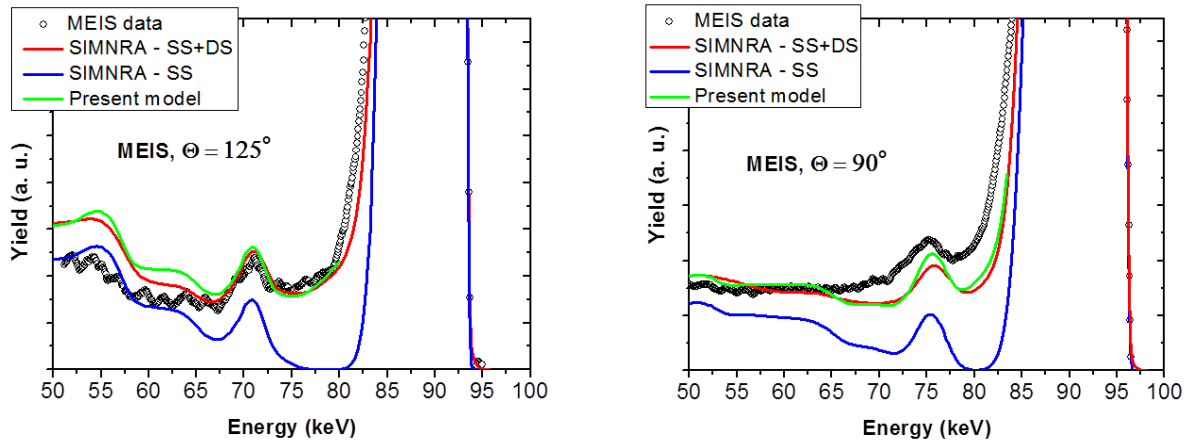

Figure 1 *MEIS spectra of a 10 nm Au/2 nm Cr_2O_3/glass layer system and SIMNRA simulations with only single scattering (SS) and single+dual scattering (SS+DS) calculations. The green line shows the low energy part of the spectrum according to our simple geometrical model for dual scattering [3]. Neutralization for the incoming He^+ projectiles is considered in the calculations.*

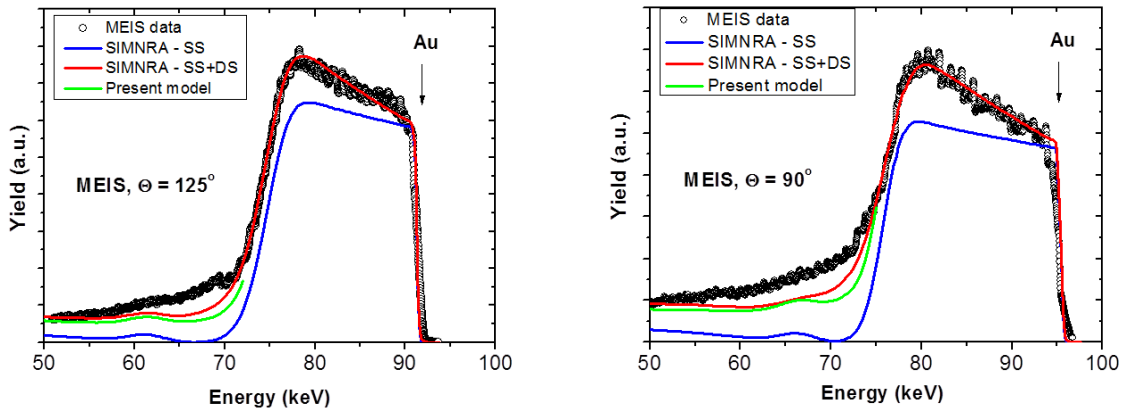

Figure 2 *Same as it is in Fig. 1 but for a 20 nm Au/2 nm Cr_2O_3/glass substrate system.*

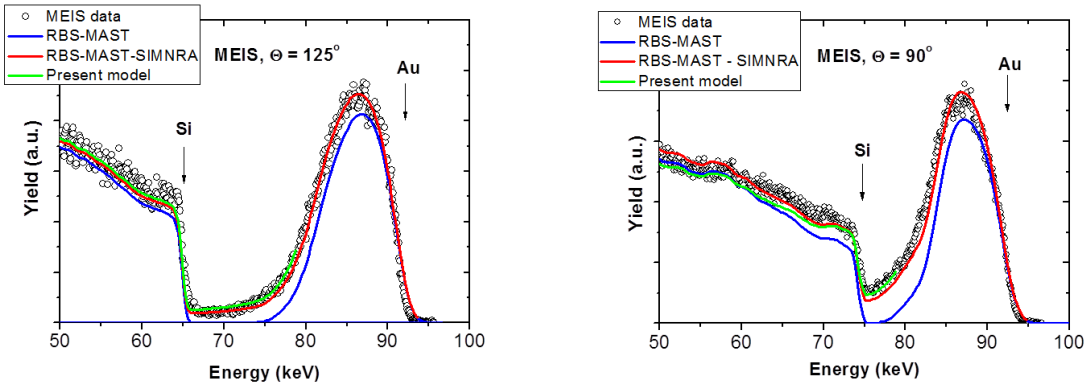

Fig. 3 *MEIS spectra of a monolayer of 25 nm diameter Au core/9 nm thick silica shell spherical nanoparticles deposited on Si substrate and 3D spectrum simulations with only single scattering (SS) and single+dual scattering (SS+DS) calculations. SS yields are calculated with RBS-MAST while DS yields are with SIMNRA, respectively. The green lines show the low energy part of the spectra according to our simple geometrical model for dual scattering [3].*

References

[1] Z. Hajnal, E. Szilágyi, F. Pászti, G. Battistig, Nucl. Instrum. Methods B 118, 1996, p. 617
[2] M. Mayer, Nucl. Instrum. Methods B 332, 2014, p.176
[3] Z. Zolnai, A. K. Rossall, J. A. van den Berg, A. Deák, S. Pothorszky, D. Zámbó, L. Illés, and G. Battistig: Large-Angle Dual Scattering Yield in the MEIS Spectra of Gold Nanostructures, Proc. HRDP 9 conference, 25-29 June 2018, Uppsala, Sweden
[4] A. K. Rossall: Examining the effect of the depth profile on the electrical properties of transition metal oxide thin films, Proc. HRDP 9 conference, 25-29 June 2018, Uppsala, Sweden

Microsystems Research Group

Group leader: Peter Fürjes
Group members: Cs. Dücső, O. Bálint-Hakkel, I. Bársony, F. Bíró, P. Földesy, Z. Hajnal, P. Hermann, V. Rakovics, I. Réti, Z. Szabó

Running projects:

- A pilot line for the next generation of smart catheters and implants — POSITION-II, H2020-ECSEL-2017-1-RIA-two-stage-783132
- Hungarian-Russian Collaborative Research Program is 2017-2.3.4-TéT-RU-2017-00006
- Intelligent Catheters in Advanced Systems for Interventions – INCITE (ENIAC CALL 2013-1)
- Multiparaméteres Point of Care in vitro diagnosztikai rendszerek fejlesztése, KTIA VKSZ_14-1-2015-0004
- Gyors húgyúti baktérium elemző mérőkészülék fejlesztése (Rapid urine bacteria analyzer), VEKOP-2.2.1-16-2017-00001 - Versenyképességi és Kiválósági Együttműködések
- Chiptechnológia alkalmazása a humán in vitro fertilizáció eredményességének javításában, GINOP-2.3.2-15 - „Stratégiai K+F műhelyek kiválósága”
- Mikrocsatornák készítése protonnyalábos mikromegmunkálással és alkalmazásuk Lab-on-a-chip eszközökben, OTKA CK 83821

In the reporting period significant efforts were invested in constructing and organising a competitive infrastructure and competence in the MEMS Laboratory of MTA EK MFA for supporting the development of biosensors, biointerfaces, microfluidic systems and medical applications of MEMS devices. These efforts focussed on development microsystems (BIOMEMS) integrable in medical diagnostic or interventional devices. The highly challenging topics attracted emerging industrial interest and increasing number of students. Accordingly the group is heavily involved in collaborations on national and international level by supporting industrial partners and assisting multidisciplinary education at partner universities.

Achievements

- Besides the development of conventional micromechanical sensors, solid background was established for the research and development bioanalytical and medical diagnostic systems supported by a dedicated laboratory for complex characterisation of microfluidic and BIOMEMS devices. Novel biosensing principles as well as sample preparation methods are proposed for medical applications expected to integrate the micro- and nanoscale transducers by embedded preparatio in microfluidic systems for Lab-on-a-Chip devices.
- The established system technology is open for the Hungarian project partners (universities, industrials and institutes) for realisation their specific complex micro- and nanofluidic systems in silicon/glass and polymer materials.
- Wide cooperative and knowledge network was established by the large number of joint research projects with Hungarian research centra: ATOMKI, BME, ELTE (Biológiai Fizika, Immunológiai Csoport), PPKE, SE, SZBK, PTE, WIGNER / Momentum Groups: Gyurcsányi E. Róbert - BME, Horváth Róbert – MTA EK MFA, Guttmann András – Pannon University / Companies: 77 Elektronika (Budapest, Hungary), CellSorter (Budapest, Hungary), Biotalentum (Gödöllő, Hungary), Diagnosticum (Budapest, Hungary), AlphaSIP (Madrid, Spain), FRK (Zabrze, Poland), Micronit (Twente, The Netherlands), Osypka (Berlin ,Germany), Philips Research (Eindhoven, The Netherlands), Tateyama Kagaku Ind. Corp. Ltd. (Toyama, Japan), Z-Microsystems (Austria).

- The scientific and processing results are directly transferred into higher education, as represented by the large number of students working in the laboratory also (13 laudated at the university TDK and 4 at OTDK), BSc, MSc diploma works (25) or PhD theses (1+2).

ECSEL JU "POSITION-II project, "Towards next generation of smart catheters and implants"[4]

The POSITION-II project is to realize a breakthrough in Europe in the development of smart catheters with embedded functions. By the introduction of open Flex to Rigid (F2R) technology platforms for miniaturization, in -tip AD conversion, wireless communication, MEMS transducer technology and encapsulation novel systems for minimal invasive surgery and medical examination will be developed. The availability of these open platforms will allow manufacturers to improve the performance of smart catheters at a lower cost and will enable the development of completely new minimally invasive smart instruments. The 46 member European consortium is led by Philips.
Our group was invited upon the previous successful cooperation in the ECSEL "INCITE" project where together with the Polish Foundation of Cardiac Surgery Development (FRK) and the Polymer Engineering group of BME we jointly developed a laparoscope demo system with tweezers integrated force sensor chips and electronics.
In the present project our group has two tasks

- Design and development of a 3D Flex-to-Rigid compatible force sensor for tip head integration of the catheter, where, alternative solutions will be evaluated and realized in response to the need of capacitive transduction. Similarly to the piezoresistive force sensor we developed in the frame the INCITE project. A force-transfer and -amplifyer rod will be formed from the handle layer of the SOI wafer, whereas the deforming membrane will be the 40μm thick device layer with isolated read-out capacitors on top. In this early phase of the project model calculations and preliminary experiments are being led to finalize the design, elaborate specific processing steps as well as the F2R compatible process flow.
- Material selection and process development for encapsulation and evaluation for biocompatible protective coatings of complex electronic devices to be implanted in the human body. Our contribution is the design and production of test chips and involvement in performing in-vivo tests.

Our generalgoal is to elaborate a capacitive type force sensor on flexible substrates. This will open the way towards various future applications in medical and robotic fields forming the basis of joint developments with domestic industrial partners in medium term.

Low power combustible-type nanosensors for gas detection in harsh environment [5]

On the basis of our previous results summarized in the excellent PhD work of Ferenc Bíró about processing of micro-hotplates and micro calorimetric gas sensors, a bilateral collaboration with the group of National Research Nuclear University MEPHI (Moscow Engineering Physics Institute) was initiated. Our joint R&D proposal was positively evaluated in both countries and the three year project started officially on April 1st, 2018 with the final goal to develop the **prototype** of solid state micro gas sensors for detection of hydrocarbons, CO and NH_3 concentrations up to their lower explosion limits.

[4] A pilot line for the next generation of smart catheters and implants — POSITION-II, H2020-ECSEL-2017-1-RIA-two-stage-783132
[5] Hungarian-Russian Collaborative Research Program is 2017-2.3.4-TéT-RU-2017-00006

In the first year the micro-hotplate structure was further improved to minimize its power consumption and temperature non-uniformities by means of novel filament geometries and applying new materials. The detrimental effect of temperature gradients arising along the filament and across the hotplate was proven. The operation temperature reduction to 500^{o}C or below plays crucial role in mass transport related degradation effects. Catalists operating efficiently at reduced temperature is also essential part of the work. This task is shared with the Russian partner and subject of the 2nd year of the project. In the reporting periode the

1. geometry of the Pt filament for uniform temperature was modified and temperature gradients << 0.5^{o}C/µm towards the perimeter were reduced. Thereby the masstransport was minimized and the lifetime of the sensor is expected to exceed the minimum one year. The heat sink contact wire wasintroduced in the centre the conventional double-spiral geometry modified such as to to provide extra power along the perimeter of the heated area. Both versions have small variations in filament diameter and widths to find the best structure. Some of the characteristic designs are shown in Fig 1. A new patterning technology of the Pt filament was also introducedreplacing the lift-off technique by a dry etching process of Pt in our DRIE system using Ar-SF_6 gas mixture. The perfect patterns and sidewalls facilitate further processing, eliminate sidewall flakes, increase yield and uniformity of filament. Identical filament pairs are badly needed in the Wheatstone-bridge configuration of the final device.

Fig. 1. Mask images of selected filament geometries for formation of uniform temperature hotplates.

2. Uniform and reproducible crystalline Si filaments were formed from SOI (silicon on insulator) wafersusing the buried oxide for achieving uniform thickness and identical geometry. Cantilevers are suspended on stress compensated SiO_2-Si_3N_4 membrane to eliminate possible ruptures of the cantilevers. Compared to metals higher resistivity of device silicon ensures higher filament resistance at the same temperature i.e. the cross section of the current routes should be increased to achieve the sufficient resistance. With the c-Si based design the electromigration can be reduced by > two orders of magnitude.

The heated area of these filaments can be completely covered on both sides with catalyst or passive pastes by drop deposition

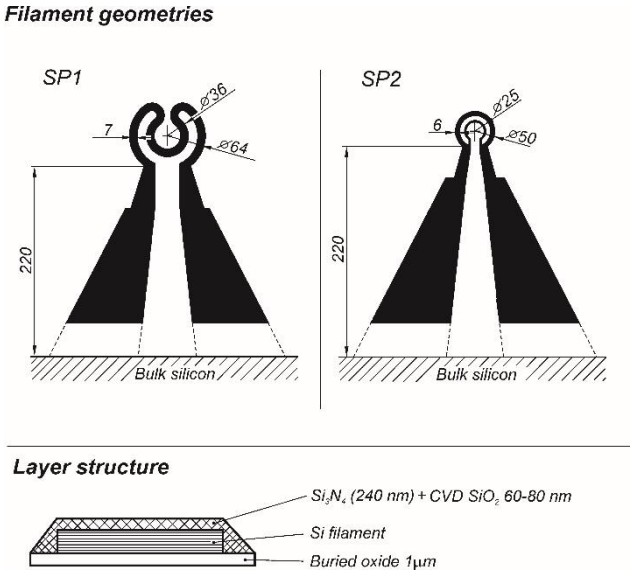

Fig. 2. *Suspended silicon filaments layouts and the layer stack below.*

Observing the resistance variations and also the "all-around" catalyst deposition, two filament geometries were designed (Fig. 2 top). The layer structure is identical for both filament geometries. The top side of the filaments are covered with Si_3N_4-SiO_2 layers, while the bottom side is covered with the buried oxide (Fig. 2 bottom). The silicon-nitride is the diffusion barrier against oxidation of silicon at the top, consequently in this design we expect the oxidation of the silicon filament to occur only at the bottom side reducing the resistance drift. The processing of the first test wafer will be expected end of January 2019.

Publications:

1. Bíró Ferenc, Metánérzékelés mikropellisztorral, PhD. védés, Pannon Egyetem, 2018.02.26.
2. Bíró, F., Hajnal, Z., Dücső, C., Bársony, I., The Role of Phase Changes in TiO_2 /Pt/TiO_2 Filaments, Journal of Electronic Materials, 47(4), (2018) pp. 2322-2329
3. Bársony, István; Bíró, Ferenc; Hajnal, Zoltán; Dücső, Csaba, Means of temperature assistance in gas sensing, In: Emerging Sensing Technologies Summit, (2018) pp. 31-33.
4. F. Bíró, .I. Bársony, Z. Hajnal, Microhotplate constraints, Advances in Microelectronics: Review, Chapter in Vol. 2, Book Series. Accepted, will be published in Q1 2019.

Biomechanical tissue characterisation by force sensitive smart laparoscope of Robin Heart Surgical Robot [6]

To obtain real-time multi-parametric information about physical and anatomic conditions of affected tissues during MIS operation is crucial for precision and safety. [1] The integrated 3D force and tactile sensors should provide these information about the different organs and tissues touched.

Integrated 3D force sensors for Minimal Invasive Surgery applications

Piezoresistive vectorial force sensors were designed according to the proposed force ranges and manufactured by 3D bulk micromachining process [2]. Two different MEMS sensors were electro-mechanically integrated into a metal laparoscope tweezers with the pre-processing electronics for

[6] Intelligent Catheters in Advanced Systems for Interventions – INCITE, ENIAC CALL 2013-1 (partners: Philips Research – The Netherlands, FRK – Poland, BME)

analogue-digital data conversion and communication with the robot control system (Fig. 1-1.). The sensors were embedded in biocompatible elastic polymer.

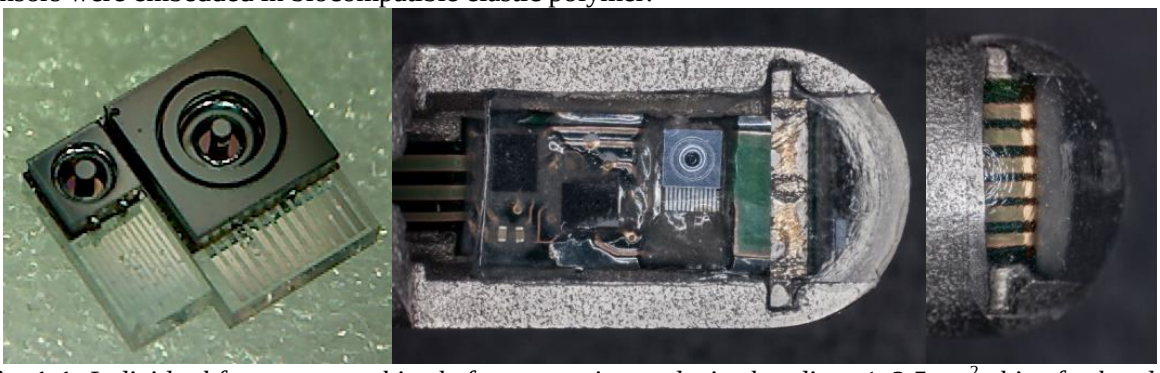

***Fig. 1-1**: Individual force sensor chips before mounting and wire bonding: 1x2.5mm^2 chips for head mounted tactile sensing (left) and 2x3mm^2 for gripping force (right). The medical grade stainless steel laparoscopic tweezers with the integrated electronics - covered by the (transparent) flexible biocompatible elastomer.*

Biomechanical measurements by robot integrated laparoscope

Tissue hardness measurements were performed using real animal tissue perpendicularly touched with the gripper. The signals of the tip tactile sensor were collected and analysed with reference to a constant uniform protrusion of the laparoscope (Fig. 1-2.).

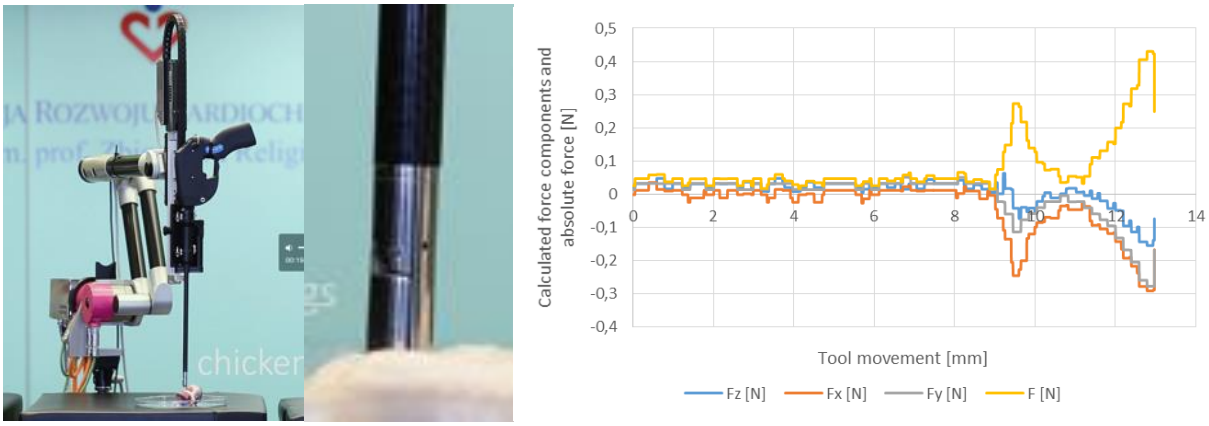

***Fig. 1-2.** Testing tissue hardness: the laparoscope protruded perpendicularly atconstant speed into a chicken wing. Measured forces (N) versus distance (mm) as the laparoscope approaches and touches chicken bone and muscular tissue. Touching depth is at 9mm.*

The measured force values clearly indicate the contact depth and the mechanical characteristics of the tissue. When pressing the soft muscle a continuous increase of force was detected starting with a slight slope. When the hard bone was pressed, a higher slope is recorded directly from the starting point on. The tissue- characteristic force signals offer the possibility of their automatic distinction.

A simple setup was constructed to mimic blood vessel and check whether the sensor built in the grasper is able to identify an artery by measuring the pulses. A liquid filled silicone tube was grasped and the signals of the force sensor were recorded along with pressure sensor readings while the microfluidic pump was operating in pulsed mode. Fig. 1-3 demonstrates that the sensitivity of the measurement depends on the preset clamping force, as expected from the blood pressure measurement protocol.

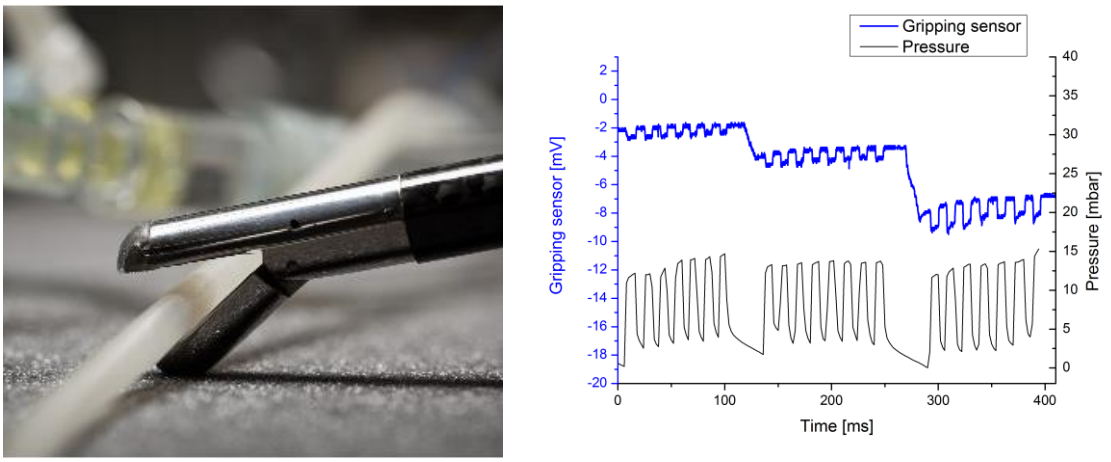

Fig. 1-3. *The signals of the grasping force sensors and the pressure sensor built in the fluidic system when applying pulse mode pressure. The three series are taken using different preset grasping forces.*

Summary
Studies of the prototype "smart" sensory laparoscopes have verified their usefulness in real-time force feedback robotic systems by identifying the state of tissue and determining the clamping force of the grasper in a surgical system. Implementing this "smart" tool into the surgery robot system, the human-machine synergy was also demonstrated by the Polish partner by applying two-directional haptic control.

References
[1] Z. Nawrat, "State of the art in medical robotics in Poland: Development of the Robin Heart and other robots", *Expert Rev. Med. Devices* 9(4), 353–359 (2012)
[2] J. Radó, Cs. Dücső, P. Földesy, G. Szebényi, Z. Nawrat, K. Rohr, P. Fürjes, „3D force sensors for laparoscopic surgery tool", Microsystem Technologies, 2017, doi:10.1007/s00542-017-3443-4

Publications
[1] Ł. Mucha, Cs. Dücső, G. Szebényi, P. Fürjes, Prototypic force feedback instrument for minimally invasive robotic surgery, Medical Robots 2018 Conference, Zabrze, Poland, 2018
[2] J. Radó, Cs. Dücső, P. Földesy, I. Bársony, K. Rohr, L. Mucha, K. Lis, W. Sadowski, D. Krawczyk, P. Kroczek, Z. Małota, G. Szebényi, H. Sántha, Z. Nawrat, P. Fürjes, Biomechanical Tissue Characterisation by Force Sensitive Smart Laparoscope of Robin Heart Surgical Robot, Proceedings of Eurosensors 2018 Conference, Graz, Austria, 2018 (Proceedings 2018, 2(13), 1035; https://doi.org/10.3390/proceedings2131035)
[3] J. Radó, Cs. Dücső, P. Földesy, G. Szebényi, H. Sántha, K. Rohr, L. Mucha, K. Lis, W. Sadowski, D. Krawczyk, P. Kroczek, Z. Małota, Z. Nawrat, P. Fürjes, Force sensitive smart laparoscope of Robin Heart Surgical Robot, Proceedings of Design, Test, Integration and Packaging of MEMS/MOEMS – DTIP 2018 Conference, Rome, Italy, 2018 (IEEE XPlore 8394204, DOI: 10.1109/DTIP.2018.8394204)

Polymer microfluidic systems for medical diagnostics [7]

Precise and fast PoC monitoring of disease related blood marker molecule or bacteria levels could be crucial in effective therapies. In a dedicated Lab-on-a-Chip (LoC) slution the microfluidic system has to transport the sample and the washing buffer to the active area of the chip, while mixing and incubating the sample with the reagents. As incubation and read-out require specified timing, precise sample handling and flow control are essential. The use of biological sample also requires bio-inert surface properties with minimized non-specific adsorption and coagulation in the channels. We target to develop a polymer based microfluidic cartridge for autonomously controlled sample transport in an integrated bioanalytical device. [1]

Autonomous microfluidic systems for blood protein detection

A microfluidic system was designed and manufactured for transporting whole blood or plasma at a precisely controlled sample rateto be integrated into Point-of-Care Lab-on-a-Chip based diagnostic devices. The detection of cardiovascular diseases was in focus in cooperation with 77 Elektronika Ltd. In the "Multiparaméteres Point of Care in vitro diagnosztikai rendszerek fejlesztése" project a specific microfluidic system was designed , actually the geometry was modified to fulfill requirements of optical detection with real blod sample. Accordingly, a new,microfluidic system compatible with the bioanalytical specifications (sample volume, targeted detection limits, surface blocking, etc.) had to be designed. With the 77 Elektronika Kft. we are developing Lab-on-a-Chip based diagnostic device for a specific project of the Science University of Pécs to support human in-vitro fertilisation also.

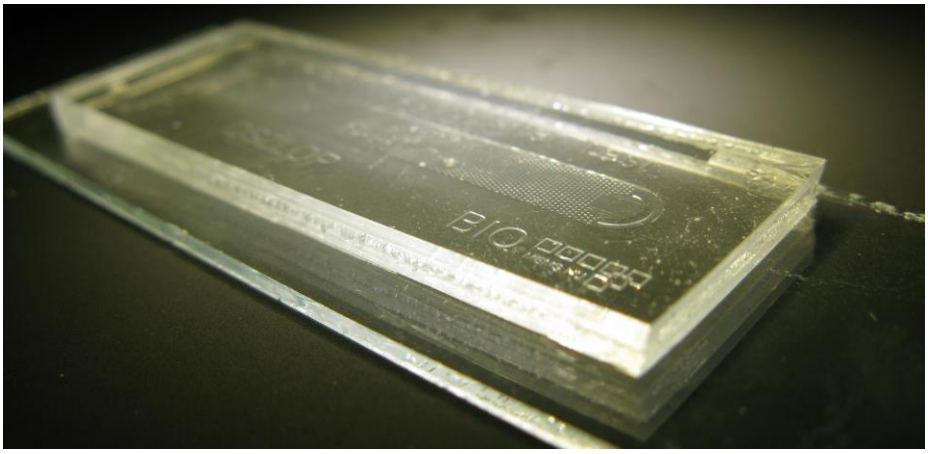

Figure 2-1. Microfluidic cartridge for testing of autonomous sample transport and preparation.

The material composition of the laboratory stage / pre-industrial cartridge was optimised for the required sample flow rate, the optical and mechanical properties. The embedding protocol of PDMS-PEO molecules was modified considering the molecular weight, concentration and physical parameters of the PDMS polymerisation process (temperature, time, surface treatments of the molding master).

[7] Multiparaméteres Point of Care in vitro diagnosztikai rendszerek fejlesztése, KTIA VKSZ_14-1-2015-0004 (cooperating partners: 77 Elektronika Ltd., BME, SE)

Gyors húgyúti baktérium elemző mérőkészülék fejlesztése (Rapid urine bacteria analyzer), VEKOP-2.2.1-16-2017-00001 - Versenyképességi és Kiválósági Együttműködések (cooperating partners: 77 Elektronika Ltd., SE)

Chiptechnológia alkalmazása a humán in vitro fertilizáció eredményességének javításában, GINOP-2.3.2-15 „Stratégiai K+F műhelyek kiválósága" (együttműködő partnerek: Pécsi Tudományegyetem, 77 Elektronika Kft., Semmelweis Egyetem, BME)

Surface modification of polymers compatible with industrial fabrication technologies
Our laboratory has been involved in the development of precision injection molding technology and surface modification processes of micro structured polymer cartridges. Hydrophilic and non-fouling features are crucial requirements of the autonomous fluid sample transport in the microfluidic cassette, therefore surface modification of the polymer substrate is necessary. We conducted wet and dry chemistry experiments to create adequate surfaces. The surfaces were characterised using several surface analytical methods. The long term stability of the surfaces was examined by contact angle measurements. Surface- chemistry functional groups were identified byAttenuated Total Reflectance Fourier Transformed Infrared (ATR FT-IR) spectroscopy. The morphology was inferred from Atomic Force Microscopy (AFM) images, whereas the thickness and homogeneity monitored by ellipsometry. The modified surfaces retained their hydrophilic character for two months period. (Fig. 2-2).

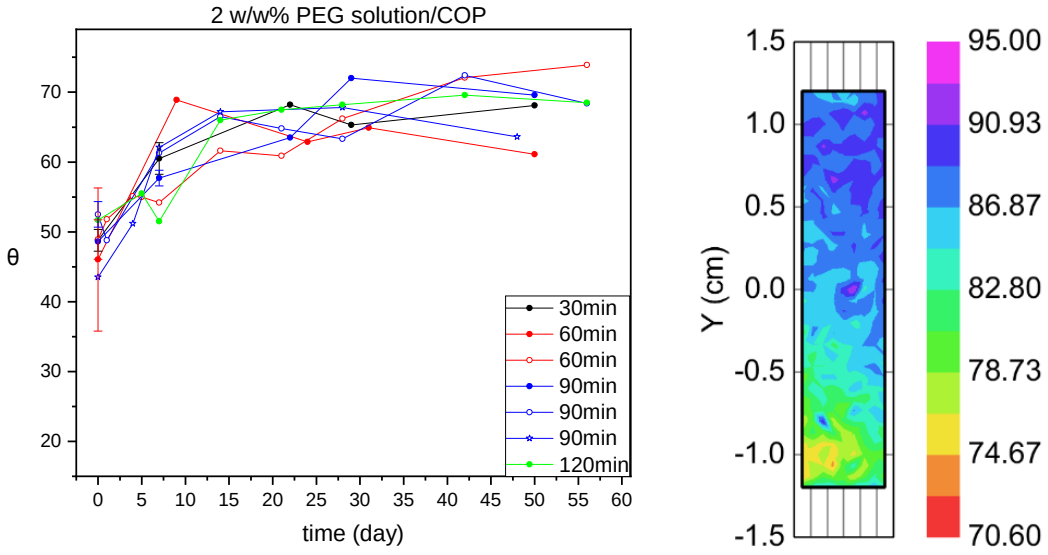

Figure 2-2. Long term stability of water contact angle (left) on hydrophilic PEG layer deposited by wet chemistry and ellipsometry thickness map (right).

The ATR FT-IR spectra showed that a homogenous hydrophylic layer could be formed on the polymer surface by wet chemical methods. Evaluation of the ellipsometry and AFM measurements revealed that the thickness of the layer is typically ~ 100-200 nm (depending on the parameters of the preparation).

High resolution silicon mold insert for injection molding microfluidic systems
Our research laboratory is participating in development precise micro-injection molding of plastics for high throughput fabrication of microfluidic systems in in cooperation with the 77 Elektronika Kft. and Z-Microsystems GmbH. The applicability of the technology is not trivial for fabrication microstructures, as the definition of the molding parameters and the development of molding master is quite critical. The MEMS Lab developed a reliable technology for fabrication molding master using bulk silicon micromachining technology by 3D Deep Reactive Ion Etching (DRIE) of crystalline silicon wafer. The final structure was developed by DRIE with adequate surface roughness and wall angle for the injection molding technique. The geometry transfer achieved by the developed molding master is demonstrated in Fig. 2-3.

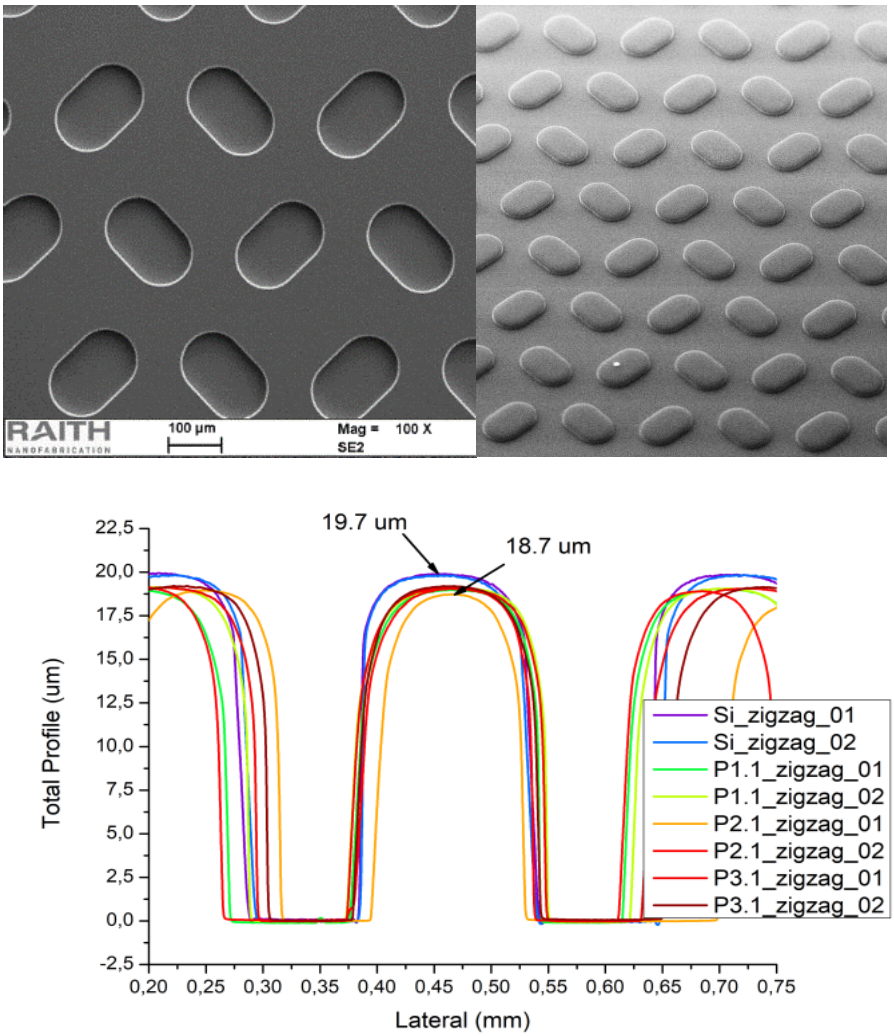

Figure 2-3. The microstructure of the fabricated silicon molding master (top left),the injection molded polymer sample (top right) and the profiles compared (below).

References

[1] L. Gervais, E. Delamarche (2009) Toward one-step point-of-care immunodiagnostics using capillary-driven microfluidics and PDMS substrates, Lab Chip 9, 3330–3337

[2] E. Holczer, P. Fürjes, Effects of embedded surfactants on the surface properties of PDMS; applicability for autonomous microfluidic systems, Microfluidics and Nanofluidics 21: 81, 2017, doi:10.1007/s10404-017-1916-5

Finite element modelling and simulation in the development of MEMS and microfluidics devices

Initial design as well as specific optimization tasks mostly involve not only the careful structural and process engineering, but also various simulations of device operation in microtechnology. Numerical simulations enable assessment of stability of the device components under various external conditions, as well as trial modifications of the studied devices, adaptation to varying requirements, etc.
Modelling and simulation also has the advantage of lower resource needs and faster trial evaluation cycles. In the following we present a couple of examples of applied models and simulations, carried out in the COMSOL finite element modelling (FEM) framework. FEM provides approximations of arbitrary accuracy for device and environmental components. Systems of coupled partial differential equations can be numerically solved in practically any configuration of device components and environmental conditions, with simplifying assumptions about the local behaviour of the various state-functions and physical variables. As multiple physical quantities are being simultaneously solved for in the iterations of the simulations, hence their colloquial name, *multiphysics*.

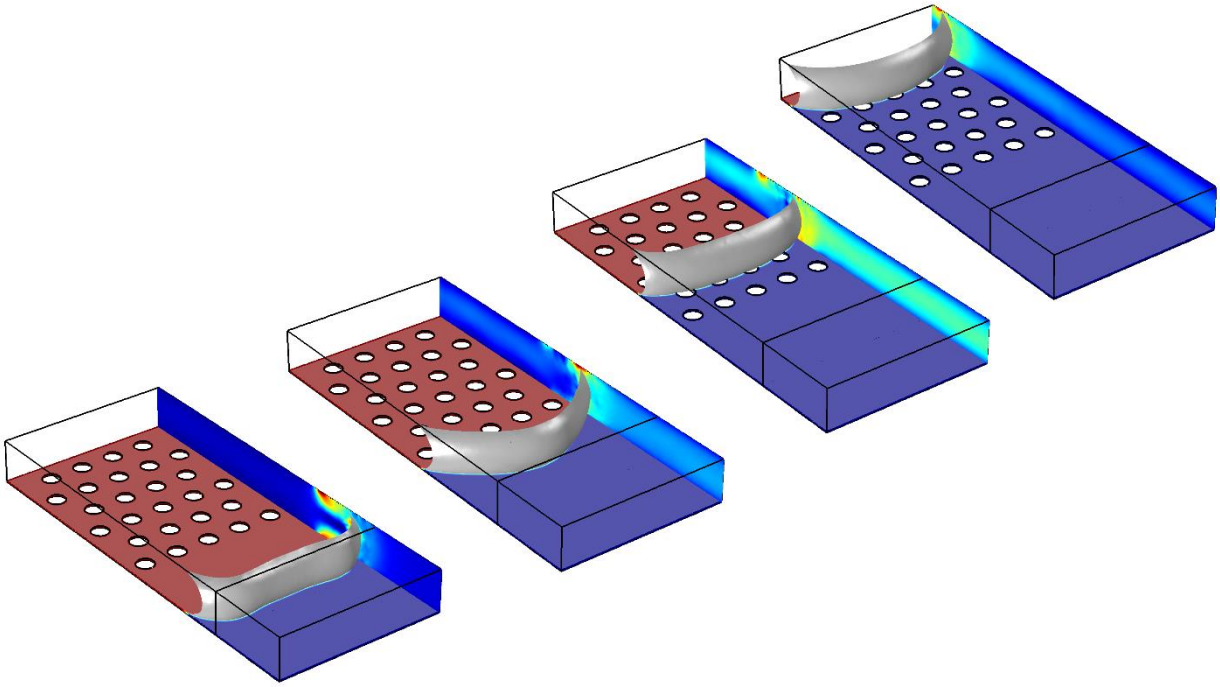

Figure 2-4. Timesteps (from left to right: 0.02, 0.08, 0.14, 0.20 ms) of water entering a surface modified capillary channel. The channel width is 200 μm, height is 50 μm. The bottom of the farther part of the channel is modified by cylindrical steps of 2 μm height. In the beginningonly the closer half of the channel is filled by the liquid, during the timesteps the changes in form and gradual progress of the air/water interface are well observable. Comparison of various surface morphologies is ongoing.

Effect of the surface morphology on capillary flow in microfluidic channels
Control of fluid flow in microchannels has been a field ofintense development in the past decade. A promising direction is the changing of wetting properties by modification of surface morphology in the channel to accelerate (or decelerate) the progress of the fluid surface at desired regions. Numerical adjustment of the interface geometry to the fluid properties and desired control parameters requires several time-dependent simulations of the behaviour of the fluid (most of the times air-water) system.

Polimer based optical waveguides for biomedical applications[8]

Optical Mach-Zender Interferometer (MZI) form the basic unit of the detecting layer of a glass supported Lab-on a Chip cassette. Based on prior optical simulations we formed waveguide structures with 2×2 μm^2 cross-section on a glass support (Fig.3-1) . We used epoxy based resists (SU-8, DWL and EpoCore) which were selected by the consortium members. Devices suitable for optical characterization were formed by using available photolithography technology.
Besides optimizing the parameters of the individual steps of the lithography process (time and dose of the exposure, mask distance, baking temperature), we also conducted experiments with different cladding layers (SU-8, EpoClad). We verified the morphology and the adhesion of the wave guide layers by Scanning Electron Microscopy (SEM). Following the successful implementation of this part of the project the MZI containing cassettes were given to the consortium partners for functional tests.
In the next stage of the development we will investigate the possibility of embedding the microstructures in material systems which are compatible with industrial technologies.

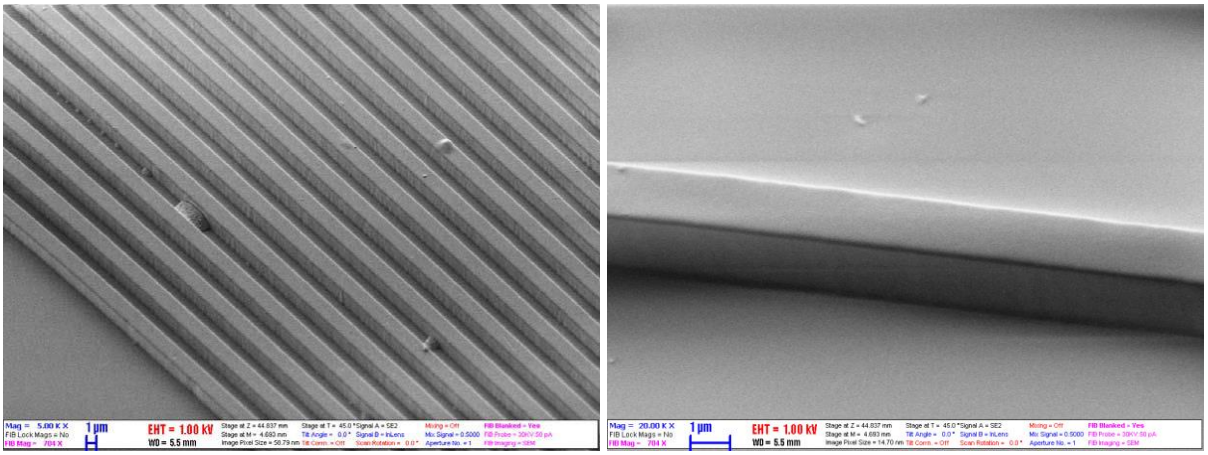

Figure 3-1. Waveguide structures of Lab-on a Chip system

Cell and particle manipulation and screening in microfluidic systems[9]

The demand for microfluidics enabling fast and effective preparation and analysis of liquid samples in microscale diagnostic (Lab-on-a-Chip) systems underlined the importance of studying these phenomena. Due to the governing physical phenomena on microscale, classical sample preparation methods, such as efficient mixing of fluids as well as size-dependent separation and sorting or filtering of corpuscles in the liquid samples becomes a challange. Novel microfluidic structures have to be developed based on the physical laws of this size domain.

Development microfluidic system for efficient separation circulating tumor cells (CTC)
In cooperation with the research groups of István Rajta and András Guttmann we participated in the design and fabrication of special microfluidic systems dedicated to sorting and separation circulating tumor cells. The channel system containing 3D tilted pillar structures of high specific surface was

[8] Gyors húgyúti baktérium elemző mérőkészülék fejlesztése (Rapid urine bacteria analyzer), VEKOP-2.2.1-16-2017-00001 - Versenyképességi és Kiválósági Együttműködések (cooperating partners: 77 Elektronika Ltd., SE)

[9] *Mikrocsatornák készítése protonnyalábos mikromegmunkálással és alkalmazásuk Lab-on-a-chip eszközökben, OTKA CK 83821 (együttműködő partnerek: ATOMKI, MTA – Pannon Egyetem – Transzlációs Glikomika Lendület Csoport)*
Gyors húgyúti baktérium elemző mérőkészülék fejlesztése (Rapid urine bacteria analyzer), VEKOP-2.2.1-16-2017-00001 – Versenyképességi és Kiválósági Együttműködések (cooperating partners: 77 Elektronika Ltd., SE)

desined according to the results of preliminary Finite Element Modelling. The behaviour of the fabricated microfluidic system was defined by analysis of the movement of human tumor cells, to validate the FEM simulation. The computational fluid dynamics (CFD) assisted chip design and the entire microfabrication process was demonstrated with some preliminary test results on flow characteristics [1].
As a continuation of our previously published work, we presented a detailed evaluation of a microfabricated cell capture device utilizing a doubly tilted micropillar array. The device was fabricated using a novel hybrid technology based on the combination of proton beam writing and conventional lithography techniques. The resulting unique hybrid device had a small central region with the doubly tilted micropillar array for improved cell capture, fabricated by PBW, while the surrounding area of the chip was generated using UV lithography. This novel combination extended the potential of conventional microstructuring techniques, generating high interest both from engineering and biological application points of views. Tilted pillars offer unique flow characteristics and support enhanced fluidic interaction for improved immunoaffinity based cell capture. The performance of the microdevice was evaluated by an image sequence analysis based in-house developed single-cell tracking system. Individual cell tracking allowed in-depth analysis of the cell–chip surface interaction mechanism from hydrodynamic point of view. Simulation results were validated by using the hybrid device and the optimized surface functionalization procedure. Finally, the cell capture capability of this new generation microdevice was demonstrated by efficiently arresting cells from a HT29 cell-line suspension.

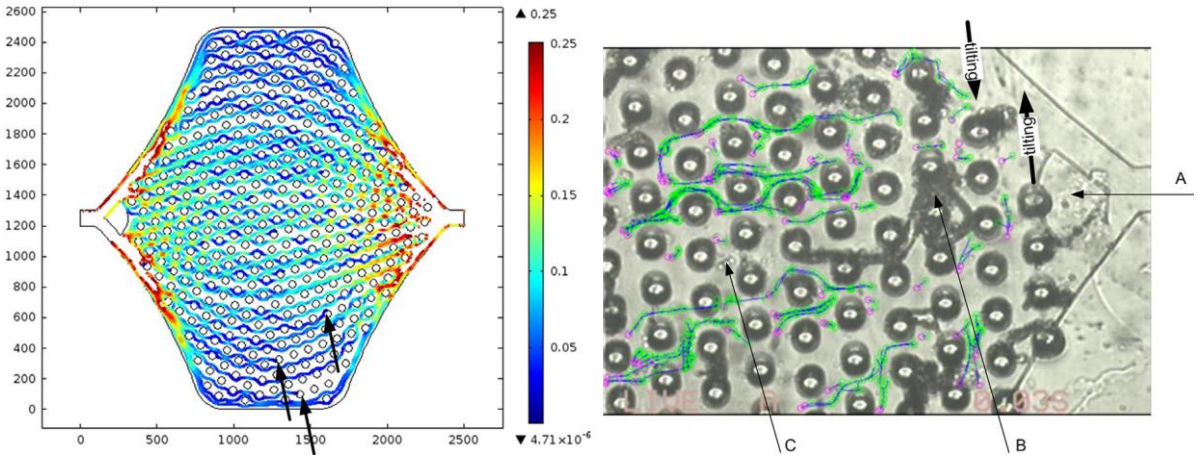

Figure 4-1. *Calculated steady-state streamlines based on the developed model, expressed in term of fluid velocity (mm/s) (left). X and Y axes represent the geometrical scaling with micrometer unit. A representative screenshot from the acquired and processed image sequence video, showing the flow distributor (A), a clogged (B) and a free flowing cell clusters (C). Blue lines represent the observed cell trajectories.*

Modelling and characterisation of droplet generation, trapping and detection in impedance based cell analytical microfluidic system

Droplet based microfluidics have developing relevance in the field of Lab-on-a-Chip technology. In these multi-phase flow devices, the continuous sheath emulsion enables to generate, manipulate, mix, focus and separate encapsulated chemical reagents or biosamples as assay of living cells. Therefore cell-analytical and diagnostic procedures can be automatized on microscale, although the precise control and monitoring of droplet parameters and behaviour are essential for their reliable application. Accordingly this work focuses on design and characterisation of a hybrid polymer microfluidic system having integrated electrode system (Fig. 4-2). The developed system is capable of creating, manipulating, trapping and monitoring droplets having precisely determined size fitted to general cell diameter. [2, 3]

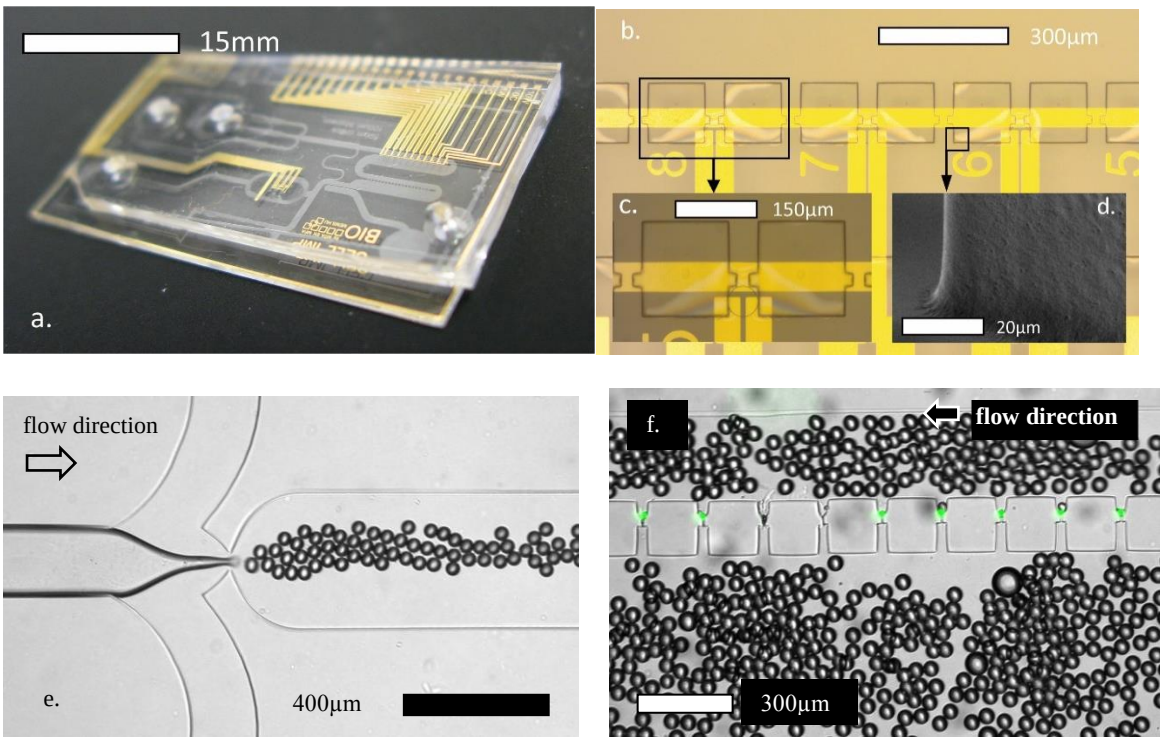

Figure 4-2. *Metal (Au) electrodes integrated in SU-8 based hybrid microfluidic system (a). For proper alignment, electric insulation and transparency the channels are formed in multi-layered SU-8 (b, c). SEM view presents the interface between the thin insulation and the thick channel forming SU-8 layers (d). Droplets generated in the two-phase microfluidic system (e) and encapsulated fluorescent beads trapped in the perforated cavities of the model microfluidic system (f).*

The influence of flow characteristics of two-phase microfluidic systems was analysed regarding the droplet generation, particle encapsulation and trapping processes. Droplets were dispersed in oil continuous phase with the requirement of precise size distribution to enable effective cell entrapment controlled by the applied flow parameters. Hydrodynamic behaviour of the microfluidic system was modelled by Finite Element Method (FEM) using COMSOL Multiphysics and compared to experimental results. The applicability of droplet based cell encapsulation and hydrodynamic trapping and the capability of impedance spectroscopy based droplet and cell detection were also characterised.

References

[1] I. Rajta, R. Huszánk, A.T.T. Szabó, G. U. L. Nagy, S. Szilasi, P. Fürjes, E. Holczer, Z. Fekete, G. Járvás, M. Szigeti, L. Hajba, J. Bodnár, A. Guttman, Tilted pillar array fabrication by the combination of proton beam writing and soft lithography for microfluidic cell capture: Part 1 Design and feasibility, Electrophoresis 37 3 pp. 498–503, 2016

[2] E. Holczer, O. Hakkel, P. Fürjes, Fabrication of hybrid microfluidic system on transparent substrates for electrochemical applications, Proceedings of Eurosensors 2017 Conference, Paris, France, 2017 (Proceedings 2017, 1(4), 326; doi:10.3390/proceedings1040326)

[3] A. B. Tóth, E. Holczer, O. Hakkel, E. L. Tóth, K. Iván, P. Fürjes, Modelling and characterisation of droplet generation and trapping in cell analytical two-phase microfluidic system, Proceedings of Eurosensors 2017 Conference, Paris, France, 2017 (Proceedings 2017, 1(4), 526; doi:10.3390/proceedings1040526)

Publications

[1] G. Járvás, T. Varga, M. Szigeti, L. Hajba, P. Fürjes, I. Rajta, A. Guttman, Tilted pillar array fabrication by the combination of proton beam writing and soft lithography for microfluidic cell capture Part 2: Image sequence analysis based evaluation and biological application, Electrophoresis 2018, 39, 534–539

[2] A. B. Tóth, E. Holczer, A. Füredi, O. Hakkel, E. L. Tóth, K. Iván, P. Fürjes, Modelling and characterisation of droplet generation, trapping and detection in impedance based cell analytical microfluidic system, Lab-on-a-Chip Europe 2018 Conference, Rotterdam, The Netherlands, 2018

Solid state nanopore and nanocapillar based bioanalytical systems [10]

Nanoporous membranes are fundamental components of the transport modulation based label free electrochemical biosensors envisioned for high sensitive molecule detection. [1] The sensitivity and the specificity of these sensors are significantly affected by the pore geometry what has to be fitted to the size and conformation of the target molecules. Precise tailoring of nanopore geometries and alignment to target molecule conformation and size improves the signal-to-noise level of the identification method - in our case the impedance spectroscopy (EIS). The pore geometry engineering is essential for reliable and reproducible manufacturing of integrable solid state nanopore-arrays in molecule diagnostic devices. Other important issue is the adequate selection of the applied material composition. Commercialization of the nanopore based biosensors or Lab-on-a-Chip devices seems to depend on the development of precise and high throughput nanofabrication techniques enabling reliable and reproducible shaping of nanopore geometries in extremely thin, but mechanically stabile solid state membranes having electrical resistance as high as possible:

- Different (5-10nm thick TiO_2, AlO_X and HfO_2) dielectric layers were deposited by ALD (atomic layer deposition) and tested electronically to select the adequate insulation layer to be able to integrate multi-electrode array for EIS measurements.

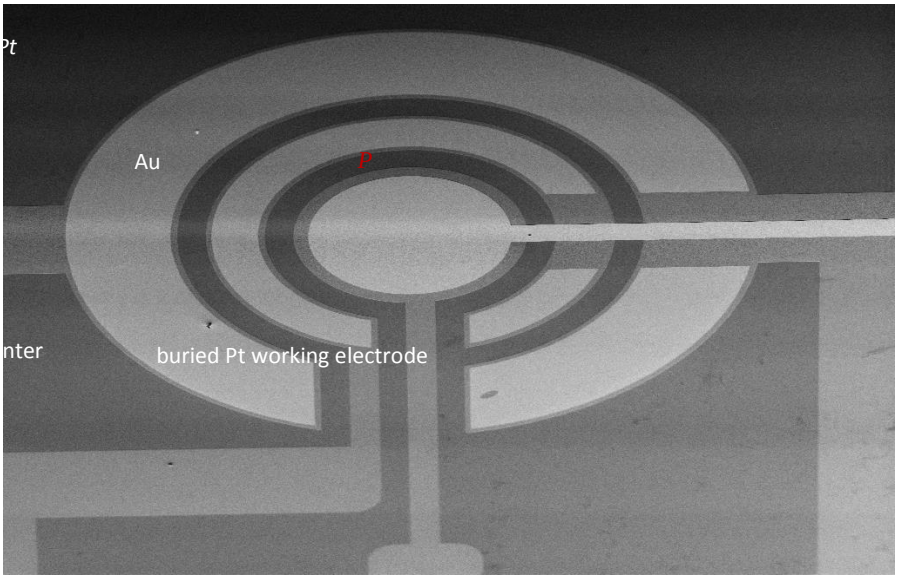

Figure 7-1. *Integrated electrodes for on-chip EIS measurement.*

[10] Multiparaméteres Point of Care in vitro diagnosztikai rendszerek fejlesztése, KTIA VKSZ_14-1-2015-0004 (cooperating partners: 77 Elektronika Ltd., BME, SE)

References
[1] Makra, A. Brajnovits, Gy. Jágerszki, P. Fürjes, R. E. Gyurcsányi, Potentiometric sensing of nucleic acids using chemically modified nanopores, Nanoscale 9 pp 739-747, 2017, doi: 10.1039/C6NR05886H

SERS active periodic 3D structure for trapping and high sensitive molecular analysis of particles or cells

Raman spectroscopy is finding many applications in biology, life sciences and other areas. Raman scattering is inherently weak, but its sensitivity can be improved by implementing surface-enhanced Raman scattering (SERS). Surface enhanced Raman scattering (SERS) evolves in the vicinity of nanostructured metallic surfaces or nanostructures achieving several orders of magnitude enhancement in the Raman signal and extremely improved sensitivity reaching the attomolar (10^{-18} M) concentration ranges [1]. This highly sensitive detection performance of SERS was utilized for analysing molecules located in the few nanometer distance or immobilised on the surface of micro and nanoparticles trapped in a specially designed microstructure.
In a previous work the highly sensitive molecule recognition performance of a specially designed surface enhanced Raman scattering (SERS) substrate was demonstrated. The general inverse pyramid structures were fabricated as cavities in perforated membrane applicable for particle and cell filtering, sorting and trapping. In the voids of the gold covered substrate size compatible particles functionalised by different molecules were trapped, their SERS signal was detected and the different molecules were recognised.

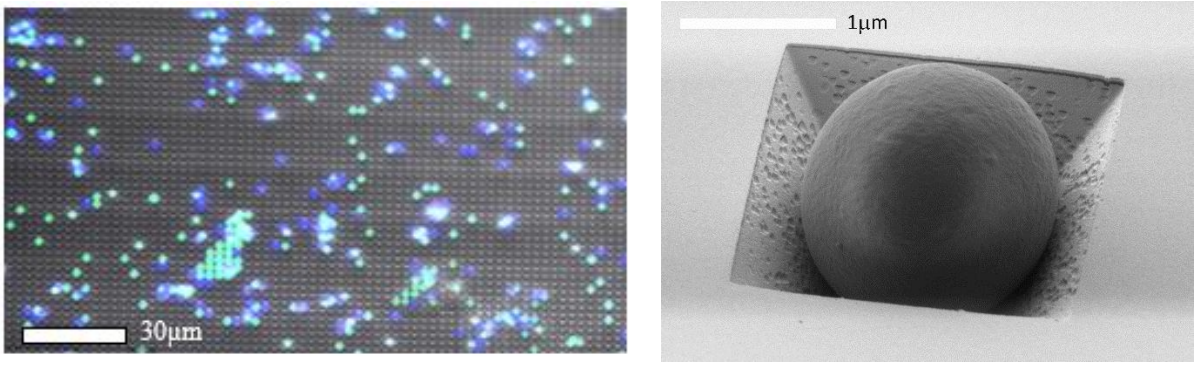

Figure 5-1. *Fluorescent beads with appropriate 2µm diameter (Sigma Aldrich - green and Spherotech - blue) entrapped in the periodic array of perforated pyramidal structures: multichannel fluorescent (left) and SEM image (right).*

The fluorescent molecules were analysed by SERS utilizing the plasmonic enhancement by the structured surface of the traps. The definite and sensitive differentiation of the molecules immobilized on the polystyrene bead surfaces are presented in Figure 5-2, where a huge increase in the Raman signal can be observed on the SERS surface.

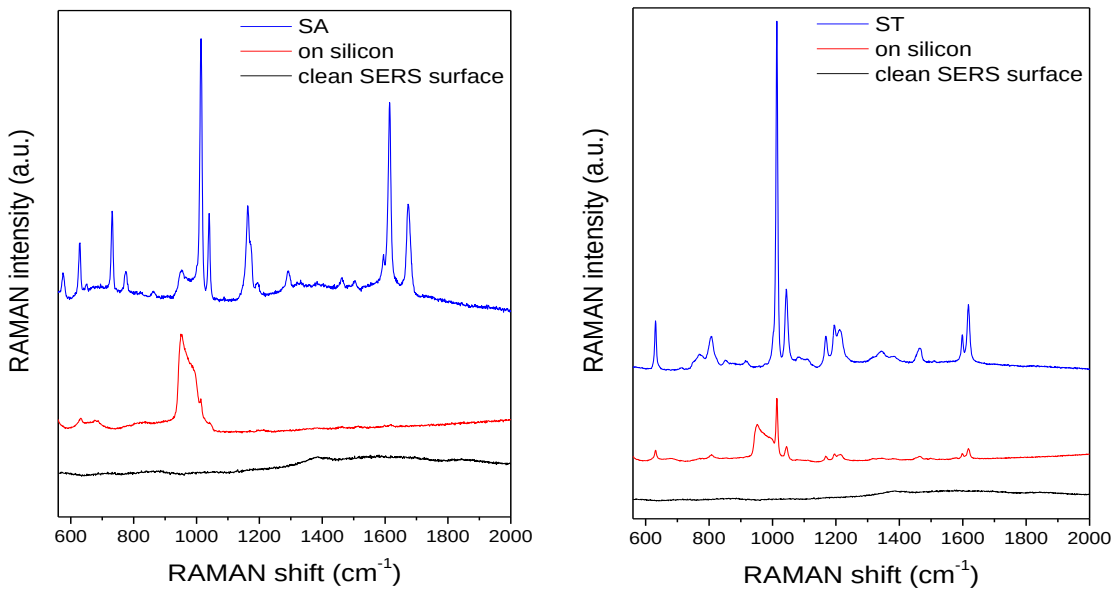

Figure 5-2. *Comparison of the SERS spectra recorded on the clean SERS substrate (black) and different fluorescent beads on silicon (red) and trapped in the periodic array (blue). SA – Sigma Aldrich and ST - Spherotech fluorescent beads, respectively.*

In our approach special size fitted SERS active substrate was prepared by micromachining techniques in silicon wafer to be applicable for particle entrapment. Subsequently, gold nanospheres were trapped in the pyramidal cavities. SERS performance of the hierarchically combined structures was analyzed and compared by using a highly diluted benzophenone solution and octadecanethiol surface functionalization. The recorder spectra are demonstrated in Fig. 5-3.

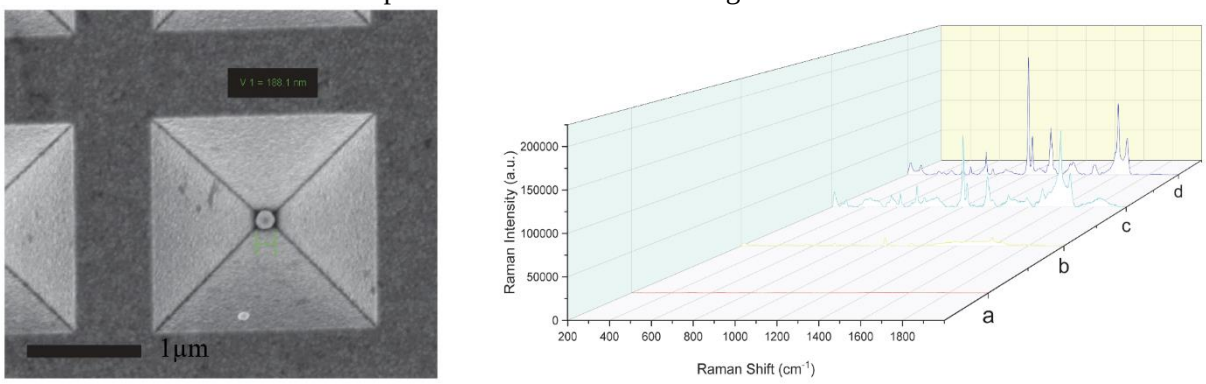

Figure 5-3. *Scanning electron microscopic images of the periodic array of gold coated inverse pyramids with the entrapped gold nanoparticle (left). Reference normal Raman (right, curve a) and surface enhanced Raman spectra of benzophenone recorded on array of gold coated inverse pyramids (right, curve b), array of gold coated inverse pyramids with entrapped nanoparticles (right curve c) and the latter with octadecanethiol surface functionalization (right, curve d).*

The applicability of special periodic 3D structure was demonstrated for simultaneous particle (or cell) or nanoparticles trapping and extremely sensitive Surface-Enhanced Raman Spectroscopy based detection of molecules immobilized on the surfaces of the confined beads.

References

[1] I. Rigó, M. Veres, P. Fürjes, SERS active periodic 3D structure for trapping and high sensitive molecular analysis of particles or cells, Proceedings of Eurosensors 2017 Conference, Paris, France, 2017 (Proceedings 2017, 1(4), 560; doi:10.3390/proceedings1040560)

Publications

[1] I. Rigó, M. Veres, O. Hakkel, P. Fürjes, Hierarchically Combined Periodic SERS Active 3D Micro- and Nanostructures for High Sensitive Molecular Analysis, Proceedings of Eurosensors 2018 Conference, Graz, Austria, 2018 (Proceedings 2018, 2(13), 1069; https://doi.org/10.3390/proceedings2131069)

[2] I. Rigó, M. Veres, P. Fürjes, SERS active periodic 3D structure for trapping and high sensitive Raman-spectroscopy of molecular surface analysis of particles or cells, Lab-on-a-Chip Europe 2018 Conference, Rotterdam, The Netherlands, 2018

Intelligent wound patch for online monitoring wound healing processes – WoundER[11]

In the clinical practice, the proper care of wounds obtained in accidents, postoperative and ulcerative ulcers is of primary importance. It is a basic expectation of the treating physician to obtain continuous or regular information on the healing of the wound. In case of a home-based hospitalization, the control of wound is time consuming and difficult for the physician, but remote monitoring of the appropriate parameters can help in effective curing. The task of the "intelligent bond" we developed is to facilitate the work of the physician and the cure of the patient by monitoring the process of healing. In case of a problem the user and the physician should be warned about the need for a check or a replacement.

An intelligent tool was developed to provide continuous information about various parameters of the wound healing, such as temperature, humidity, and the tightness of the bandage. [1] Targeting afinal wireless, point-of-care application we focused on the minimisation of the energy consumption of the electronics. Appropriate sensors were chosen and integrated into a flexible PCB. Low power consumption electronics were also developed to solve the preliminary signal processing and communication tasks using Bluetooth protocol. Data processing and visualisation software was also developed. For testing the proper functionality of the sensor system, as well as their influence on the operation behaviour of the sensors various tests and calibrations were elaborated by using different wound dressings applied in medical practice.

[11] National Research, Development and Innovation Fund (NKFIA) via NVKP_16-1-2016-0018

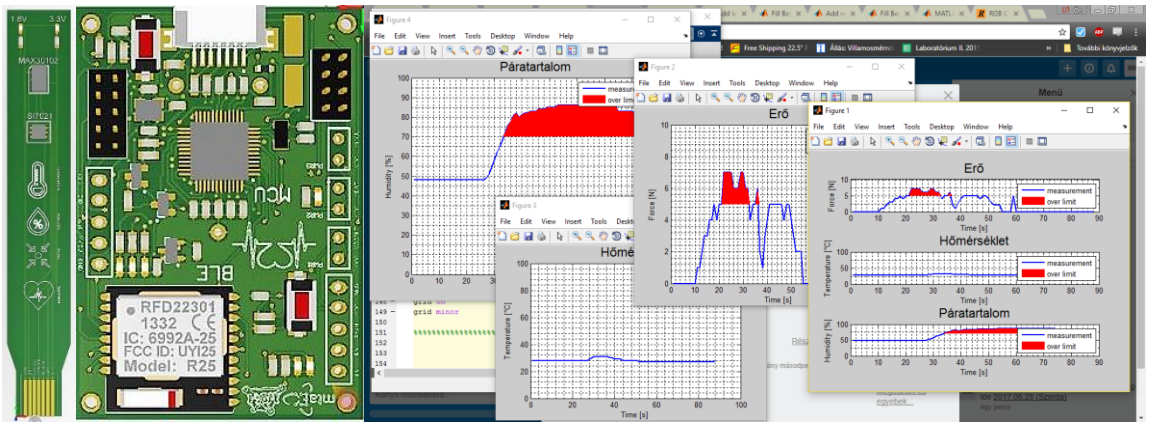

(a) *(b)* *(c)*

Figure 6-1. *Flexible PCB for sensors (a) and signal processing electronics (b) for wound healing monitoring system. The sensor data can be visualised in the application specific software (c) – WoundER / PC.*

References

[1] Tim R. Dargaville, Brooke L. Farrugia, James A. Broadbent, Stephanie Pace, Zee Upton, Nicolas H. Voelcker, Sensors and imaging for wound healing: A review, Biosensors and Bioelectronics 41 (2013) 30–42

Thin Film Physics Department

Head: Dr. Katalin Balázsi, Ph.D., senior scientist

Research Staff

- Ildikó CORA, Ph.D.
- Zsolt CZIGÁNY, D.Sc.
- Zsolt FOGARASSY, Ph.D.
- Viktória KOVÁCSNÉ-KIS, Ph.D.
- János LÁBÁR, D.Sc,
- Riku LOVICS, Ph.D.
- Fanni MISJÁK, Ph.D. (on leave, Univ. Ulm)
- Béla PÉCZ, D.Sc., deputy general director of Centre for Energy Res., MFA director
- György Zoltán RADNÓCZI, Ph.D.
- György SÁFRÁN, C.Sc.
- Attila SULYOK, Ph.D.
- Fruzsina SZIRA, Ph.D. (from November)
- Orsolya TAPASZTÓ, Ph.D.
- Lajos TÓTH, C.Sc.

- Árpád BARNA, D.Sc., Prof. emeritus
- Péter B. BARNA, D.Sc., Prof. emeritus
- György GERGELY, D.Sc., Prof. emeritus.
- Miklós MENYHÁRD, D.Sc., Prof. emeritus
- György RADNÓCZI, D.Sc., Prof. emeritus

Ph.D. students

- Erzsébet DÓDONY
- Mónika FURKÓ
- Klára HAJAGOS-NAGY (maternity leave from October)
- Nikolett HEGEDŰS (from September)
- Tamás KOLONITS
- Nikolett OLÁH (maternity leave)
- Adél RÁCZ
- Márton SZENDRŐ (to July)
- Haroune Rashid BEN ZINE ("Hungaricum stipendium")
- Awais QUADIR ("Hungaricum stipendium" to November)
- Soukaina LAMNINI ("Hungaricum stipendium" from February)
- Mohamed AFROIU ("Hungaricum stipendium" from September)

Technical Staff

- Noémi SZÁSZ
- Sándor GURBÁN
- Andor KOVÁCS
- Viktor VARGA

- Andrea J. FENYVESINÉ
- Valéria OSVÁTH (maternity leave)
- Tamás ZAGYVA (50%)
- Zsolt DALLOS (50%)

The Thin Film Physics Department, based on its half-a-century experience in the field continued its research towards modern trends in materials science. In 2018, one of the important research fields in basic science was the development of the polycrystalline coatings. Further, several international basic scientific projects and collaborations supported the research of modern semiconductor layers, hetero transitions, and 2D semiconductor layers. Another strong research line was the structural build-up of ceramics and bioceramics, including both basic and applied research. In case of technical ceramics, Si_3N_4 composites with or without addition (graphene, carbon nanotube) were studied. In case of bioceramics, improvement of hydroxyapatite development was achieved in the framework of European and domestic projects. The third intense line and uniqueness of the Department (in national and international level) was the transmission electron microscopy. Effect of microstructure on detailed material properties was demonstrated by TEM studies and it was shown that optimal structures could be reached in a controlled way. All topics were supported by methodical developments based on electron diffractions.
In 2018, 38 papers appeared in refereed journals with a cumulative impact factor of 115. In addition, 14 papers in conference proceedings were published with no impact factor. Members of the group presented

11 invited lectures, 26 oral talks and 24 posters at national and international conferences. The group received 1900 independent citations in the examined interval of the last two years. The FEMS Junior Euromat 2018 conference – the main event for young material scientists - was organized in Budapest between July 8 and 12, by the members of Thin Film Physics Department.
Research members of the group lectured three courses at universities and four members held laboratory practices. All courses were for full semester (Roland Eötvös University - ELTE, and Budapest University of Technology and Economics - BME, and Óbuda University - OE). In addition, 12 PhD students were supervised.
Social activity of the group is landmarked by 15 memberships in different committees of the Hungarian Academy of Sciences and in boards of societies, giving one elected representative to the General Assembly of the Hungarian Academy of Sciences.

Investigation of metal (Ni) induced lateral crystallization (MILC) of amorphous Si thin films at low temperature

TÉT-10-1-2011-0570

G. Z. Radnóczi, B. Pécz, I. Stoimenos, N. Frangis, N. Vouroutzis (AU, Thessaloniki)

The well-known MILC process was studied at low temperature to characterize the various ways of crystallization taking part in the process. At low temperature crystallization is dominated by the movement of the $NiSi_2$ particles forming the characteristic whiskers (Figure 1a). Further growth of the whisker sidewalls is supressed in contrast to experiments carried out at higher temperatures. Consequently, the morphology of the resulting crystalline structure will be dominated by whiskers growing in various directions. Whiskers growing in 111-type directions often change growth direction to other equivalent 111-type direction forming a 70.5°kink.
Tetrahedral $NiSi_2$ inclusions forming during crystallization and previously observed in Si whiskers grown by the MILC process were also observed in these experiments confirming that the whisker growth is very similar to other experiments (Figure 1b).
Analytical measurements were also carried out using the newly installed Themis microscope's SuperX detector system to confirm the presence of Ni at whisker tips. Unfortunately, the preparation process (etching the glass substrate under the 50 nm thick a-Si/Si film) mostly removed the $NiSi_2$ clusters leading the whisker growth, however in some exceptional cases enough silicide was preserved. Such a whisker tip is imaged in STEM-HAADF mode and shown in the figure below together with the elemental map for Ni and Si (Figure 1c).

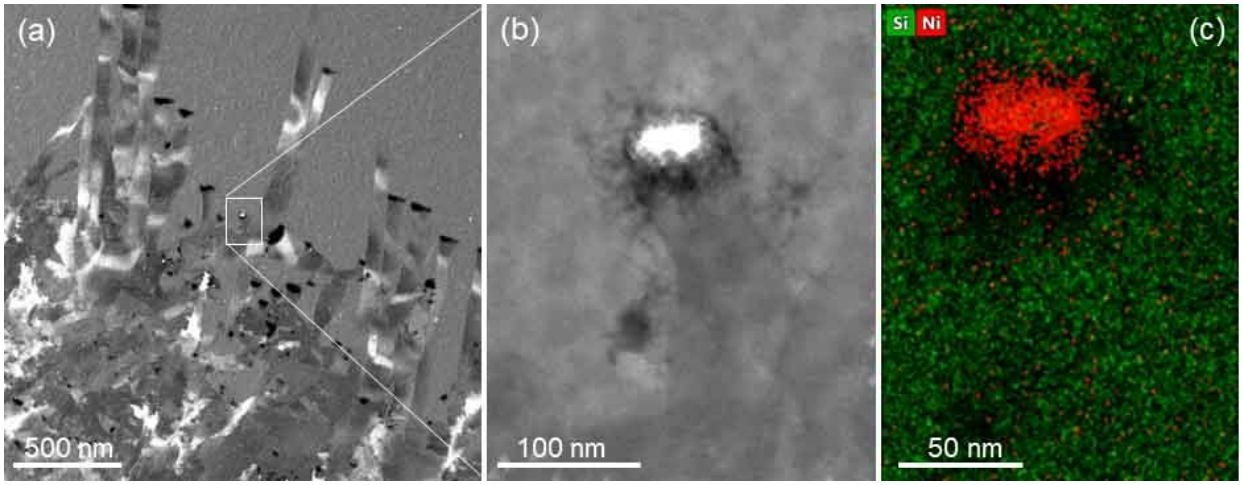

Figure 1*. a.) HAADF overview image of a group of mostly parallel whiskers. Black regions at the whisker tips are holes where the $NiSi_2$ clusters were etched during preparation. b.) an exceptional whisker with a preserved $NiSi_2$ cluster showing as a bright region due to Z-contrast and c.) EDX elemental map of Ni and Si of the region imaged in b.)*

Reference

N. Vouroutzis, J. Stoemenos, N. Frangis, G. Z. Radnóczi, D. Knez, F. Hofer, and B. Pécz, Structural characterization of poly-Si Films crystallized by Ni Metal Induced Lateral Crystallization, Scientific Reports volume 9, Article number: 2844 (2019)

Design of corrosion resistive SiC nano-layers

A. S. Rácz, M. Menyhárd

We have demonstrated earlier that applying ion beam induced mixing (IBM) at room temperature on C/Si/C/Si/C multilayer structures nano-sized SiC production occurred. It has also been shown that the appearance of nano-sized SiC rich layer improves considerably the corrosion resistance of the irradiated sample. A correlation between the corrosion resistance of the sample and the amount and distribution of SiC determined by AES depth profiling has been found [A.S. Racz et al., ACS Appl. Mater. Interfaces, 2017, 51, 44892–44899]. This observation provides the possibility of tailoring corrosion resistance of a given sample; one must determine and produce the SiC amount and distribution necessary to reach the desired corrosion resistance. If one wishes to design a protective coating allowing for various constrains concerning the layer structure, determining the optimal irradiation conditions using an experimental approach is rather time consuming and expensive, however. Therefore, we looked for applying simulation techniques.

Here we report on corrosion resistance measurements on samples produced by IBM at room temperature applying various irradiation conditions and samples containing C and Si layers of various thicknesses and numbers being on Si substrate. For ion bombardment we have used the easily available Ar^+ and Xe^+ ions. The amount and distribution of the SiC has been determined by TRIDYN simulation (not by AES depth profiling). The effective areal density of SiC (introduced in our previous work) was calculated from the SiC distribution and an excellent correlation between these quantities and the measured corrosion resistances has been found (Figure 2). Therefore, having any request for a given corrosion resistance by the help of the TRIDYN simulation we can deteremine the irradiation conditions considering the other constrains by the layer thicknesess and numbers as well. This enables a high freedom for the design of the protective coating layer.

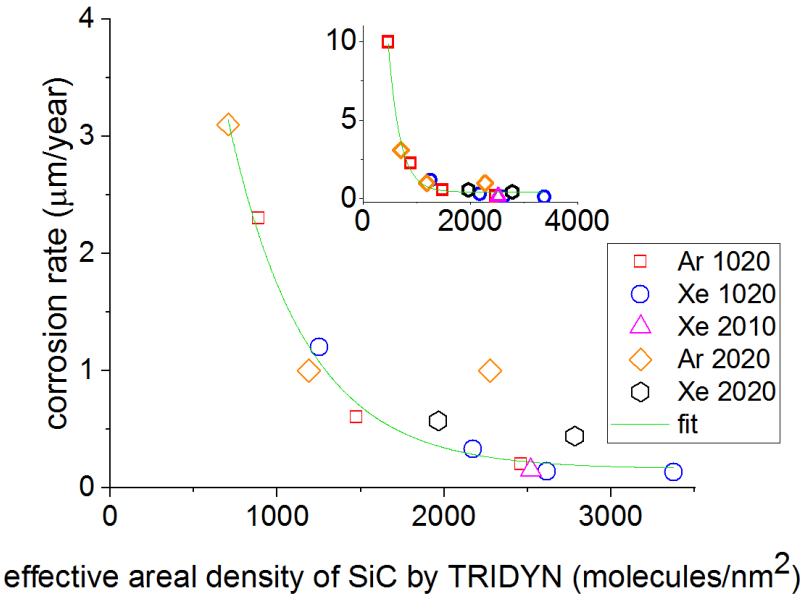

Figure 2. *The experimentally measured corrosion rate vs. effective areal density of SiC determined by TRIDYN simulation; inset enlarged y axis.*

[1] A.S. Racz, M. Menyhard: Design of corrosion resistive SiC nano-layers, ACS Appl. Mater. Interfaces, 2018, 10 (26), pp 22851–22856.

Highly Safe GaN Metal-Oxide-Semiconductor Transistor Switch (SAFEMOST)

L. Tóth, Zs. Fogarassy, I. Cora, D. Gregušová (IEE), J. Kuzmík (IEE) and B. Pécz

In the frame of the international SAFEMOST project, we continued the complex structural study of the InGaN/AlGaN/GaN heterostructures prepared by our colleagues at IEE SAS, Bratislava. The main goal was to influence the electrical polarization of the layers through incorporation of a suitable mechanical stress and thus reaching normally-off operation of the switching device.
In 2018, installation of a new aberration corrected TEM (of the type FEI Themis) in our lab opened new possibilities in our characterization spectrum. The use of the aberration corrected objective lens improved the point-to-point resolution by a factor of two (down to 0.09 nm). Also, use of several new methodologies (like scanning transmission techniques with various detectors, EDS mapping, etc.) became possible in the lab.

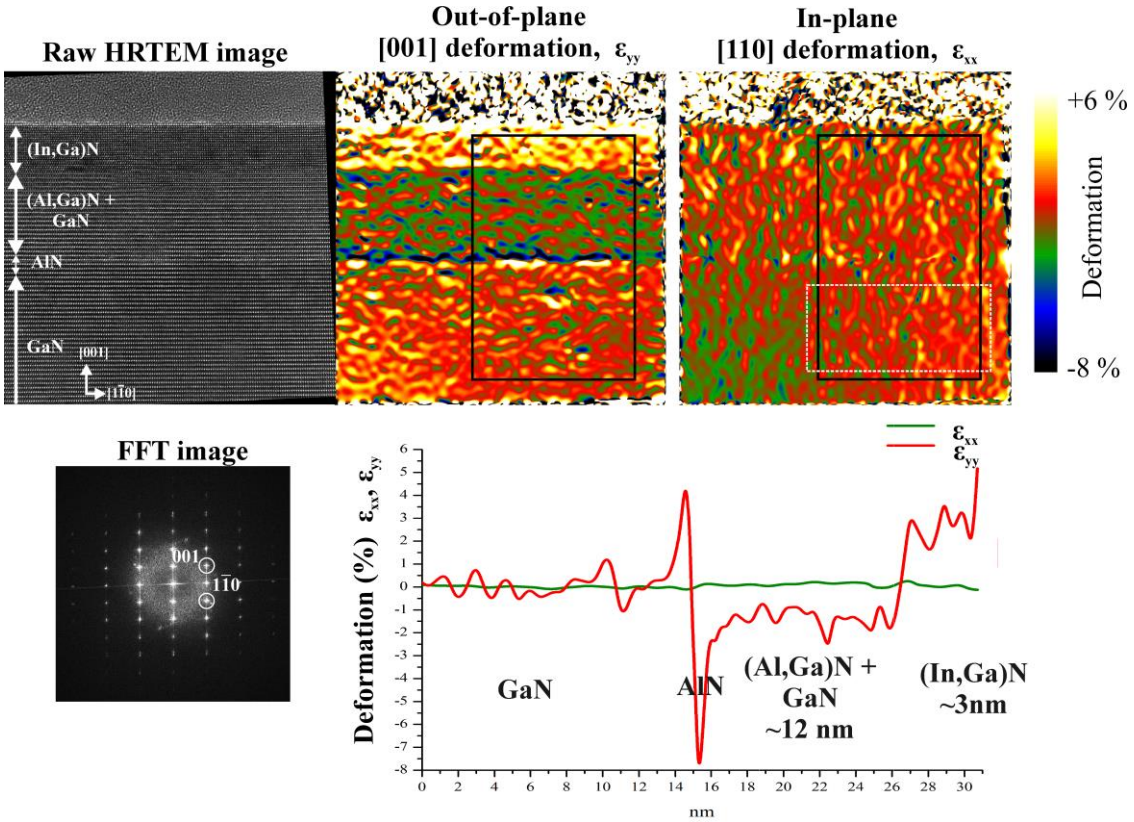

Figure 3. *Determination of local variation of the deformation tensor in a InGaN/AlGaN/GaN sample by means of the GPA technique in the aberration corrected new Themis electron microscope.*

By applying the new Themis electron microscope, local variation of the of the strain tensor components were determined using geometrical phase analysis (GPA) technique (Figure 3). Starting from high resolution images of the cross-sectional specimens and their Fourier transform, the in-plane and out-of-plane deformation components of the crystal lattice were calculated with a special software (relative to a non-deformed reference area in the same TEM lamella). It turned out that the in-plane strain component is practically zero, while the out-of-plane component followed the chemical composition of the layer structure. This means large negative strain in the AlN layer, small (1-2%) negative change in the AlGaN, and somewhat larger (3-4%) positive strain in the InGaN film (Figure 4). The elemental maps taken with the EDS system confirmed our observation. This result supports the model of the Slovakian colleagues on

the polarization effects observed by electrical measurements. These samples were found be suitable for the realization of normally-off MOS HEMT transistors after some additional processing steps.

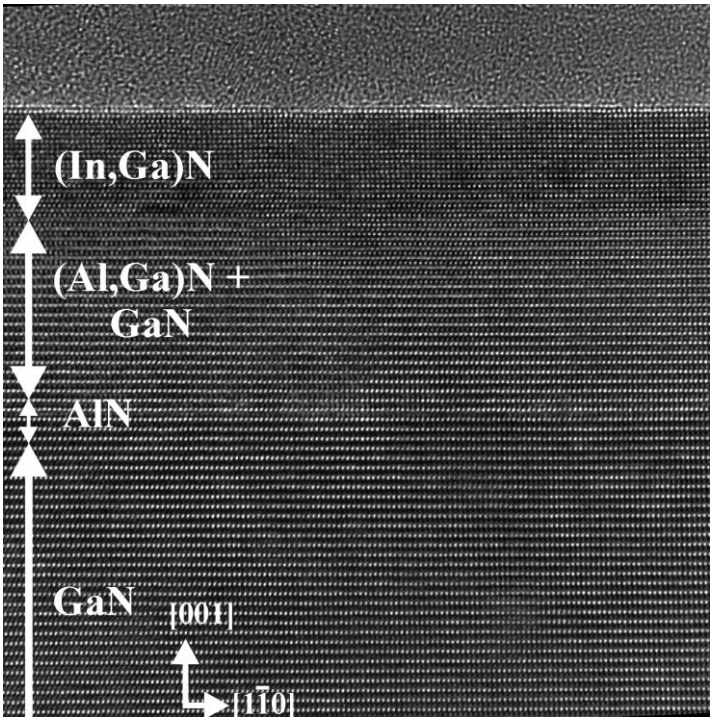

Figure 4. *High resolution micrograph of the InGaN/AlGaN/GaN cross sectional sample taken with the new 200 kV Themis electron microscope used for the above GPA analysis.*

In situ TEM and ex situ heating experiments on κ-Ga_2O_3

MTA Postdoctoral Fellowship and bilateral CNR- MTA

I. Cora[a], Zs. Fogarassy[a], B. Pécz[a], F. Mezzadri[b], F. Boschi[b], M. Bosi[b], R. Fornari[b], A. Recnik[c]
[a]MTA EK MFA, [b]IMEM-CNR, Parma, [c]Jožef Stefan Institute, Ljubljana

Ga_2O_3 is a wide bandgap semiconducting oxide (~4.7 eV), promising for UV optoelectronics and power electronics. Ga_2O_3 layers were grown onto (001) surface of α-Al_2O_3 by vapor phase epitaxy[1]. *Ex situ* heated samples up to 1000 °C and studied by XRD, DSC, TEM and simulations using JEMS software package. The *in situ* heating of cross sectional and plan view TEM lamella was also done in TEM up to 980°C in order to follow and study the κ→β (orthorhombic to monoclinic) structural transformation.
The structure of κ-Ga_2O_3 is ordered in 5-10 nm large (110)-twinned domains, and each domain has an orthorhombic structure with *Pna*2_1 space group symmetry[2]. This phase is a new polymorph among the Ga-oxides.
During the *in situ* heating experiment the structural changes and the transformation was acquired on movie and the samples were studied in detail (BF, HRTEM, SAED, simulations). Fornari *et al.* [3] earlier studied the DSC curve of the transformation and they reported a weak endothermic bent up to 650°C. We connect this bent to the moving of grain/twin boundaries, antiphase boundaries, and the enlargement of domain size in the material. Between the very spectacular κ→β phase transformation we identified no amorphous phase.
The kinetically driven phase transformation from κ to β is topotaxial, since the direction of the oxygen stacking is the same. We determined the structural relationship between the two phase and we modelled the interface. Beside the β and κ, the metastable γ phase also appears at lateral interface between β/κ and next to κ as well.
With the *ex situ* heating (up to 820°C with 2°C/min speed) of κ-Ga_2O_3 we had another transformation. We found the κ→γ phase transformation (Figure 5). The γ-Ga_2O_3 is cubic metastable phase. We studied its crystal structure by HRTEM and SAED and concluded a most probable crystal structure of it. The interface between them was also studied.

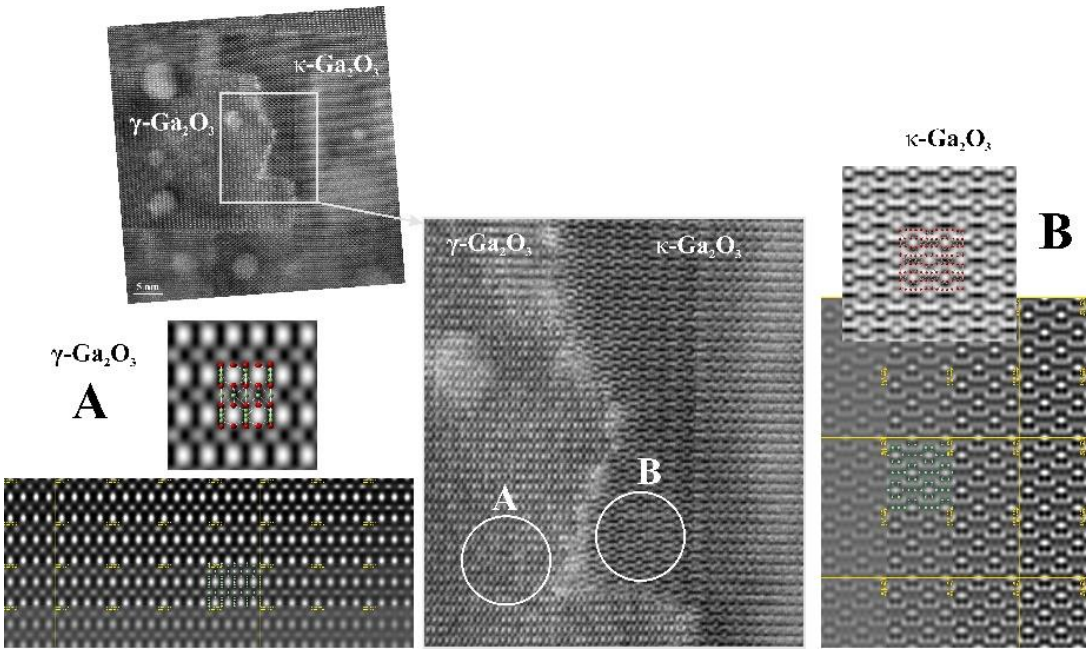

Figure 5. *The interface of the transformation on HRTEM image in the middle. Left from the interface ('A') the symmetry averaged, filtered HRTEM image of γ phase with the simulated one for comparison. Right from the interface ('B') is the same but for the κ-Ga_2O_3.*

References:

[1] F. Mezzadri, G. Calestani, F. Boschi, D. Delmonte, M. Bosi and R. Fornari. *Inorg. Chem.* 55, 12079. (2016)
[2] I. Cora, F. Mezzadri, F. Boschi, M. Bosi, M. Čaplovičová, G. Calestani, I. Dódony, B. Pécz, R. Fornari. *CrystEngComm* 19:(11) 1509-1516. (2017)
[3] R. Fornari, M. Pavesi, V. Montedoro, D. Klimm, F. Mezzadri, I. Cora, B. Pécz, F. Boschi, A. Parisini, A. Baraldi, C. Ferrari, E. Gombia, M. Bosi. *Acta Materialia* 140, 411-416. (2017)

The influence of bath additives on the thermal stability of nanocrystalline Ni films processed by electrodeposition

T. Kolonits (MFA, ELTE, PhD student), L. Péter (Wigner), I. Bakonyi (Wigner), J. Gubicza (ELTE, supervisor) and Zs. Czigány (MFA, supervisor)

The effect of various organic additives (such as saccharin and trisodium-cytrate) on the microstructure (grain size, dislocation and twin densities), mechanical properties and thermal stability of electrodeposited Ni films was investigated by X-ray diffraction (XRD) line profile analysis and transmission electron microscopy (TEM). The main task of the project is to investigate the thermal stability of different initial microstructures which could be formed by solving organic additives in the original electrolyte.

The electrodeposited layers were deposited at room temperature at low current density onto copper substrate. The basic electrolyte mainly contained nickel-sulphate ($NiSO_4 \cdot 7\ H_2O$) and boric acid (H_3BO_3). XRD and TEM grain size and phase analysis was carried out to determine the microstructure. Hardness tests were made to examine the mechanical properties. Heat treatment (at 400, 500, 600, 750 and 1000 K) was applied to investigate the stability of the micro and macro properties.

According to our former research [1] even a small amount of organic additives has a significant effect on the microstructure (grain size, defect density and texture) of nanocrystalline Ni films. In this work three different microstructures were formed: the organic additive free bath resulted a large grain size (90-130 nm), a low dislocation density ($13 \times 10^{14}\ m^{-2}$) and a (220) type texture. Trisodium citrate resulted a moderate grain size (60-80 nm) and dislocation density ($30 \times 10^{14}\ m^{-2}$) and the direction of the texture was changed into (200). The additive saccharin resulted in the smallest grain size (20-30 nm), the largest defect density ($160 \times 10^{14}\ m^{-2}$), the highest hardness and the texture was eliminated. The differences were caused by the presence of incorporating sulfur and sodium [1].

The changes of the hardness and the microstructure can be followed on Figure 6. It was found that the layer with additive saccharin which showed the highest hardness on room temperature has the worst thermal stability since the high defect density led to a large driving force for recrystallization; the recrystallization process occurred between 750-1000 K and took place in a few minutes. The best thermal stability was achieved in the layer processed with trisodium-cytrate as recrystallization has not been observed even after heating up to 1000 K.

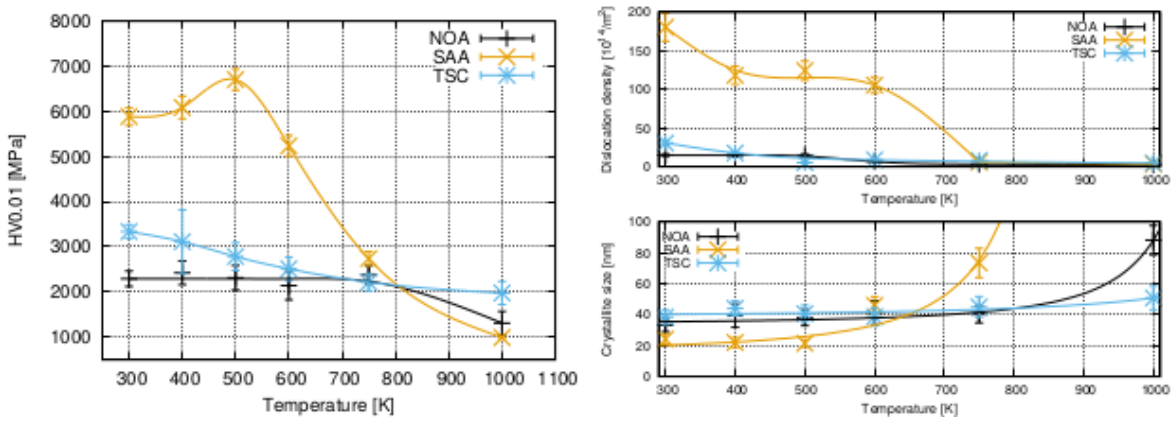

***Figure 6**. Hardness, dislocation density and crystallite size of heat treated electrodeposited nanocrystalline nickel layers*

References:

[1] Kolonits, T., Jenei, P., Péter, L., Bakonyi, I., Czigány, Z., & Gubicza, J. Effect of bath additives on the microstructure, lattice defect density and hardness of electrodeposited nanocrystalline Ni films - Surface and Coatings Technology, (2018). 349: 611-621.

Structure and mechanical properties of hard and tough WBC layers – possible industrial application.

S. Mirzaei (Brno), M. Alishahi (Brno), P. Soucek (Brno), L. Zábransky (Brno), V. Buršíková (Brno), M. Stupavská (Brno), V. Peřina (Rež), K. Balázsi (MFA), Zs. Czigány (MFA), P. Vašina (Brno)

A cooperation of Thin Film Physics Dpt. and Dpt. of Physical Electronics Masaryk University is running since 2016 in research of WBC thin films. The main challenge in deposition of protective coatings is to produce films, which simultaneously exhibit high hardness and enhanced fracture toughness. Nowadays, popular ceramic-based protective coatings show difficulties to cope with these increased demands due to their inherent brittleness. Materials exhibiting such seemingly contradictory combination of mechanical properties - high hardness and moderate ductility - was already realized experimentally in Mo_2BC and recently predicted by ab-initio calculations in crystalline X_2BC system (X = Ti, V, Zr, Nb, Mo, Hf, Ta, W). Our aim is to produce fracture tough WBC protective coatings and in the long run to produce the theoretically predicted W_2BC crystalline phase which was predicted to have the best mechanical properties in the X_2BC family. However, low enthalpy of formation of W_2BC phase and existence of WB and WC phases instead of W_2BC phase indicate difficulties of deposition of crystalline W_2BC phase. Our results were published in Surface and Coatings Technology [1,2]. In these two papers we have investigated the mechanical, bonding and structural properties of the film at fixed C content with variation of B/W ratio and constant B content with changing C/W ratio, especially in the vicinity of the composition range of W_2BC. WBC films were deposited by combination of DC magnetron sputtering of W and B_4C targets and pulsed DC sputtering for C in Ar at 500ºC. The pulsed regime resulted in 2.5 times increase of ion flux at 350 kHz and 65% duty cycle compared with DC sputtering. Bonding structure and mechanical properties were investigated by XPS and nanoindentation, respectively. Structural properties were investigated by TEM (including HRTEM and SAED) using JEOL3010 equipment at MFA. It was determined, that the coatings far from the composition of W_2BC phase are amorphous, while those coatings close to W_2BC composition are nanocomposites containing nanocrystals with size of ~5nm embedded into an amorphous matrix (Figure 7). A certain level of short range ordering can be observed even in the amorphous films which is manifested in short, curved and irregular lattice fringes in the HRTEM images. All the layers exhibited high hardness (>20GPa) so they all can be classified as hard coatings. The level of crystallinity played no crucial role in determining the hardness of the coating, while the effect of the coating structure and bonding was clear – the densest coating with the highest relative amount of W-B bonds exhibited the highest hardness of ~ 29 GPa (Figure 8).
We are planning to continue the research with coatings deposited in industrial deposition chamber and other members of X_2BC family (e.g. Mo_2BC).

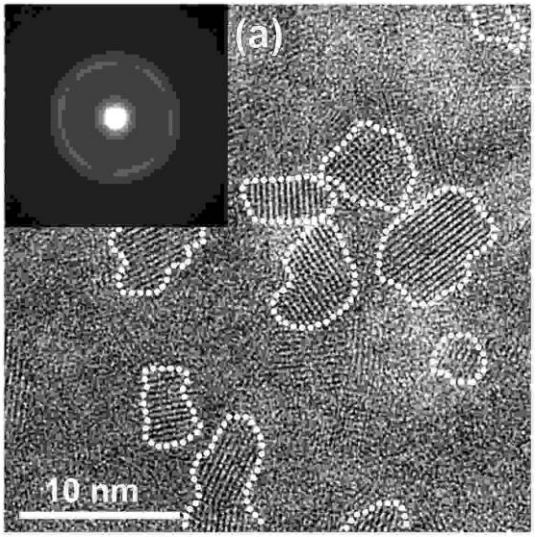

Figure 7. *HRTEM image and SAED pattern of $W_{53}B_{17}C_{30}$ film. The film has nanocomposite structure with nanocrystals embedded in the amorphous matrix.*

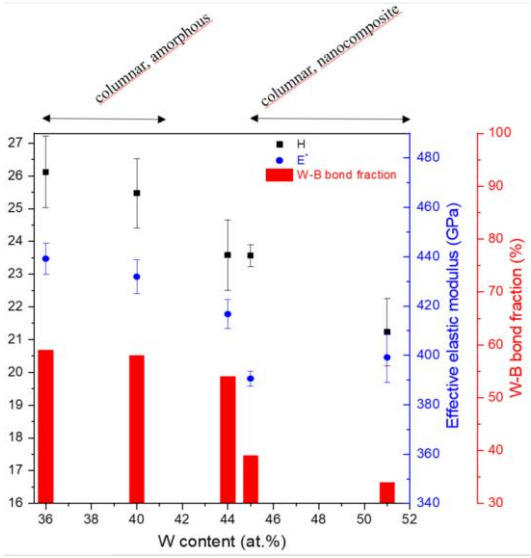

Figure 8. *Hardness and Youngs's modulus correlates with fraction of stiff W-B bonds for sputter deposited $W_xB_{70-x}C_{30}$ coatings*

References:

[1] M. Alishahi , S. Mirzaei, P. Soucek, L. Zábranský, V. Buršíková, M. Stupavská, V. Peřina, K. Balázsi, Zs. Czigány, P. Vašina, Evolution of structure and mechanical properties of hard yet fracture resistant W-B-C coatings with varying W and C content Surface and Coatings Technology 340 (2018) 103-111

[2] Saeed Mirzaei, Mostafa Alishahi, Pavel Souček, Lukas Zábranský, Vilma Buršíková, Monika Stupavská, Vratislav Peřina, Katalin Balázsi, Zsolt Czigány and Petr Vašina, On the origin of the hardness of fracture resistant W-B-C coatings with varying B/W ratio, Surface and Coatings Technology 358(2019)843-849

NEW TYPE FUNCTIONAL ALLOY FILMS

OTKA NN 112156

F. Misják[1], K. Hajagos-Nagy[1], M. Čaplovičová[2], G. Radnóczi[1]

[1]Research Centre for Energy Research, Hungarian Academy of Sciences
[2]Slovak University of Technology in Bratislava, University Science Park Bratislava Centre

Effect of growth temperature on the growth of CoCrFeNiCu high entropy alloy (HEA) films

Five-component CoCrFeNiCu HEA films were deposited by DC magnetron sputtering using spark-melted targets at background pressure of 6×10^{-8} mbar with a deposition rate of ~10 nm/min. The working pressure was 3×10^{-3} mbar by applying 99.9 % pure Argon as sputtering gas. Films were deposited onto thermally oxidized (100)-oriented Si wafers. The growth was carried out at room temperature, as well as, elevated temperature of 380 ^{o}C.
The nanostructure of the films was analyzed by transmission electron microscopy (TEM) in a Philips CM20 microscope at 200 kV accelerating voltage. HREM measurements were made in a 200 kV JEOL JEM ARM 200cF microscope. Samples for TEM investigation were produced in cross section views, embedding the films in Ti rings and grinded by mechanical polishing to about 50 μm thickness. The thinning was then followed by Ar^{+} ion milling at grazing incidence.
The structure of the films grown at room temperature is single-phase FCC and corresponds to zone T structure, with a well expressed <111> texture. Width of the columns is uniform about ~25 nm and the growth competition region is about 50 nm thick in the 500 nm thick film. The columns are rather defective, the main defects are planar defects, stacking faults and twin lamellae. Their density is very high; it is around 2-3 faults/nm (Figure 9). As the film is grown in good vacuum conditions ($p=6x10^{-8}$ mbar) no impurity effects are expected to be present. The impingement rate of oxygen/metallic species is $\sim5x10^{-3}$. The five-constituent components are randomly distributed in the FCC structure; no ordering or separation of components is detected.

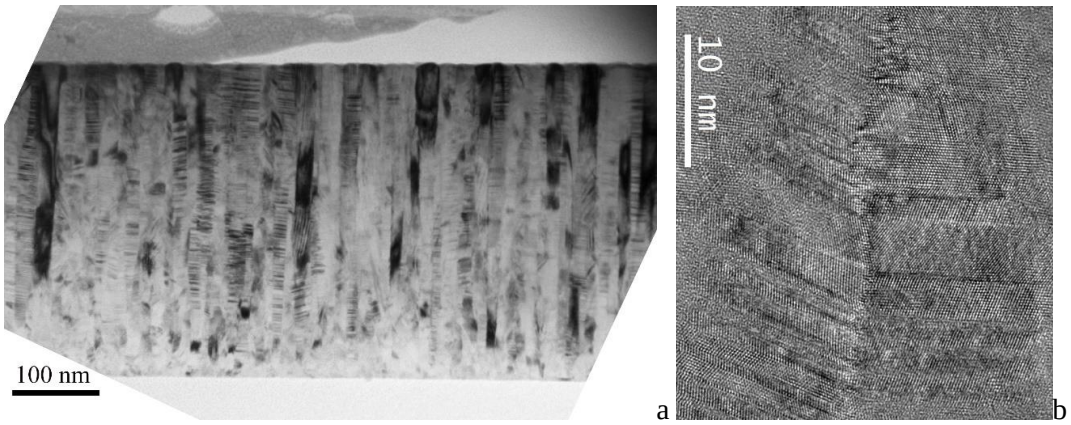

Figure 9. *Overall (a) and high resolution (b) image of CrFeCoNiCu alloy film grown at 20^{o}C substrate temperature and $6x10^{-8}$ mbar background pressure.*

The morphology of the film grown at 380 ^{o}C substrate temperature corresponds to the transition between zones II and III of the structure zone model and possesses dominant single phase FCC structure. Repeated nucleation is clearly observed (Figure 10a), meaning the formation of a covering or blocking layer during the growth of alloy crystallites.

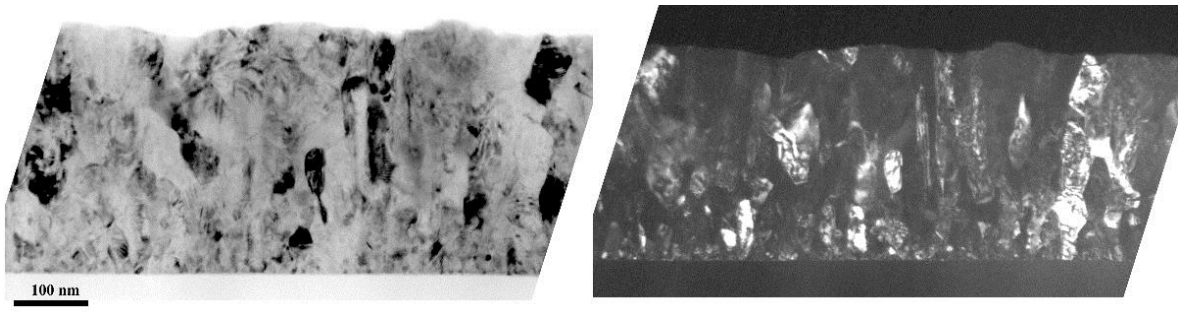

a)

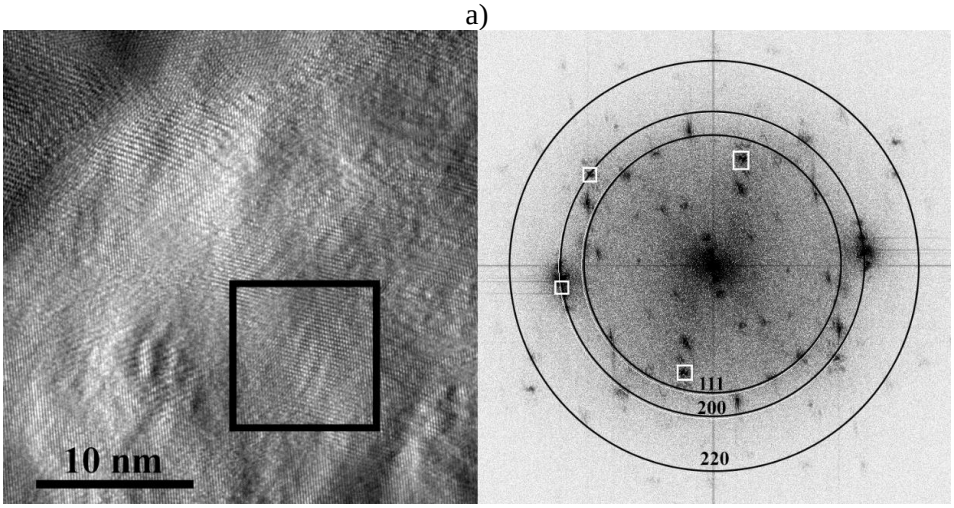

b)

Figure 10. *Overall bright field and dark field (a) and high resolution and FFT (b) images of CrFeCoNiCu alloy film grown at 380^{o}C substrate temperature and 4x10^{-6} mbar background pressure.*

This is also supported by the random crystallographic orientation of the grains. The vacuum during growth was maintained at p=4x10^{-6} mbar, resulting in an impingement ratio of impurity to metal species ~1x10^{-1}.

This impingement ratio can result in the formation of a covering layer (either oxide or nitride or their mixture) leading to repeated nucleation. The FFT (Fast Fourier Transform) obtained from the high resolution image shows the presence of the FCC reflections (those falling on the rings in Figure 10b) but shows the presence of other reflections as well, indicating the formation of second crystalline phases in the film. Their quantity is however small, as they are not detectable in the overall diffraction patterns obtained from the film.

TEM study of copper silicides

E. Dódony (PhD student), G. Z. Radnóczi (supervisor)

Copper-silicides attracted considerable interest due to their wide range of applications. Cu_3Si is an important phase of the family (Figure 11). It is used in ultrapure silicon synthesis for photovoltaic and electric devices, as contact material in microelectronics and as catalyst for carbon nanowire and semiconductor production. Despite the importance of copper-silicides, their phase and structural relations are not entirely solved yet. Due to their importance, we are studying the formation of copper-silicides in thin amorphous silicon (a-Si) films. A 10 nm thick a-Si film was transferred to copper grid (Cu-grid) and heated in-situ in a Philips CM20 transmission electron microscope. During the heating the Cu-grid acted as an unlimited source for the diffusion of metal into the a-Si film. Silicide formation started at 500 °C (Figure 12). We observed the η-Cu_3Si-phase and its modulations during our experiments.

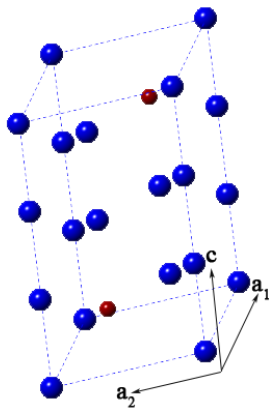

***Figure 11**. Structural model of Cu_3Si; space group: P-3m1, a_0: 4.06 Å, c_0: 7.33 Å*

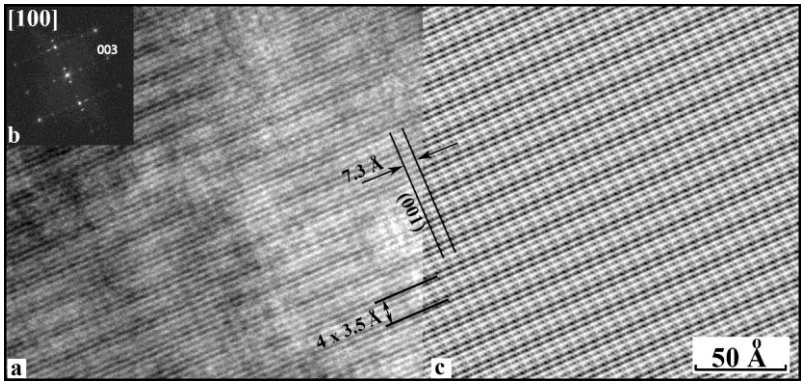

***Figure 12.** Raw [100] projected experimental HRTEM image of modulated Cu_3Si with four times of the (100) periodicity (= 14.0 Å) of the basic structure (a), its Fourier-transform (b) and the Fourier-filtered experimental image (c)*

For the phase and structural measurements, we recorded high resolution (HRTEM) images and selected area electron diffraction (SAED) patterns, under Jeol3010 and Philips CM20 transmission electron microscopes, respectively. By analyzing SAED patterns and HR images, we found that the η-phase's structural model does not fit our experimental data and that many modulations of the phase formed under the experimental conditions.

Through measurements, calculations and modelling we gave a new structural model for the η-Cu_3Si-phase (Figure 11) and solved two of the many modulations formed by the different ordering of the Cu – Si atoms forming supercells. One is shown in Figure 12 with modulation in the ***a*** direction with four times periodicity of the basic Cu_3Si structure.

The influence of artificial aging on the microstructure of an Al-Zn-Mg-Zr alloy processed by equal channel angular pressing

2017-2.3.4-TÉT-RU-2017-00005, VEKOP-2.3.3-15-2016-00002

J. L. Lábár (MFA), J. Gubicza[1], J. Lendvai[1] and N. Q. Chinh[1]

[1]Department of Materials Physics, Eötvös Loránd University

There is a large interest in age-hardenable Al-Zn-Mg alloys (7xxx series) due to their technological and practical importance, as these alloys can be treated to have a preferable combination of ductility and strength, as well as reasonable weldability and corrosion resistance. If a supersaturated Al-Zn-Mg alloy is aged under different conditions, various metastable and stable precipitates may form. Therefore, aging can be used for tailoring mechanical behavior of these alloys. Although, the microstructure obtained by ECAP has been extensively studied in the literature, the effect of artificial aging on the precipitation and the strength of SPD-processed supersaturated Al-Zn-Mg alloys has not been clarified so far.
In this paper, the effect of artificial aging on the microstructure and hardness of an ultrafine-grained (UFG) Al-4.8%Zn-1.2%Mg-0.14%Zr (wt.%) alloy was studied. The UFG microstructure with an average grain size of about 260 nm was obtained by severe plastic deformation (SPD) applying four passes of equal channel angular pressing (ECAP) at room temperature. Then, artificial aging was performed on the ECAP-processed samples at 120 °C and 170 °C for 2 h.

The size and morphology of the matrix grains and the precipitates were characterized by transmission electron microscopy (TEM). Thin TEM-lamellae were prepared by Ar-ion milling with special care taken to avoid heating (and possible transformation) of the samples during preparation. TEM and energy-disperse X-ray spectroscopy (EDS) examinations were performed in a Titan Themis G2 200 STEM equipped with a four-segment Super-X EDS detector. The corrector for the spherical aberration (Cs) was applied at the imaging part, while no probe-correction was present. Image resolution limit is 0.08 nm in phase-contrast HRTEM mode, while resolution is 0.16 nm in STEM Z-contrast imaging mode (recorded with a Fishione high-angle annular dark-field (HAADF) detector). HRTEM images were recorded at 200 keV with a 4k × 4k CETA 16 CMOS camera. EDS data were recorded (together with the HAADF signal) in spectrum-image (SI) mode, where individual X-ray count data can later be post-processed pixel-by-pixel and elemental intensities (and quantified elemental concentrations) can be obtained from any post-selected regions. In that way, distribution of concentrations can be visualized along any lines or over any area.
In the ECAP-processed sample Guinier-Preston (GP) zones, $MgZn_2$ precipitates and a high dislocation density were observed (Figure 13). After aging at 120 °C, coarse $MgZn_2$ precipitates were formed in the grain boundaries, leading to softening, while the dislocation density did not decrease (Figure 14). Annealing at 170 °C yielded a growth of the matrix grains to ~530 nm with a significant decrease of the dislocation density (Figure 15). In addition, GP zones disappeared and $MgZn_2$ precipitates were formed in both the grain interiors and the boundaries. This overaging of the precipitate structure and the decrease of the dislocation density resulted in a lower hardness than after annealing at 120 °C. It was found that the hardness-reduction due to the change of the precipitate structure at 170 °C was higher than that caused by the decrease of the dislocation density.

This research was supported by the Hungarian-Russian bilateral Research program (TÉT) No. 2017-2.3.4-TÉT-RU-2017-00005 and by grant no. VEKOP-2.3.3-15-2016-00002 of the European Structural and Investment Funds.

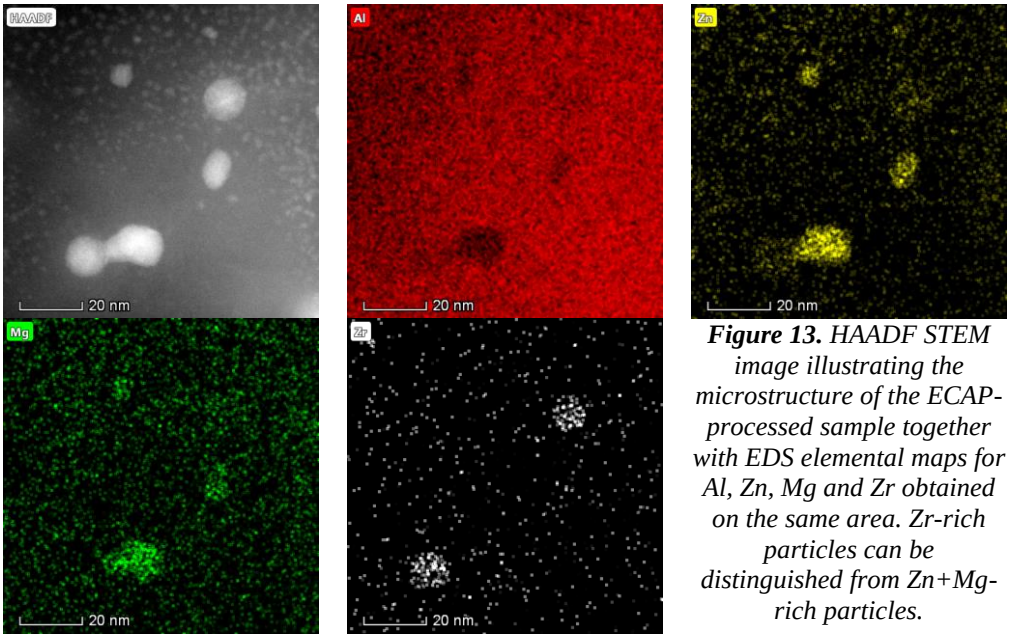

Figure 13. *HAADF STEM image illustrating the microstructure of the ECAP-processed sample together with EDS elemental maps for Al, Zn, Mg and Zr obtained on the same area. Zr-rich particles can be distinguished from Zn+Mg-rich particles.*

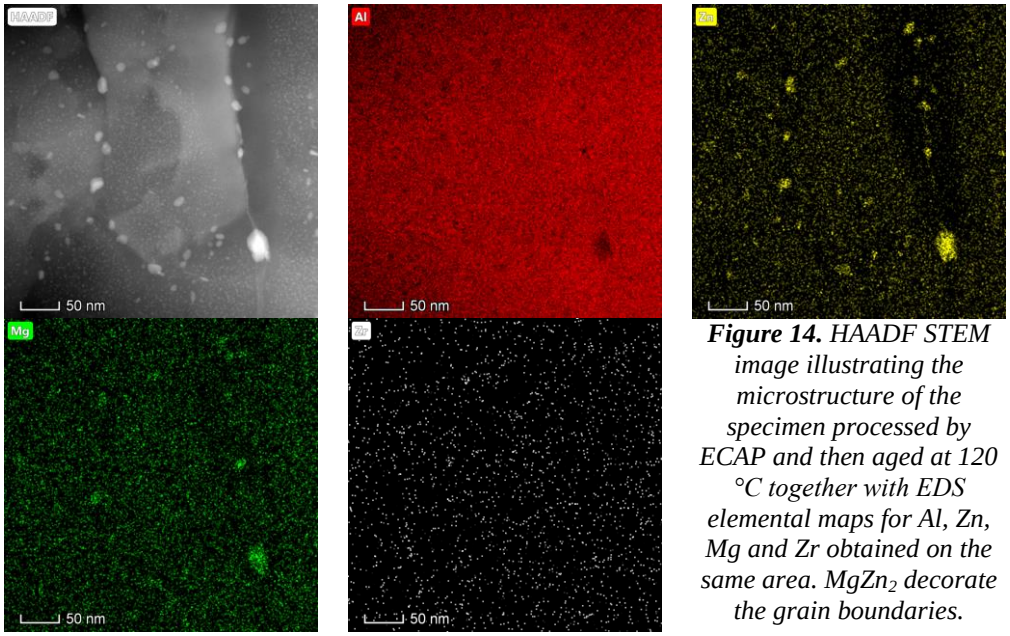

Figure 14. *HAADF STEM image illustrating the microstructure of the specimen processed by ECAP and then aged at 120 °C together with EDS elemental maps for Al, Zn, Mg and Zr obtained on the same area. $MgZn_2$ decorate the grain boundaries.*

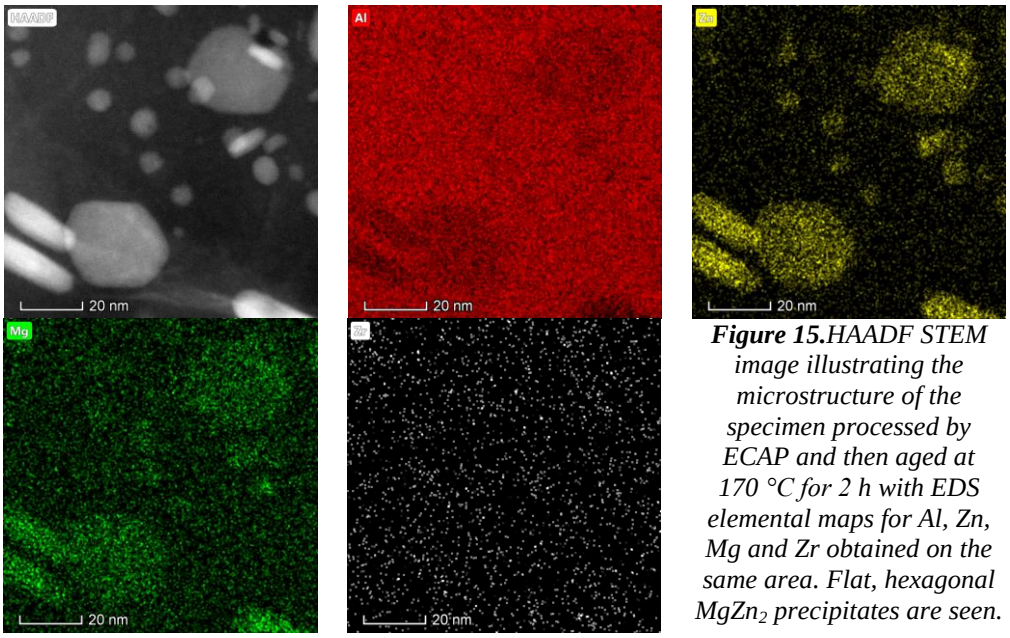

Figure 15.*HAADF STEM image illustrating the microstructure of the specimen processed by ECAP and then aged at 170 °C for 2 h with EDS elemental maps for Al, Zn, Mg and Zr obtained on the same area. Flat, hexagonal* $MgZn_2$ *precipitates are seen.*

Wear mechanism of spark plasma sintered MWCNTs reinforced zirconia composites under dry sliding conditions

S. Lamnini (PhD student), K. Balázsi (supervisor), C. Balázsi (supervisor)

Multiwall carbon nanotubes (MWCNTs) reinforced ceramics matrix served not only as enhancing factor of the mechanical properties, but also enabled the formation of an intrinsic solid lubricant effect, thus affording low friction response and remarkable wear resistance. However, controversial results have been often reported with different concentrations. In this work, multiwall carbon nanotubes (MWCNTs) reinforced 8 mol. % yttria-stabilized zirconia (8YSZ) composites were synthesized using ball milling and spark plasma sintering (SPS, at 1400 °C) in different compositions (0, 1, 5, 10 wt. % MWCNTs). The aim of our investigation is to provide an explicit understanding of the wear mechanism features evaluated after friction-test against Si_3N_4 balls used as a counterpart, which can contribute largely to avoid the easier mechanical failure. Furthermore, the effect of sliding speed namely at low (V1= 0.036 m/s) and high (V2= 0.11 m/s) was also highlighted (Figure 16). In fact, an outstanding wear improvement at low sliding speed (V1) was reported with the addition of 1 wt. % of MWCNTs. This was most likely attributed to two main raisons: 1) the formation of a perfectly continuous and uniform tribo-film. 2) the improved flexural strength, fracture toughness and density. Based on Scanning Electron Microscopy (SEM) and Energy Dispersive X-ray spectroscopy (EDS) results, we have concluded that the applied sliding speed, grain size /geometry, surface roughness, MWCNTs content and its dispersion into the matrix, altogether plays a vital role to beneficially or adversely influence the tribological performance of the composites.

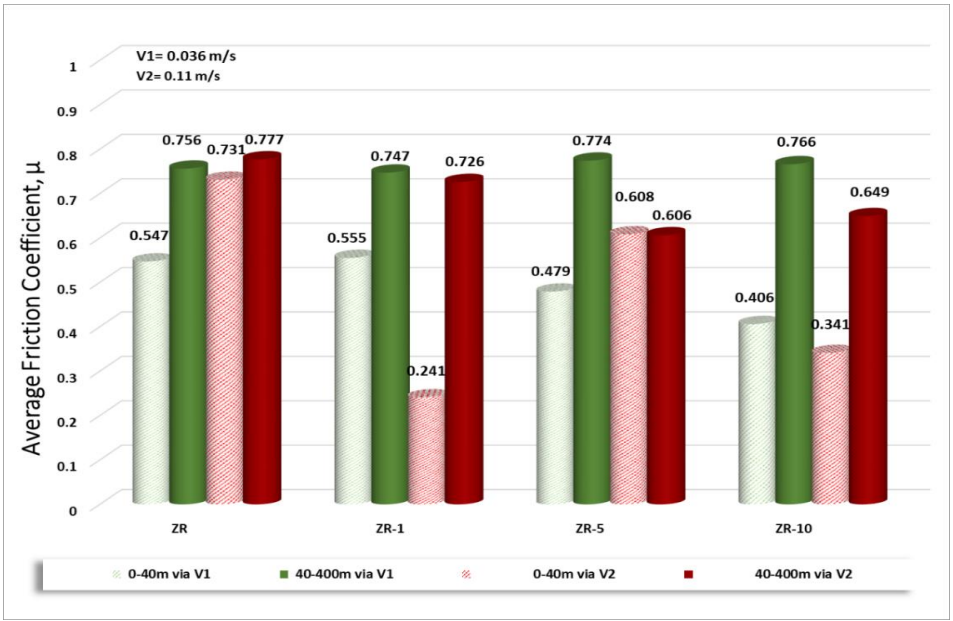

Figure 16. *Comparative graph presenting the Average Friction Coefficient (μ) during transitory state (0-40m) and steady state (40-400m) for all the composites tested at fix normal load (5N) and different sliding rates (V1=0.036 m/s, V2=0.11 m/s).*

Examination of milled h-BN addition on sintered Si_3N_4h-BN ceramic composites

OTKA NN127723 FLAG.ERA "Ceranea"

K. Balázsi, M.Furkó, Zs. Fogarassy, C. Balázsi

Silicon nitride (Si_3N_4) ceramics containing 1 and 5 wt.% of hexagonal boron nitride (h-BN) have been prepared by attrition milling and hot-isostatic pressing using three different milling conditions. Thorough morphological characterizations have been carried out to reveal the influence of the milling parameters on the size of the h-BN additives. The results confirmed significant decrease in h-BN particle size by increasing milling time. The transmission electron microscopy (TEM) observations revealed that the h-BN particles were evenly incorporated into the ceramic matrix (Figure 17). Moreover, the increase of the h-BN content decreased significantly the hardness of materials and the hardness values were higher when the size of h-BN was larger (Figure 18).

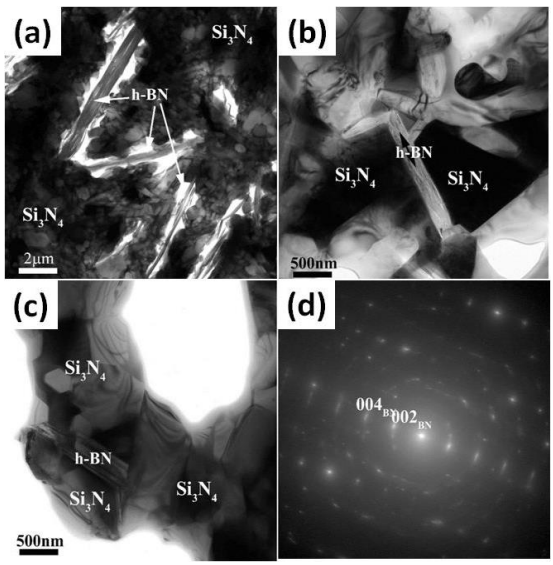

Figure 17. *Bright-field (BF) TEM images of B1/5 (a) C2/1 (b) and D3/1 (c) samples as well as selected area electrondiffraction (SAED) on one h-BN platelet within the B1/5 sample (d).*

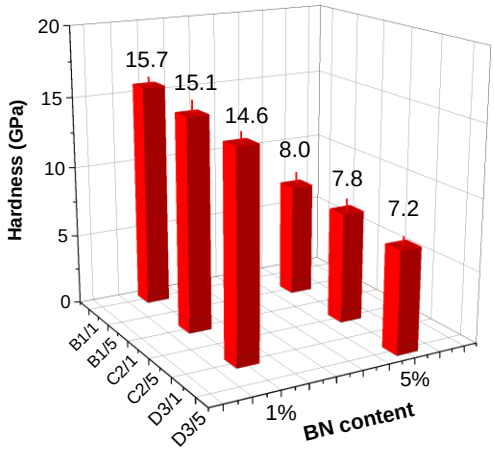

Figure 18. *Hardness measurement on Si_3N_4/h-BN composite samples containing 1 and 5 wt.% h-BN additives prepared with different methods. B1/1 and B1/1 samples: h-BN added without pre-milling, C2/1 and C2/5 samples: h-BN added 30 minutes before the milling, D3/1 and D3/5 samples: h-BN added at the beginning of the milling*

CO_2 reforming of methane by Ni–In/SiO_2 catalyst with no coke formation

J. Károlyi, M. Németh, C. Evangelisti, G. Sáfrán (MFA), Z. Schay,
A. Horváth, F. Somodi

The current opinion is that the reduction of carbon dioxide with methane (dry reforming of methane (DRM) $CO_2 + CH_4 = 2CO + 2\ H_2$) would be a suitable reaction, since the product is synthesis gas, which is one of the most important feedstock of chemical industry [1-3]. Unfortunately, carbon deposits more readily form on nickel than on noble metal surfaces during the reaction leading to fast deactivation of the catalyst. Potential catalysts for CO_2 – methane dry reforming were tested in a cooperation of MTA EK Surface Chemistry and Catalysis Laboratory and CNR, Institute of Molecular Science and Technologies Milano [4]. It was shown that the presence of 2 wt% indium on the surface of a 3 wt%Ni/SiO_2 catalyst prevented coke formation during dry reforming of methane.
In efforts to understand the mechanism, TPR revealed that indium was unstable against sintering without nickel on the silica surface, however in the bimetallic catalyst it was in metallic state and mixed with nickel after reduction at 700 °C. The presence of indium profoundly changed the adsorption properties of nickel, as CO-TPD measurements suggested. XPS measurements showed changes in the electronic structure of nickel on the Ni–In/SiO_2 catalyst after reduction, moreover, they revealed the presence of bimetallic particles which surface composition found to be $Ni_{2.2}In$, lower than the expected Ni_3In, referring to indium enrichment on the surface.

***Table 1**. Hydrogen consumption during TPR and the average particle size and dispersion of nickel calculated based on the results of CO pulse chemisorption.*

	3 wt% Ni/SiO_2			3 wt%Ni–2 wt%In/SiO_2		
	1st	2nd	3rd	1st	2nd	3rd
H_2 (cm^3 /g) [a]	9.8	10.3	10.5	15.4	15.3	14.7
CO (cm^3 /g)	0.4	0.8	0.7	1.3	0.7	0.6
D (%) [b]	4.3	7.1	6.0	11.7	5.8	5.2
d (nm) [b]	23.4	14.3	16.9	8.6	17.5	19.5

[a]Values at standard temperature and pressure (22414 cm^3 /mol).
[b]Values calculated from the amount of chemisorbed CO.

Simultaneously, HRTEM analysis of the bimetallic catalyst showed the presence of NiIn and Ni_2In alloy nanoparticles. TEM analysis of the spent catalysts after 24h time on stream showed that the average particle size of the bimetallic catalyst was slightly smaller than that of the monometallic catalyst.
Based on the present results, the higher catalytic activity and outstanding carbon tolerance of the bimetallic Ni–In/SiO_2 catalyst is the consequence of a structural and electronic effects of indium.

References
[1] S. Wang, G.Q. (Max) Lu, G.J. Millar, Energy Fuels 10 (4) (1996) 896.
[2] M.-S. Fan, A.Z. Abdullah, S. Bhatia, ChemCatChem 1 (2) (2009) 192.
[3] G. Centi, S. Perathoner, Catal. Today 148 (3–4) (2009) 191.
[4] J. Károlyi, M. Németh, C. Evangelisti, G. Sáfrán, Z. Schay, A. Horváth, F. Somodi,
Journal of Industrial and Engineering Chemistry 58 (2018) 189–201.

Thinning of TEM samples (know-how)

György Sáfrán, Noémi Szász

Introduction

Conventional preparation of TEM samples in MTA EK MFA is carried out by Ar-ion beam thinning so that the sample is mounted on the holder by carbon paste. Carbon contamination of samples is a severe problem when working with new generation C_s-corrected Transmission Electron Microscopes (TEM). High intensity beam in HRTEM and STEM modes may, unfortunately, deposit artefacts of cracking products from the migrating residue of the carbon paste. The deposited contamination raise difficulties or balks the TEM investigation. Fixing the sample with carbon paste is difficult and time consuming. Furthermore, it is risky, since during its removal the sample may be spoiled with the dissolved carbon paste. Consequently, using carbon paste is disadvantageous from the point of view of both preparation and TEM study of the samples! The installation of the C_s-corrected TEM "THEMIS" in the Thin Films Physics Laboratory arise the need to further develop our thinning technology and to skip carbon paste.

New technology and sample holder design

In order to replace carbon paste used earlier for mounting the samples a new sample holder (Figure 19) has been constructed that implements mechanical fixing of the sample. In addition, with carbon-free technology in mind, we changed the composition of glue that embeds the slabs of samples into the Ti disk: instead of Araldite mixed with carbon powder we use Gatan G1 with alumina or Ti-powder (Figure 20).

Results

The new mechanical construction, together with the new composition of embedding glue, was tested in our lab during daily TEM sample preparations over the year 2018. It showed, undoubtedly, that the new solution provides reliable, clean, mounting of samples, good heat conductance, small access angle of ion beam, backlight illumination- and centering possibility. Besides, it is simple and cheap, easy to manufacture, and compatible with all variations of sample holders from IV 3 till IV7.

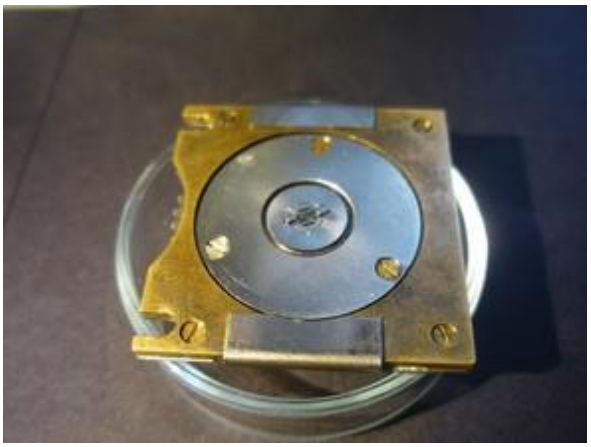

Figure 19. *View of the newly designed holder for ion beam thinning of TEM samples. The sample is fixed mechanically with Ti clamps.*

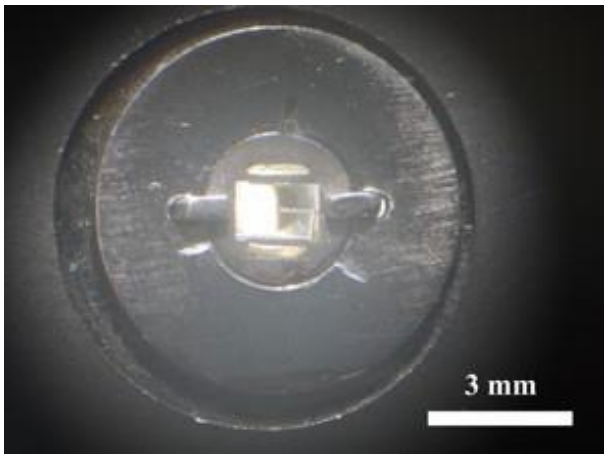

Figure 20. *Seat plate with the sample and the fixing clamps. The offset position demonstrates that the construction permits sample centering.*

Exploitation of know how

Beside daily utilization in the Thin Films Physics Laboratory the know-how of the new construction has been sold for 3MFt to TECHNOORG LINDA, manufacturer of our ion beam thinning equipment.

Micro-combinatorial analysis of concentration dependent properties of binary films

G. Sáfrán, T. Lohner, B. Kalas, P. Petrik, Zs. Zolnai, M. Serényi, M. Fried, G. Dobrik, J. Gubicza (ELTE), N.Q. Chinh (ELTE)

A "one sample concept" combinatorial method has been worked out and patented for an efficient TEM study of concentration dependent properties of binary films [1,2]. The new technique called „μ-combinatory" has been adapted to further analytical measurements e.g. AES, XRD, RBS, ellipsometry, nanoindentation. Contrary to traditional "multiple sample combinatorial techniques" we synthetize a single sample of suitable size that exhibits a concentration gradient and includes all compositions of a binary system. The μ-combinatorial sample for TEM appears as a thin gradient film on a 3mm diameter TEM grid, while for other analytical measurements the gradient sample is deposited on a 25x10 mm^2 wafer. That permits a very efficient, even automated, analysis of the microstructure, physical and chemical properties and the collection of complete data libraries within a single measuring session. A major technical progress in 2018 was that the manual control has been replaced by a processor unit controlling both power of DC magnetrons and synchronized movement of the mechanics.
The efficiency of the method is demonstrated by achievements as below.

AlMg system: In a cooperation with N.Q. Chinh (ELTE) TEM and nano-hardness studies of the AlMg system were carried out in the technologically relevant range of 0-30 Mg%. Figure.1. shows the microstructure revealed by TEM and SAED of MgAl at 1%, 10% and 30% Mg content indicating that Mg addition radically decreases grain size. Pure Al layer shows fcc Al phase with large grains of typically 60-120nm. By adding 1w% Mg the grain size decreases to 30-100nm. Up to about 10% Mg the fcc Al(Mg) solid solution phase is present exhibiting 20-40nm grains. At 25% Mg and above (30%), however, a very fine grained Al_3Mg_2 phase appears beside the still existing fcc Al(Mg) that shows 10-20 nm size grains (Figure 21).
Nanoindentation measurements pointed out that 1% Mg content increases hardness to 3-times of that of Al, followed by monotonous increase to a saturation of 4.5-times of Al at 20% Mg.

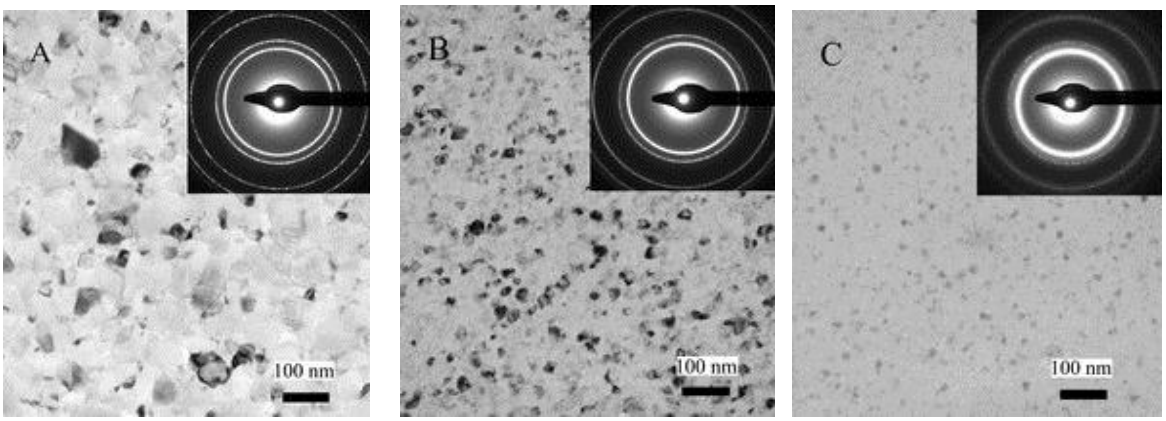

***Figure 21**. BF TEM and SAED of MgAl μ-combinatorial sample measured at (a) 1%, (b) 10% and (c) 30% Mg content places revealed 30-100nm, 20-40nm and 10-20nm grain sizes, respectively: Mg addition decreases, remarkably, the grain size and, simultaneously, increases hardness.*

SiGe system: TEM, RBS, and ellipsometry investigations were carried out, together with researchers of the Photonics Laboratory, on non-hydrogenated μ-combinatorial SiGe samples. The concentration diagrams, depicted in Figure 22, measured by RBS and EDS along the length of the 25x10mm^2 size μ-combinatorial sample show linear change with the position. The full range concentration dependence of

refractive index **n** and absorption **k** of a-SiGe (Figure 23) was determined and plotted in a color-coded map by ellipsometry in the λ=400-1600 nm wavelengths range [3,4]. The extracted diagrams show Vegard's low-like, linear dependence of **n** and **k** on composition. Similarly, XRD measurements (by J. Gubicza, ELTE) of SiGe layers crystallized by annealing also showed Vegard's low-like, linear dependence of lattice parameter on composition.

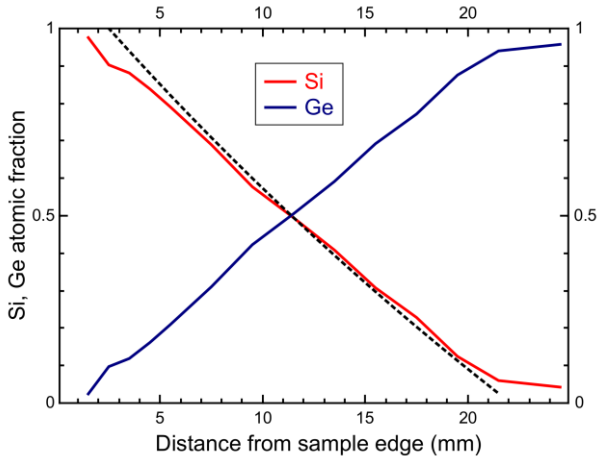

Figure 22. *Concentration diagrams measured along the gradient of a μ-combinatorial SiGe sample (25x10mm^2 size) by RBS (continuous) and EDS (- - -), respectively.*

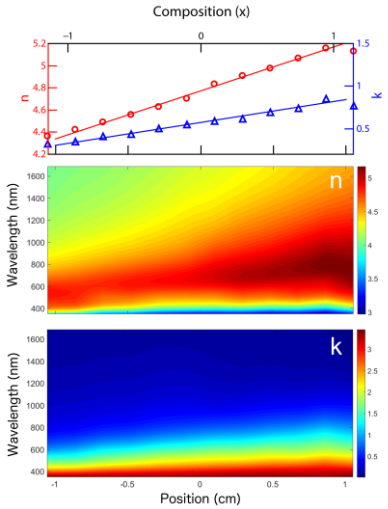

Figure 23. *Color-coded maps of refractive index **n** and absorption **k** of a-SiGe as a function of composition at wavelengths of λ=400-1600 nm. Top: cleared diagrams of **n** and **k** at λ=849.7 nm. (Positions of -1, 0 and 1 cm correspond to Si_xGe_{1-x}= 1, 0.5 and 0, respectively.)*

References

[1] Sáfrán György: Hung. Patent #P1500500.
[2] György Sáfrán: Ultramicroscopy 187 (2018) 50–55
[3] T. Lohner, B. Kalas, P. Petrik, Zs. Zolnai, M. Serényi,G. Sáfrán: Appl. Sci. 2018(8) 826
[4] OTKA K129009 "Efficient, combinatorial synthesis and analysis of cutting edge functional materials"
[5] Hungarian Development and Innovation Operative Program GINOP-2.1.7-15-2016-02073 The development of the μ-combinatorial method and device is done in a co-operation of MTA EK MFA and Holocom

Development and characterization of multi-element doped hydroxyapatite coatings on metallic implant materials

M. Furkó (PhD student), C. Balázsi (supervisor)

The aim of this research work is to develop coatings onto implant materials which possess both antimicrobial and biocompatible properties. Coatings were prepared by pulse current deposition technique. The pure hydroxyapatite (HAp) layer was doped and co-deposited with Ag^{+}, Zn^{2+}, Mg^{2+} and Sr^{2+} ions (Figure 24). The corrosion and biodegradable properties of layers were studied by carrying out electrochemical impedance spectroscopy measurements in simulated body fluid (SBF) using three-electrode open cell over a long time period. The biocompatible characteristics of layers were investigated by seeding osteoblast-like MG-63 cells onto the samples' surface. The most corrosion rate of coating increase with immersion time, which proves its biodegradable property (Figure 25).

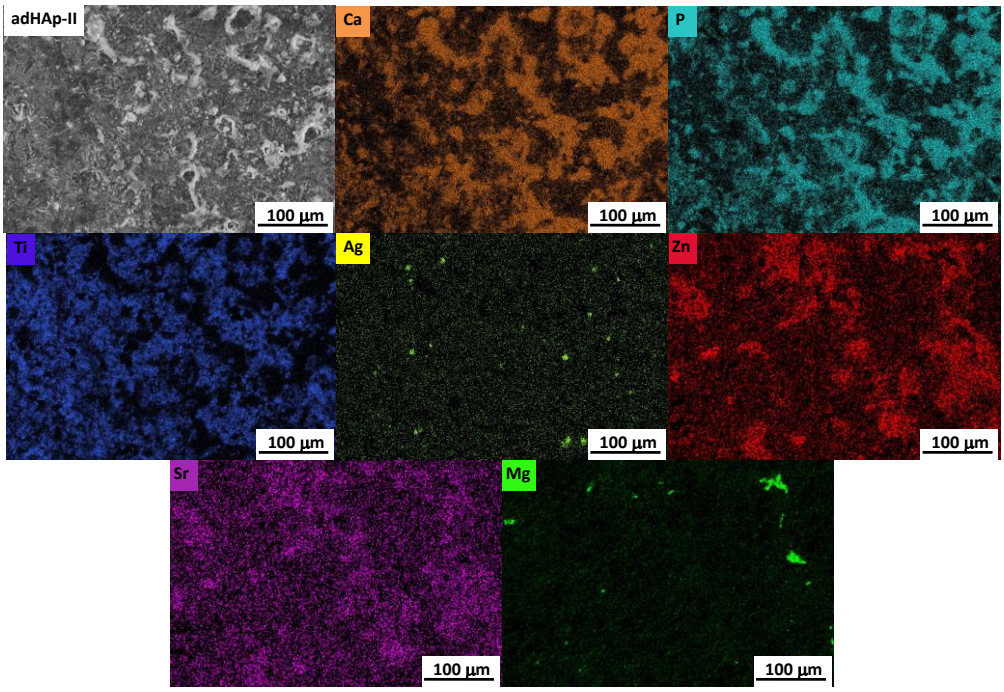

Figure 24*. The elemental map of the composition of multi-element doped HAp (reference - silver, Ca - orange, P - blue, Ti – dark blue, Ag - yelow, Zn - red, Sr - purple, Mg - green).*

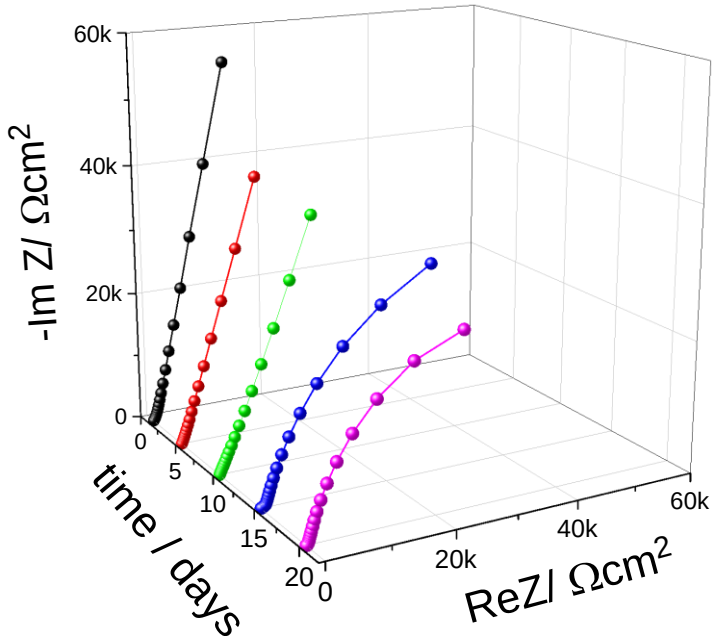

***Figure 25**. Nyquist diagrams of multi-element doped HAp coated Ti6Al4V alloy. The curves were recorded several times over a two-week period in SBF solution at 37 °C.*

Ceramic dispersed austenitic strengthened steels (CDSS)

H. R. Ben Zine (PhD student), F. Cinar Sahin (ITU Istanbul), Zs. Czigány, K. Balázsi (supervisor), C. Balázsi (supervisor)

In this work, the 316L austenitic strengthened stainless steel based composites were developed by powder technology. Attrition milling and sintering were used for production of CDSS with 0.33 wt% and 1 wt% nanosized SiC addition. The highly efficient attrition milling provided an efficient size reduction of the 316L steel grains and homogeneous distribution of the ceramic nanoparticles before sintering process. Spark plasma sintering (SPS) was used for fast compaction of milled powder mixtures. The density of composites decreased with increasing the amount of SiC due to its lower density. The SiC addition improved the hardness of the 316L, the 316L/1 wt% SiC shows lower hardness compared to the 316L/0.33 wt% SiC composite due to its lower density. A simultaneous transgranular and intergranular fracture behaviour (Figure 26) have been observed after the 3 points bending test of the 316L/1wt% SiC composite where an average bending strength high as 1127.4 MPa has been recorded at room temperature. In the case of the 316L/0.33wt% SiC the samples were just bended due to their higher ductility. Tribological properties of the sintered composites have been studied, and it was observed that the addition of the SiC improves the tribological properties of the 316L stainless steel. Friction coefficients of 0.962, 0.879 and 0.930 have been measured, respectively, for all of the sintered reference sample 316L, 316L/ 0.33 wt% SiC and the 316L/1wt% SiC composites. The investigation of the sintered composites by TEM confirmed the distribution of the ceramic particles to the grains boundaries (Figure 27).

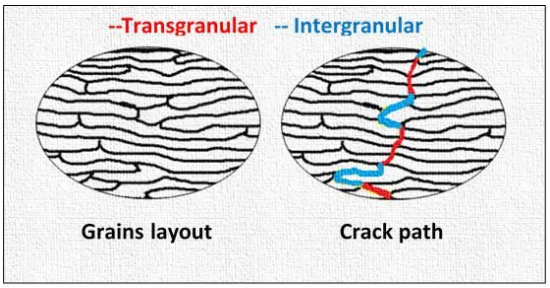

Figure 26. *Schematic views of fracture propagation.*

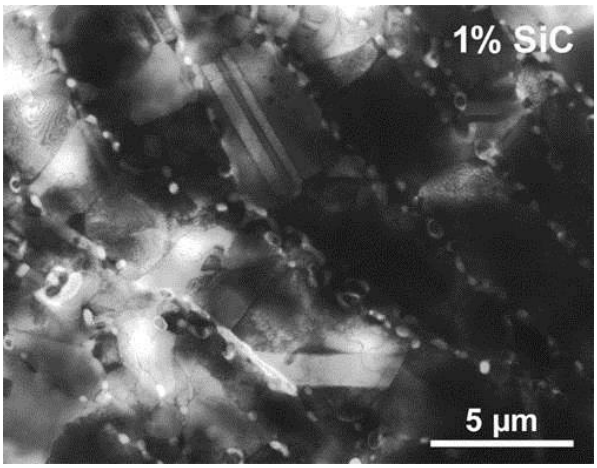

Figure 27*. TEM image of CDSS with 1 wt% SiC addition.*

New approaches in the development of Hypoallergenic implant material in Orthopaedics: steps to personalised medicine

EU FP7 "HypOrth"

K. Balázsi, Zs. Fogarassy, V. Varga, T. Zagyva, D. Delfonse (Mathys, Switzerland), C. Lohman (Magdeburg Un., Germany), J. Lorenzen (Teknologisk Institute, Denmark), C. Balázsi

Conventional materials of endoprostheses, such as Metal-on-Metal (MoM) are not suitable for all people, as some individuals develop adverse immune reactions to the constituents of metal alloys. The process, which leads to this adverse immune reaction and why some individuals react to the implanted materials whereas others do not, are not yet understood. The main aspect of our project was the development of the novel material combination for endoprostheses with excellent hypoallergenic and antibacterial properties. This new biomaterial was developed from raw waste biogenic materials as seashells using combination of the powder technology with novel electrodeposition method – electrospraying.

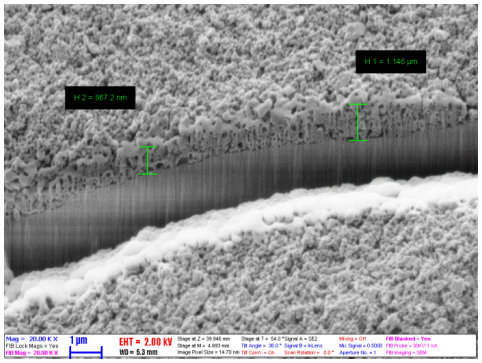

Figure 28. *SEM image of electrosprayed hydroxyapatite film on TiAlV implant surface*

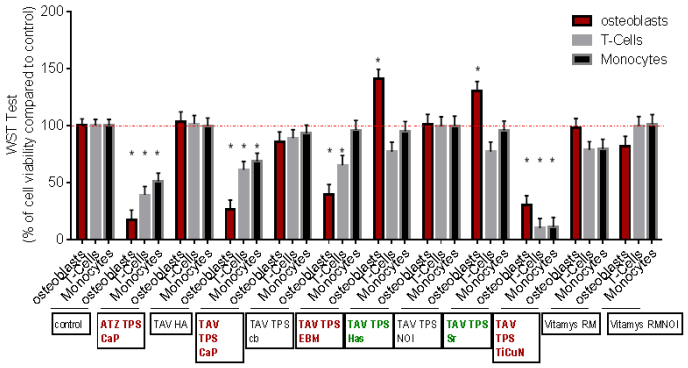

Figure 29. *Test of implant material combinations (bioceramic and coating) for biocompatibility and osteointegration*

Nanosized bioactive powder from seashells was prepared by highly efficient attritor milling. Electrospraying was used as a coating technology for the bioceramics film deposition (Figure 28). We confirmed that these coatings contained important trace elements as strontium or magnesium which increased the osteointegration activity. Moreover, the seashell derived coating (TAV TPS HAS) exhibited the highest biocompatibility among the examined coatings (Figure 29). We also confirmed that the properties of coatings after sterilization were similar from the point of view of structure, adhesion and biocompatibility to starting as-received bioactive coatings. The detailed steps of preparation and characterization are confidential. The project was successfully accomplished and the final report was accepted by EU Commission.

Graphene-ceramic composites for tribological application in aqueous environments

OTKA NN 114422 M.ERA-NET"Grace"

C. Balázsi, Zs. Fogarassy, V. Varga, M. Knoch (FCT), J. Dusza (IMR SAS, Slovakia), A. Kailer (IMW Franhoufer, Germany), K. Balázsi

The M-ERANET „Grace" project was oriented to the development of advanced Si_3N_4/ graphene and SiC/graphene ceramic composites. There is a strongly growing demand for highly wear resistant and reliable ceramic materials that may be widely used in industrial applications and energy production. Special attention is paid to components that are used under severe conditions and only lubricated by the surrounding media that are mainly aqueous. Reliability and efficiency of these components need to be improved by using high performance ceramics with superior tribological and mechanical properties.
Recent basic research of the project partners on the development of graphene containing ceramic composites showed that the realization of the nanocomposites with remarkably increased wear resistance and fracture toughness was possible. Multilayered graphene (MLG) was prepared by attritor milling at 10 h intensive milling of few micrometer sized graphite powders. The large quantity, low cost and quick preparation process are main strengths of our MLG. Si_3N_4/MLG nanocomposites were prepared by attritor milling and sintered by hot pressing (HP). The Si3N4 ceramics were produced with 1 wt%, 3 wt%, 5 wt% and 10 wt% content of MLG. The tribological behavior of composites in aqueous environment was investigated (Figure 30). This study showed decrease of wear at increased MLG content (Figure 31).

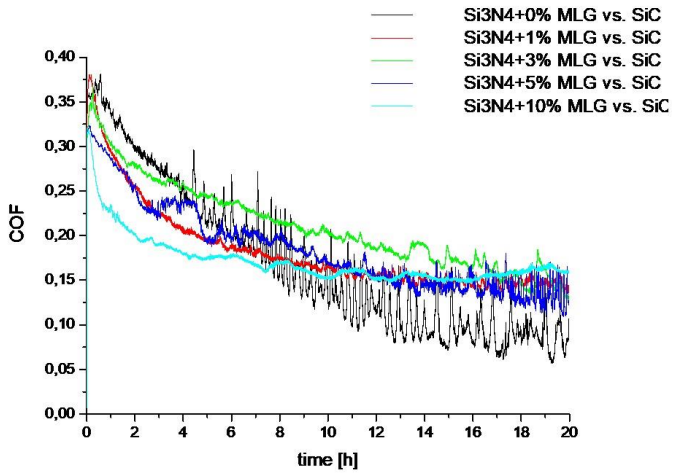

Figure 30. *Friction property of Si3N4 / MLG composites with different MLG content.*

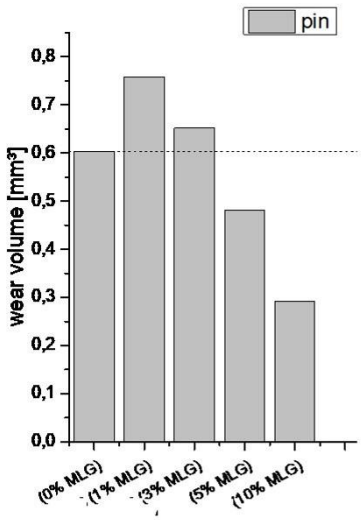

Figure 31. *Wear of composites as function of MLG content.*

Our current knowledge in the field of ceramic nanocomposites shows that is possible to make ceramic materials by incorporating graphene into the Si_3N_4 and SiC structure. The new approach is very promising, since ceramic microstructures can be designed with high toughness and provides improved wear resistance at low friction.

Nanobiosensorics Momentum Goup

Head: Dr. Robert HORVATH, Ph.D., Senior Scientist

Research Staff

- Robert HORVATH, Ph.D.
- Sándor KURUNCZI, Ph.D.
- Inna SZÉKÁCS, Ph.D.
- Beatrix PÉTER, Ph.D.
- Boglárka KOVÁCS, Ph.D.

Ph.D. students / Diploma workers

- Enikő FARKAS, Ph.D. student
- András SAFTICS, Ph.D. student
- Ágoston NAGY, Ph.D. student
- Tamás GERECSEI, PhD student
- Kristóf KLIMENT, PhD student
- Aurél PRÓSZ, MSc student
- Nicolett KANYÓ, MSc student
- Milán SZTILKOVICS, MSc student
- Olga NÉMETH, MSc student
- Brigitta RUSZNÁK, MSc student
- Barbara TÜRK, MSc student
- Kinga Dóra KOVÁCS, MSc student

The research profile of the Nanobiosensorics Group is the development and application of label-free optical biosensors, the mathematical modeling of the relevant biological and biophysical processes. Building on their broad national and international collaborative network the group conducts research in the fields of instrument development, monitoring of cell secreted extracellular vesicles, development of protein-based functional coatings, adhesion studies on human cancer and immune cells, and theoretical modeling. In 2014, the application for an ERC Consolidator Grant by the head of the research group received qualification category “A (fully meets the ERC excellence criteria and should be funded if sufficient funds are available)” after the interview in Brussels, but the funding line did not reach this proposal due to budgetary constraints. However, using this achievement the Group could successfully apply for funding from NKFIH in the framework of the ERC_HU call. In the framework of this project they aim single cell manipulation and label-free sensing. Building on this expertise, in 2018 they won an Élvonal (NKFIH) research project for single cell biosensing.

Bacteria repellent layer made of flagellin

"Lendület" LP2012-26/2012, OTKA ERC_HU_15 117715, GINOP-2.3.2-15-2016-00017, OTKA NN 117849

B. Kovacs, D. Patko, A. Klein (University of Pannonia, Veszprém), B. Kakasi (University of Pannonia, Veszprém), A. Saftics,S. Kurunczi, F. Vonderviszt (University of Pannonia, Veszprém), R. Horvath

The development of bacteria repellent surface coatings is critical in various fields ranging from biosensing to health care, biotechnology and food production. In the present study we exploit that the protein flagellin rapidly forms a dense and oriented monolayer on hydrophobic surfaces upon adsorption from aqueous solution. This oriented layer mimics the surface of bacterial flagellar filaments and has excellent bacteria repellent properties. *In situ* OWLS (Optical Waveguide Lightmode Spectroscopy) measurements were used to monitor on-line both the formation of the protein layer on the silanized sensor surface and subsequent bacterial adhesion (see Fig.1). The adhered cells were also visualized by fluorescent microscopy and the formed protein film was characterized by AFM (Atomic Force Microscopy). In parallel control experiments, the adherence of bacteria was measured on bare hydrophobic surfaces as well. Both OWLS and microscopy results well confirmed that the flagellin coating drastically reduced the adhesion of *E. coli* cells. Therefore, a novel type of bacteria repellent layer made of flagellin is demonstrated [1].

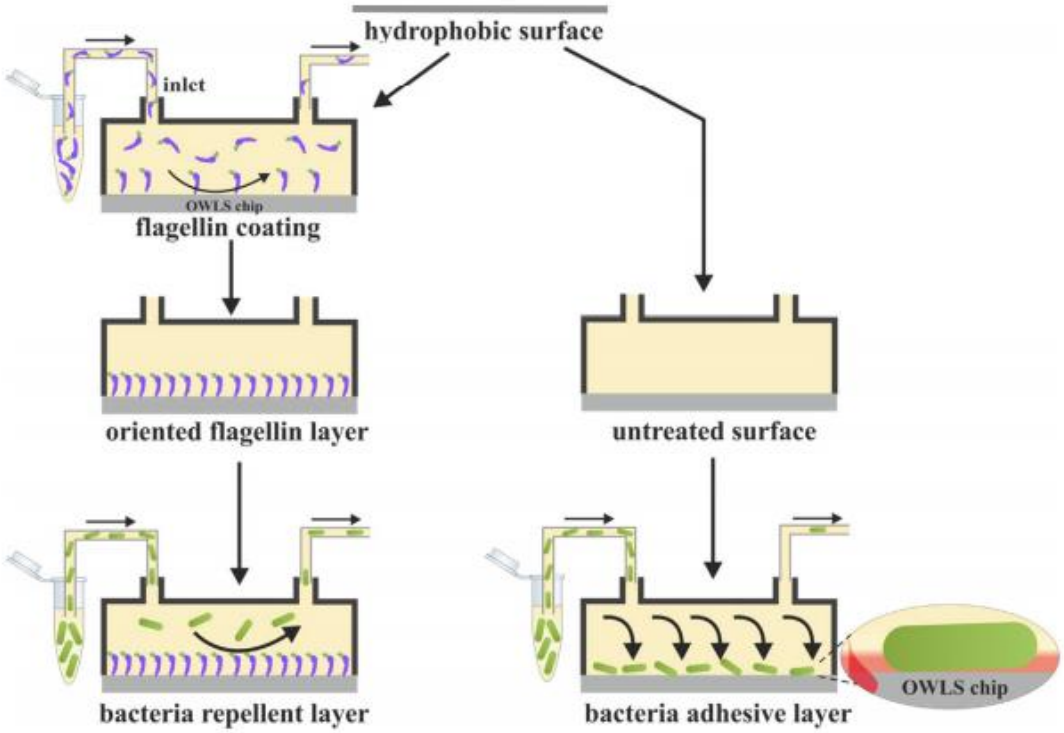

Figure 1. *Schematic representation of the differences between the bacterial adhesion on the flagellin coated and on the uncoated hydrophobic surface.*

[1] Kovacs, B.; Patko, D.; Klein, A.; Kakasi, B.; Kurunczi, S.; Vonderviszt, F.; Horvath, R. Bacteria repellent layer made of flagellin. Sens. Actuator B-Chem., 2018, 257, 839–845.

Kinetics and structure of self-assembled flagellin monolayers on hydrophobic surfaces in the presence of Hofmeister salts: Experimental measurement of the protein interfacial tension at the nanometer scale

MTA "Lendület" LP2012-26/2012, OTKA ERC_HU_15 117715, OTKA KH 126900, NKFI-6, OTKA K 124932, GINOP-2.3.2-15-2016-00017, OTKA NN 117849

B. Kovacs, A. Saftics, A. Biro, S. Kurunczi, B. Szalontai (University of Pannonia, Veszprém), B. Kakasi (University of Pannonia, Veszprém), F. Vonderviszt (University of Pannonia, Veszprém), A. Der (HAS Biological Research Centre, Szeged), R. Horvath

Flagellins (building blocks of bacterial flagellar filaments) does not preferentially adsorb on hydrophilic substrates, but very rapidly forms an oriented, dense and stable monolayer on hydrophobic surfaces, where the hypervariable D3 domain (one of the four flagellin domains) is oriented toward the solution. It presents a repellent surface coating to bacteria or cancer cells, thus this property can be utilized in biosensors and biofunctionalized surfaces. In this work, we monitored the adsorption–desorption kinetics and adsorbed layer structure of the bacterial protein flagellin in the presence of Hofmeister salts by a surface sensitive label-free optical biosensor (optical waveguide lightmode spectroscopy, OWLS). The recorded OWLS data were analyzed by a computer code using a set of coupled differential equations modeling the adsorption–desorption process. By supposing reversibly and irreversibly adsorbed protein states with different adsorption footprints, the kinetic data could be perfectly fitted. We revealed that the proteins adsorbing in the presence of kosmotropic salts had smaller footprints, leading to a more oriented and densely packed layer. Kosmotropic salts increased both the adsorption rate constant and the transition rate constants from the reversibly to the irreversibly adsorbed state (see Fig. 1). In contrast, chaotropic salts increased the desorption rate constant and led to decreased adsorbed mass and a more loosely packed film. Neither circular dichroism spectroscopy in bulk solutions or Fourier transform infrared spectroscopy of surface-adsorbed flagellins could reveal significant structural changes due to the presence of the Hofmeister salts, and supported our conclusions about the adsorption mechanism. On the basis of the measured kinetic and structural data (footprints of adsorbed proteins), we developed a model to calculate the protein–water-substrate interfacial tension in the presence of Hofmeister salts, and compared the experimentally obtained values with related literature data. The calculated values are consistent with previously published data of surface tension changes, and—to the best of our knowledge—represent the first experimental results for this quantity [1].

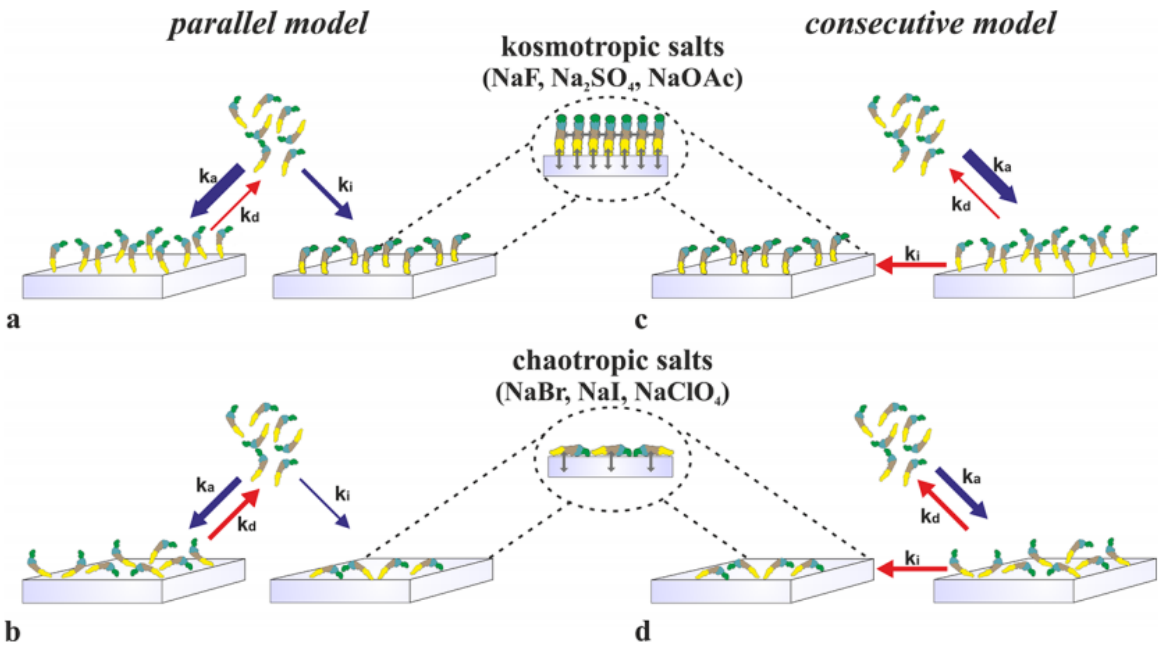

Figure 1. *Schematic illustration of the adsorption kinetics of flagellin proteins on a hydrophobic surface.*

[1] Kovacs, B.; Saftics, A.; Biro, A.; Kurunczi, S.; Szalontai, B.; Kakasi, B.; Vonderviszt ,F.; Der, A.; Horvath, R. Kinetics and Structure of Self-Assembled Flagellin Monolayers on Hydrophobic Surfaces in the Presence of Hofmeister Salts: Experimental Measurement of the Protein Interfacial Tension at the Nanometer Scale. J. Phys. Chem. C 2018, 122, 21375−21386.

Interaction of positively charged gold nanoparticles with cancer cells monitored by an in situ label-free optical biosensor and transmission electron microscopy

MTA "Lendület" LP2012-26/2012, OTKA ERC_HU_15 117715, OTKA KH 126900, MedinProt

B. Peter, I. Lagzi (BME, Budapest), S. Teraji (KIT, Kyoto, Japan), H. Nakanishi (KIT, Kyoto, Japan), L. Cervenak (Semmelweis University, Budapest), D. Zámbó, A. Deák, K. Molnár (Eötvös Lóránd University, Budapest), M. Truszka (Eötvös Lóránd University, Budapest), I. Szekacs, R. Horvath

Functionalized nanoparticles (NPs) can penetrate into living cells and vesicles, opening up an extensive range of novel directions. For example, NPs are intensively employed in targeted drug delivery and biomedical imaging. However, the real-time kinetics and dynamics of NP−living cell interactions remained uncovered. In this study, we in situ monitored the cellular uptake of gold NPs −functionalized with positively charged alkaline thiol− into surface-adhered cancer cells, by using a high-throughput label-free optical biosensor employing resonant waveguide gratings. The characteristic kinetic curves

upon NP exposure of cell-coated biosensor surfaces were recorded and compared to the kinetics of NP adsorption onto bare sensor surfaces. We demonstrated that from the above kinetic information, one can conclude about the interactions between the living cells and the NPs (see Fig.1). Real-time biosensor data suggested the cellular uptake of the functionalized NPs by an active process. It was found that positively charged particles penetrate into the cells more effectively than negatively charged control particles, and the optimal size for the cellular uptake of the positively charged particles is around 5 nm. These conclusions were obtained in a cost-effective, fast, and high-throughput manner. The fate of the NPs was further revealed by electron microscopy on NP-exposed and subsequently fixed cells, well confirming the results obtained by the biosensor. Moreover, an ultrastructural study demonstrated the involvement of the endosomal−lysosomal system in the uptake of functionalized NPs and suggested the type of the internalization pathway. NPs may act as model systems to imitate host cell-bacteria interactions and penetration in biosensor measurements. Furthermore, these measurement settings and results can be applied to study the uptake of NPs by bacteria as well [1].

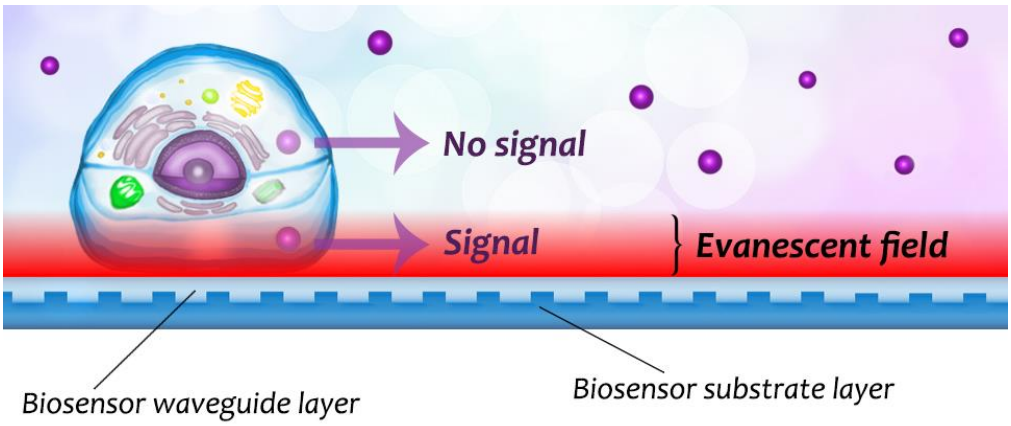

Figure 1. *Schematic illustration of the concept of evanescent labelfree biosensors in NP uptake detection.*

[1] Peter, B.; Lagzi, I.; Teraji, S.; Nakanishi, H., Cervenak, L.; Zámbó, D.; Deák, A.; Molnár, K.; Truszka, M.; Szekacs, I.; Horvath, R Interaction of Positively Charged Gold Nanoparticles with Cancer Cells Monitored by an in Situ Label-Free Optical Biosensor and Transmission Electron Microscopy. ACS Appl. Mater. Interfaces 2018, 10, 26841−26850.

High-resolution adhesion kinetics of EGCG-exposed tumor cells on biomimetic interfaces: Comparative monitoring of cell viability using label-free biosensor and classic end-point assays

MTA "Lendület" LP2012-26/2012, OTKA ERC_HU_15 117715, OTKA KH 126900, OTKA K 104275

B. Peter, R. Ungai-Salanki (Eötvös Lóránd University, Budapest), B. Szabó (Eötvös Lóránd University, Budapest), A. G. Nagy, I. Szekacs, Sz. Bősze (Eötvös Lóránd University, Budapest), R. Horvath

A high-throughput label-free resonant waveguide grating biosensor, the Epic BenchTop was utilized to in situ monitor the adhesion process of cancer cells on Arg-Gly-Asp tripeptide (RGD) displaying biomimetic polymer surfaces. Using highly adherent human cervical adenocarcinoma (HeLa) cells as a model system, cell adhesion kinetic data with outstanding temporal resolution were obtained. We found that pre-exposing the cells to various concentrations of the main extract of green tea, the (−)-epigallocatechin gallate (EGCG), largely affected the temporal evolution of the adhesion process. For unexposed and low dosed cells, sigmoid shaped spreading kinetics was recorded. Higher dose of EGCG resulted in a complete absence of the sigmoidal character, and displayed adsorption-like kinetics. By using the first derivatives of the kinetic curves, a simple model was developed to quantify the sigmoidal character and the transition from sigmoidal to adsorption-like kinetics (see Fig.1). The calculations showed that the transition happened at EGCG concentration of around 60 μg/mL. Using the 3-(4,5-dimethylthiazol-2-yl)-2,5-diphenyltetrazolium bromide end-point assay, we concluded that EGCG is cytostatic but not cytotoxic. The effect of EGCG was also characterized by flow cytometry. We concluded that, using the introduced label-free methodology, the shape of the cell adhesion kinetic curves can be used to quantify in vitro cell viability in a fast, cost-effective, and highly sensitive manner [1]. This method probably can be used with bacterial cells as well to demonstate the antibacterial effects of certain further natural compounds.

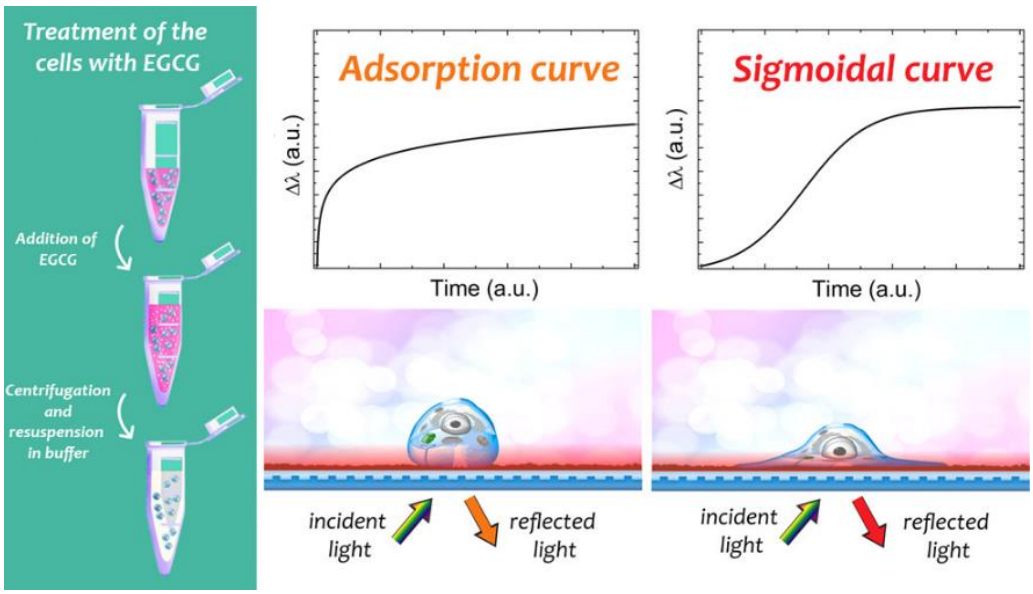

Figure 1. *Schematic illustration of the working principle of the Epic BT biosensor and the steps of the measurement (left). In case of adsorption kinetic curve, the cell attaches but does not adhere onto the biosensor surface. This phenomenon indicates a nonliving, "dead" process. Note, it also occurs when proteins adsorb onto the surface. In case of sigmoidal kinetic curve, the cells adhere onto the biosensor surface. This phenomenon indicates a "living" process.*

[1] Peter, B.; Ungai-Salanki, R.; Szabó, B.; Nagy, A.G.; Szekacs, I.; Bősze, Sz.; Horvath, R. High-resolution adhesion kinetics of EGCG-Exposed tumor cells on biomimetic interfaces: Comparative monitoring of cell viability using label-free biosensor and classic end-point assays. ACS Omega 2018, 3, 3882−3891.

Label-free optical biosensor for real-time monitoring the cytotoxicity of xenobiotics: A proof of principle study on glyphosate

MTA "Lendület" LP2012-26/2012, OTKA ERC_HU_15 117715, OTKA K 109865

E. Farkas, A. Szekacs (Agro-Environmental Research Institute, Budapest), B. Kovacs, M. Olah (Agro-Environmental Research Institute, Budapest), R. Horvath, I. Szekacs

Rapid and inexpensive biosensor technologies allowing real-time analysis of biomolecular and cellular events have become the basis of next-generation cell-based screening techniques. Our work opens up novel opportunities in the application of the high-throughput label-free Epic BenchTop optical biosensor in cell toxicity studies. The Epic technology records integrated cellular responses about changes in cell morphology and dynamic mass redistribution of cellular contents at the 100–150 nm layer above the sensor surface. The aim of the present study was to apply this novel technology to identify the effect of the herbicide Roundup Classic, its co-formulant polyethoxylated tallow amine (POEA), and its active ingredient glyphosate, on MC3T3-E1 cells adhered on the biosensor surface (sse Fig.1). The half maximal inhibitory concentrations of Roundup Classic, POEA and glyphosate upon 1 h of exposure were found to be 0.024%, 0.021% and 0.163% in serum-containing medium and 0.028%, 0.019% and 0.538% in serum-free conditions, respectively (at concentrations equivalent to the diluted Roundup solution). These results showed a good correlation with parallel end-point assays, demonstrating the outstanding utility of the Epic technique in cytotoxicity screening, allowing not only high-throughput, real-time detection, but also reduced assay run time and cytotoxicity assessment at end-points far before cell death would occur [1].

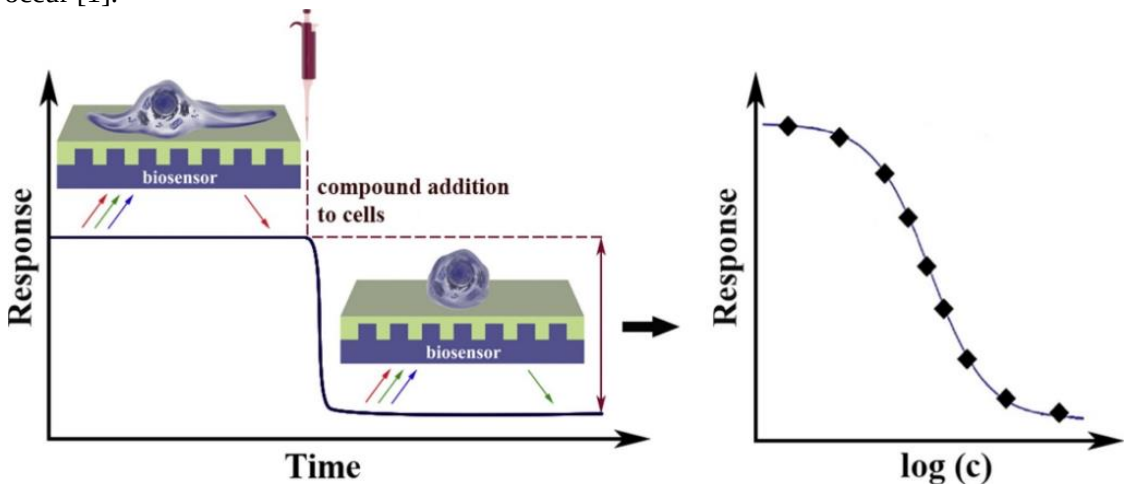

Figure 1. *Schematic representation of the measurement and data evaluation methodology.*

[1] Farkas, E.; Szekacs, A.; Kovacs, B.; Olah, M.; Horvath, R.; Szekacs, I. Label-free optical biosensor for real-time monitoring the cytotoxicity of xenobiotics: A proof of principle study on glyphosate. J. Haz. Mat. 2018, 351,80-89.

Integrin targeting of glyphosate and its cell adhesion modulation effects on osteoblastic MC3T3-E1 cells revealed by label-free optical biosensing

MTA "Lendület" LP2012-26/2012, OTKA ERC_HU_15 117715, OTKA KH 126900, NVKP_16-1-2016-0049, OTKA K 109865

I. Szekacs, E. Farkas, B.L. Gemes (Agro-Environmental Research Institute, Budapest), E. Takacs (Agro-Environmental Research Institute, Budapest), A. Szekacs (Agro-Environmental Research Institute, Budapest), R. Horvath

Cell adhesion is the crucial event in numerous physiological and pathophysiological processes. Foreign substances can affect cellular processes through receptors, ion channels, enzymes, binding proteins or the cytoskeleton. Biosensor techniques and their application in different areas, including cytotoxicology, is becoming of growing significance. Whole cell-based sensors gain utmost importance due to their capability to measure comprehensive and functional effects of different xenobiotics.

An evanescent filed based surface-sensitive resonant waveguide grating (RWG) biosensor was applied for high-throughput label-free detection of impacts of the world leading herbicide active ingredient glyphosate on cell adhesion in real time and quantitative evaluation. In the present study we discovered and thoroughly examined a new, yet unidentified, properties of glyphosate as cell adhesion modulator. The RWG technique was employed for measuring kinetics of cell adhesion to glyphosate adsorbed on biosensor surfaces and by measuring the antagonistic action of glyphosate on cell binding to Arg-Gly-Asp (RGD)-displaying polymer surfaces (see Fig.1). The results obtained demonstrate that living preosteoblastic cells can adhere to glyphosate adsorbed on the sensor surface, showing ligand-specific kinetics. Soluble glyphosate significantly reduces cell adhesion via blocking RGD-specific integrins in a concentration-dependent manner, as also validated by competitive binding assays to recombinant receptor αvβ3 in both enzyme-linked immunosorbent assay (ELISA) and biosensor formats. Using this novel methodology, the half maximal inhibitory concentration (IC_{50}) for glyphosate in living osteoblastic cells was determined to be 20.6 mM. The affinity of glyphosate to cell adhesion receptors is also determined. The introduced methodology is fast, sensitive, and biological effects were revealed using intact, living cells [1].

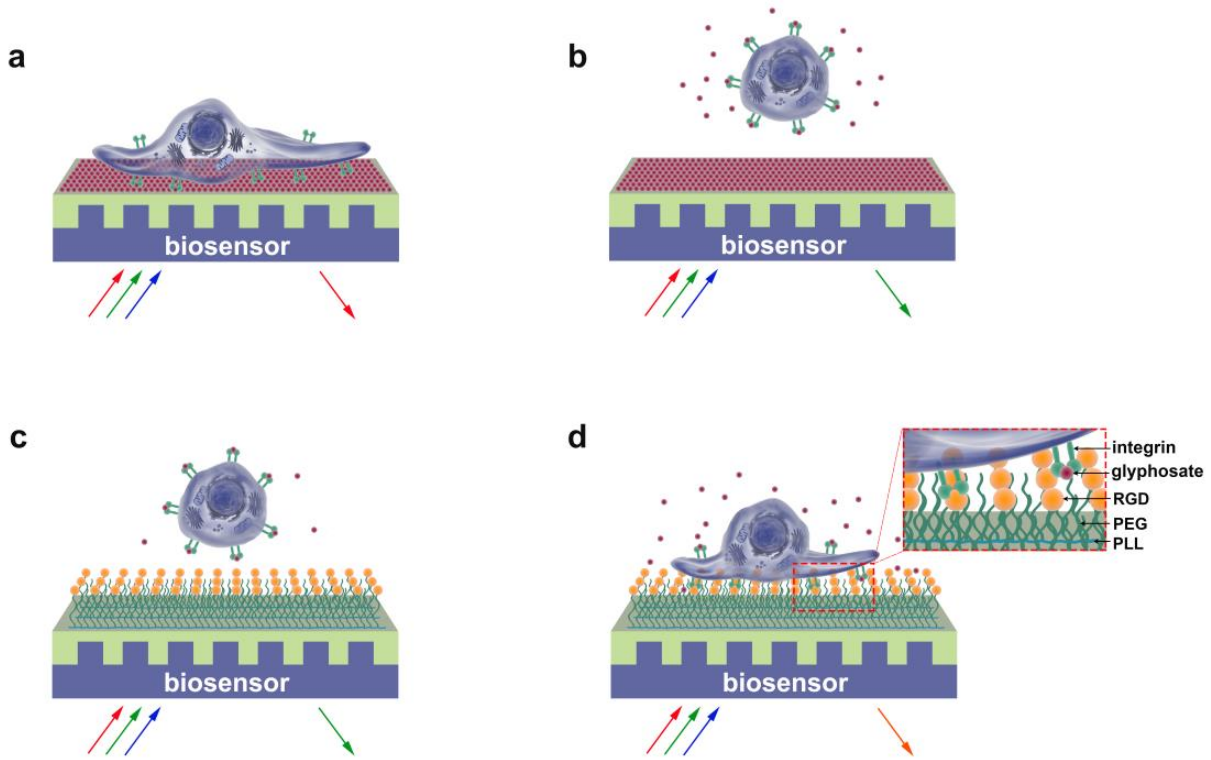

Figure 1. *Schematic illustration of the working principle of the cell-based biosensor and the concentration-dependent effects of glyphosate on cell adhesion. (a) MC3T3-E1 cells spread on a sensor surface treated with 0.1% glyphosate solution. (b) Inhibition of cell adhesion by glyphosate at 0.2–1.7% concentration in the solution (with complete blockage achieved at 1.7%). (c) Prevention of cell adhesion onto PP:PPR surface by preincubation of the cells with glyphosate at 0.47% concentration in the solution. (d) Detaching MC3T3-E1 cells adhered to a surface modified with PP:PPR by glyphosate at 0.9% concentration in solution.*

[1] Szekacs,I.; Farkas, E.; Gemes, B.L.; Takacs, E.; Szekacs, A., Horvath, R. Integrin targeting of glyphosate and its cell adhesion modulation effects on osteoblastic MC3T3-E1 cells revealed by label-free optical biosensing. Sci. Rep. 2018, 8, 17401.

In situ viscoelastic properties and chain conformations of heavily hydrated carboxymethyl dextran layers: a comparative study using OWLS and QCM-I chips coated with waveguide material

MTA"Lendület" LP2012-26/2012, OTKA ERC_HU_15 117715, OTKA KH 126900

A. Saftics, Gy. A. Prósz, B. Türk, B. Peter, S. Kurunczi, R. Horvath

Hydration, viscoelastic properties and dominant structure of thin polymer layers on the surface of waveguide material were evaluated using optical waveguide lightmode spectroscopy (OWLS) and quartz crystal microbalance (QCM) methods. The fundamentally different principles of the two applied label-free biosensors enable to examine analyte layers from complementary aspects, e.g. to determine the amount of bound water in hydrated layers. In this study, a new QCM instrument with impedance measurement (QCM-I) was introduced. Its specially designed sensor chips, covered by thin film of waveguide material (SiO_2-TiO_2), supply identical surface as used in OWLS sensors, thus enabling to perform parallel measurements on the same type of surface. Viscoelastic analysis of the measured data was performed by our evaluation code developed in MATLAB environment, using the Voinova's Voigt-based model. *In situ* deposition experiments on the ultrathin films of poly(L-lysine)-*graft*-poly(ethylene glycol) (PLL-*g*-PEG) were conducted for instrumental and code validation. Additionally, a novel OWLS-QCM data evaluation methodology has been developed based on the concept of combining hydration and viscoelastic data with optical anisotropy results from OWLS measurements (see Fig. 1). This methodology provided insight into the time-dependent chain conformation of heavily hydrated nano-scaled layers, resulting in unprecedented structural, hydration and viscoelastic information on covalently grafted ultrathin carboxymethyl dextran (CMD) films, which are basically antifouling coatings that can be specifically conjugated by adhesive motifs in order to arrange cells and bacteria on biosensor surfaces. The measured mass values as well as hydration and viscoelastic properties were compared with the characteristics of PLL-*g*-PEG layers [1].

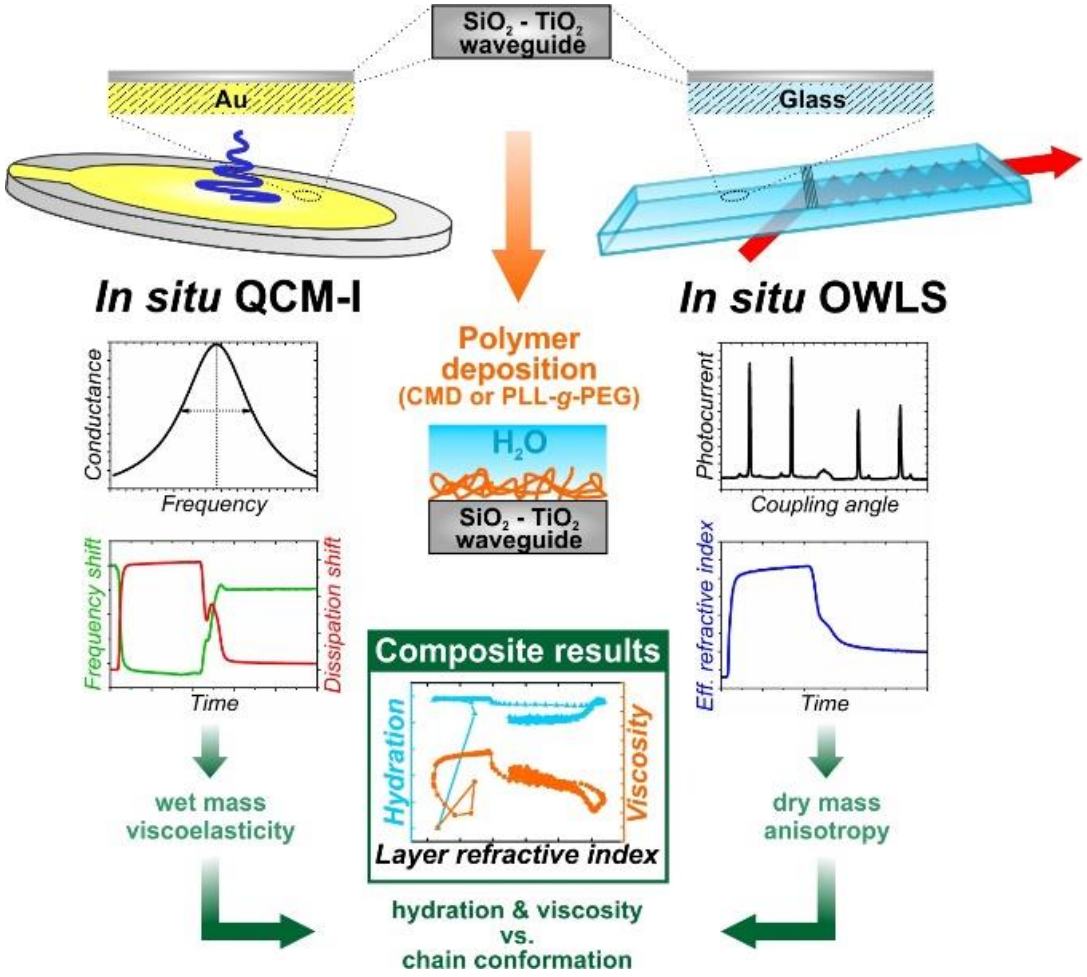

Figure 1. *Schematic representation of the measurement and data evaluation methodology developed and applied in this work.*

[1] Saftics, A.; Prósz, Gy.A.; Türk,B.; Peter, B.; Kurunczi, S.; Horvath, R. In situ viscoelastic properties and chain conformations of heavily hydrated carboxymethyl dextran layers: a comparative study using OWLS and QCM-I chips coated with waveguide material.
Sci. Rep. 2018, 8, 11840.

Complex Systems Department

Head: Dr. György Szabó D.Sc., scientific advisor

Research Staff

- Balázs Király
- István Borsos
- Zoltán Juhász PhD.
- Géza Ódor D.Sc., scientific advisor
- Attila Szolnoki D.Sc., scientific advisor

Ph.D. students / Diploma workers

- Kristóf Hódsági (BME, BSc-MSc student)
- Vince Varga (BME, BSc student)

The research field of the group is the investigation of complex systems by the methods of statistical physics in equilibrium as well as non-equilibrium states.
The theoretical investigation of multi-agent evolutionary game models studies processes supporting fair behavior of individuals by numerically analyzing mathematical models when a player's own interest opposes that of the community. Mathematical models have been used to investigate the effect of one kind of penalties, the combinations of the rules of strategy updates, and systems in which the income of the players is obtained from two or three interconnection systems (communities).
Decomposing matrices into elementary (orthogonal) components allows the identification and frequency analysis of elementary interactions causing social dilemmas in potential games. The systematic examination of elementary interactions of evolutionary matrix games unearthed two newer versions of social dilemmas. In the first case the macroscopic system develops into a state of higher average income, because of the greater number of possible microscopic states. In the second case the anomalous consequence of cyclic symmetry-breaking forces the system develops into the state of lower average income. Because of the cyclic dominance, however, this system returns to the initial state, where the newer and newer similar avalanche phenomena cause huge fluctuations both in the proportions of the strategies and in the incomes.

Using traditional concepts and methods of statistical physics the universal properties of avalanche phenomena were analyzed in ropes made of many threads. Similar catastrophe analyses were performed in models appearing in the interconnected network of electric plants. They extended the investigation of the general characteristics of the Griffiths phase to inhomogeneous networks of modular structure.
The increase of data in folk music and genetic data sets implies the continuous improvement of algorithms to analyze them. The newly developed algorithms are able both to identify clusters and to follow the evolutionary inheritance of clusters, both in genetic (haplogroup) features and in popular characteristics of folk music tunes.

Competition and partnership between conformity and payoff-based imitations in social dilemmas

OTKA K 120785

A. Szolnoki and X. Chen

Learning from a partner who collects a higher payoff is a frequently used working hypothesis in evolutionary game theory. One of the alternative dynamical rules is when the focal player prefers to follow the strategy choice of the majority in the local neighborhood, which is often called a conformity-driven strategy update. In this work we assumed that both strategy learning methods are present and compete for space within the framework of a coevolutionary model.
We have shown that there are parameter regions, like strong snowdrift game situations at high temptation (*T)* or high sucker's payoff *(S)* values where the competition of different learning methods results in the unambiguous victor of payoff-driven strategy learning. Here the role separating cooperator-defector pairs provide so high collective payoff value that cannot be beaten by a homogeneous domain which would be a consequence of a conformity-driven learning method.

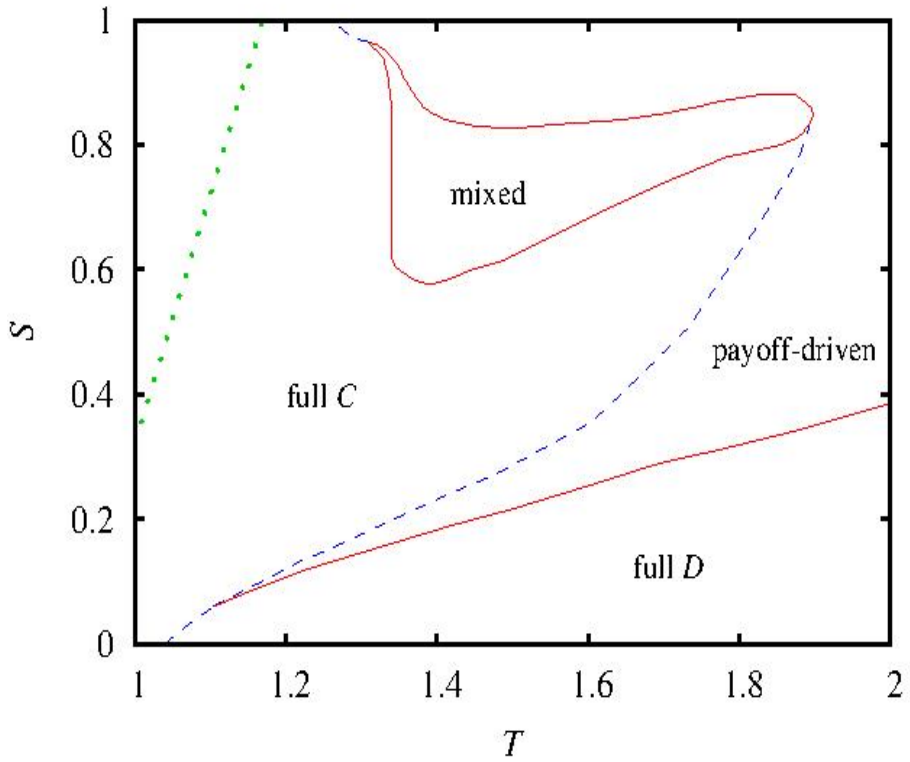

Figure 2*. Phase diagram of snowdrift game where payoff-driven and conformity-driven strategy learning protocols are competing for space. Full C (full D) label marks the para-meter regions where only co-operator (defector) strategies survive in the stationary state. 'Payoff- driven' label marks the region where payoff-driven strategy learning protocol pre-vails and related cooperator and defector players form a stable winning solution. The phase denoted by 'mixed' label shows where all learning protocols and all strategies coexist. For comparison, green dotted line marks the border of full cooperator state when only payoff-driven learning protocol is available for players in a uniform system.*

Nevertheless, for less sharp snowdrift game regions at smaller *T* and *S* values the coevolution of different learning methods is useful to reach a full cooperative state that would not be reachable otherwise. In the latter case the homogeneous cooperator domains can invade the whole space by enjoying the advantage of conformity-driven learning method. Interestingly, in the stag-hunt game region the simultaneous presence of different learning methods reveals a novel way of collaboration that cannot be observed otherwise. Here conformity-driven cooperators can resist the invasion of payoff-driven defectors and neighboring payoff-driven cooperators can attack conformity-driven defectors successfully. The expected symmetry is broken for defectors because conformity-driven (o_D) and payoff-driven (p_D) states cannot form similarly efficient alliance. In this way the active partnership of different types of cooperator players allows them to extend the full cooperator state to those parameter values which belonged to the sovereignty of defectors in the classic payoff-driven model.

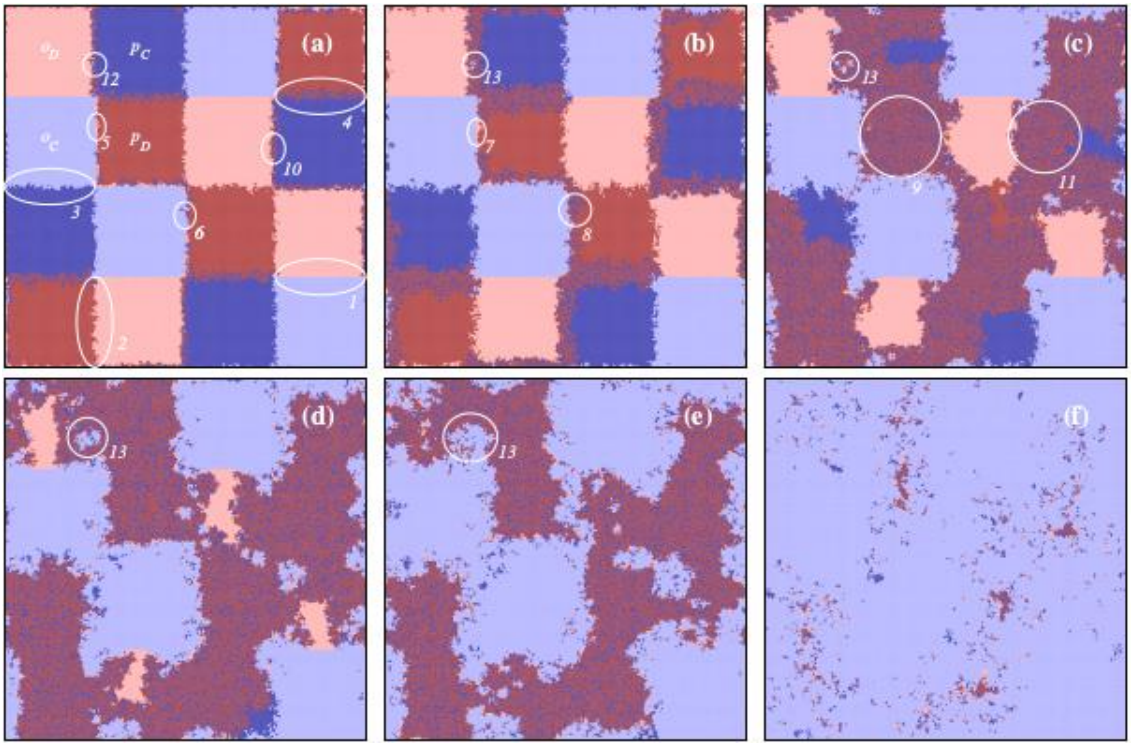

Figure 2. *Spatial evolution of the four competing states in a 400×400 system at T=1.4 and S=0.4 where the simulation is launched from a prepared patch-like initial state where all kind of interfaces between competing players can be found. In this way we can monitor all emerging pattern formations simultaneously via a single run. Here dark (light) blue denotes payoff-driven (conformity-driven) cooperators, while dark (light) red marks payoff-driven (conformity-driven) defectors, as it is marked by white labels in panel (a). This panel represents the early stage of evolutionary process after 20 MCSs. Further stages of the evolutionary process are shown at 50, 150, 250, 350, and 800 MCSs. Finally the system evolves into a homogeneous oC state (not shown). The circles and ellipses highlight the specific invasion fronts between different types of domains.*

This work was published in *New J. Phys.* **20** (2018) 093008.

Griffiths phases in infinite-dimensional, non-hierarchical modular networks

OTKA K109577

Géza Ódor, Silvio Ferreira, Wesley Cota

Griffiths phases (GPs), generated by the heterogeneities on modular networks, have recently been suggested to provide a mechanism, rid of fine parameter tuning, to explain the critical behavior of complex systems. One conjectured requirement for systems with modular structures was that the network of modules must be hierarchically organized and possess finite dimension. We investigate the dynamical behavior of an activity spreading model, evolving on heterogeneous random networks with highly modular structure and organized non-hierarchically. We observe that loosely coupled modules act as effective rare-regions, slowing down the extinction of activation. As a consequence, we find extended control parameter regions with continuously changing dynamical exponents for single network realizations, preserved after finite size analyses, as in a real GP. The avalanche size distributions of spreading events exhibit robust power-law tails. Our findings relax the requirement of hierarchical organization of the modular structure, which can help to rationalize the criticality of modular systems in the framework of GPs. (*Scientific. Reports 8 (2018), 9144*)

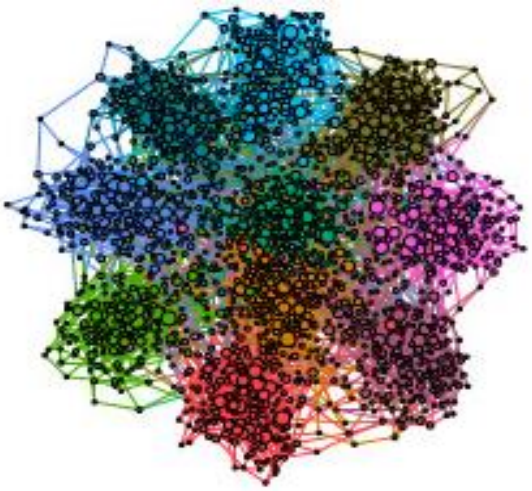

Figure 1. *Example a of modular structure. Networks with 100 modules of same size of 200 nodes and number of inter-modular connections k = 10, representing loosely and densely connected modular graphs, respectively. The network degree distribution is given by* $P(k) \sim k^{-2.7}$. *Connected modular structures can clearly be observed.*

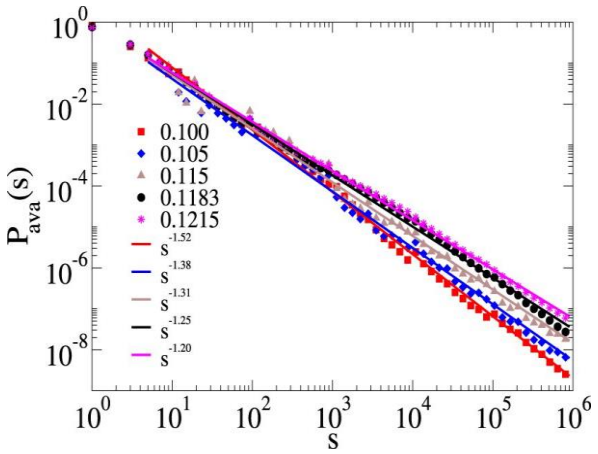

Figure 2. *Avalanche size distributions of the SIS spreading on a single MMN. Only topological disorder is considered and the number of modules is* 10^3. *Different values of* λ *are indicated by the legends. Simple PL tail fits are also shown.*

Correlation analysis of jointly propagating genetic and musical characteristics of modern and ancient populations in Eurasia and America – a simultaneous quest for ancient human populations and their musical parent languages

Z. Juhász, H. Pamjav et al.

In this study, we aimed to illustrate the efficiency of correlation analysis of musical and genetic characteristics in research for certain common ethnic and ethno-musical roots of the mankind. The comparison of the results to archaeogenetic data shows that correlations of recent musical and genetic data may reveal past cultural and migration processes resulting in recent connections. (Accepted for publication in Molecular Genetics and Genomics.)

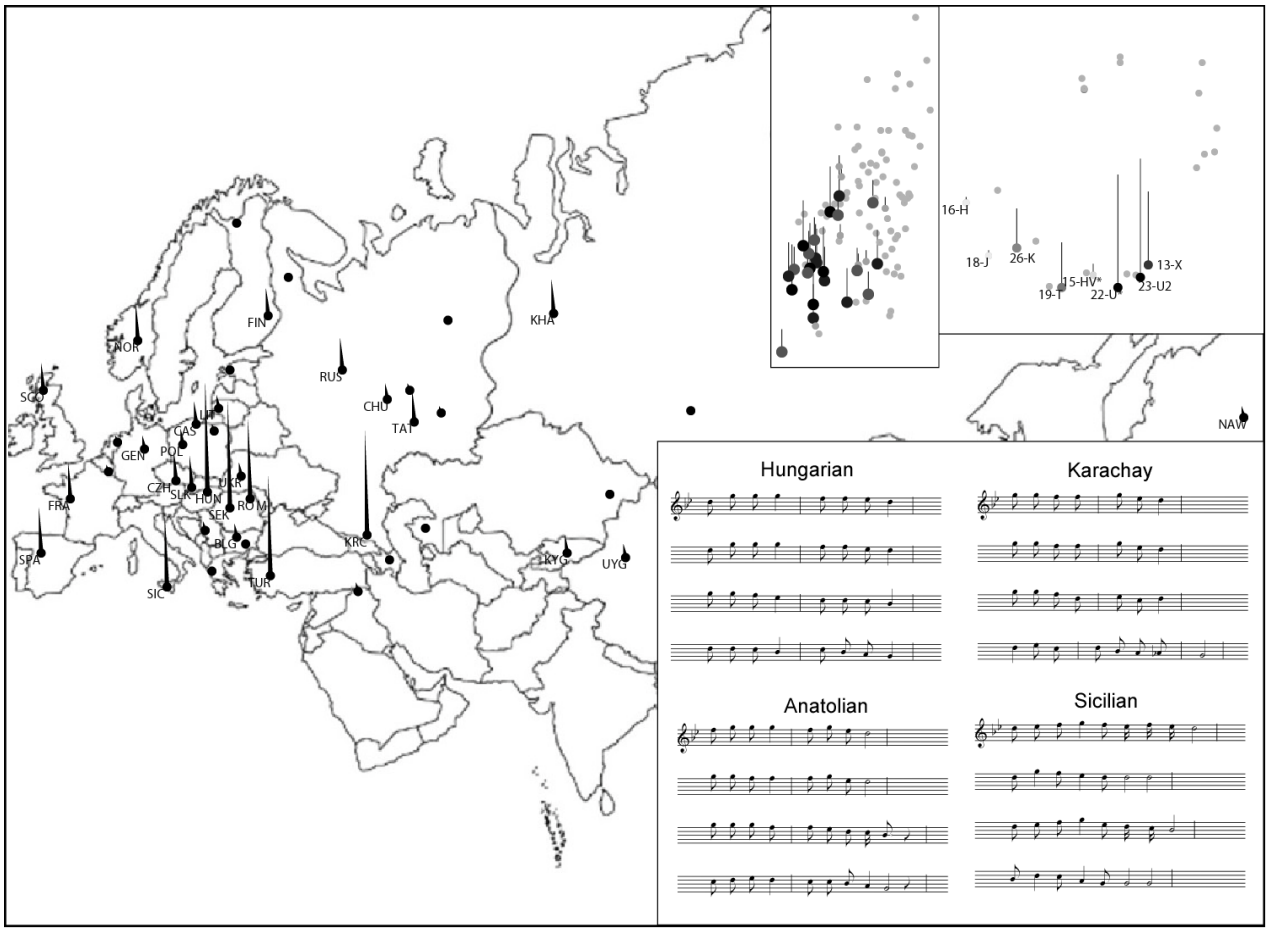

Figure 1. *Geographical distribution of the common mean weight vectors derived from similar rank lists of the populations studied, belonging to the musical types and haplogroups indicated in the right upper part. The result refers to an association of haplogroups X, U*, U2, HV*, T, K, J and H, as well as melody types of descending melody contours and high ranges. The highest weights of this association of genetic and musical types are found in Anatolia, the Carpathian Basin, the Caucasus and Sicily. The given haplogroup association was compared to ancient archaeogenetic samples, and it was found to be dominant in Neolithic farmer populations in the Fertile Crescent, so the corresponding association of melody types may be attributed to one of the well-known Neolithic migrations. Four closely related melodies arising from Hungary, the Caucasus-area (Karachay), Anatolia and Sicily verify the existence of this hypothetical musical parent language*

Seminar talks

- 2018. január 24, 11h Ódor Géza: "A topologikus heterogenitások hatása elektromos hálózatokban"
- 2018. február 14, 11h Szabó György: "Mátrixjátékok anatómiája"
- 2018. február 21, 11h Matteo Bosi, IMEM-CNR (Parma, Italy): "Epsilon-Ga2O3 polymorph: epitaxial growth, properties, and possible applications"
- 2018. március 14, 11h Juhász Zoltán: „Genetikai és népzenei korrelációk öntanuló algoritmusokkal"
- 2018. március 21, 11h Borsos István: "Gépi tanulás: áttörés a szellemi játékok (sakk, go) számítógépes elemzésében"
- 2018. március 28, 11h Tapasztó Orsolya: "Szilícium-nitrid kerámiák tribológiai tulajdonságainak javítása néhány rétegű grafén adalékolásával"
- 2018. április 11, 11h Lábadi Zoltán: Fotolumineszcencia spektroszkópia: helyzet az MFA-ban, lehetőségek, távlatok.
- 2018. április 18, 11h Horváth Zoltán György (Wigner FK): "KFKI anno" (Alulnézet)
- 2018. április 25, 11h Prof. Nikolay G. Galkin (Head of Optics and Electrophysics Laboratory Institute of Automation and Control Processes Far Eastern Branch of Russian Academy of Sciences): "Double hetero- and nanostructures based on silicon and semiconductor silicides of transition and alkaline earth metals"
- 2018. május 9, 11h Kádár György: "Elkésett elismerés: Bolyai és Károlyházy"
- 2018. június 6, 11h órakor Oláh Nikolett: „Biokompatibilis titán-karbid/amorf szén nanokompozit bevonat előállítása és különböző módszerekkel végzett vizsgálatai"
- 2018. június 21, 11h Sameer Sapra (Department of Chemistry, Indian Institute of Technology Delhi, India) „Light Harvesting from II-VI Semiconductor Heteronanostructures"
- 2018. augusztus 3, 11h Prof. Z. J. Ding (Hefei National Laboratory for Physical Sciences at Microscale and Department of Physics) „Extracting optical properties from reflection electron energy loss spectroscopy spectra by reverse Monte Carlo method"
- 2018. szeptember 26, 11h Furkó Mónika (EK MFA, Vékonyréteg laboratórium): „Biokompatibilis és antibakteriális biokerámia bevonatok előállítása és jellemzése"
- 2018 október 3, 11h Pósa László (EK MFA): "Memrisztív kapcsolások vékonyrétegekben"
- 2018. október 10, 11h Schiller Róbert (EK MFA): "Ionbesugárzás hatása fémek kontakt potenciáljára"
- 2018. október 17, 11h Csaba György (Pázmány Péter Katolikus Egyetem, Információs Technológiai és Bionikai Kar): Spin alapú számítóeszközök
- 2018. november 14, 11h Dodony Erzsébet: „Cu-Si eta-fázis szerkezetének pontosítása TEM mérések alapján"
- 2018. november 28, 11h Saftics András: Dextrán alapú hidrogél rétegek fejlesztése bioszenzorikai alkalmazásokhoz
- 2018. december 11, 10h Dr. Mohsen Samadi - Khoshkhoo, (Carl Zeiss Microscopy GmbH) „X-Ray Microscopy of a high spatial resolution – a new technology approach for the research laboratory"
- 2018. december 12, 11h Blanka Magyari-Köpe (Stanford University) „Memristors for Artificial Intelligence Systems – What Have We Learned from Ab Initio Simulations?"

List of MFA publications 2018

[1] P. Z, O. Hakkel, G. Szíjjártó, and T. A, "Adsorption and transformations of ethanol over ceria based model catalysts," *CATALYSIS TODAY*, vol. 306, pp. 145–153, 2018.

[2] J. Radó, C. Dücső, P. Földesy, G. Szebényi, Z. Nawrat, K. Rohr, and P. Fürjes, "3D force sensors for laparoscopic surgery tool," *MICROSYSTEM TECHNOLOGIES*, vol. 24, no. 1, pp. 519–525, 2018.

[3] G. Járvás, T. Varga, M. G. Szigeti, L. Hajba, P. Fürjes, I. Rajta, and A. Guttman, "Tilted pillar array fabrication by the combination of proton beam writing and soft lithography for microfluidic cell capture Part 2: Image sequence analysis based evaluation and biological application," *ELECTROPHORESIS*, vol. 39, no. 3, pp. 534–539, 2018.

[4] J. Károlyi, M. Németh, C. Evangelisti, G. Sáfrán, Z. Schay, A. Horváth, and F. Somodi, "Carbon dioxide reforming of methane over Ni–In/SiO2 catalyst without coke formation," *JOURNAL OF INDUSTRIAL AND ENGINEERING CHEMISTRY*, vol. 58, pp. 189–201, 2018.

[5] M. Furko, Z. May, V. Havasi, Z. Kónya, A. Grünewald, R. Detsch, A. R. Boccaccini, and C. Balázsi, "Pulse electrodeposition and characterization of non-continuous, multi-element-doped hydroxyapatite bioceramic coatings," *JOURNAL OF SOLID STATE ELECTROCHEMISTRY*, vol. 22, no. 2, pp. 555–566, 2018.

[6] M. Furko, V. Havasi, Z. Kónya, A. Grünewald, R. Detsch, A. R. Boccaccini, and C. Balázsi, "Development and characterization of multi-element doped hydroxyapatite bioceramic coatings on metallic implants for orthopedic applications," *BOLETIN DE LA SOCIEDAD ESPANOLA DE CERAMICA Y VIDRIO*, vol. 57, no. 2, pp. 55–65, 2018.

[7]J. Szívós, S. Pothorszky, J. Soltys, M. Serényi, H. An, T. Gao, A. Deák, J. Shi, and G. Sáfrán, "CoPt/TiN films nanopatterned by RF plasma etching towards dot-patterned magnetic media," *APPLIED SURFACE SCIENCE*, vol. 435, pp. 31–38, 2018.

[8] J. Kelling, G. Odor, and S. Gemming, "Dynamical universality classes of simple growth and lattice gas models," *JOURNAL OF PHYSICS A-MATHEMATICAL AND THEORETICAL*, vol. 51, no. 3, 2018.

[9] B. Kovacs, D. Patko, A. Klein, B. Kakasi, A. Saftics, S. Kurunczi, F. Vonderviszt, and R. Horvath, "Bacteria repellent layer made of flagellin," *SENSORS AND ACTUATORS B-CHEMICAL*, vol. 257, pp. 839–845, 2018.

[10] I. Szekacs, N. Orgovan, B. Peter, B. Kovacs, and R. Horvath, "Receptor specific adhesion assay for the quantification of integrin–ligand interactions in intact cells using a microplate based, label-free optical biosensor," *SENSORS AND ACTUATORS B-CHEMICAL*, vol. 256, pp. 729–734, 2018.

[11] G. Greco, F. Giannazzo, P. Fiorenza, S. Di Franco, A. Alberti, F. Iucolano, I. Cora, B. Pecz, and F. Roccaforte, "Barrier Inhomogeneity of Ni Schottky Contacts to Bulk GaN," *PHYSICA STATUS SOLIDI A-APPLICATIONS AND MATERIALS SCIENCE*, vol. 215, no. 9, 2018.

[12] B. Urbán, P. Szabó, D. Srankó, G. Sáfrán, L. Kollár, and R. Skoda-Földes, "Double carbonylation of iodoarenes in the presence of reusable palladium catalysts immobilised on supported phosphonium ionic liquid phases," *MOLECULAR CATALYSIS*, vol. 445, pp. 195–205, 2018.

[13] Z. Kasztovszky, K. Lázár, K. V. Kovács, A. Len, J. Füzi, A. Markó, and K. Biró, "A novel approach in the mineralogy of Carpathian mahogany obsidian using complementary methods," *QUATERNARY INTERNATIONAL*, vol. 467, pp. 332–341, 2018.

[14] Z. Szabó, I. Cora, Z. Horváth, J. Volk, and Z. Baji, "Hierarchical oxide nanostructures fabricated with atomic layer deposition and hydrothermal growth," *NANO-STRUCTURES & NANO-OBJECTS*, vol. 13, pp. 100–108, 2018.

[15] M. Seifikar, B. P. Christian, J. Volk, J. Radó, I. E. Lukács, R. Dauksevicius, R. Gaidys, V. Lebedev, A. Viana, and E. P. O'Reilly, "Direct observation of spontaneous polarization induced electron charge transfer in stressed ZnO nanorods," *NANO ENERGY*, vol. 43, pp. 376–382, 2018.

[16] A. Bouvet-Marchand, A. Graillot, J. Volk, R. Dauksevicius, C. Sturm, M. Grundmann, E. Saoutieff, A. Viana, B. Christian, V. Lebedev, J. Rado, I. E. Lukacs, K. N Q, D. Grosso, and C. Loubat, "Design of UV-crosslinked polymeric thin layers for encapsulation of piezoelectric ZnO nanowires for pressure-based fingerprint sensors," *JOURNAL OF MATERIALS CHEMISTRY C*, vol. 6, no. 3, pp. 605–613, 2018.

[17] D. P. Szekrényes, S. Pothorszky, D. Zámbó, Z. Osváth, and A. Deák, "Investigation of Patchiness on Tip-Selectively Surface-Modified Gold Nanorods," *JOURNAL OF PHYSICAL CHEMISTRY C*, vol. 122, no. 3, pp. 1706–1710, 2018.

[18] G. Szabó and G. Bunth, "Social dilemmas in multistrategy evolutionary potential games," *PHYSICAL REVIEW E: COVERING STATISTICAL NONLINEAR BIOLOGICAL AND SOFT MATTER PHYSICS (2016-)*, vol. 97, no. 1, 2018.

[19] D. Merkel, D. Bessas, G. Bazsó, A. Jafari, R. Rüffer, A. Chumakov, N. Khanh, S. Sajti, J.-P. Celse, and D. Nagy, "In situ study of electric field controlled ion transport in the Fe/BaTiO 3 interface," *MATERIALS RESEARCH EXPRESS*, vol. 5, no. 1, 2018.

[20] A. Szolnoki and M. Perc, "Evolutionary dynamics of cooperation in neutral populations," *NEW JOURNAL OF PHYSICS*, vol. 20, no. 1, 2018.

[21] G. Sáfrán, "'One-sample concept' micro-combinatory for high throughput TEM of binary films," *ULTRAMICROSCOPY*, vol. 187, pp. 50–55, 2018.

[22] J. Gyulai, "Ionsugaras technikáktól a nanoszerkezetekig," *FIZIKAI SZEMLE*, vol. 68, no. 1, pp. 3–8, 2018.

[23] S. Gurbán, P. Petrik, M. Serényi, A. Sulyok, M. Menyhárd, E. Baradács, B. Parditka, C. Cserháti, G. Langer, and Z. Erdélyi, "Electron irradiation induced amorphous SiO 2 formation at metal oxide/Si interface at room temperature; electron beam writing on interfaces," *SCIENTIFIC REPORTS*, vol. 8, no. 1, p. 2124, 2018.

[24] M. Streckova, T. Sopcak, R. Stulajterova, M. Giretova, L. Medvecky, A. Kovalcikova, and K. Balazsi, "Needle-less electrospinning employed for calcium and magnesium phosphate coatings on titanium substrates," *SURFACE AND COATINGS TECHNOLOGY*, vol. 340, pp. 177–189, 2018.

[25] M. Alishahi, S. Mirzaei, P. Souček, L. Zábranský, V. Buršíková, M. Stupavská, V. Peřina, K. Balázsi, Z. Czigány, and P. Vašina, "Evolution of structure and mechanical properties of hard yet fracture resistant W-B-C coatings with varying C/W ratio," *SURFACE AND COATINGS TECHNOLOGY*, vol. 340, pp. 103–111, 2018.

[26] B. Király and G. Szabó, "Entropy Affects the Competition of Ordered Phases," *ENTROPY*, vol. 20, no. 2, 2018.

[27] Z. Molnár, V. Bódai, G. Szakacs, B. Erdélyi, Z. Fogarassy, G. Sáfrán, T. Varga, Z. Kónya, E. Tóth-Szeles, R. Szűcs, and I. Lagzi, "Green synthesis of gold nanoparticles by thermophilic filamentous fungi," *SCIENTIFIC REPORTS*, vol. 8, 2018.

[28] Z. Fogarassy, N. Oláh, I. Cora, Z. E. Horváth, T. Csanádi, A. Sulyok, and K. Balázsi, "The structural and mechanical characterization of TiC and TiC/Ti thin films grown by DC magnetron sputtering," *JOURNAL OF THE EUROPEAN CERAMIC SOCIETY*, vol. 38, no. 7, pp. 2886–2892, 2018.

[29] Z. Danku, Z. Wang, and A. Szolnoki, "Imitate or innovate: Competition of strategy updating attitudes in spatial social dilemma games," *EUROPHYSICS LETTERS*, vol. 121, no. 1, 2018.

[30] C. H. Ágoston, C. B. Örs, B. Szabolcs, S. Örs, K. Pál, and F. Zoltán, "A multimodal microtool for spatially controlled infrared neural stimulation in the deep brain tissue," *SENSORS AND ACTUATORS B-CHEMICAL*, vol. 263, pp. 77–86, 2018.

[31] P. Sipos, K. V. Kovács, R. Balázs, A. Tóth, I. Kovács, and T. Németh, "Contribution of individual pure or mixed-phase mineral particles to metal sorption in soils," *GEODERMA*, vol. 324, pp. 1–8, 2018.

[32] B. Gajdics, J. Tomán, F. Misják, G. Radnóczi, and Z. Erdélyi, "Spinodal decomposition in nanoparticles-experiments and simulation," *DEFECT AND DIFFUSION FORUM*, vol. 383, pp. 89–95, 2018.

[33] F. Bíró, "Metánérzékelés mikropellisztorral = Micro-pellistor for methane detection," Pannon Egyetem, 2018.

[34] T. Sopcak , L. Medvecky, T. Zagyva, M. Dzupon, J. Balko, K. Balázsi, C. Balázsi, "Characterization and adhesion strength of porous electrosprayed polymer–hydroxyapatite composite coatings," *RESOLUTION AND DISCOVERY*, vol. 3, no. 2, pp. 17–23, 2018.

[35] B. Kovács, "Flagellin alapú biomimetikus felületek jellemzése és élő sejtek adhéziójának nyomon követése jelölésmentes optikai bioszenzorokkal = Characterization of flagellin-based biomimetic coatings and monitoring of cell adhesion with label-free optical biosensors," Pannon Egyetem, 2018.

[36] G. Radnóczi, B. Bert, D. Diederik, and F. Misják, "Nagyentrópiás ötvözet-vékonyrétegek szerkezete," *FIZIKAI SZEMLE*, vol. 68, no. 3, pp. 81–85, 2018.

[37] E. Farkas, A. Szekacs, B. Kovacs, M. Olah, R. Horvath, and I. Szekacs, “Label-free optical biosensor for real-time monitoring the cytotoxicity of xenobiotics: A proof of principle study on glyphosate,” *JOURNAL OF HAZARDOUS MATERIALS*, vol. 351, pp. 80–89, 2018.

[38] G. Kádár, “Parallels of Belated Recognition: Bolyai János and Károlyházy Frigyes,” *UNIVERSE*, vol. 4, no. 1, 2018.

[39] M. Fried, *Felületek és vékonyrétegek vizsgálata polarizált fénnyel*. Budapest: Óbudai Egyetem, 2018.

[40] T. W. Pyrcz, R. Garlacz, K. Kertész, L. P. Biró, and Z. Bálint, “An imperfect imago? Post-mating loss of iridescent scales in Cheimas butterflies may change female from attractive to cryptic (Lepidoptera: Nymphalidae: Satyrinae),” *JOURNAL OF NATURAL HISTORY*, vol. 52, no. 19–20, pp. 1333–1350, 2018.

[41] G. Vértesy and I. Tomáš, “Nondestructive magnetic inspection of spot welding,” *NDT & E INTERNATIONAL*, vol. 98, pp. 95–100, 2018.

[42] A. Qadir, Z. Fogarassy, Z. E. Horváth, K. Balazsi, and C. Balazsi, “Effect of the oxidization of Si3N4 powder on the microstructural and mechanical properties of hot isostatic pressed silicon nitride,” *CERAMICS INTERNATIONAL*, vol. 44, no. 12, pp. 14601–14609, 2018.

[43] R. B. Z. Haroune, B. Katalin, and B. Csaba, “EFFECT OF THE alfa-Si3N4 ADDITION ON THE TRIBOLOGICAL PROPERTIES OF 316L STAINLESS STEEL PREPARED BY ATTRITION MILLING AND SPARK PLASMA SINTERING,” *ANYAGOK VILÁGA*, vol. XV, no. 1, pp. 9–16, 2018.

[44] R. B. Z. Haroune, B. Csaba, and B. Katalin, “Study of different ceramic additions effect on the 316L morphological properties during attrition milling,” *ANYAGOK VILÁGA*, vol. XV, no. 1, pp. 36–42, 2018.

[45] A. Zátonyi, Á. Szabó, F. Fedor, Á. Horváth, A. Pongrácz, and Z. Fekete, “Trendek a polimer alapú mikroimplantátumok fejlesztésében,” *ANYAGOK VILÁGA*, vol. 15, no. 1, pp. 17–33, 2018.

[46] T. Lohner, B. Kalas, P. Petrik, Z. Zolnai, M. Serényi, and G. Sáfrán, “Refractive Index Variation of Magnetron-Sputtered a-Si1−xGex by ‘One-Sample Concept’ Combinatory,” *APPLIED SCIENCES-BASEL*, vol. 8, no. 5, 2018.

[47] A. Klein, M. Kovacs, A. Muskotal, H. Jankovics, B. Toth, M. Posfai, and F. Vonderviszt, “Nanobody-Displaying Flagellar Nanotubes,” *SCIENTIFIC REPORTS*, vol. 8, 2018.

[48] M. L. Debreczeni, I. Székács, B. Kovács, A. Saftics, B. Péter, S. Kurunczi, J. Dobó, R. Horváth, and L. Cervenak, “Jelölésmentes optikai rendszer kidolgozása endotélsejtek működésének komplex vizsgálatára.” 2018.

[49] Ü. Antal, F. Zoltán, D. László, N. Szilvia, and N. Ákos, “Contact problems in GaAs-based solar cells,” *ACTA POLYTECHNICA HUNGARICA*, vol. 15, no. 6, pp. 99–124, 2018.

[50] G. Vértesy, I. Tomáš, B. Bálint, S. Gyimóthy, J. Pávó, T. Uchimoto, and T. Takagi, “Investigation of the role of a nonmagnetic spacer in local wall thinning inspection,” *INTERNATIONAL JOURNAL OF APPLIED ELECTROMAGNETICS AND MECHANICS*, vol. 57, no. 2, pp. 235–245, 2018.

[51] J. Radó, C. Dücső, P. Földesy, G. Szebényi, H. Sántha, K. Rohr, L. Mucha, K. Lis, W. Sadowski, D. Krawczyk, P. Kroczek, Z. Małota, Z. Nawrat, and P. Fürjes, “Force sensitive smart laparoscope of Robin Heart Surgical Robot,” in *20th Symposium on Design, Test, Integration and Packaging of MEMS and MOEMS, DTIP 2018*, 2018, pp. 104–107.

[52] I. Nyirő-Kósa, Á. Rostási, É. Bereczk-Tompa, I. Cora, M. Koblar, A. Kovács, and M. Pósfai, “Nucleation and growth of Mg-bearing calcite in a shallow, calcareous lake,” *EARTH AND PLANETARY SCIENCE LETTERS*, vol. 496, pp. 20–28, 2018.

[53] A. Palinkas, P. Kun, A. A. Koos, and Z. Osvath, “Dynamic strain in gold nanoparticle supported graphene induced by focused laser irradiation,” *NANOSCALE*, vol. 10, no. 28, pp. 13417–13425, 2018.

[54] T. Hristova-Vasileva, P. Petrik, D. Nesheva, Z. Fogarassy, J. Lábár, S. Kaschieva, S. Dmitriev, and K. Antonova, “Influence of 20 MeV electron irradiation on the optical properties and phase composition of SiOx thin films,” *JOURNAL OF APPLIED PHYSICS*, vol. 123, no. 19, 2018.

[55] M. Serényi, C. Frigeri, and R. Schiller, “Vegard’s-law-like dependence of the activation energy of blistering on the x composition in hydrogenated a-SixGe1-x,” *JOURNAL OF ALLOYS AND COMPOUNDS*, vol. 763, pp. 471–477, 2018.

[56] K. Lázár, L. Varga, K. V. Kovács, T. Fekete, Z. Klencsár, S. Stichleutner, L. Szabó, and I. Harsányi, "Electric explosion of steel wires for production of nanoparticles: Reactions with the liquid media," *JOURNAL OF ALLOYS AND COMPOUNDS*, vol. 763, pp. 759–770, 2018.

[57] W. Cota, G. Ódor, and S. C. Ferreira, "Griffiths phases in infinite-dimensional, non-hierarchical modular networks," *SCIENTIFIC REPORTS*, vol. 8, no. 1, 2018.

[58] B. Fulop, Z. Tajkov, J. Peto, P. Kun, J. Koltai, L. Oroszlany, E. Tovari, H. Murakawa, Y. Tokura, S. Bordacs, L. Tapaszto, and S. Csonka, "Exfoliation of single layer BiTeI flakes," *2D MATERIALS*, vol. 5, no. 3, 2018.

[59] T. Kolonits, P. Jenei, L. Péter, I. Bakonyi, Z. Czigány, and J. Gubicza, "Effect of bath additives on the microstructure, lattice defect density and hardness of electrodeposited nanocrystalline Ni films," *SURFACE AND COATINGS TECHNOLOGY*, vol. 349, pp. 611–621, 2018.

[60] K. Nagy and F. Misják, "In-situ transmission electron microscopy study of thermal stability and carbide formation in amorphous Cu-Mn/C films for interconnect applications," *JOURNAL OF PHYSICS AND CHEMISTRY OF SOLIDS*, vol. 121, pp. 312–318, 2018.

[61] K. H. Nagy, G. Radnóczi, and F. Misják, "Model study of carbide formation at Cu-Mn/low-k dielectric interfaces using in-situ TEM." 2018.

[62] G. Radnóczi, F. Misják, K. Nagy, and M. Čaplovičová, "Effect of Growth Temperature on the Structure of CoCrFeNiCu High Entropy Alloy Films." 2018.

[63] Z. A, F. F, B. Zs, and F. Z, "In vitro and in vivo stability of black-platinum coatings on flexible, polymer microECoG arrays," *JOURNAL OF NEURAL ENGINEERING*, vol. 15, no. 5, 2018.

[64] X. Chen and A. Szolnoki, "Punishment and inspection for governing the commons in a feedback-evolving game," *PLOS COMPUTATIONAL BIOLOGY*, vol. 14, no. 7, 2018.

[65] Z. Kovács, E. Schafler, K. V. Kovács, P. Szommer, and Á. Révész, "High pressure torsion of a Vitreloy bulk metallic glass near the glass transition temperature," *JOURNAL OF NON-CRYSTALLINE SOLIDS*, vol. 498, pp. 25–31, 2018.

[66] L. Yang, M. Menyhárd, A. Sulyok, K. Tőkési, and Z. Ding, "Optical properties and excitation energies of iridium derived from reflection electron energy loss spectroscopy spectra," *APPLIED SURFACE SCIENCE*, vol. 456, pp. 999–1003, 2018.

[67] A. Cigáň, P. Lobotka, A. Dvurečenskij, M. Škrátek, G. Radnóczi, M. Majerová, Z. Czigány, J. Maňka, I. Vávra, and M. Mičušík, "Characterization and magnetic properties of nickel and nickel-iron nanoparticle colloidal suspensions in imidazolium-based ionic liquids prepared by magnetron sputtering," *JOURNAL OF ALLOYS AND COMPOUNDS*, vol. 768, pp. 625–634, 2018.

[68] S. Bietti, F. Basset, D. Scarpellini, A. Fedorov, A. Ballabio, L. Esposito, M. Elborg, T. Kuroda, Á. Nemcsics, L. Toth, C. Manzoni, C. Vozzi, and S. Sanguinetti, "Ga metal nanoparticle-GaAs quantum molecule complexes for terahertz generation," *NANOTECHNOLOGY*, vol. 29, no. 36, 2018.

[69] M. Alshahed, L. Heuken, M. Alomari, I. Cora, L. Toth, B. Pecz, C. Wachter, T. Bergunde, and J. Burghartz, "Low-Dispersion, High-voltage, Low-Leakage GaN HEMTs on Native GaN Substrates," *IEEE TRANSACTIONS ON ELECTRON DEVICES*, vol. 65, no. 7, pp. 2939–2947, 2018.

[70] A. Szolnoki and X. Chen, "Reciprocity-based cooperative phalanx maintained by overconfident players," *PHYSICAL REVIEW E: COVERING STATISTICAL NONLINEAR BIOLOGICAL AND SOFT MATTER PHYSICS (2016-)*, vol. 98, no. 2, 2018.

[71] Ö. C.Boros, Á. C. Horváth , S. Beleznai , Ö.Sepsi, S. Lenk , Z. Fekete, P. Koppa "Optical and thermal modeling of an optrode microdevice for infrared neural stimulation," *APPLIED OPTICS*, vol. 57, no. 24, pp. 6952–6957, 2018.

[72] Zs. Berces, J. Pomothy, Á. Cs. Horváth, T. Kőhidi, É. Benyei, Z. Fekete, E. Madarász, A. Pongrácz "Effect of nanostructures on anchoring stem cell-derived neural tissue to artificial surfaces," *JOURNAL OF NEURAL ENGINEERING*, vol. 15, no. 5, 2018.

[73] A. Szolnoki and D. Z, "Dynamic-sensitive cooperation in the presence of multiple strategy updating rules," *PHYSICA A - STATISTICAL MECHANICS AND ITS APPLICATIONS*, vol. 511, pp. 371–377, 2018.

[74] R. Dedoncker, P. Djemia, G. Radnóczi, F. Tétard, L. Belliard, G. Abadias, N. Martin, and D. Depla, "Reactive sputter deposition of CoCrCuFeNi in nitrogen/argon mixtures," *JOURNAL OF ALLOYS AND COMPOUNDS*, vol. 769, pp. 881–888, 2018.

[75] G. Vértesy, A. Gasparics, and I. Tomáš, "Inspection of Local Wall Thinning by Different Magnetic Methods," *JOURNAL OF NONDESTRUCTIVE EVALUATION*, vol. 37, no. 3, 2018.

[76] G. Piszter, K. Kertész, Z. E. Horváth, L. P. Biró, and Z. Bálint, "Ikarusz boglárka lepkék szerkezeti és pigment eredetű színeinek stresszállósága," *FIZIKAI SZEMLE*, vol. 68, no. 7–8, pp. 225–229, 2018.

[77] I. Bányász, S. Pelli, G. Nunzi-Conti, G. Righini, S. Berneschi, E. Szilágyi, A. Németh, M. Fried, P. Petrik, E. Agócs, B. Kalas, Z. Zolnai, N. Khanh, I. Rajta, G. Nagy, V. Havranek, V. Vosecek, M. Veres, and L. Himics, "Design, Ion beam fabrication and test of integrated optical elements," in *Proceedings of the 6th International Conference on Photonics, Optics and Laser Technology*, vol. 1, 2018, pp. 279–285.

[78] A. Szolnoki and X. Chen, "Competition and partnership between conformity and payoff-based imitations in social dilemmas," *NEW JOURNAL OF PHYSICS*, vol. 20, no. 9, 2018.

[79] A. Racz and M. Menyhard, "Design of Corrosion Resistive SiC Nanolayers," *ACS APPLIED MATERIALS & INTERFACES*, vol. 10, no. 26, pp. 22851–22856, 2018.

[80] K., Bán, M. Nagy, Á. Cziráki, Zs. Fogarassy "The Study Of Heat Affected Zone In Soft Magnetic Glassy Ribbons During Laser Cutting," in *Advanced Manufacturing and Repair Technologies in Vehicle Industry*, 2018.

[81] D. Music, P. Schmidt, Z. Czigány, G. Greczynski, R. W. Geyer, and M. Hans, "Electrical resistivity modulation of thermoelectric iron based nanocomposites," *VACUUM*, vol. 157, pp. 384–390, 2018.

[82] Z. Bálint, S. Sáfián, A. Hoskins, K. Kertész, A. Koós, Z. Horváth, G. Piszter, and L. Biró, "The Only Blue Mimeresia (Lepidoptera: Lycaenidae: Lipteninae) Uses a Color-Generating Mechanism Widely Applied by Butterflies," *JOURNAL OF INSECT SCIENCE*, vol. 18, no. 3, 2018.

[83] A. Saftics, G. Prósz, B. Türk, B. Peter, S. Kurunczi, and R. Horvath, "In situ viscoelastic properties and chain conformations of heavily hydrated carboxymethyl dextran layers: a comparative study using OWLS and QCM-I chips coated with waveguide material," *SCIENTIFIC REPORTS*, vol. 8, 2018.

[84] G. Kapoor, L. Péter, É. Fekete, J. Lábár, and J. Gubicza, "The influence of Mo addition on the microstructure and its thermal stability for electrodeposited Ni films," *MATERIALS CHARACTERIZATION*, vol. 145, pp. 563–572, 2018.

[85]

Z. Juhász, E. Dudás, and H. Pamjav, "A new self-learning computational method for footprints of early human migration processes," *MOLECULAR GENETICS AND GENOMICS*, vol. 293, no. 6, pp. 1579–1594, 2018.

[86] I. Bársony, F. Bíró, Z. Hajnal, and C. Dücső, "Means of temperature assistance in gas sensing," in *Emerging Sensing Technologies Summit*, 2018, pp. 31–33.

[87] A. Deák, "Nanorészecskék önszeveződése," *FIZIKAI SZEMLE*, vol. 68, no. 9, pp. 295–298, 2018.

[88] A. Lengyel, Z. Homonnay, K. Kovács, Z. Klencsár, S. Németh, R. Szalay, V. Kis, F. Fodor, Á. Solti, M. Ristic, S. Music, and E. Kuzmann, "Characterization of nanomagnetites co-precipitated in inert gas atmosphere for plant nutrition," *HYPERFINE INTERACTIONS*, vol. 239, no. 1, 2018.

[89] F. Bíró, Z. Hajnal, C. Dücső, and I. Bársony, "The Role of Phase Changes in TiO2/Pt/TiO2 Filaments," *JOURNAL OF ELECTRONIC MATERIALS*, vol. 47, no. 4, pp. 2322–2329, 2018.

[90] A. Nemcsics, A. Urmos, and L. Toth, "Droplet Epitaxy and its Possibilities in Nano-electronics," *International Symposium on Next-Generation Electronics*, vol. 2018, pp. 122–124, 2018.

[91] N. M. Freitag, T. Reisch, L. A. Chizhova, P. Nemes-Incze, C. Holl, C. R. Woods, R. V. Gorbachev, Y. Cao, A. K. Geim, K. S. Novoselov, J. Burgdoerfer, F. Libisch, and M. Morgenstern, "Large tunable valley splitting in edge-free graphene quantum dots on boron nitride," *NATURE NANOTECHNOLOGY*, vol. 13, no. 5, pp. 392–397, 2018.

[92] B. Kovacs, A. Saftics, A. Biro, S. Kurunczi, B. Szalontai, B. Kakasi, F. Vonderviszt, A. Der, and R. Horvath, "Kinetics and Structure of Self-Assembled Flagellin Monolayers on Hydrophobic Surfaces in the Presence of Hofmeister Salts: Experimental Measurement of the Protein Interfacial Tension at the Nanometer Scale," *JOURNAL OF PHYSICAL CHEMISTRY C*, vol. 122, no. 37, pp. 21375–21386, 2018.

[93] I. Bársony, F. Bíró, Z. Hajnal, and C. Dücső, "Means of temperature assistance in gas sensing," in *Emerging Sensing Technologies Summit*, 2018, pp. 31–33.

[94] J. Balogh, P. Süle, L. Bujdosó, Z. E. Horváth, D. Kaptás, A. Kovács, D. G. Merkel, A. Nakanishi, S. Sajti, and L. Bottyán, "Asymmetric alloy formation at the Fe-on-Ti and Ti-on-Fe interfaces," *JOURNAL OF PHYSICS-CONDENSED MATTER*, vol. 30, no. 45, 2018.

[95] Z. Zolnai, D. Zámbó, Z. Osváth, N. Nagy, M. Fried, A. Németh, S. Pothorszky, D. Szekrényes, and A. Deák, "Gold Nanorod Plasmon Resonance Damping Effects on a Nanopatterned Substrate," *JOURNAL OF PHYSICAL CHEMISTRY C*, vol. 122, no. 43, pp. 24941–24948, 2018.

[96] Z. Danku, G. Ódor, and F. Kun, "Avalanche dynamics in higher-dimensional fiber bundle models," *PHYSICAL REVIEW E: COVERING STATISTICAL NONLINEAR BIOLOGICAL AND SOFT MATTER PHYSICS (2016-)*, vol. 98, no. 4, 2018.

[97] G. Vértesy, "Nondestructive investigation of wall thinning in ferromagnetic material by Magnetic adaptive testing: influence of yoke size," *BADANIA NIENISZCZĄCE I DIAGNOSTYKA*, vol. 2, pp. 45–49, 2018.

[98] P. Jenei, C. Balázsi, Á. Horváth, K. Balázsi, and J. Gubicza, "The influence of BN additives on the phase composition, microstructure and mechanical properties of 316L steel consolidated by spark plasma sintering," *IOP CONFERENCE SERIES: MATERIALS SCIENCE AND ENGINEERING*, vol. 426, no. 1, 2018.

[99] D. Zambo, D. P. Szekrenyes, S. Pothorszky, N. Nagy, and A. Deak, "SERS Activity of Reporter-Particle-Loaded Single Plasmonic Nanovoids," *JOURNAL OF PHYSICAL CHEMISTRY C*, vol. 122, no. 41, pp. 23683–23690, 2018.

[100] H. Nakanishi, A. Deak, G. Hollo, and I. Lagzi, "Existence of a Precipitation Threshold in the Electrostatic Precipitation of Oppositely Charged Nanoparticles.," *ANGEWANDTE CHEMIE-INTERNATIONAL EDITION*, vol. 57, no. 49, pp. 16062–16066, 2018.

[101] J. Gyulai, "Anyagtudomány és anyagmérnökség – ennek néhány egyedi vonása a kelet-közép-európai térség (KKE) országaiban," *ACTA MATERIALIA TRANSYLVANICA (HU)*, vol. 1, no. 1, pp. 5–11, 2018.

[102] B. Peter, R. Ungai-Salanki, B. Szabo, A. G. Nagy, I. Szekacs, S. Bosze, and R. Horvath, "High-Resolution Adhesion Kinetics of EGCG-Exposed Tumor Cells on Biomimetic Interfaces: Comparative Monitoring of Cell Viability Using Label-Free Biosensor and Classic End-Point Assays," *ACS OMEGA*, vol. 3, no. 4, pp. 3882–3891, 2018.

[103] B. Peter, I. Lagzi, S. Teraji, H. Nakanishi, L. Cervenak, D. Zambo, A. Deak, K. Molnar, M. Truszka, I. Szekacs, and R. Horvath, "Interaction of Positively Charged Gold Nanoparticles with Cancer Cells Monitored by an in Situ Label-Free Optical Biosensor and Transmission Electron Microscopy," *ACS APPLIED MATERIALS & INTERFACES*, vol. 10, no. 32, pp. 26841–26850, 2018.

[104] D. Beke, A. Fučíková, T. Z. Jánosi, G. Károlyházy, B. Somogyi, S. Lenk, O. Krafcsik, Z. Czigány, J. Erostyák, K. Kamarás, J. Valenta, and A. Gali, "Direct Observation of Transition from Solid-State to Molecular-Like Optical Properties in Ultrasmall Silicon Carbide Nanoparticles," *JOURNAL OF PHYSICAL CHEMISTRY C*, vol. 122, no. 46, pp. 26713–26721, 2018.

[105] P. Sipos, T. Németh, V. Kovács Kis, N. Zajzon, C. Choi, and Z. May, "Potentially Toxic Metal-Bearing Phases in Urban Dust and Suspended Particulate Matter: The Case of Budapest, Hungary," in *Urban Pollution*, 2018, pp. 371–383.

[106] F. Riesz, "Structured-illumination Makyoh-topography: optimum grid position and its constraints," *SURFACE TOPOGRAPHY: METROLOGY AND PROPERTIES*, vol. 6, no. 4, 2018.

[107] V. G. Mansurov, Y. G. Galitsyn, T. V. Malin, S. A. Teys, E. V. Fedosenko, A. S. Kozhukhov, K. S. Zhuravlev, I. Cora, and B. Pecz, "Formation of a Graphene-Like SiN Layer on the Surface Si(111)," *SEMICONDUCTORS*, vol. 52, no. 12, pp. 1511–1517, 2018.

[108] J. Radó, P. Udvardi, S. Soleimani, L. Kenda Peter, I. Bársony, P. Révész, and J. Volk, "Low-Frequency Piezoelectric Accelerometer Array for Fully Implantable Cochlear Implants," *PROCEEDINGS*, vol. 2, no. 13, 2018.

[109] J. Pető, T. Ollár, P. Vancsó, Z. I. Popov, G. Z. Magda, G. Dobrik, C. Hwang, P. B. Sorokin, and L. Tapasztó, "Spontaneous doping of the basal plane of MoS2 single layers through oxygen substitution under ambient conditions," *NATURE CHEMISTRY*, vol. 10, no. 12, pp. 1246–1251, 2018.

[110] A. Kovalčíková, M. Húlan, R. Sedlák, M. Fides, C. Balázsi, M. Mihaliková, and J. Dusza, "Thermal Shock Resistance of Si3N4/hBN Ceramic Composites," *KEY ENGINEERING MATERIALS*, vol. 784, pp. 73–78, 2018.

[111] K. Kertész, G. Piszter, Z. Bálint, and L. Biró, "Optical Vapor Sensing on Single Wing Scales and on Whole Wings of the Albulina metallica Butterfly," *SENSORS*, vol. 18, no. 12, 2018.

[112] I. Szekacs, E. Farkas, B. L. Gemes, E. Takacs, A. Szekacs, and R. Horvath, "Integrin targeting of glyphosate and its cell adhesion modulation effects on osteoblastic MC3T3-E1 cells revealed by label-free optical biosensing," *SCIENTIFIC REPORTS*, vol. 8, 2018.

[113] V. K. Kis, M. Fábián, and J. Lábár, "Mineralogical applications of ePDF analysis of amorphous materials - need for validation." 2018.

[114] M. Fábián and V. K. Kis, "Bioactive glasses: structure characteristics and bone regeneration application." 2018.

[115] V. Kovács Kis, M. Fábián, I. Székács, I. Kovács, J. Lábár, and Z. Kovács, "Structural investigations on bioactive glasses," in *A Magyar Mikroszkópos Társaság éves konferenciája*, 2018.

[116] M. Fábián and V. K. Kis, "Neutron diffraction and Raman spectroscopic study of bioactive silica based glasses." 2018.

[117] V.K. Kis, Zs. Dallos, Zs. Czigány, D. Nagy, I. Dódony "HRTEM study of bone mineral nanocrystals." 2018.

[118] K. V. Kovács, Z. Dallos, Z. Czigány, D. Nagy, and I. Dódony, "Discrepancies between the nanostructure of bone apatite and hydroxylapatite. An HRTEM study." 2018.

[119] Z. Dallos, K. V. Kovács, F. Kristály, and I. Dódony, "Heating experiments on bone apatite to observe structural alterations." 2018.

[120] K. Kiss, T. Szeniczey, K. Karlinger, K. Z. Mészáros, E. Szvák, E. Molnár, A. Marcsik, A. Sklánitz, L. Szabó, Z. Dallos, K. V. Kovács, K. Buczkó, and T. Hajdu, "A possible case of metastatic cancer from Kehida-Fövenyes (7 - 8 century)." 2018.

[121] B. Péter, E. Farkas, E. Forgács, A. Saftics, B. Kovács, S. Kurunczi, I. Székács, A. Csámpai, S. Bősze, and R. Horváth, "A zöld tea polifenol hatása a sejtadhéziós mátrixra és a sejtadhézióra: vizsgálatok jelölésmentes optikai bioszenzorokkal." 2018.

[122] B. Péter, E. Farkas, E. Forgács, A. Saftics, B. Kovács, S. Kurunczi, I. Székács, A. Csámpai, S. Bősze, and R. Horváth, "A zöld tea polifenol hatása a sejtadhéziós mátrixra és a sejtadhézióra: vizsgálatok jelölésmentes optikai bioszenzorokkal." 2018.

[123] P. Beatrix, "Living cells and copolymer coatings exposed to green tea polyphenol (EGCg): dynamic investigations using label-free optical biosensors." 2018.

[124] P. Beatrix, "Living cells and copolymer coatings exposed to green tea polyphenol (EGCg): dynamic investigations using label-free optical biosensors." 2018.

[125] E. Farkas, A. Székács, B. Kovács, M. Oláh, R. Horváth, and I. Székács, "Xenobiotikumok hatásának tanulmányozása MC3T3-E1 sejtvonalon jelölésmentes bioszenzorral." 2018.

[126] E. Farkas, A. Székács, B. Kovács, M. Oláh, R. Horváth, and I. Székács, "Jelölésmentes optikai bioszenzor alkalmazása xenobiotikumok letapadt sejtekre gyakorolt hatásának meghatározásához." 2018.

[127] M. Gartner, C. Lete, M. Chelu, H. Stroescu, M. Zaharescu, C. Moldovan, C. Brasoveanu, M. Gheorghe, S. Gheorghe, A. Duta, Z. Labadi, B. Kalas, A. Saftics, M. Fried, P. Petrik, E. Toth, H. Jankovics, and F. Vonderviszt, "Electrochemical Sensors for Detection of Different Ionic Species (Nitrites/Nitrates and Heavy Metals) in Natural Water Sources," *INTERNATIONAL SEMICONDUCTOR CONFERENCE*, vol. 2018, pp. 329–332, 2018.

[128] D. Bazeia, B. F. de Oliveira, and A. Szolnoki, "Phase transitions in dependence of apex predator decaying ratio in a cyclic dominant system," *EUROPHYSICS LETTERS*, vol. 124, no. 6, 2018.

[129] B. Katalin, F. Mónika, F. Zsolt, and B. Csaba, "Examination of milled h-BN addition on sintered Si3N4/h-BN ceramic composites," *PROCESSING AND APPLICATION OF CERAMICS*, vol. 12, no. 4, pp. 357–365, 2018.

[130] J. Radó, C. Dücső, P. Földesy, I. Bársony, K. Rohr, L. Mucha, K. Lis, W. Sadowski, D. Krawczyk, P. Kroczek, Z. Małota, G. Szebényi, H. Sántha, Z. Nawrat, and P. Fürjes, "Biomechanical Tissue Characterisation by

Force Sensitive Smart Laparoscope of Robin Heart Surgical Robot," *PROCEEDINGS*, vol. 2, no. 13, pp. 1035–1038, 2018.

[131] K. Kliment, B. Mácsik-Valent, K. Nagy, B. Péter , E. Farkas, I. Székács, R. Horváth , A. Erdei, I. Kurucz "Real-Time Monitoring of Integrated Cellular Responses of Primary B Cells upon Simultaneous Receptor Engagement." 2018.

[132] M. Szappanos, J. Radó, G. Battistig, P. Földesy, and J. Volk, "Energy Harvesting Powered Wireless Vibration Analyser," *PROCEEDINGS*, vol. 2, no. 13, 2018.

[133] E. Dodony, G. Z. Radnóczi, and I. Dódony, "Observations in the low temperature copper - silicon system." 2018.

[134] A. Prósz, A. Saftics, B. Péter, S. Kurunczi, and R. Horváth, "Biológiai vékonyrétegek és élõ sejtek mechanikai tulajdonságainak vizsgálata kvarckristály mikromérleggel," *FIZIKAI SZEMLE*, vol. 68, no. 12, pp. 416–420, 2018.

[135] C. S. Daróczi, *MTA EK MFA Yearbook 2017*. Budapest: MTA Energiatudományi Kutatóközpont, 2018.

[136] G. Vértesy and I. Tomáš, "Influence of magnetizing current's speed in Magnetic Adaptive Testing," *JOURNAL OF ELECTRICAL ENGINEERING-ELEKTROTECHNICKY CASOPIS*, vol. 69, no. 6, pp. 461–463, 2018.

[137] G. Odor and B. Hartmann, "Heterogeneity effects in power grid network models," *PHYSICAL REVIEW E: COVERING STATISTICAL NONLINEAR BIOLOGICAL AND SOFT MATTER PHYSICS (2016-)*, vol. 98, no. 2, 2018.

[138] A. Horvath, N. Nagy, G. Vertesy, and R. Schiller, "The effect of ion irradiation on the electron work function of stainless steel," *MATERIALS CHEMISTRY AND PHYSICS*, vol. 217, pp. 541–546, 2018.

[139] Á. G. Nagy, A. Bonyár, and R. Horváth, "A nanofluidikai atomerőmikroszkóp: FluidFM," *ELEKTRONIKAI TECHNOLÓGIA ÉS GYÁRTÁSINFORMATIKA*, vol. 2018, no. 1, pp. 4–8, 2018.

[140] E. Agocs and R. K. Attota, "Enhancing optical microscopy illumination to enable quantitative imaging," *SCIENTIFIC REPORTS*, vol. 8, 2018.

[141] P. Petrik, "Solar cells with photonic and plasmonic structures," in *Spectroscopic Ellipsometry for Photovoltaics*, vol. 1, 2018, pp. 509–522.

[142] I. Rigó, M. Veres, O. Hakkel, and P. Fürjes, "Hierarchically Combined Periodic SERS Active 3D Micro- and Nanostructures for High Sensitive Molecular Analysis," *PROCEEDINGS*, vol. 2, no. 13, 2018.

[143] I. Rigó, M. Veres, L. Himics, T. Váczi, and P. Fürjes, "Preparation and Characterization of SERS Substrates of Different Morphology," in *Advanced Nanotechnologies for Detection and Defence against CBRN Agents*, 2018, pp. 63–68.

[144] Z. Balint, G. Piszter, K. Kertesz, and L. P. Biro, "Physiology of butterflies: the various roles of wing scales presented via case studies (Lepidoptera: Lycaenidae)," *MITTEILUNGEN DER DEUTSCHEN GESELLSCHAFT FÜR ALLGEMEINE UND ANGEWANDTE ENTOMOLOGIE*, vol. 21, pp. 309–312, 2018.

[145] J. Gyulai, "Materials Science and Engineering – Some Aspects in Central and Eastern European (CEE) Countries," *ACTA MATERIALIA TRANSYLVANICA (EN)*, vol. 1, no. 1, pp. 5–11, 2018.

[146] V. Mansurov, Y. Galitsyn, T. Malin, S. Teys, K. Zhuravlev, I. Cora, and B. Pécz, "van der Waals and Graphene-Like Layers of Silicon Nitride and Aluminum Nitride," in *2D Materials*, 2018.

[147] A. Pongrácz, S. Barna, I. Lukács, L. Illés, H. Liliom, P. Lajer, B. Csernyus, Á. Szabó, Z. Bérces, Z. Fekete, P. Lőw, and K. Schlett, "Modification of Glial Attachment by Surface Nanostructuring of SU-8 Thin Films," *PROCEEDINGS*, vol. 2, no. 13, p. 1016, 2018.